Holographic Optical Elements in Dichromated Gelatin

Ian Russell Redmond

Submitted for the degree of Doctor of Philosophy.

Heriot-Watt University

Department of Physics

May 1989

List of Figures

Acknowledgements

I would like to give my thanks to my supervisor, Prof. Andrew Walker for his support and guidance, and especially for his knowledge where mine was lacking. A useful old fish is Andy. Also thanks to Prof. Smith, without whose efforts the DCG lab could never have been built, and to Ronald Reagan for financing half of the lab, although I doubt if he ever knew it.

Thanks especially to Harvey Richardson and Jeff Hunter, the department VAX experts, for their help both in the implementation of the models in this thesis, and in the use of the typesetting program, LaTeX, in which this thesis is produced.

This work has been supported by the Science and Engineering Research Council through a CASE studentship in collaboration with British Aerospace plc at Filton in Bristol. I would like to thank B.Ae. for their support, especially Alan Levenston and Nick Roberts, and hope that this thesis will be of use to them. Thanks also to Pilkington Brothers plc at Lathom for the supply of some of the gelatin layers used in the thesis.

Thanks to the following people who have directly or indirectly assisted me in the work leading to this thesis; Brian Robertson, Mohammed Taghizadeh, Frank Tooley, Nick Craft, Jimmy Moffat and David Craig.

Abstract

The properties, preparation and processing of dichromated gelatin (DCG) are detailed, and procedures for the control of the holographic properties of DCG, including reproducible high performance, are given. Transmission holographic gratings are investigated and analysed by coupled wave theory, including the effects of higher diffraction orders, non-uniformities in depth and saturation of the index modulation. The theory is extended in an investigation of transmission fan-out holograms, giving the most complete picture to date of these devices due to the inclusion of cross-coupling effects in both the absence and presence of cross-gratings, and the consideration of the effects of saturation and spatially varying modulation due to beating between gratings. Efficiency and uniformity are principally studied. Comparison with theory is qualitatively correct, and quantitatively better than previous theories. Conformal reflection gratings are also described by a theory involving depth non-uniformities. Finally, a selection of real devices are given, with their design considerations, including holographic attenuators, fan-out devices and lenses, both for the same wavelength as recording and for different. A ray tracing model is given and used in lens optimisation for use at wavelengths different from the recording wavelength.

Chapter 1

Introduction

Holography began with Gabor's idea [GAB48] to extend Bragg's X-ray microscope principle [BRA39] in order to increase the magnification of electron miroscopes. Electron microscopes were limited by the spherical aberration of the magnetic lenses used to focus an electron beam. Gabor realised that the coherent recording on a photographic plate of the interference between the scattered field from an object and a plane or spherical 'reference' wave could, when re-illuminated by the reference wave, completely reconstruct the scattered 'object' wave by diffraction. He intended to replay this 'hologram' (meaning 'whole image' from the Greek) with visible light, thereby getting a magnification due to the great wavelength change. The technique was never very successful, partly due to the hologram's on-axis nature, which meant the image was mixed up with both the transmitted reference beam, and the extraneous 'conjugate' image.

The invention of the laser provided a light source with much greater coherence, allowing off-axis holograms to be recorded with a Helium-Neon laser [LEI62], sep-

arating the image and the reference beam. Since that time, lasers have improved (the Argon-ion laser being the main addition for holographic use), although the Helium-Neon laser is still the most widely used laser for holography. The main advances have been in holographic materials, such as improved photographic materials suitable for the recording of reflection holograms (which have a greater resolution requirement than Gabor's transmission holograms), and in processing techniques, such as bleaching of photographic materials [CAT65]. Dichromated gelatin was re-discovered rather than invented, since it can easily be obtained from conventional photographic materials [SHA68], and had been used as an alternative photographic material since the 1830's. DCG has proved to be one of the best holographic materials, and its preparation and use will form a significant part of this thesis.

Holograms may be thought of as devices which redirect light in a controlled way, unlike a photograph which simply scatters light in all directions. This leads to the three dimensional properties of holographic images, which change their appearance as the viewer moves around the hologram in exactly the same way as the object itself changes its appearance. A hologram can also be considered a memory of the two waves used to record it, so that illuminating it with either one will recreate the other. Therefore, if the reference wave is a plane wave, and the object wave is spherical, then illuminating it after recording and developing with a plane wave will cause a spherical wave to be generated. This is identical to the operation of a conventional lens, and is the principle behind holographic optical elements (HOE's). An HOE may therefore duplicate the action of any

optical element simply by recording the desired input and output waves. The proviso is that perfect operation is achieved only when the illuminating wave is an exact duplicate of the recording wave, in direction, curvature and wavelength. The broadening of the operating parameters of HOE's is the subject of much work, including, in part, this thesis.

The work contained in this thesis began in a department which had essentially no experience of dichromated gelatin, and very little of holography. It began as a result of optical computing research, and a need for power-supply and 'wiring' methods analogous to those in electronics.

Following the successful development of optically nonlinear devices suitable for optical digital computing, efforts were directed at demonstrating digital circuits using these devices in parallel, ultimately in large arrays, in order to demonstrate the parallelism advantage that optics shows over electronics. The problem then came that arrays had to be supplied with power, and arrays had to be interconnected with each other. There is general agreement that HOE's in one form or another are the devices best suited to these tasks. HOE's can provide re-routing of beams, focussing, and fan-out functions simply and, in the right material, with high efficiency. The right material is thought by many to be dichromated gelatin, or DCG, since in many ways it is an almost ideal holographic medium. It exhibits close to 100% diffraction efficiency in simple gratings with negligible scatter and absorption, and has a resolution on the molecular scale, suitable for visible and UV operation. It can also be processed in relatively thick layers ($> 100\mu$m), allowing control over wavelength and angular selection properties, as well as high efficiency

volume operation in the near infra-red.

The main disadvantages with DCG are its poor reproducibility, and its sensitivity to environmental conditions prior to sealing. The use of an environmentally controlled laboratory in which holograms are kept throughout all stages of exposure and processing largely eliminates these problems. Under these conditions, DCG becomes a manageable holographic material which may be controlled in its response by processing and exposure techniques. A detailed practical analysis of the treatment of DCG is given in chapter 2. Methods are given for pre-processing and post-processing, including methods of post-tuning the efficiency of holograms, and protecting them against thermal and laser damage.

Chapter 3 investigates the internal structure of transmission holograms, and develops a theory which includes the effects of higher-order diffraction, saturation and non-uniformities in DCG. The theory successfully accounts for all the observed grating responses. Chapter 4 extends the modelling to fan-out holograms - an area of particular interest in optical computing, and compares experiment with theory. The investigation given is believed to come closer to the facts than any previous studies. A number of effects unique to fan-out holograms are investigated and quantified as far as possible.

Chapter 5 performs a similar analysis to chapter 3 on conformal reflection holograms, again developing a theory which accounts for non-uniformities and comparing it with experiment.

Chapter 6 discusses a number of real HOE's made for specific applications, including attenuators, beamsplitters, polarising beamsplitters, fan-out devices,

lenses and lens arrays, and wavelength-shifted lenses. The ray tracing model used to optimise such lenses is given, and includes the effects of thickness and refractive index changes during processing, and measures of the Bragg mismatch which affects diffraction efficiency.

The HOE's program has proved itself to be a significant spinoff area, which continually generates interest and finds applications in many areas of optics. Most of the HOE's discussed in detail in the thesis have been 'commissioned', some from optical computing research within the department, and some from external organisations, such as Ferranti (holographic mirror for a head-up display, and the fibre link HOE) and AT&T Bell laboratories (850nm lens array). This demonstrates that HOE's in DCG are a practical complement to conventional optics, and, at present, the only type of HOE's capable of holding this position.

Chapter 2

Dichromated Gelatin.

2.1 Introduction

It was recognised in the 1830's that some biological organic colloids, such as gelatin, albumen and fish glue undergo photochemical hardening, or tanning when chromates or dichromates are present in the material. When sufficiently hardened by exposure to light, these colloids become insoluble in water, and so an image can be created by simply washing away the unexposed, unhardened areas. This image is in the form of a relief, or phase, image on the transparent colloid. It can be made visible by dying. Alternatively, carbon particles may be dispersed through the medium which are retained in the hardened areas during washing to form a black and white image. If the colloid is exposed to the interference pattern of two coherent waves, a hologram will result, initially as a surface relief phase hologram, after washing. Note that both the thickness of the layer and its local density is affected by photochemical hardening, so that the phase modulation results from

two sources. In the case of gelatin, which of these is the dominant feature can be controlled by the processing and the 'bias hardness' of the gelatin. 'Hardness' in this case specifically refers to the solubility of gelatin. If the gelatin is hard, it may only absorb a limited amount of water, which is insufficient to cause separation of the gelatin molecules into solution. It should be noted that there are a number of aspects to hardness, which will be discussed in more detail in section 2.1.2

Of the various photosensitive colloids, gelatin is the most useful for three main reasons: 1) It can absorb large quantities of liquids quickly (particularly water), facilitating processing. 2) It can easily be produced in uniform films from less than 1μm to over 500μm in thickness of good optical quality. 3) Its photosensitive properties can be controlled by chemical hardening and the processing of the gelatin.

The best sensitising chromate to use is ammonium dichromate, partly due to its high solubility in water which allows a high concentration of dichromate in the gelatin layer before crystallisation occurs on drying.

Gelatin itself is derived from the natural protein, collagen, which is obtained mainly from pigskin and calfskin, via a lengthy chemical process which breaks down the collagen into polypeptide chains of amino acids. These chains are typically 80nm long and have the chemical form shown in figure 2.1. Because of the biological origin, the exact composition, and therefore properties, of gelatin vary greatly from different sources. R represents an amino acid residue, such as glycine.

When gelatin solutions of greater than 1% are allowed to dry, the gel phase

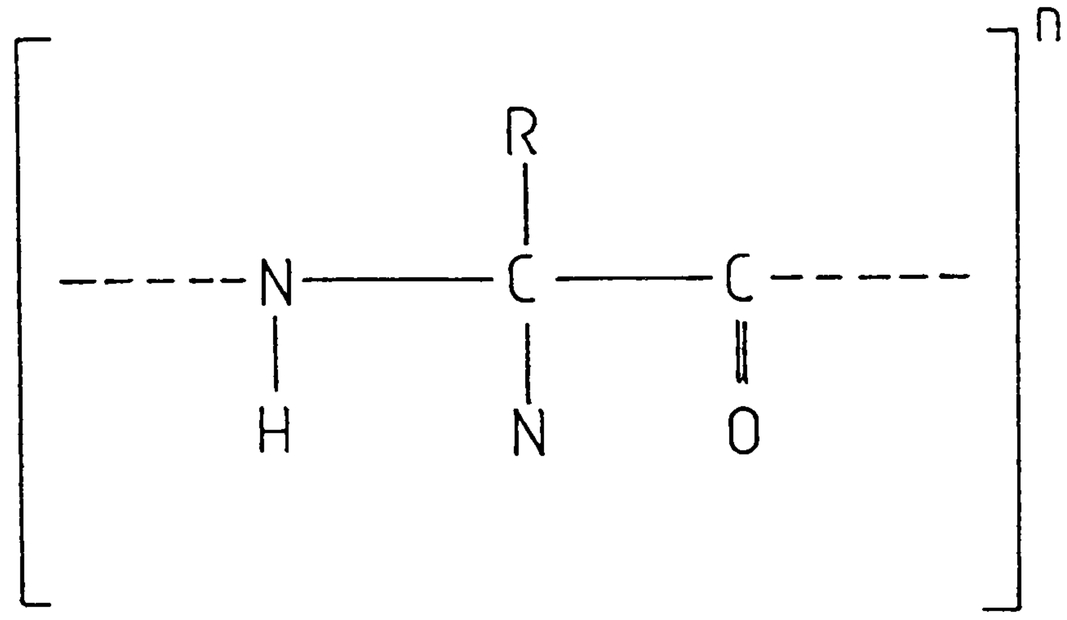

Figure 2.1: Unit of the polypeptide chain of gelatin.

results. This is a clear, rigid, crystalline form of gelatin. By adding water a gelatin solution is again formed, unless the gel has been hardened in the interim. When hardened, the gel can still absorb large quantities of water, typically two to three times its own mass, and swell, but remain intact, and then dry again to a gel. It is this gel state of gelatin which is of interest in holography, because the gelatin is sufficiently rigid to retain the photo-induced image, and may be processed (as described in section 2.2.4) to amplify this image.

2.1.1 The photochemical reaction.

Gelatin can be photochemically hardened in the presence of chromates or dichromates. On a molecular scale, 'hardening' means crosslinking the gelatin chains together more tightly by means of molecular complexes. In the photochemical reaction, this occurs via the chromium Cr^{3+} ion. The Cr^{6+} ion is introduced by sensitising the gel in a solution of the chromate, most usually ammonium dichromate, and allowing the gel layer to dry again. On exposure to light in the presence

of the oxidisable gelatin molecule and some water (in equilibrium with the water in the atmosphere), the Cr^{6+} ion is reduced to Cr^{3+}. The Cr^{3+} ions formed by this reaction react with two carboxyl groups on neighbouring gelatin molecules to form a coordinated complex which crosslinks the two molecules. These crosslinks are very strong and very stable, and effectively harden the gelatin, and reduce its ability to absorb water. The sensitivity to light of the photochemical reaction varies between chromate compounds, but the only known chromate which is more sensitive than ammonium dichromate is pyridine dichromate [SHA68]. However, gelatin sensitised with this is less stable, with a shorter shelf life of hours rather than days. Also, pyridine dichromate is a very hazardous substance to use.

Since the photochemical reaction involves at most only a few chromate ions, and the adjacent gelatin molecules, the spatial resolution of the reaction is very high. It is known that DCG can record spatial periods smaller than 200nm [MEY77]. Further, Fillmore and Tynan show that the sensitivity is flat for spatial periods between 0.4μm and 10μm [FIL71].

2.1.2 Hardness.

The critical property of gelatin for use in holography is its hardness. Hardness may be defined in terms of many parameters, including melting point, ability to swell in water, and mechanical hardness or rigidity (defined via the depth of indentation resulting from the impact of a ball bearing on the gelatin).

If the gelatin is soft, its solubility is high, its ability to swell with water is high, its melting point is low, and its rigidity is low. Therefore, a relief image will

tend to form as the unexposed regions will wash away. If the layer is harder, then none of the layer can dissolve, but an image in density (and refractive index) is recorded. However, if the layer is too hard, the refractive index change available will be very small. DCG is of interest mainly for its volume holographic properties, hence we are mostly concerned with creation of refractive index modulation rather than surface relief. This means that the 'bias' hardness of the gelatin needs to be controlled in order to obtain an insoluble layer which has a sufficient refractive index modulation available to form efficient holograms. In practice the gelatin can be insoluble but still be too soft, causing high levels of scatter in the final hologram, and it can be too hard, making it too insensitive to light, and possibly limited in its achievable efficiency.

There are a number of methods which are capable of hardening gelatin (or *tanning*, as it is also known), including exposure to UV light, baking, and the use of many different types of chemicals both organic and inorganic [MEE44].

The simplest method of hardening is by baking. Baking the layer at around 100 to 110°C will harden a gelatin layer, eventually to a degree sufficient to use the gelatin for DCG. This has been used successfully in this work to harden completely unhardened layers and takes a matter of weeks if the gelatin is not to be burned. Hardening by heating appears to occur by linking the carboxyl groups, and as explained below, this is undesirable for holographic gelatin.

The photochemical reaction can be used to achieve bias hardness by exposure to ultra-violet light, or sensitising with a chromate and exposing uniformly to light of wavelength shorter than about 500nm. (This spectral component is used because

the dichromate ion absorption spectrum drops to zero at wavelengths longer than about 530-580nm, depending on the particular chromate and the gelatin used.)

Chromium, or rather the Cr^{3+} ion, is the most effective inorganic hardening agent. Usually the chromium salt is added to the gelatin, and then heated to achieve the required hardening effect. Chromium ions appear to primarily harden by forming crosslink complexes between both the carboxyl -COO^- groups and to a lesser extent, the amino -NH_2 groups on neighbouring molecules. The pH of gelatin solutions influences the effectiveness of chromium, and is more effective in more acid solutions. pH should always be kept below 6. Pre-hardening gelatin with chromium obviously reduces the ability of chromium to harden in a photochemical reaction. For this reason, pre-hardening should preferably be done with a substance which crosslinks other sites on the gelatin chains.

Other inorganic salts can be used to harden gelatin, such as those containing iron, thorium, titanium, zirconium and uranium oxide. Aluminium salts have been used more frequently, although they are not as effective as chromium, and the result is only semi-permanent. All of these salts form crosslinks with the -COO^- groups.

Organic hardening agents subdivide into aldehydes, ketones and quinones. Not all compounds of each type are useful, and often pH is critical. By far the best organic hardener is formaldehyde H-CHO, which has long been used in the photographic industry as an emulsion hardener. Its hardening properties extend to collagen and untreated animal hides, and it is this property that makes formaldehyde useful as an animal preservative. Organic hardeners require a pH above 5

to operate effectively, and in general provide desirable crosslinking between the NH_2 groups, leaving the -COO^- groups free for the photochemical reaction. The formaldehyde reaction is greatly accellerated by heat. The only other aldehyde which is known to be used with gelatin for DCG is the carboxylic aldehyde mucochloric acid.

The final group of hardening agents are the noble metal salts, in particular hydrogen hexachloroplatinate hydrate $H_2PtCl_6.6H_2O$ (chloroplatinic acid or platinic chloride) [MAZ82]. These have the desirable features that they bind amino, rather than carboxyl groups, and that sensitised layers appear to be more stable, due to oxidation of the reduction agents responsible for the dark reaction in DCG. These factors mean that the gelatin is at the same time both more sensitive and more stable than gelatin hardened by organic methods.

2.1.3 Modulation formation in DCG.

The refractive index variation available via the photochemical reaction in section 2.1.1 and simple washing of the exposed layer is insufficient for practical holography. The modulation must be amplified, and this can be achieved by using Shankoff's processing technique [SHA68]. Essentially, this simply involves dehydrating the washed gelatin layer rapidly by immersing it in a bath of isopropanol. The isopropanol takes the place of the water, and then the layer is dried in air, where the isopropanol evaporates rapidly. This leaves a greatly amplified refractive index pattern in the dry gel layer. In practice, less rapid dehydration via increasing concentrations of isopropanol is usually used in order to improve uniformity

and reduce scatter.

The mechanism for this amplification is still not definitely known. Curran and Shankoff originally thought that the rapid drying induced sufficient stress in the gelatin to form voids or cracks [CUR70], but this should give rise to high levels of scatter. Indeed, this may well be the case when layers are dried too rapidly, at which point severe scatter often appears.

It has been suggested that much smaller voids or 'vacuoles' are responsible for the refractive index modulation [CAS76]. More recently some authors have proposed that the processing allows a still less dramatic rearrangement of gelatin molecules resulting from a differential swelling in the water being frozen by rapid dehydration [CHA80,MCG80,CUL82]. The differential swelling results from a differential 'pliability' between hard and soft areas, and the distribution is frozen by removing the water before the gelatin can relax. This theory can explain most of the observed features of DCG, such as the influence of drying rate and temperature, and the effect of uniform exposure.

2.2 Practicalities.

2.2.1 Gelatin layers.

Layers of gelatin suitable for use in holography can be obtained by a number of methods. These divide into two main techniques; modifying existing gelatin layers, usually photographic emulsions, and forming gelatin layers directly onto substrates.

Pre-processing photographic layers involves removing unwanted silver halides and dyes, and usually altering the hardness of the gelatin to optimise it for use as DCG. Most commonly, the photographic emulsions used are Kodak 649F spectroscopic plates [LIN69]. In fact the dye in Kodak 649F plates is compatible with the ammonium dichromate sensitiser, so that leaving the dye in the layer increases its sensitivity [MCG80]. Layers from Agfa 8E75 or 8E56 plates need to be softened by soaking in hot water [OLI84], whereas layers from Kodak 649F plates often need to be hardened before use with salts such as those used in hardening fixers [CHA79]. In general, however, other hardening techniques as mentioned in section 2.2.2 have been successfully used during this work to increase the hardness of both photographic and unhardened layers. A typical pre-processing formula for 649F plates is given in section 2.2.3

Producing gelatin layers from raw gelatin powder is more difficult than pre-processing photographic plates, but it allows flexibility in the important features of layer thickness and hardness. Controlling hardness by using organic hardening agents allows greater index modulation. This is particularly important in thin ($<15\mu$m) layers, where hardening by salts or baking may limit maximum efficiencies to well below the theoretical maximum. Holograms in DCG up to 120μm have been successfully processed [MCC85,DUN85] and are of great interest in narrow-band filter applications. No photographic layers are made which are this thick, and there is no other commercial source of gelatin layers, so these layers must be produced by the user.

Gelatin layers can be produced by dip-coating, doctor blading, gravity set-

tling, spin-coating or casting [MEY77,MCC73]. Dip-coating was originally used by Shankoff, and then Lin [LIN69], but this method tends to produce wedge shaped films. To dip-coat a gelatin layer, the glass substrate is simply pulled from a gelatin solution at a controlled rate and angle. Doctor blading [BRA69,MCC73] involves pouring an excess of gelatin solution onto a levelled substrate and quickly drawing a bar at fixed height over the plate to leave a controlled quantity of gelatin. Gravity settling is similar, except that a measured quantity of gelatin solution is poured onto the plate [CUL82]. The layer then dries to a thin film, which will be flat across a central area, to within about 1cm from the edge of the plate. Early in this work, layers were successfully produced which had a flatness uniformity of better than $\pm 3\%$ in this 'flat' region.

Commercial companies involved in dichromated gelatin generally use spin-coating or casting. Spin coating uses commercially available equipment already used for coating photoresists, and is therefore a well tried and tested technique. In spin-coating, gelatin solution is poured onto the centre of a rapidly rotating substrate, and is forced outwards by radial forces to leave an even layer. Gelatin tends to build up at the edges, so the edges are not used, or removed.

Casting involves pouring gelatin solution between two accurately spaced flat, parallel, plates, the substrate and the base plate. The substrate should adhere strongly to the gelatin, while the base plate should repel it. The former can be achieved by carefully cleaning the plate, and the latter by using a plexiglas base plate [MCC73] or by treating the base plate with a release agent, such as concentrated dimethyldichlorosilane, or the commercial release agent, Repelcote, from

BDH, which is 2% dimethyldichlorosilane in 1,1,1 trichloroethane, a de-greasing agent. Commercial photographic companies often use a 'subbing' agent on their substrates to improve adhesion. McCauley et al [MCC73] give a subbing formula for use on plexiglass substrates. This is of particular interest since a plexiglass substrate can be non-planar, allowing fabrication of holograms on curved substrates. Curved substrates are of interest for use in a head-up display in an aircraft pilot's helmet, and in holographic laser safety goggles [MAG85].

Casting on plane glass substrates has successfully been used in this work to produce gelatin films of superior optical quality to that of pre-processed 649F layers and with greater dynamic range. The procedure used to produce these layers is given below.

1. Clean the substrates.

   (a) Clean the plates in hot running water.

   (b) Rinse in deionised water.

   (c) Clean in acetone with ultrasonic agitation for 15 minutes.

   (d) Clean in methanol with ultrasonic agitation for 15 minutes.

   (e) Clean in 5% Decon 90 with ultrasonic agitation for 15 minutes.

   (f) Rinse in deionised water.

   (g) Immerse in 2% H_2SO_4 15 minutes with agitation.

   (h) Rinse in deionised water.

   (i) Allow to dry.

   (j) Bake at 150°C to drive out water.

2. Apply the release agent to the base plate. Pure dimethyldichlorosilane is applied using paper towel evenly over the plate. *This stage must be done with care in a fume cupboard, as the fumes are highly toxic. Rubber gloves must also be used, and precautions taken against static discharges or ignition as dimethyldichlorosilane is extremely flammable.* It is then allowed to evaporate (1 hour) and the grease film is removed using isopropanol. The plate is cleaned with lens tissue and dust gun.

3. Prepare the gelatin. The gelatin is bloom strength 200 to 260 pigskin gelatin from Leiner Gelatins of Mid Glamorgan. A 10% solution of gelatin is made using de-ionised water (10g/100ml) and is heated to 50°C on a hotplate with continuous stirring. When the solution is ready it is filtered through 30μm filter paper.

4. Harden the gelatin. Formaldehyde is added to make a concentration of 0.5% to 1% with the mass of gelatin. It is added as 3.8% w/v solution in methanol (usually supplied as 38%, which is diluted 1+9). The formaldehyde is added drop by drop into a rapidly stirring solution to avoid strands of hardened gelatin forming.

5. Remove the bubbles from solution. Immerse the gelatin solution in its flask in an ultrasonic bath at 50°C for 15 minutes. Then replace on the hotplate.

6. Remove dust from the substrates and place on the base plate. The substrates are separated from the base plate by an accurate distance. Metal shim or nylon or mylar sheet of controlled thickness may be used. For less accurate

layers, microscope cover slides can be used. These are 140 to 150μm thick and give layers of about 12μm.

7. Heat the plates using an infra-red lamp above the plates. The infra-red lamp should maintain the plates at 40 to 50°C.

8. Cast the layers. Use a pipette at the gelatin temperature to apply the gelatin along one edge of the substrate in one go. Avoid introducing bubbles into the layers or the solution. Replace the gelatin in the ultrasonic bath if necessary.

9. Turn off the lamp and allow the gelatin to set but not dry completely. The setting should be slowed down by placing substrates and base plate in a fridge. This reduces the strains induced and avoids peeling. The plates should be set sufficiently to remove after one day. They can then be removed in one smooth movement and allowed to dry completely in the fridge. It is particularly important that the drying of the exposed layers occurs in a dust-free environment.

10. If necessary, leave the layers for one month to reach final hardness.

2.2.2 Hardening gelatin.

In order to make holograms in DCG, it is necessary to control the hardness of the gelatin, and therefore it is necessary to be able to measure hardness. This is most easily done in a quantifiable way by measuring the amount of water the gelatin layer may absorb [SAM80]. This is expressed as a swelling ratio, defined as

$$S = (w_s - w_o)/w_o \tag{2.1}$$

Where w_s is the mass of the swollen gelatin layer and w_o is the mass of the dry gelatin layer. To obtain S, the weight of the substrate plus dry layer is taken first. Then the layer is swollen by soaking in water at 20°C for 10 minutes, followed *immediately* by weighing (because there is only a fraction of a gram of water contained in the gelatin, which rapidly evaporates). Finally the gelatin is removed from the substrate by scalpel or household bleach, and the substrate weighed in order to calculate w_s and w_o. The ideal value for S for holographic gelatin is in the region of 2 to 3. Kodak 649F plates have S=2.0 to 2.5, depending on processing, whereas Agfa 8E75 plates have S=0.25, corresponding to a much harder gelatin, usuitable for holography in this form. Unhardened gelatin layers typically have S values of 5 to 8. These layers are so soft that they may dissolve completely in water.

Hardening of layers derived from photographic emulsion is usually done by soaking the layer in a hardening salt, such as sodium metabisulphite, or in a hardening photographic fixer. These are usually sufficient if any hardening is required, as most photographic gelatins are already pre- hardened. More often it is necessary to soften the gelatin by soaking at a high temperature, such as in the case of Agfa 8E layers (90°C for 10 minutes) [OLI84].

Hardening of layers produced by other methods, such as casting, is usually done at the gelatin solution stage. Most commonly, this is done by adding ammonium dichromate to the solution and baking at high temperature (100°C to 150°C) after

the gelatin has set or by adding an organic hardener to the solution. Baking layers containing ammonium dichromate gives films which are stable immediately after baking. It also allows the layers to be produced with the sensitiser already present, eliminating a separate sensitising (and drying) step. The hardening obviously involves the same caboxyl sites that are used in the photochemical reaction, and hence the gelatin has a limited refractive index modulation available.

Using an organic hardener such as formaldehyde allows up to ten times the modulation available by salt hardening to be obtained. Unfortunately, the aldehyde hardening reactions are much slower, typically taking weeks to months for completion. The properties of the gelatin layers will be changing during this time, making holographic results also variable. The reactions can be speeded up by gently baking the layers in a sealed environment (to contain the formaldehyde vapour).

2.2.3 Preprocessing.

Most of the experiments in this thesis have been performed on Kodak 649F spectroscopic plates. As already mentioned, these need to be preprocessed to a suitable condition for use as DCG layers. The process used is outlined below. It is similar to that used by Chang [CHA71]. The fixing step removes silver halides in the layer, and the high temperature wash eliminates small crystallites in the gel and promote larger stronger crystals. This creates a stronger gel less liable to the break up that Chang considers is the cause of the strong scatter often seen in a processed layer. The ramped temperature increase is to prevent reticulation,

(break-up of the gel under severe stress) and the second fixing stage pre-hardens the layer slightly. It was found in practice that this method has the advantage of reproducibility over simpler preprocessing schemes (such as simply fixing and drying) in that variations between batches of plates were reduced, and good optical quality layers consistently result. Variations in sensitivity still are present, but these can be compensated for by exposure, sensitiser concentration, and processing temperature if necessary.

Kodak 649F preprocessing

1.	25% Agfa g334 fixer (part A).	10 minutes	20°C
2.	Water wash, increasing the temperature from 20 to 32°C at 1.5°/min.		
3.	Wash	15 minutes	32°C
4.	25% g334 fixer plus 5% hardener	10 minutes	20°C
5.	Wash	15 minutes	20°C
6.	Dry in circulating air	overnight	20°C

2.2.4 Processing.

The standard processing procedure used is outlined below. This should be taken as the processing used unless otherwise stated. The procedure is based on a more gradual dehydrating of the gelatin than in Shankoff's original method, and includes two additional steps before washing which further harden the layer, and remove

the dichromate more effectively than washing. Sodium metabisulphite was first suggested by Lin [LIN69]. An alternative is to use a hardening fixer, such as Kodax Rapid fixer [CHA79].

Standard processing procedure

1.	0.5% $(NH_4)_2Cr_2O_7$ (Ammonium dichromate)	5 minutes	20°C
2.	0.5% $Na_2S_2O_7$ (Sodium metabisulphite)	5minutes	20 °C
3.	Wash in de-ionised water	10minutes	20°C
4.	50% Isopropanol/deionised water	3minutes	20°C
5.	75% Isopropanol/deionised water	3minutes	20°C
6.	Isopropanol	3minutes	20°C
7.	Dry in circulating air	$\geq$1 hour	20°C

Sodium metabisulphite (or a hardening fixer) performs the dual function of rapidly removing the sensitiser from the gelatin and further hardening the gelatin. Omitting the metabisulphite requires the gelatin to be washed for much longer in order to remove the sensitiser (typically one hour for 649F layers, but as much as four hours for 60μm layers). This leaves holograms with lower light absorption, but which are often too soft and have poor optical quality. Figure 2.2 shows a spectrophotometer transmission scan of a 60μm gelatin layer on glass which had been sensitised and processed by washing for three hours and dehydrating with isopropanol baths of 20 minutes duration each. Figure 2.3 shows the transmission scan of a 60μm plate which was sensitised and processed by the standard

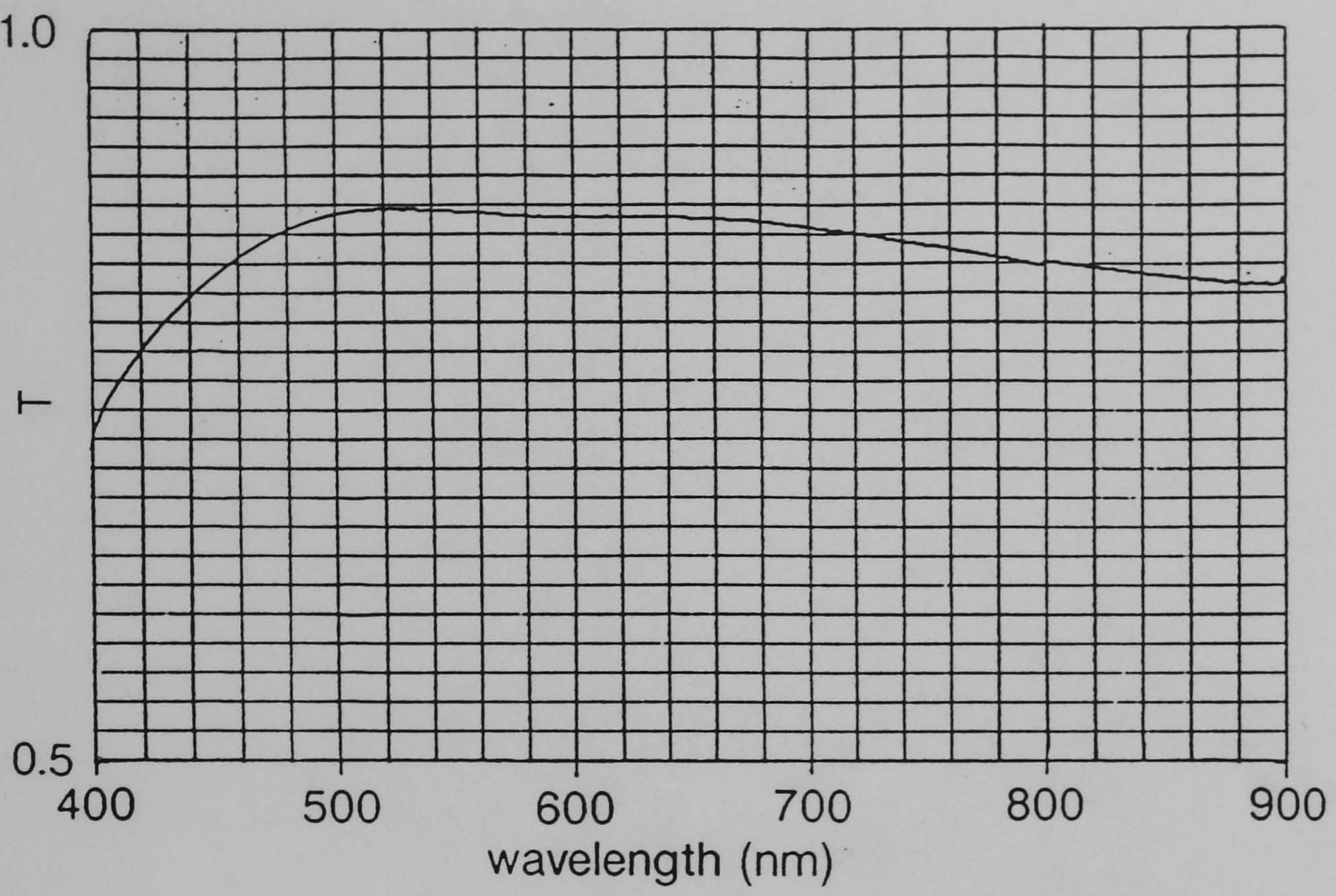

Figure 2.2: Transmission of wash-processed 60μm layer.

formula with 20 minute bath times, and including the sodium metabisulphite pre-wash hardening bath. These graphs show that the metabisulphite introduces a significant level of absorption into the gelatin. This is undesirable from the point of view of efficiency and of power handling capability, hence processing without bisulphite is generally desirable and should be used whenever scattering is not of great importance, and provided the gelatin is not too soft.

Attempts to use sodium metabisulphite after the wash failed to harden the gelatin, indicating that its hardening action arises via a reaction with the sensitiser. The gelatin must therefore be prehardened to a greater degree in order to get good optical quality and low absorption.

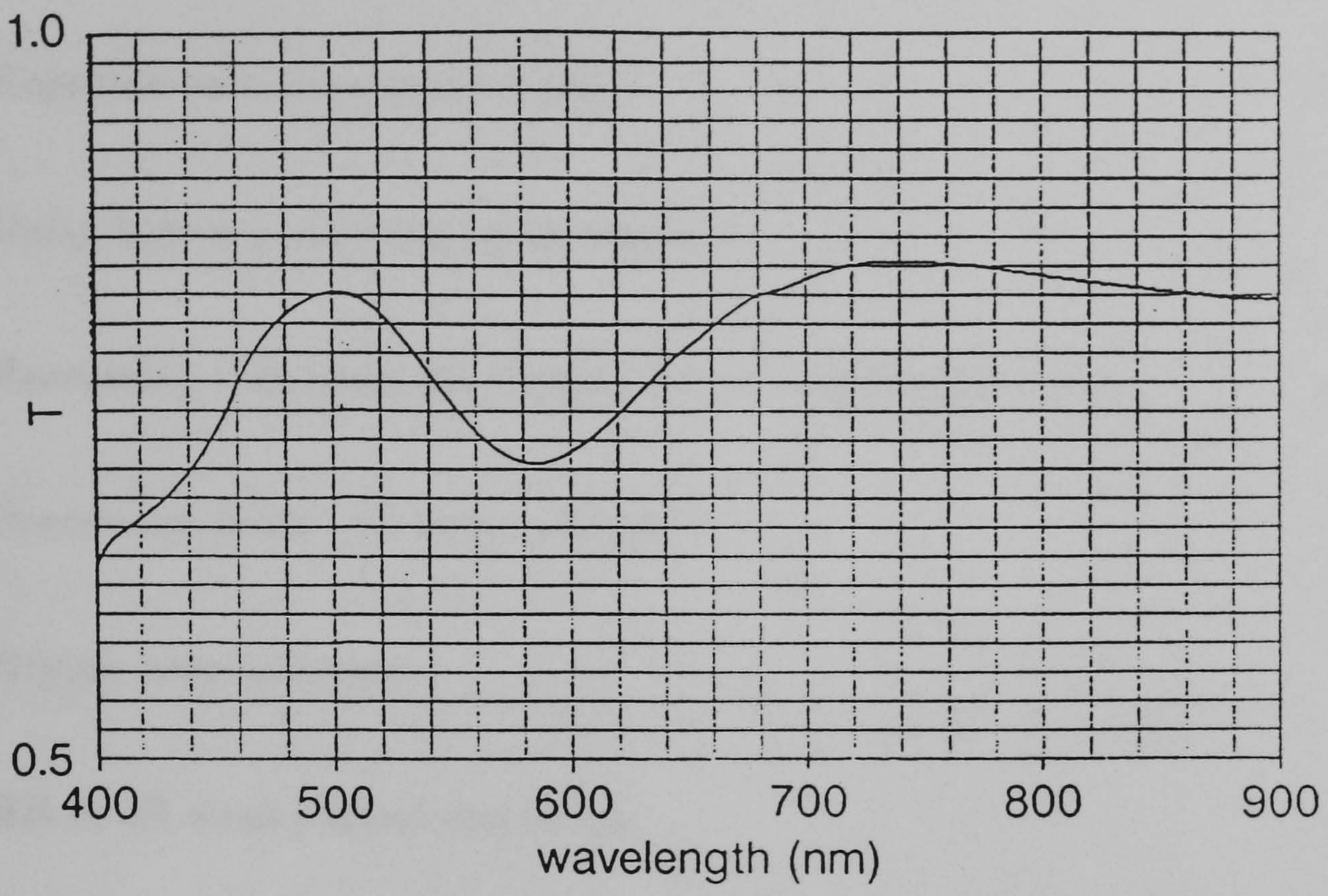

Figure 2.3: Transmission of standard-processed 60μm layer.

2.2.5 Factors affecting the properties of holograms.

Much of the usefulness of DCG stems from the abilty to control many of the properties of the final hologram in the processing stages. Cullen and McGrew [CUL82,MCG80] outline most of the factors affecting DCG. Some of these factors can make DCG more difficult to use, most noticably, its dependance on relative humidity and its limited shelf life. Outlined below are all of the known factors which affect holograms made in DCG.

1. Initial gelatin hardness, thickness and origin.

2. Sensitiser composition and concentration (And presence of wetting agent).

3. Drying rate after sensitising.

4. Delay before exposure (dark reaction).

5. Exposure conditions: λ, exposure energy, angles of beams.

6. Exposure rate (irradiance levels).

7. Delay before processing (dark reaction).

8. Processing chemicals. Hardeners, no. of dehydration baths.

9. Processing times and temperatures.

10. Drying time and rate.

11. RH in all steps carried out in air.

12. Throughout *all* processing steps above, temperature and pH.

These effects are discussed in [MCG80] and [CUL82]. Broadly, the environmental factors of temperature, relative humidity (RH) and pH must be controlled to ensure reproducible results. Also, as in photography, processing times must be controlled, and sufficient agitation used to ensure even processing.

Temperature.

Increasing the temperature increases the diffusion rates into the gelatin, and hence the speed of reactions. Thus dehydration also occurs more rapidly, increasing the sensitivity of the gelatin. This is also true in the final air drying step, where drying under forced air and/or at higher temperature aids evaporation of the alcohol and increases sensitivity. According to the model in section 2.1.3, the gelatin's differential swelling distribution is frozen before it can completely relax.

It is known that excessively high alcohol dehydration rates cause spatial nonuniformities in the sensitivity of holograms. In this work it has been found also that air drying steps are similarly affected. This includes drying after sensitising, and drying after processing. If, for example, a hologram is sensitised, and then immediately dried vertically in a convection oven at 40°C, nonuniformities will be found especially within 1cm from the bottom of the plate. These are similar to drying marks found on photographic emulsions. These marks are significantly reduced by drying more slowly at room temperature. Similar results are found due to drying after processing.

High dehydration rates also cause nonuniformities throughout the depth of the hologram [MCG80]. This appears to take the form of a greater swelling near the surface of the film. This has also been observed by Cullen [CUL82]. From studies of reflection holograms, where the fringe planes are substantially parallel to the surface of the hologram, Cullen observed that angular and wavelength bandwidths are different when viewed from the two sides of the hologram. When viewed from the gelatin side, it has a larger bandwidth than when viewed from the glass side. Again this appears to agree with the model, since dehydration will occur much more rapidly from the surface, forming a water-free barrier to further alcohol movement. This is discussed more in section 2.2.5.

Relative Humidity.

Relative humidity also affects reaction rates, but it has two distinct effects. Firstly, high RH slows down the drying rate in air, and therefore reduces sensitivity when

drying a processed hologram. Secondly, the presence of small amounts of water in a sensitised layer encourages a dark reaction which hardens the hologram and therefore reduces its sensitivity. By contrast, the dark reaction in an *exposed* hologram *increases* its sensitivity, apparently due to the presence of the Cr^{3+} ion in exposed regions, which accelerates the reduction of Cr^{6+}. This then has the apparent effect of an accelerated dark reaction in exposed areas, which in turn appears as an increasing index modulation after exposure.

It is known that water is a necessary chemical for the photochemical reaction to occur (see section 2.1.1). It is thought likely that the dark reaction is the same reaction only occuring more slowly in the absence of light. This is because the dark-reacted layer is darker in colour than a freshly sensitised one, and the photochemical reaction also results in darkening, as the Cr^{6+} (yellow-orange) ions are reduced to Cr^{3+} (brown). It therefore looks possible that the same reduction reaction occurs in the dark reaction. High RH is known to increase the dark reaction rate. This could be due to the higher concentration of water available to take part in the reaction. Cullen states that the shelf life of sensitised plates can be increased by storage at 10 to 15°C in a 35 to 40% RH environment. This is consistent with reducing reaction rates.

pH.

As mentioned in section 2.2.2, pH is known to affect the solubility of gelatin and the hardening ability of most hardening chemicals. Mees [MEE44] describes the pH properties of gelatin, and in particular states that the solubility and the degree

of swelling in water depend on pH. Most physical properties of gelatin have a minimum at a pH value known as the isoelectric point. The isoelectric point is characteristic of the gelatin, and depends on how it was initially processed.

McGrew [MCG80] notes the dependence of peak reconstruction wavelength and scatter in holograms on pH. Cullen [CUL82] also mentions the effect of sensitiser pH on peak reconstruction wavelength. This can be seen as the effect of pH on sensitised thickness due to its effect on swelling. Hardness, represented by scatter in a processed hologram, is apparently also affected, possibly being related to the effect of pH on solubility.

In this work, the effects of pH have been minimised by using fixed pH levels in all liquids. This can be done by using de-ionised water for solutions, and pure alcohols and chemicals.

Processing times.

All reactions in DCG, whether chemical or diffusion, take a finite time to complete. The photochemical reaction during exposure, and the pre-wash reduction and hardening steps are chemical and diffusion reactions. That is, a chemical reaction takes place, once the chemical has diffused into the gelatin. The dehydration steps, however, are purely diffusion, whereby the concentration of water in the gelatin is progressively reduced. No chemical process takes place. In the case of the dehydration steps, the diffusion rate is important, as the object is to rapidly dehydrate the gelatin, thereby removing the 'elasticity' from the layer and leaving an amplified phase image. The maximum rate of dehydration is limited by the

rate of diffusion of alcohol into (and water out of) the layer. Also, it appears that the amplitude of the index modulation is greater at the surface than in the bulk of the gelatin. It is possible that this is due to a varying rate of dehydration, that rate being greater at the surface. This variation can be understood if we assume that the alcohol cannot move freely around in 'dry' gelatin. This appears to be justified by Meyerhofer's observations [MEY77]. Therefore, the dry surface acts as a barrier to further diffusion of alcohol into the gelatin.

2.2.6 Reprocessing.

One of the unique features of dichromated gelatin is that holograms can be reprocessed without losing the stored interference pattern. Exposure creates permanent cross-linking which cannot be destroyed by normal processing. Holograms may be reprocessed to alter many of the properties discussed in section 2.2.5. Lin [LIN69] originally mentioned reprocessing, stating that holograms appeared to be able to be reprocessed without any degradation, and could be reprocessed without limit. However Cullen [CUL82] verifies observations made during this work that degradation occurs with subsequent processing unless they are reprocessed within a few hours. He also observes that scatter increases with the number of reprocessings. Chang [CHA76] shows that the reprocessing can be altered to increase or decrease sensitivity, by altering temperature and the hardening step prior to washing. Again, higher temperature processing leads to higher sensitivity.

2.2.7 Baking.

Following processing, the properties of a DCG hologram can also be altered by baking. The baking step has three distinct effects on a hologram:

1. Water is driven from the gelatin.

2. The gelatin is partially melted, reducing index modulation.

3. The thickness of the layer is reduced.

The first feature results in an increase in index modulation, and an increase in the melting point of the gelatin (see [MEE44] and section 2.2.8). The increase of index modulation when water is removed is a continuation of the dehydration step in the processing, which is incomplete in the respect that the gelatin will always contain a small amount of water in equilibrium with the atmosphere. Baking implies a hotter and therefore lower relative humidity environment, and thus a lower equilibrium content.

In this work, the effects of baking have been investigated for two purposes:

- To protect holograms at high temperatures.

- To alter the efficiency of holograms after processing.

The damage of a DCG hologram at high temperature is discussed in section 2.2.8. The second item here has been investigated as a method of improving the yield of hologram production. It is still found that holograms treated identically at every stage of the process do not yield identical results. As section 2.2.5 describes, there are a very large number of variables in the complete DCG process, and

quantifiying all of them and subsequently ensuring tolerances in the process is a major undertaking. However, baking processed holograms allows them to be 'tuned' to the desired efficiency, and in the case of reflection holograms, allows tuning of the peak wavelength (although this is a result of the third effect of baking, the decrease in thickness).

Efficiency tuning of a transmission hologram may be accomplished by initially overexposing the hologram, so that its index modulation is greater than that required for maximum efficiency. The hologram is then processed as normal and allowed to dry. It is then baked at a temperature slightly greater than the gelatin's melting point. The 'safe' temperature at which the hologram could be held without change was found to be about 70°C, and the baking temperature for tuning was typically 100°C. At this temperature the hologram was tested every 5 minutes and the index modulation observed to decrease. For an overexposed hologram, this initially results in an increase in efficiency, until it reaches its maximum, at which point the hologram is transferred to the 'safe' temperature, to keep it dry, and sealed. This can successfully bake the hologram back onto its peak efficiency. It is only necessary to ensure the hologram is overexposed. Typical overexposure margins are about 50%, and baking times 10 minutes to an hour.

Figure 2.4 illustrates the effect of baking on the transmission of hologram gratings at the Bragg angle. The graph shows the transmission of a range of gratings on the same plate which were recorded with different exposures around the value which was known to give maximum efficiency (and therefore minimum transmission). Curve 1 shows the initial results after processing and drying. Curve

2 shows the effect of baking for 15 minutes at 100°C. This temperature has been sufficient to partially destroy the modulation, effectively reducing the modulation, and moving the minimum transmission to higher exposure values. Values after a further 30 minutes at 20°C are shown by curve 3. Rather than remaining close to curve 2, modulation has dropped further. This is due to the re-absorption of water from the atmosphere. Carefully drying the gelatin again at this point would increase the modulation back up to curve 2. Curve 4 shows a further drop in modulation as the layer is left at 20°C for a further 20 hours. Curve 5 clearly shows the effect of drying by further baking for 15 minutes at 100°. This time, the modulation has increased again as water is driven out, leaving a greater index modulation. The modulation is not reduced as it was in curve 2 because baking has a hysteretic effect on the melting temperature. On cooling after baking, the gelatin will not take up as much water again, and its melting point will not drop back down so far. Further baking at the same temperature will therefore have primarily a drying effect, and a reduced effect on the modulation. The increase in modulation in curve 5 is therefore mostly due to drying. Curve 6 shows the reverse effect after 2 hours at 20°C, where the modulation has dropped again with the re-absorption of water. This time it has dropped below curve 4, indicating that there must have been some melting of the gelatin during the last baking spell.

Note that as modulation is varied by baking and drying, the position of the minimum (corresponding to *maximum* diffraction efficiency) moves along the exposure axis. Therefore, if a single hologram is deliberately overexposed, its efficiency may be carefully 'baked back' to a maximum, using our knowledge of the mech-

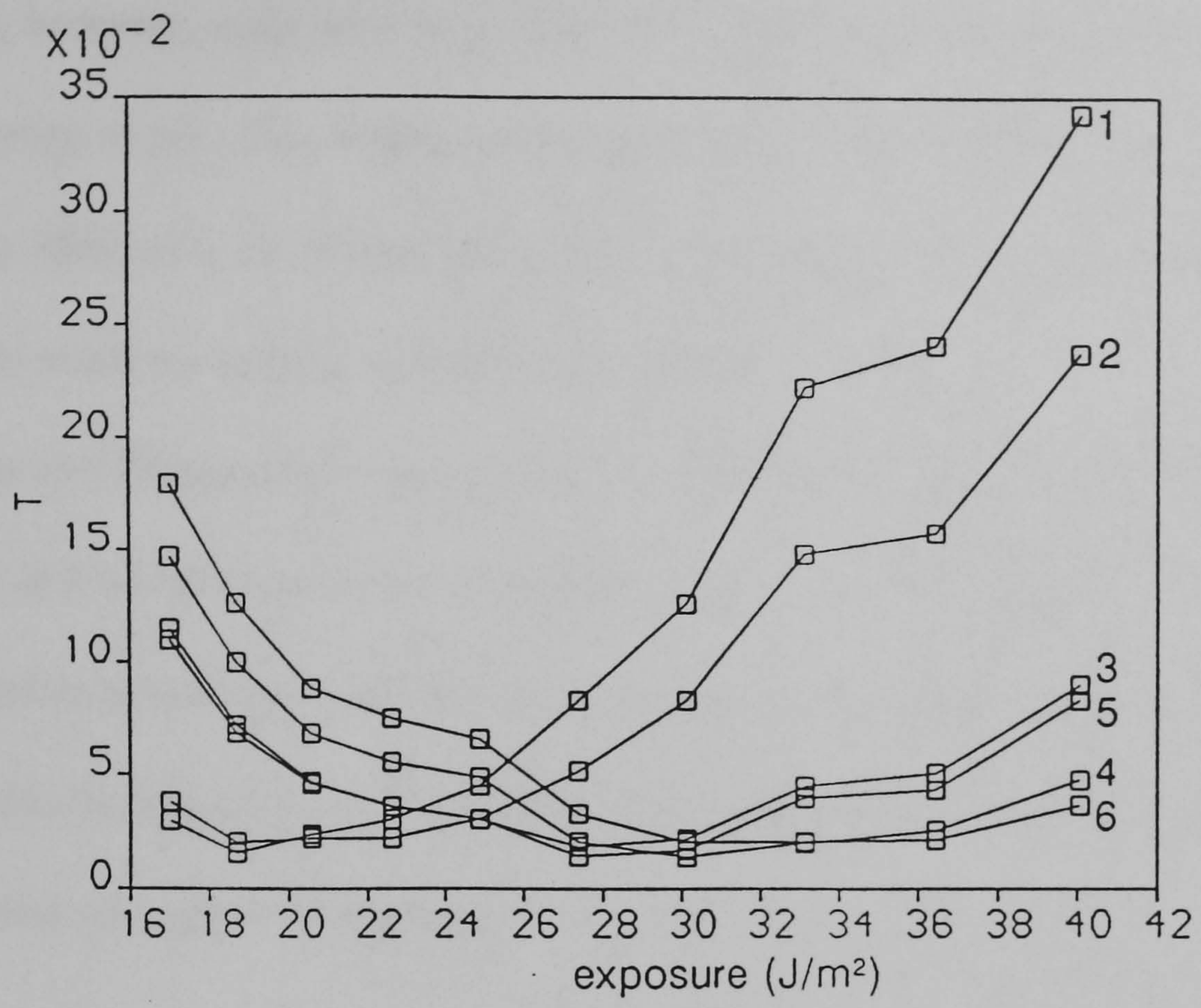

Figure 2.4: The effect of baking on diffraction efficiency.

anisms at play. This technique has been successfully used in this work to tune hologram efficiencies to a peak, but may equally be used to position efficiency at any specified value, for example, in a beamsplitter hologram with a chosen splitting ratio.

The final feature of baking is that of the thickness change. Normally it is found that a processed hologram will have an altered Bragg replay angle. Typically this is about 1° to 2° in such a sense as to suggest swelling. In fact there is a net swelling relative to the sensitised state, but there is also a decrease in bulk refractive index which operates in the opposite sense to the swelling, and cancels the effect of swelling to some extent [MEY72,NEW87]. This will be discussed more in chapter 3.

Baking, however, only acts to reduce the thickness of the layer, and therefore alter the Bragg angle. This thickness change can be successfully produced without a change in efficiency, by baking just under the melting point. Typically this was done in this work by baking at 60°C for 10 to 30 minutes.

Also the net Bragg angle change can be made to change sign, typically over a total range of 4° in a 12μm layer. Note that a change in Bragg angle does *not* occur in a symmetric geometry transmission hologram, i.e. when the fringe planes are perpendicular to the surface. This shows that only a thickness change is involved, and no lateral change of dimension.

2.2.8 Protection of holograms.

Protection of holograms is necessary for applications where they are to be used in a high temperature or high humidity environment. Holograms may easily be protected against humidity by carefully sealing the entire hologram with a cover plate and non-porous optical cement. The edges of the gelatin must not be exposed as water can eventually diffuse into the layer over a period of weeks to months.

Protecting against thermal damage is more difficult, however. Often this will be required in a military environment, but it also may be required in the normal operating conditions of some holographic optical elements, especially where irradiance levels in excess of 100 W/m^2 may occur. Under these circumstances, any absorption in the hologram can result in an excessive temperature in the gelatin which can destroy the index modulation, and even cause charring, and lead to catastrophic damage in the layer. Protection of gelatin holograms is often briefly

mentioned in literature, with little or no quantitative data, and authors are more often concerned with relative humidity limits. Wang et al observed dynamic damage due to excessive power levels [WAN88] with no suggestion of the cause.

The damage of a DCG hologram at high temperature is because the gelatin melts, and so the index modulation pattern is destroyed. However, the melting point is dependent on the the water content in the layer, being lower when more water is present. Therefore the water must be removed from the gelatin in order to increase the melting point and protect the hologram up to higher temperatures. This can be done by baking, but the temperature must be gradually increased, so that as the water is driven out, the melting point rises ahead of the baking temperature. It has been found in this work that the initial melting point is between 60 and 70°C for the particular procedures used, so that baking at 60°C noticably increases the damage threshold temperature with no change in efficiency. Curves are given in figure 2.5 from results obtained in this department [ROB88]. These show the effect of long term baking on the efficiency of two holograms. H1 was unbaked, and H2 was baked by ramping up the oven temperature from 40°C to 70°C over 1 hour in order to increase its melting point. The baking in the graph was carried out at 60°C.

Chang and Leonard [CHA79] suggest that vacuum drying is a better method to protect a hologram as the fringe structure is unaffected, and they state that their holograms (from 649F plates) are stable up to 110°C. However, their measurements only prove that their holograms were stable at 100°C for one hour. Note that a sealed hologram will be more susceptible to thermal damage for a given water

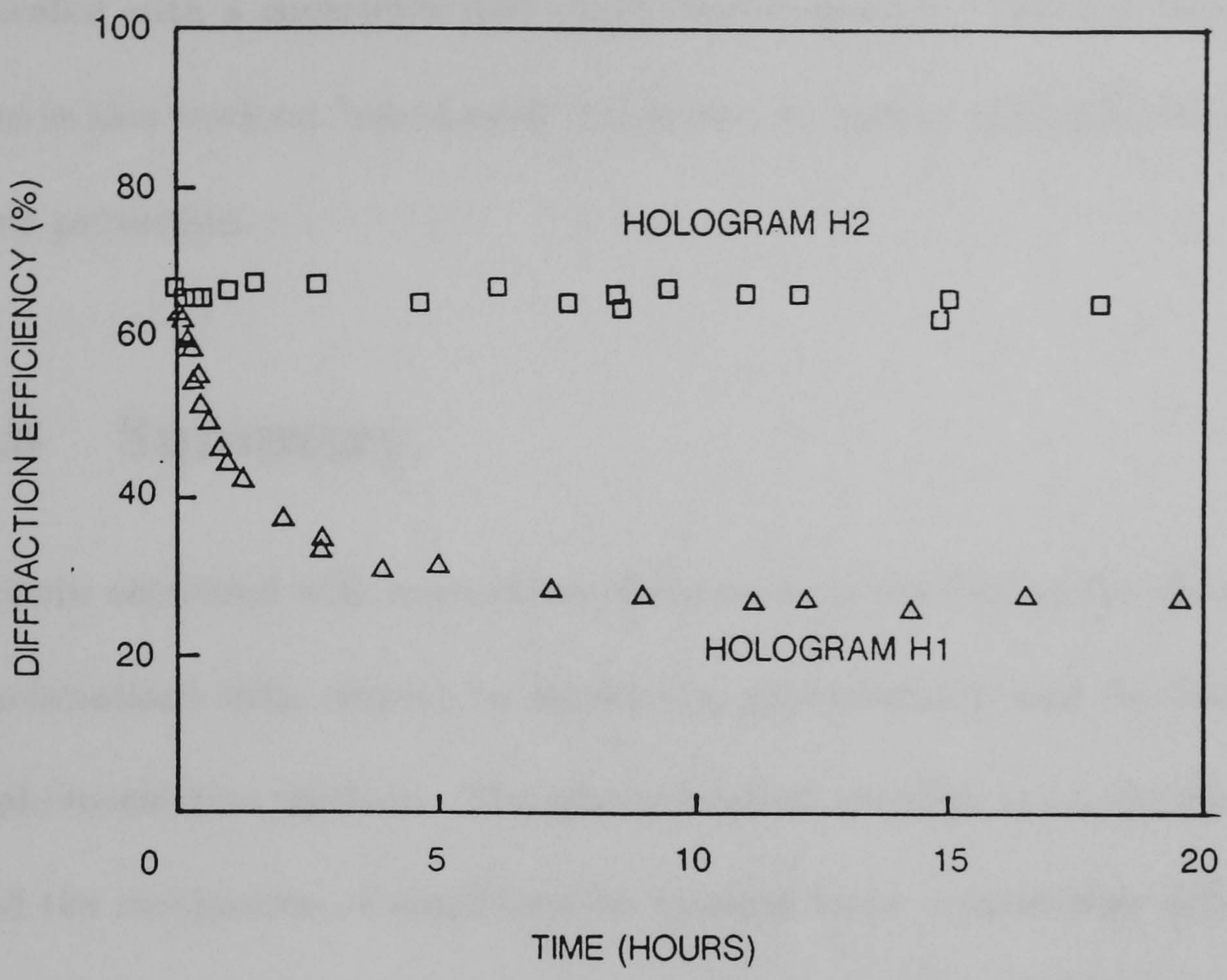

Figure 2.5: The effect of baking to protect a hologram.

content, because the water cannot escape. This means the melting temperature cannot rise as the gelatin heats up as it would do if water was able to be driven out.

With any drying technique it is necessary to seal the hologram in the dry state, so that it cannot re-absorb water which would lower its melting temperature again. This is not easy since the hologram immediately begins to re-absorb water from the air as soon as it is removed from the drying environment. This is rapid enough to mean that the hologram must be sealed in the dry environment. One convenient way to do do this is simply to seal the hologram on a hotplate once it has been suitably dried. The hotplate keeps the hologram and the air around it hot. The hologram is therefore in a low humidity environment. Once a hologram has been dried, it can be rapidly transferred to a hotplate which will keep it dry while it

is sealed with a coverplate and (dry) optical cement. This has been successfully used in this work on 'baked-back' holograms to 'freeze' their efficiency and improve their protection.

2.3 Summary.

Gelatin sensitised with ammonium dichromate is the best of the chromated colloid combinations with respect to sensitivity, processability and flexibility for use as a photosensitive medium. The photochemical reaction is on the molecular scale, and the mechanism of amplification appears to be a molecular diffusion process, resulting in an extremely high optical resolution. The recorded image is therefore essentially continuous and non-granular. The final image is a close to a pure phase image, allowing very high diffraction efficiencies to be achieved in practice.

These features make DCG the best available holographic medium in most holographic optical element applications. Its main disadvantages are generally low sensitivity, complete insensitivity to light of wavelength longer than 530nm or so, and the number of factors which influence the performance and reproducibility of DCG, particularly its short shelf life, due to a dark reaction, and environmental conditions. However, many of these factors may also be used to advantage to control the final properties of a hologram, such as thickness and bandwidth. Sensitivity and available refractive index modulation may also be controlled, but there is a trade-off with associated optical scatter. The sensitivity to actinic (blue-green) light is typically 10^{-3} to 10^{-4} times that of silver halide holographic materials.

Post-processing helps to compensate for reproducibility problems, allowing con-

trolled reduction of thickness and index modulation. Baking or vacuum drying increases the melting temperature, and hence the irradiance damage threshold of a hologram. Reprocessing allows further attempts to be made to alter modulation or bandwidth.

Chapter 3

Transmission Holograms.

The simplest type of hologram is that which is recorded in the region of interference between two plane waves. This arrangement, shown in figure 3.1, gives rise to an interference pattern with fringes which bisect the interfering beams. The hologram records these fringes throughout its depth.

This arrangement will produce a transmission hologram, so called because on replay with one of the original beams, the Bragg-diffracted beam will be transmitted through the hologram. If recording beams are incident from opposite sides of the medium, a reflection hologram is formed which produces a Bragg-diffracted beam on the same side as the incident beam. These two types of holograms have significantly different properties, and reflection holograms will be discussed in detail in chapter 5.

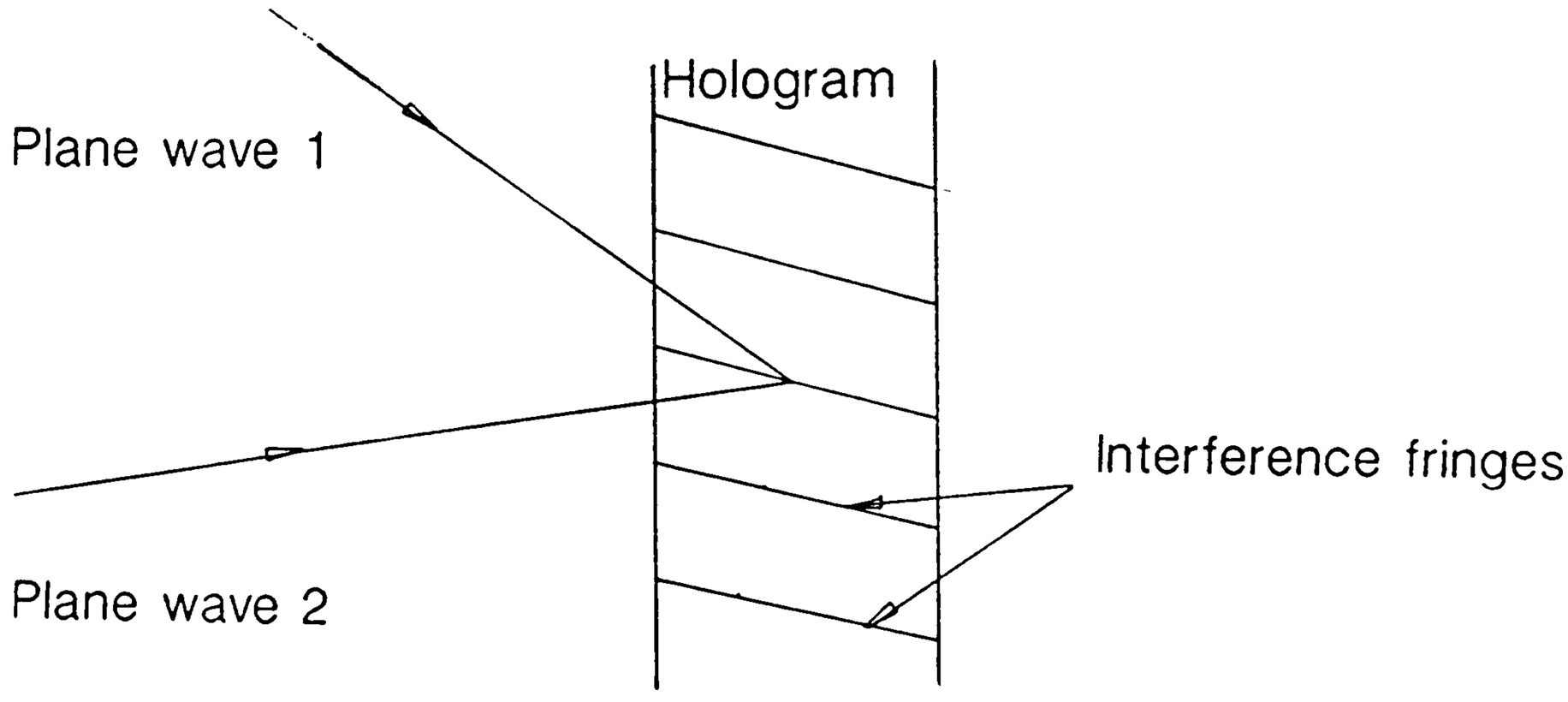

Figure 3.1: Arrangement for recording a holographic grating.

3.1 Experimental.

3.1.1 Hologram exposure geometry.

Shown in figure 3.2 is the experimental arrangement used to produce most of the transmission gratings investigated in this thesis. For optimum quality gratings, the beams are expanded and spatially filtered after the beamsplitter, and small portions of the centre of the resulting gaussian beams are used to ensure a good approximation to plane waves. This in turn assures a good approximation to a planar grating is recorded with with uniform modulation and hence uniform efficiency. All lenses used should be anti-reflection coated to avoid unwanted interference fringes which would modulate the amplitude of the hologram fringes.

The arrangement shown uses imaging systems to simultaneously provide locally

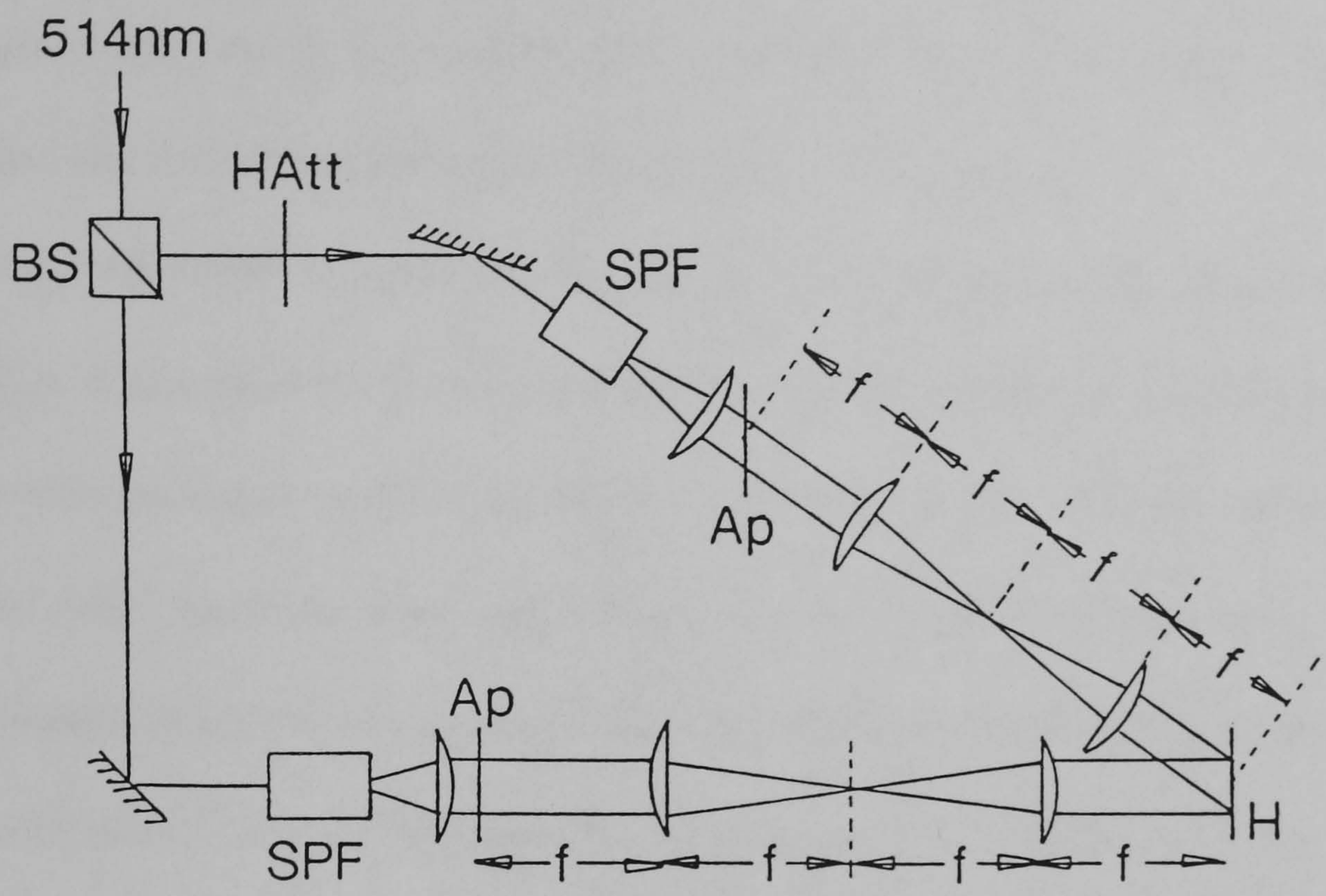

Figure 3.2: Experimental arrangement to produce transmission gratings.

plane waves and to sharply image apertures onto the hologram. This eliminates problems due to diffraction from apertures distant from the hologram. In a similar arrangement for holographic lenses this technique allows efficient close packing of small aperture holograms (<1mm).

The hologram is mounted on an y-z stepper motor stage which is automatically controlled in conjunction with the shutter by a micro-computer. This technique allows automated exposure of test plates and arrays of identical holograms with positioning accuracies of better than $\pm 20\mu$m.

3.1.2 Hologram exposure considerations.

The stepper motor must be de-energised during exposures as it vibrates slightly when energised. The laser source used to record holograms was a Coherent Innova

90/6 argon ion laser with a temperature stabilised Fabry-Perot etalon for single frequency operation. The coherence length of the laser is in excess of three metres, so that the matching of beam path lengths is not critical.

Care was taken to minimise the effects of vibration, air movement and thermal settling of components in order to obtain repeatable high quality holograms. The laser was mounted on wooden blocks and foam pads to reduce vibration coupled to the table resulting from the cooling water which flows through the laser. The air conditioning in the laboratory was turned off ten minutes before exposure, and curtains placed around the table during exposure to stop air currents.

Thermal settling of the optics and the plate were investigated using a Helium-Neon laser interferometer with the optic under test as one mirror. This indicated that at least 10 minutes should be left after the plate is in position for it to reach equilibrium. The heating effect in the gelatin layer during exposure was also investigated by HeNe interferometer using the exposed area of gelatin as a reflector in one arm. This is of particular importance in DCG as, due to its insensitivity to light, high exposures are required. This experiment indicated that, during exposure to 488nm light, irradiances should be kept below 50 W/m^2 in order to keep expansion of the gelatin layer to less than $\lambda/20$, assuming a 5% sensitised 15μm layer on glass at room temperature. At 514nm this figure is higher, at around 200 W/m^2 due to lower absorption. These values correspond to irradiance absorptions in the gelatin of approximately 75% and 25% respectively. This unfortunately tends to limit minimum exposure times to around 10 to 100s seconds for a maximum efficiency, depending on sensitivity.

It was also found that aluminium mirrors have sufficient absorption that they heat up and expand by up to $\lambda/10$ with an unexpanded 1.5mm diameter 500mW beam of 514nm light. Therefore dielectric mirrors or prisms must be used to direct unexpanded beams. Expansion of aluminium mirrors is negligible at normal exposure irradiance levels ($<200 W/m^2$), so they may be used with expanded beams. Care must similarly be taken with neutral density filters, whether they are aluminium coated or absorbing glass types.

It is found in practice that *all* of the above factors *must* be controlled to ensure repeatability.

3.2 Theoretical.

Before discussing actual methods used in analysing holographic gratings, it should be noted that these theories may use assumptions about the 'thickness' of holograms in order to simplify calculations. Holographic thickness is distinct from physical thickness, and it refers to the extent of Bragg effects in holograms. These effects result from the three-dimensional nature of the fringe planes in a grating due to a real physical thickness. It does not depend only on physical thickness, however. Many properties of holograms are greatly influenced by the thickness of the recording medium, such as bandwidths and efficiencies. Holograms are usually said to be in the 'thick' or 'thin' regimes, and these terms are best explained in terms of the replay properties of the holograms.

A thick grating is is one where we assume only two beams, the zero and first order diffracted beams, to be present when replayed close to the Bragg angle.

Such a hologram is said to be in the 'Bragg' regime. This is the assumption which Kogelnik makes in his coupled wave theory [KOG69]. This assumption in fact would only be wholly valid in an infinitely thick hologram, but the resulting theory gives the best physical insight into the mechanisms of thick, or volume holograms. In practice, finite thickness means that higher order diffracted beams, both transmitted and reflected, will be present. Usually higher orders will have smaller amplitudes than the zero and first orders, as they will generally not satisfy the Bragg condition which leads to efficient diffraction. Note that the Bragg condition exists for any grating of finite thickness, but for thinner holograms its effect on relative diffracted powers and angular selectivity is reduced, until the hologram can be said to be in the thin or Raman-Nath regime.

Whether or not the 'thick' assumption is valid, (and hence whether higher diffracted orders are insignificant), depends on wavelength, optical thickness, refractive index modulation and fringe slant. The situation is further complicated by the effects of absorption and non-uniformities in holographic gratings. However, the definition that Kogelnik used, which was derived from Phariseau's acoustic diffraction grating theory [PHA56], is still a good, simple indication of thickness. It uses the Q parameter

$$Q = \frac{2\pi\lambda d}{n\Lambda^2} \tag{3.1}$$

where λ is the replay wavelength, d the hologram physical thickness, n the bulk refractive index and Λ is the fringe spacing. When $Q \gg 1$, the grating is considered thick. Otherwise, it is considered to be thin.

Gaylord and Moharam point out [GAY81], based on earlier analysis [MOH80],

[MOH80A], that the distinction between thick and thin gratings depends on whether it is the diffraction regime (i.e. Raman-Nath or Bragg) or the angular and wavelength selectivity which is the desired important feature. The selectivity distinction is rather vague, although simple in its application, whereas the diffraction regime distinction allows for real situations where the grating can be *neither* thick or thin, and *both* thick and thin. In such situations rigorous theories which make no assumptions about thickness should be used [BUR66,MOH81A,CHU70] to predict performance accurately.

3.2.1 Methods of analysis.

There are three principle methods which have been used to analyse volume holograms. They are;

- Modal theory.
- Thin grating decomposition.
- Coupled-wave theory.

Burckhardt used the rigorous modal approach [BUR66,BUR67] which was exact, but complicated, requiring a computer solution in all cases. The approach was also used by Chu and Tamir [CHU70] and Kaspar [KAS73], who included non-sinusoidal index profiles in his analysis. Su and Gaylord extended the method further with a less rigorous model than Burckhardt, which allowed arbitrary diffraction orders, and arbitrary periodic grating profile [SU75].

The thin grating decomposition approach was introduced by Alferness [ALF75A], [ALF76]. As its name suggests, this method decomposes the hologram into many slabs which individually may be considered as thin gratings. Propagation through the hologram may be calculated allowing multiple diffraction orders, and multiple superimposed gratings. Hence any grating shape may be considered by decomposition into its Fourier component gratings. Again, this method does not yield simple analytic expressions for a simple hologram. The equivalence of the thin grating decomposition method and the rigorous modal approach has been described by Magnusson and Gaylord [MAG78B].

3.2.2 Coupled wave theory.

The most widely used techniques for theoretically investigating volume hologram properties are those using coupled wave theory. This is principally because it is intuitively straightforward, and in Kogelnik's simplified theory it provides simple, accurate expressions for thick holograms of all types at the Bragg angle.

This method was first used for volume gratings by Raman and Nath [RAM35], when it was applied to diffraction of light by ultrasonic waves in liquids. The method was first applied to holography by Kogelnik [KOG69]. Kogelnik's theory made several assumptions which have since been found to be not strictly valid with common holgraphic materials, such as DCG and photographic materials, but the results nevertheless give a very accurate account of many hologram properties with simple analytic expressions. This, and the clear physical insight that simple coupled wave theory provides makes it an attractive method. As will be seen

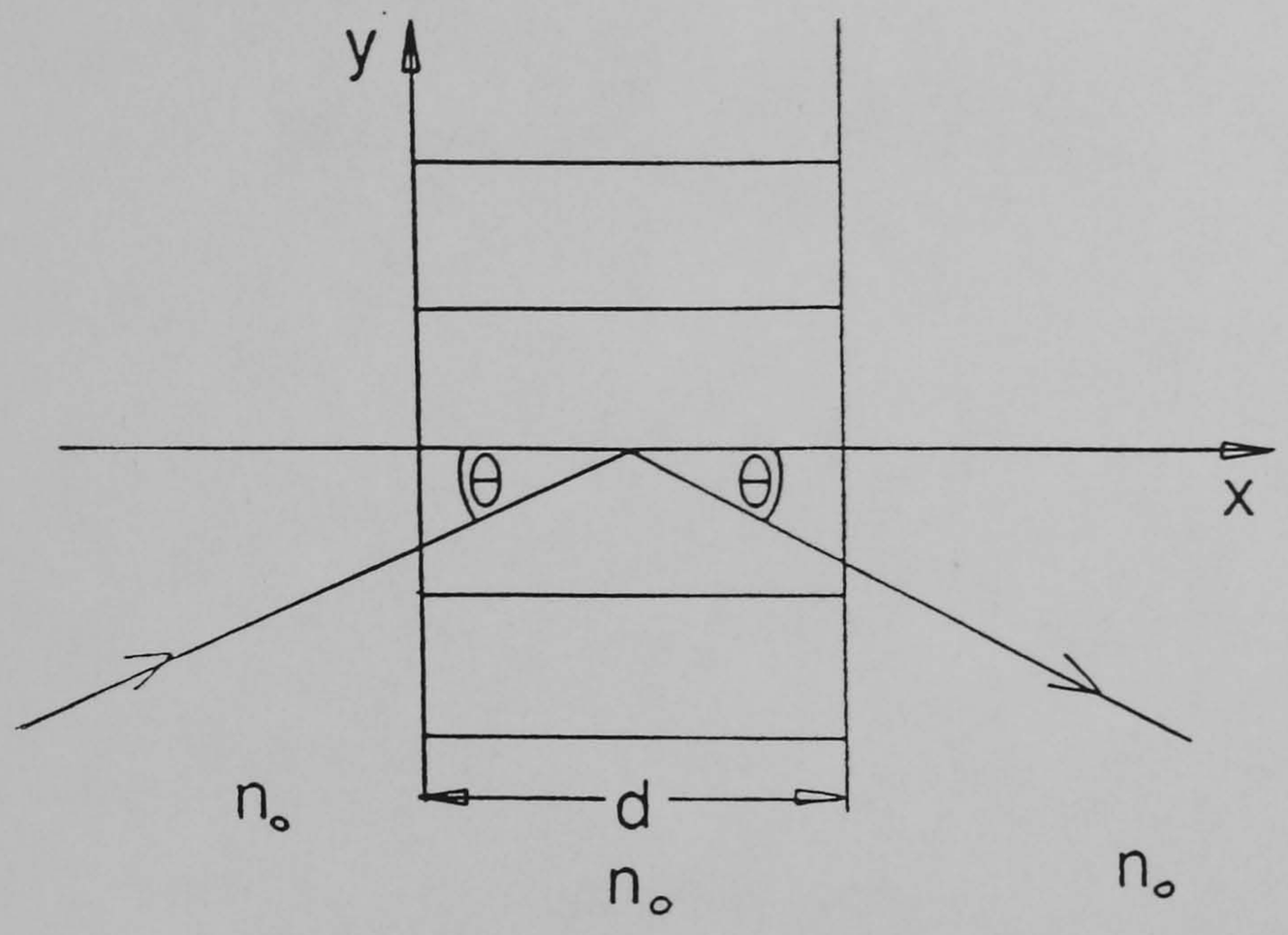

Figure 3.3: Geometry used in Kogelnik's theory.

shortly, with simple extensions to the theory and computer implementation, it can also be a very powerful technique.

Kogelnik's theory begins with the following assumptions:

1. All waves are plane and infinite.

2. Only the incident wave and the 1st order diffracted wave are assumed to be be present (the thick hologram assumption).

3. The interchange of energy between the two waves is slow (terms in $\frac{d^2A}{dx^2}$ may be ignored).

4. The modulation of absorption and refractive index is sinusoidal.

5. Bulk absorption is small.

The resulting expression for the diffracted amplitude of a lossless volume phase transmission grating shown in figure 3.3 is

$$S(d) = \frac{-i\exp(-i\chi)\sin(\Phi^2+\chi^2)^{1/2}}{(1+\chi^2/\Phi^2)^{1/2}} \tag{3.2}$$

where

$$\Phi = \frac{\pi n_1 d}{\lambda\cos\theta} \tag{3.3}$$

and

$$\chi = \vartheta d/2\cos\theta \tag{3.4}$$

$$\vartheta = \Delta\theta\cdot K\sin(\psi-\theta_0) - \Delta\lambda\cdot K^2/4\pi n_0 \tag{3.5}$$

n_1 is the amplitude of the sinusoidal refractive index modulation, θ_0 the Bragg angle and ψ the fringe slant angle made with the y axis. K is the magnitude of the grating vector. ϑ is known as the dephasing term and the above definition is valid for small deviations $\Delta\theta$ and $\Delta\lambda$ from the Bragg condition. Diffraction efficiency is given by

$$\eta = |S(d)|^2 \tag{3.6}$$

$$= \frac{\sin^2(\Phi^2+\chi^2)^{1/2}}{1+\chi^2/\Phi^2} \tag{3.7}$$

At exact Bragg incidence, $\Delta\theta = \Delta\lambda = 0$, and so

$$\eta = \sin^2\left(\frac{\pi n_1 d}{\lambda\cos\theta}\right). \tag{3.8}$$

3.2.3 Extensions to the coupled wave model.

Many extensions have been made to the coupled wave theory to improve accuracy and widen the scope of its application. The effects of internal reflections from the hologram boundaries were discussed by Kogelnik [KOG67], and Owen et al [OWE83]. The effect of absorption during recording leading to non-uniform modulation with depth was investigated by Uchida [UCH73], Kubota [KUB76,KUB78] and Killat [KIL77]. A bulk change in refractive index was investigated by Owen and Solymar [OWE80] and Solymar [SOL78]. Kubota discovered the bending of fringes inside a hologram, which he ascribed to the release of stress in photographic films, and investigated theoretically [KUB79]. Kermisch modelled the same situation by decomposing the hologram into a number of smaller uniform gratings [KER66].

More recently, Moharam and Gaylord have developed an exact coupled wave method, which is fundamentally different from other coupled wave approaches [MOH81A]. They show by comparison of approximate methods with their rigorous one that for transmission holograms, inclusion of higher diffraction orders is more important than inclusion of the second derivatives of the field amplitudes, whereas with reflection holograms, the opposite is true. This is fortunate when modelling transmission holograms, because it is relatively easy to include higher diffraction orders in a standard coupled wave formulation, but it is very difficult to include the second derivatives.

Real time, or dynamic, effects have been studied by Magnusson and Gaylord [MAG76], Newell [NEW85] and Ninomiya [NIN73]. In dichromated gelatin, the

effect is a progressive increase in absorption with exposure, which is probably the same reaction as the slow dark reaction resulting from the reduction of chromium ions. Newell showed that in fact, a pure absorption grating is being created during exposure. This absorption grating is removed by processing when the sensitiser is washed out.

Non-linear effects in modulation were studied by Syms et al in silver halide materials [SYM83], showing evidence of strong saturation of the refractive index modulation. Similar effects in DCG are observed in this thesis.

Multiple independent gratings, as opposed to harmonic gratings, were investigated by Case [CAS75], and later in more detail by Slinger and Solymar [SLI86]. These will be discussed further in chapter 4.

The more general form of non-uniformities with depth have been investigated in dichromated gelatin by Au et al [AU87] and Newell [NEW87]. Also nonlinear recording effects, such as those already described have been studied by Slinger et al [SLI85] in silver halide emulsions, and Newell [NEW87] in dichromated gelatin.

The effects of harmonic gratings and higher order diffraction have been studied by Magnusson and Gaylord [MAG77], Alferness [ALF75], and Kowarschik [KOW78]. Magnusson and Gaylord used the model to investigate diffraction from arbitrary grating shape thick phase holograms built up from harmonic gratings.

3.3 The extended coupled wave model.

For this thesis, a coupled wave model was developed which combined the work of Magnusson and Gaylord, Slinger and Solymar, and Au et al. The model includes

the following improvements on the simple two-wave model;

1. Multiple diffracted orders are allowed.

2. Grating harmonics are permitted (and therefore non-sinusoidal grating profiles).

3. The grating may be non-uniform with depth in respect to bulk refractive index, modulation and fringe spacing.

4. Average refractive index and thickness changes between recording and replay are allowed.

Items 1 and 2 allow us to investigate the effects of non-sinusoidal index profiles, item 3 allows for the effects of absorption during recording and non-uniform processing effects, and item 4 allows for the real physical changes that happen in DCG between sensitising and the final processed hologram.

3.3.1 Derivation.

Wave propagation inside a hologram as illustrated in figure 3.4 is described by the scalar wave equation

$$\nabla^2 E + k^2 E = 0. \tag{3.9}$$

where

$$k^2 = (\omega^2/c^2)n(r)^2 - 2j(\omega/c)n(r)\alpha(r) \tag{3.10}$$

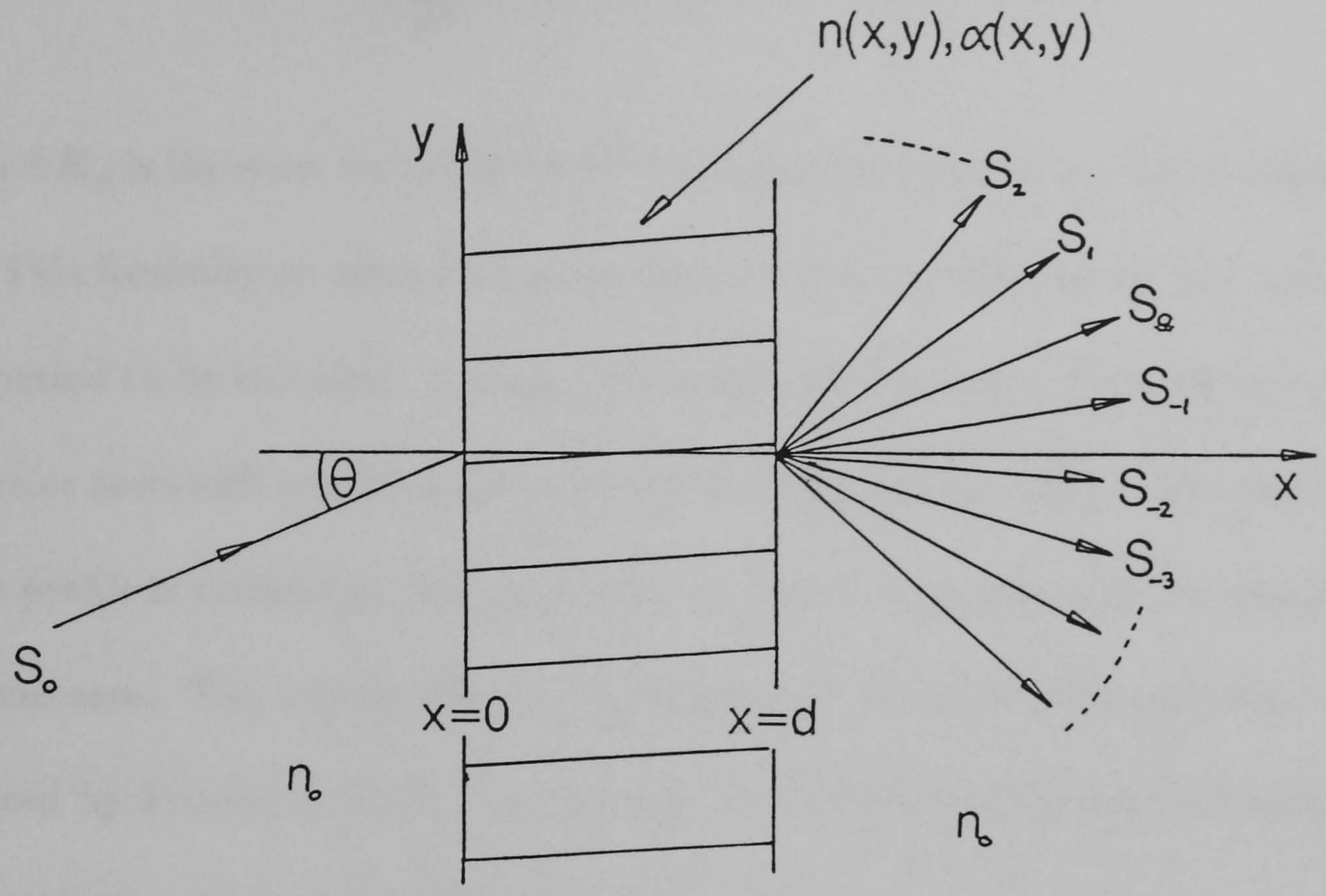

Figure 3.4: Model of a thick hologram.

and

$$n(r) = n_0 + \Delta n \tag{3.11}$$

$$\alpha(r) = \alpha_0 + \Delta\alpha. \tag{3.12}$$

n_0 and α_0 are the average refractive index and absorption within the hologram. Δn and $\Delta\alpha$ are the spatially varying refractive index and absorption modulations which totally describe the profiles within the hologram. In general, Δn and $\Delta\alpha$ may be expressed as Fourier sums;

$$\Delta n = \sum_{g,h} [n_{ch} \cos(h\boldsymbol{K}_g.\boldsymbol{r}) + n_{sh} \sin(h\boldsymbol{K}_g.\boldsymbol{r})] \tag{3.13}$$

$$\Delta\alpha = \sum_{g,h} [\alpha_{ch} \cos(h\boldsymbol{K}_g.\boldsymbol{r}) + \alpha_{sh} \sin(h\boldsymbol{K}_g.\boldsymbol{r})] \tag{3.14}$$

where $h\boldsymbol{K}_g$ is the wave vector of the h^{th} harmonic grating of a fundamental grating, $\boldsymbol{K}_g$. This formulation allows for a number of arbitrary gratings of any orientation and period to be included. A single grating of arbitrary periodic profile, such as a square or sawtooth profile, may be modelled using only one $\boldsymbol{K}_g$ and its harmonics. If the profile is symmetric, the phase can be chosen such that only the cosine terms are non-zero. The composition of the grating in terms of its harmonics may be deduced by Fourier analysis. In this way, the model may be reduced specifically to investigate saturated profiles.

Combining equations 3.10, 3.11 and 3.12 gives

$$k^2 = \beta_0^2 - 2i\alpha_0\beta_0 + 2\beta_0[(2\pi/\lambda)\Delta n - i\Delta\alpha] \tag{3.15}$$

where $\beta_0 = 2\pi n_0/\lambda$ and λ is the free-space replay wavelength.

We assume a solution of the form

$$E = \sum_i A_i \mathrm{e}^{-j(\boldsymbol{k}_i.\boldsymbol{r})} \tag{3.16}$$

where $A_i(x)$ is the amplitude of the ith diffracted wave whose wave vector is $\boldsymbol{k}_i$. The problem now is to specify the various $\boldsymbol{k}_i$.

Starting with a single sinusoidal grating with grating vector, $\boldsymbol{K}$, the wave

vector of the first order Bragg diffracted beam, $\boldsymbol{k}_1$, is given by

$$\boldsymbol{k}_1 = \boldsymbol{k}_0 - \boldsymbol{K} \tag{3.17}$$

where $\boldsymbol{k}_0$ is the incident wave vector. This vector relation is known as the $\boldsymbol{K}$ vector closure relation, because the three vectors form a closed triangle. In addition, $\boldsymbol{k}_0$ and $\boldsymbol{k}_1$ are equal in magnitude, as must any diffracted beam be, since magnitude depends only on wavelength, and this remains constant in 'linear' diffraction (as opposed to diffraction involving non-linear effects which may cause sum and difference frequencies to be generated). This gives us the familiar Ewald sphere representation of diffraction, where all wave vectors form radius vectors of a circle, their directions given by the diffraction equations. The grating vector forms a chord joining the ends of an incident and diffracted beam. This is illustrated in figure 3.5.

At this point, it should be noted that there are two possible ways to represent off-Bragg diffraction and higher diffraction orders. Kogelnik used $\boldsymbol{K}$ vector closure also for non-exact Bragg incidence. This implies a diffracted wave with a wave vector which differs in length from that of the incident wave. This method is valid close to the Bragg angle if the appropriate model is used. Many authors, such as Magnusson and Gaylord [MAG77], have used this method for higher diffraction orders with the diffracted direction of the ith order given by

$$\boldsymbol{k}_i = \boldsymbol{k}_0 - i\boldsymbol{K}. \tag{3.18}$$

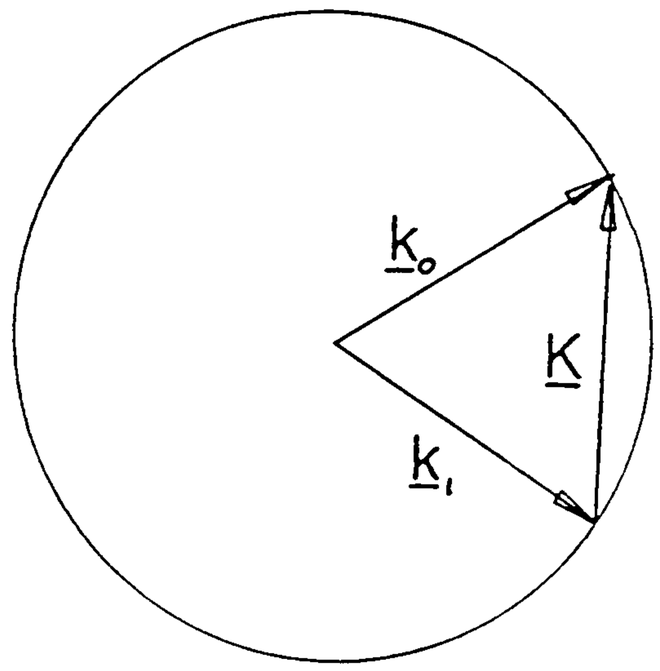

Figure 3.5: Ewald sphere representation of two-wave diffraction.

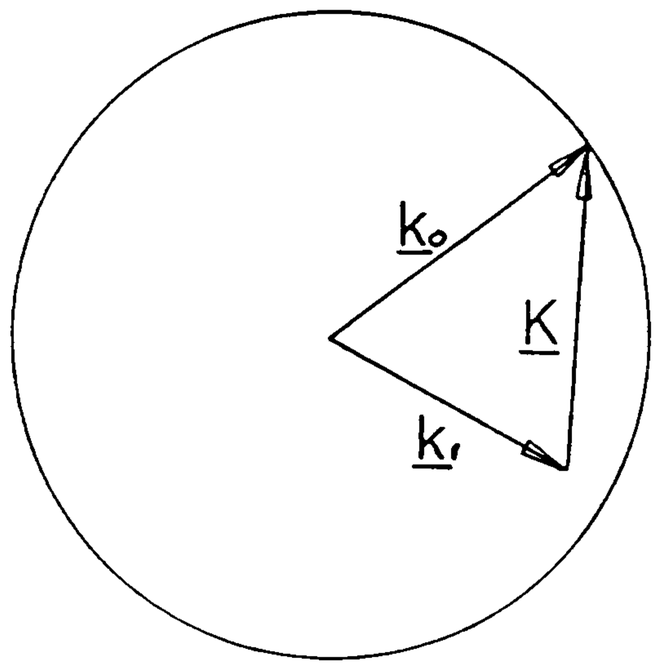

Figure 3.6: $\boldsymbol{K}$ vector closure at off-Bragg incidence.

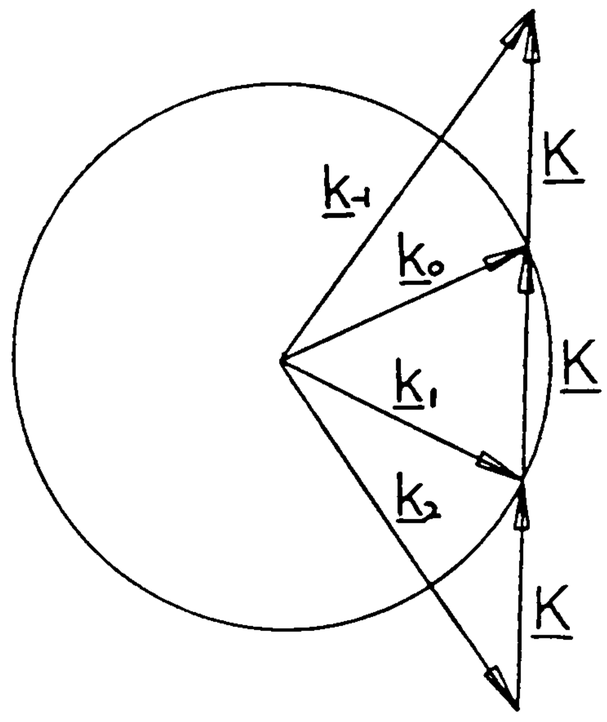

Figure 3.7: $\boldsymbol{K}$ vector closure for higher orders.

The +1, -1 and -2 orders are illustrated in figure 3.7.

However, a more physical, and more accurate approach was taken by Syms and Solymar [SYM83] who used the vector components form of the standard grating equation to define diffracted directions;

$$k_{iy} = k_{0y} - iK_y \tag{3.19}$$

where we are only dealing with the y components of the wave vectors (since only the components of **K** in the surface of the hologram affect diffracted directions, and in this case there is no z component), and magnitudes are conserved. The only difference this makes to the coupled wave theory is to make the off-Bragg de-phasing term more complicated. The model presented here uses this more

accurate method for defining the diffracted directions and calculating their powers. Obviously, additional fundamental gratings could be included, but this possibility will be left until chapter 4.

If we substitute equations 3.13 and 3.16 into 3.9, and neglect second derivatives on the grounds that wave amplitudes are assumed to change slowly on the scale of a wavelength, we get a set of simultaneous equations of the form;

$$\frac{dA_l}{dx}k_{lx}/\beta + A_l(\alpha_0 + j\vartheta_l) + j\left[\sum_{a,b}\kappa_a A_b\right] = 0. \tag{3.20}$$

A_l is the amplitude of wave l with wave vector $\boldsymbol{k}_l$, and k_{lx} is the x component of $\boldsymbol{k}_l$. The dephasing term, ϑ, is defined by

$$\vartheta_l = \left(\frac{k_{lx}^2 - k_{lx}k'_{lx}}{\beta}\right) + \left(\frac{\beta^2 - k^2}{2\beta}\right) \tag{3.21}$$

where k'_{lx} is the x component of $\boldsymbol{k}$ as given by equation 3.18. κ_a is the coupling constant of grating a, with refractive index modulation amplitude Δn_a, and absorption modulation amplitude, $\Delta\alpha_a$, given by

$$\kappa_a = \frac{\pi\Delta n_a}{\lambda} - \frac{j\Delta\alpha_a}{2}. \tag{3.22}$$

In the computer model, all $\Delta\alpha$'s are set to zero, since in dichromated gelatin, absorption modulation is generally negligible. As Newell showed, however, significant absorption gratings may be formed on exposure prior to processing [NEW87]. These are removed by processing.

The summation represents the collection of waves, A_b, which are directly coupled to wave l. Therefore, what has to be considered is which A_b's are coupled to each A_l, and via which gratings (given by κ_a). This problem divides into three areas:

- Higher diffraction orders of a sinusoidal grating.
- Diffraction orders from harmonic gratings.
- General multiple interaction diffraction from a collection of arbitrary gratings.

We will discuss items 1 and 2 here, but leave item 3 for chapter 4.

As a convenient method for expressing the various interactions between waves, the set of equations, 3.20 can be expressed in matrix form as follows;

$$\begin{bmatrix} \frac{dA_0}{dx} \\ \frac{dA_1}{dx} \\ \vdots \\ \frac{dA_L}{dx} \end{bmatrix} = - \begin{bmatrix} B_0 A_0 \\ B_1 A_1 \\ \vdots \\ B_L A_L \end{bmatrix} - C \begin{bmatrix} j\beta A_0/k_{0x} \\ j\beta A_1/k_{1x} \\ \vdots \\ j\beta A_L/k_{Lx} \end{bmatrix} \tag{3.23}$$

where B_l is given by

$$B_l = \frac{(\alpha + j\beta)\vartheta_l}{k_{lx}} \tag{3.24}$$

and C is the coupling matrix, defined by

$$C = \begin{bmatrix} c_{11} & c_{12} & \cdots & c_{1L} \\ c_{21} & c_{22} & \cdots & c_{2L} \\ \vdots & \vdots & & \\ c_{L1} & c_{L2} & \cdots & c_{LL} \end{bmatrix} \tag{3.25}$$

and the c's are given by

$$c_{ij} = \begin{cases} \kappa_a & \text{if wave } i \text{ couples to wave } j \text{ by grating } a, \\ 0 & \text{if there is no direct coupling.} \end{cases} \tag{3.26}$$

κ_a is the grating which couples waves i and j. In general every wave will couple via every grating to a set of diffracted waves, although the coupling effect may be weak. Then, each of these waves may again couple via each grating to form another set, and so on. However, in typical cases, diffraction angles are large, and so higher diffraction orders are limited in number by the geometry of diffraction. Also, powers in the higher orders that do exist are usually only a small fraction of the main diffracted powers, and so often these may be ignored, leading to a reduction of the size of the numerical problem. It is a property of the mathematical formulation that each equation in $\frac{dA_i}{dx}$ only contains terms in the neighbouring diffraction orders. For example, if A_i represents the amplitude of the ith diffraction order of some grating, the equation in $\frac{dA_i}{dx}$ contains terms in A_{i-1} and A_{i+1} only due to that particular grating.

3.3.2 Generating the coupling matrix and associated waves.

First, we take the simplest case of Kogelnik's two-wave model. The only orders involved are the zero and minus first orders with wave vectors $\boldsymbol{k}_0$ and $\boldsymbol{k}_{-1}$, connected by a single sinusoidal grating with wave vector $\boldsymbol{K}_1$, which are related by $k_{-1y} = k_{0y} - K_{1y}$. Hence we only have two differential equations in A_0 and A_{-1}, which represent the amplitudes of $\boldsymbol{k}_0$ and $\boldsymbol{k}_{-1}$. A_0 couples only to A_{-1} and vice-versa via κ. Therefore the coupling matrix is

$$\boldsymbol{C} = \begin{bmatrix} c_{(-1)(-1)} & c_{(-1)(0)} \\ c_{(0)(-1)} & c_{(0)(0)} \end{bmatrix} = \begin{bmatrix} 0 & \kappa_1 \\ \kappa_1 & 0 \end{bmatrix}. \tag{3.27}$$

Note that the subscript signs have been reversed for the matrix formulation, so that now the minus first order corresponds to the first Bragg order. This is more consistent than the Bragg notation. Now $\boldsymbol{k}_i = \boldsymbol{k}_0 + i\boldsymbol{K}$. If the positive first order is also included, $\boldsymbol{k}_1$, then $\boldsymbol{k}_{-1}$ and $\boldsymbol{k}_1$ are given by

$$k_{-1y} = k_{0y} - K_{1y} \tag{3.28}$$

$$k_{1y} = k_{0y} + K_{1y}. \tag{3.29}$$

The coupling matrix becomes

$$\boldsymbol{C} = \begin{bmatrix} 0 & \kappa_1 & 0 \\ \kappa_1 & 0 & \kappa_1 \\ 0 & \kappa_1 & 0 \end{bmatrix}. \tag{3.30}$$

If we now include the minus second order, $\boldsymbol{k}_{-2}$ and plus second order, $\boldsymbol{k}_2$, following the same reasoning, we get

$$\boldsymbol{C} = \begin{bmatrix} 0 & \kappa_1 & 0 & 0 & 0 \\ \kappa_1 & 0 & \kappa_1 & 0 & 0 \\ 0 & \kappa_1 & 0 & \kappa_1 & 0 \\ 0 & 0 & \kappa_1 & 0 & \kappa_1 \\ 0 & 0 & 0 & \kappa_1 & 0 \end{bmatrix} \tag{3.31}$$

where the array element subscripts now extend from -2 to 2. We now introduce the second harmonic grating, $\boldsymbol{K}_2$, with half the period of $\boldsymbol{K}$. This grating now diffracts the zero order into the $\boldsymbol{k}_{-2}$ and $\boldsymbol{k}_2$ directions as defined above, and diffracts $\boldsymbol{k}_{-1}$ into $\boldsymbol{k}_1$ and $\boldsymbol{k}_{-3}$ (if we had included it), and so on. No new directions are generated, unless higher orders are allowed. The coupling matrix becomes

$$\boldsymbol{C} = \begin{bmatrix} 0 & \kappa_1 & \kappa_2 & 0 & 0 \\ \kappa_1 & 0 & \kappa_1 & \kappa_2 & 0 \\ \kappa_2 & \kappa_1 & 0 & \kappa_1 & \kappa_2 \\ 0 & \kappa_2 & \kappa_1 & 0 & \kappa_1 \\ 0 & 0 & \kappa_2 & \kappa_1 & 0 \end{bmatrix}. \tag{3.32}$$

Similarly, inclusion of the third harmonic grating, $\boldsymbol{K}_3$, leads to a coupling

matrix

$$C = \begin{bmatrix} 0 & \kappa_1 & \kappa_2 & \kappa_3 & 0 \\ \kappa_1 & 0 & \kappa_1 & \kappa_2 & \kappa_3 \\ \kappa_2 & \kappa_1 & 0 & \kappa & \kappa_2 \\ \kappa_3 & \kappa_2 & \kappa_1 & 0 & \kappa_1 \\ 0 & \kappa_3 & \kappa_2 & \kappa_1 & 0 \end{bmatrix}. \tag{3.33}$$

This shows how to extend this model to any system of harmonic gratings and higher diffraction orders.

3.3.3 Non-uniformities.

Up to this point, the model has assumed uniform modulations of n and α throughout the depth of the hologram. In order to include such non-uniformities, all that is necessary is to make both n and α functions of x. This in fact is possible using numerical algorithm computer packages, some of which allow the solution of a system of ordinary differential equations with respect to x, while allowing the inclusion of x-varying parameters. However, it was found in practice that such routines were impractically slow, and it was possible to break the grating structure down into a number of uniform slabs of depth δx. This structure may instead be treated by solving with constant coefficients for each slab in turn, using final field amplitudes from the previous slab as its initial values. By comparing results from the model using a very large number of slabs, it was found to be sufficient to take only the order of ten to twenty separate slabs to reach a high degree of accuracy. This does depend, however, on the degree of non-uniformities within a

specific hologram.

The non-uniformities initially allowed were quadratic in fringe x coordinate (representing a swelling or shrinking effect), and quadratic in Δn, such as might be caused by absorption during recording, or by processing effects. The other parameter which should be allowed to vary is the bulk refractive index, n_0. It has been shown that this is indistinguishable in its effect from that of a non-uniformity in K_x [AU87], and that therefore without an independent means of distinguishing these effects, it is arbitrary which one is varied. It can also be taken that the form of a non-uniformity in n_0 for a particular grating will be similar to that of K_x, apart from scaling.

The form of the non-uniformities included is as follows;

$$\Delta n(x') = \Delta n_0 \left[1 - b/12 + ax' + bx'^2\right] \tag{3.34}$$

$$K_x(x') = K_y \left[K_{x0}/K_y - d/12 + cx' + dx'^2\right] \tag{3.35}$$

where a, b, c and d are the non-uniformity parameters, and the grating vector, k has a magnitude given by

$$|K| = \frac{2\pi}{\Lambda} \tag{3.36}$$

and a direction perpendicular to the fringes. Λ is the fringe spacing. x' is a normalised depth coordinate such that $-0.5 < x' < +0.5$. The terms $b/12$ and $d/12$ are included in order that the average refractive index and fringe spacing are unaffected, and hence the Bragg angle shift due to the non-uniformity parameters is minimised.

3.3.4 Computer solution.

The above model was converted into a computer program in Fortran 77 for a VAX 8700 mainframe computer, using NAG (Numerical Algorithms Group) routines for solving the system of differential equations. These routines use a standard fourth order Runge-Kutta technique, suitable for well behaved systems such as this, where we expect no discontinuities or singularities. Since the equations are complex, they must be separated into real and imaginary equations before solution. Therefore, if a solution involving N waves is required, $2N$ simultaneous equations must be solved. The solutions are then recombined to give amplitudes which are converted into diffraction efficiencies by normalising total amplitudes. Angles of propagation must also be taken into account, hence diffraction efficiency is given by

$$\eta_i = (\cos\theta_i / \cos\theta_0) A_i(d) A_i^*(d). \tag{3.37}$$

3.4 Exposure response.

The typical diffraction efficiency results for a test plate (number 22073) made with a range of exposure values is shown in figure 3.8. The gelatin was supplied as a 28μm thick layer, and therefore all processing times were extended to ten minutes per bath to ensure the penetration of chemicals. The gratings on the plate were recorded at 514nm and measured at 633nm. Results have been corrected for reflection and absorption losses measured in a clear area of gelatin. Given on the graph are the diffraction efficiency values at the principle Bragg angle (diamonds),

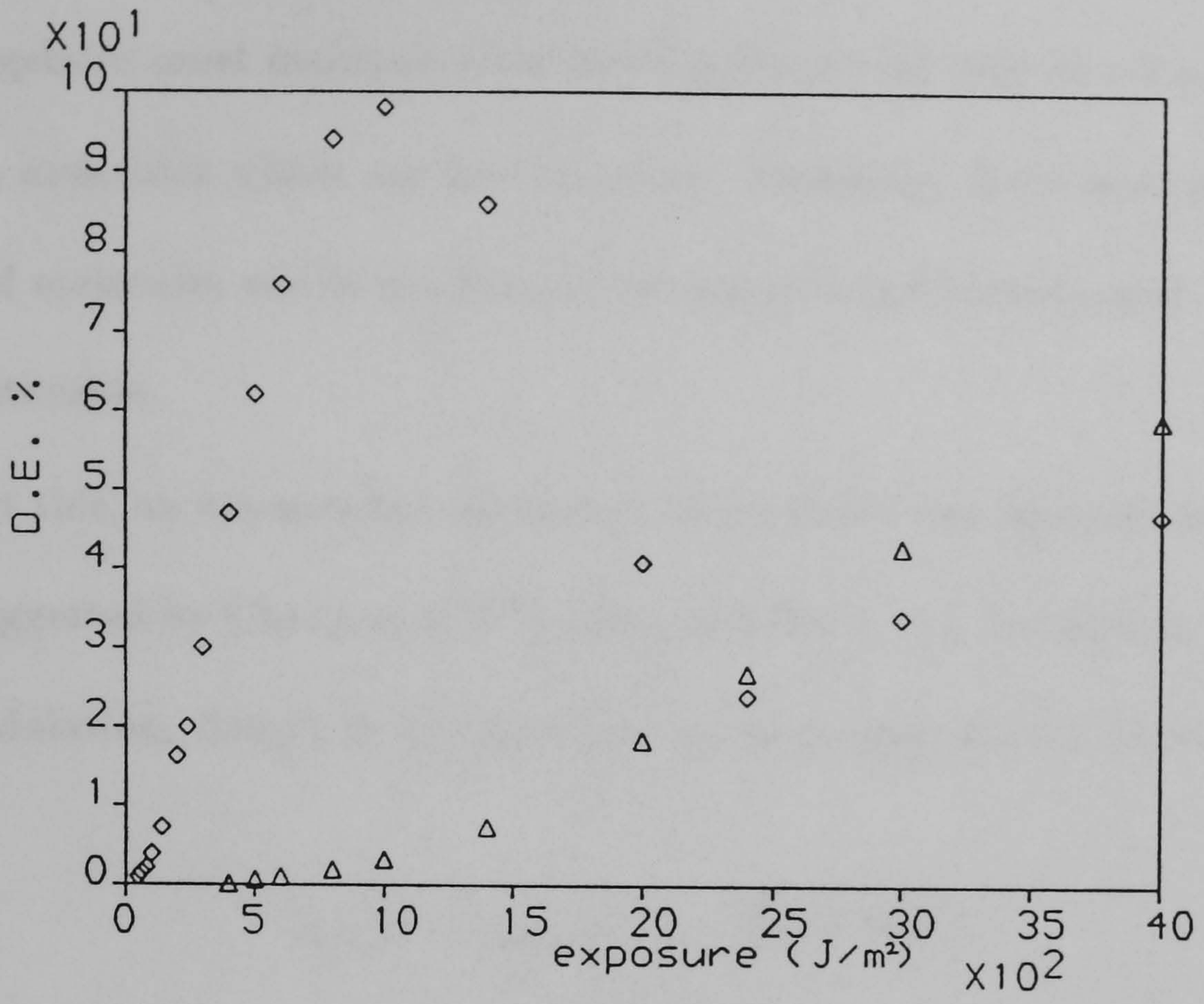

Figure 3.8: Diffraction efficiency vs exposure. Hologram 22073.

and at an angle corresponding to the second order Bragg angle (triangles).

From figure 3.8 it can be seen that the first order Bragg exposure response is not exactly as predicted by simple coupled-wave theory. The portion up to the first peak behaves as expected, like a $\sin^2$ function, but with increasing exposure, a second zero should be reached. Instead, a minimum is reached, and then efficiency rises again. The graph is also apparently stretching towards the right. This gives a clue to the possible cause of the discrepancy - saturation of the refractive index.

3.4.1 Saturation.

Whatever the mechanism underlying the refractive index modulation, there will be some limit to the change that can be induced. In the theory suggested in chapter 2, the mechanism relies on diffusion of gelatin molecules. In a pre-hardened layer,

since the gelatin must maintain some rigidity, there can only be a limited number of gelatin molecules which are free to move. Therefore, there are only a limited number of molecules which can form a refractive index pattern, and the medium is then saturable.

To test this, an exponential saturation of the index was included in the model, as first suggested by Chang et al [CHA80]. This leads to a description of refractive index modulation, $\Delta n(y)$, in the direction of the grating vector, of the form

$$\Delta n(y) = \Delta n_m \left(1 - e^{-\frac{\beta E}{\Delta n_m}(1+\cos y)}\right) \tag{3.38}$$

where Δn_m is the difference between the base refractive index, n_0 and the saturated value, β is a sensitivity term, and E represents exposure energy. Note that the driving term of $E(1 + \cos y)$ is *inside* the exponential. This leads to non-sinusoidal modulation which therefore contains other frequency components. These must all be harmonics of the driving frequency. Figure 3.9 shows harmonic strengths plotted against exposure (or modulation) obtained by Fourier analysis of the saturated function.

This graph shows that the fundamental component, which contributes to the measured diffraction efficiency, reaches a peak and drops, while the second harmonic continues to rise for around three times as long before peaking. To compare this theory to the experiment, it is first necessary to obtain the index modulation values from the experimental results. This was done by putting the experimental parameters into the coupled wave model and deducing the Δn's from best fits. This is accurate even with Kogelnik's model, since the angles between adjacent

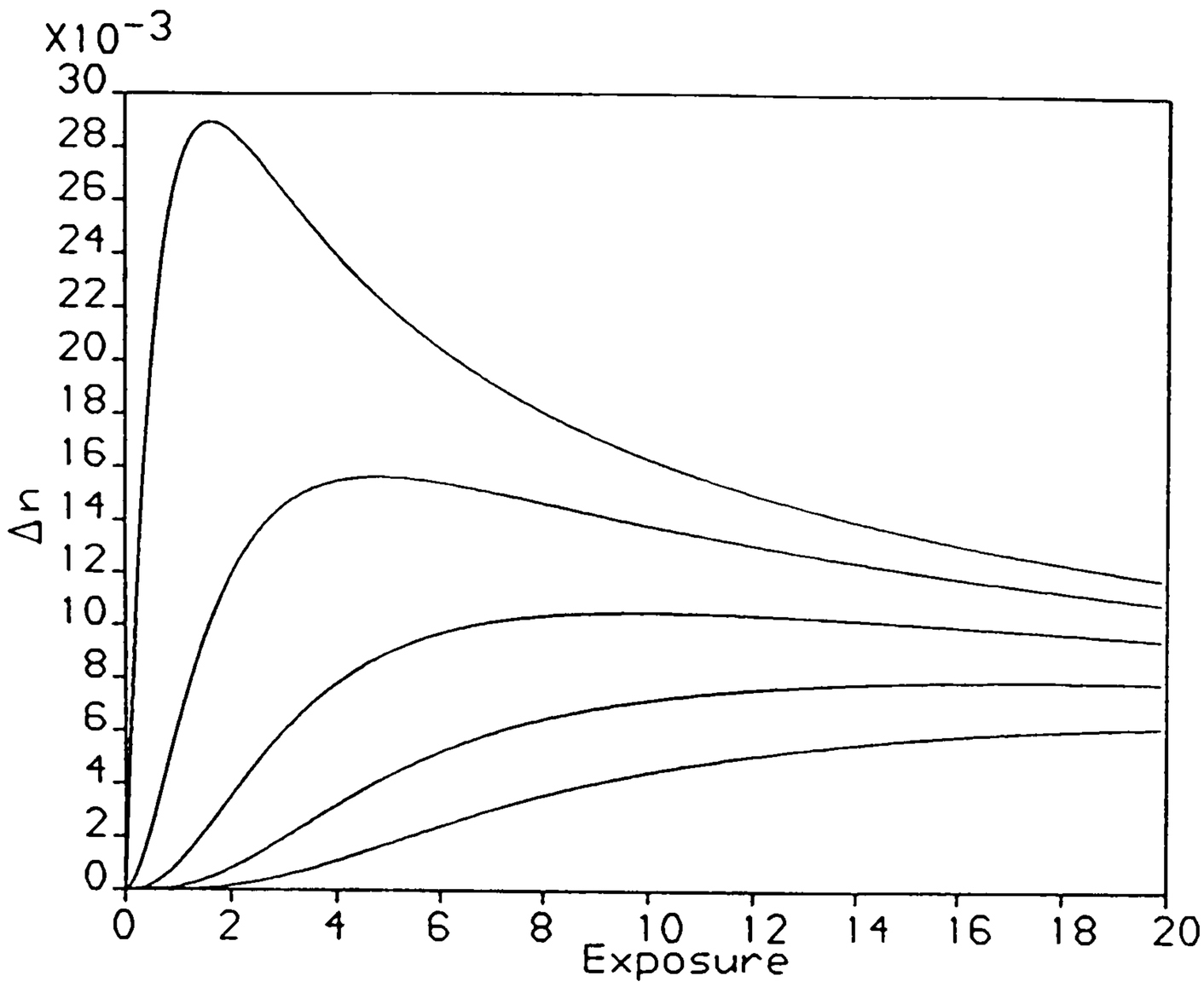

Figure 3.9: R.I. modulation harmonic strengths vs. exposure (arbitrary scale).

Bragg angles are large enough to ensure negligible coupling, and also the hologram is sufficiently thick that only a single first diffraction order from any one grating is significant at a time. This was observed experimentally, and verified with the computer model, with higher orders included.

The amplitudes of both the first and second harmonics of hologram 22073 were calculated by this method and are plotted in figure 3.10. Diamonds represent the first harmonic and triangles the second. Also on this graph are theoretical grating amplitudes obtained by fourier analysis of the saturated index profile described in eqn 3.38. It can be seen that a very good fit can be obtained, using $\beta = 1.6 \times 10^{-5}\mathrm{m}^2/\mathrm{J}$ and $\Delta n_m = 0.041$.

Note that the second harmonic grating may have two possible phases, separated by π, which give identical diffraction responses, but only one of these, with the

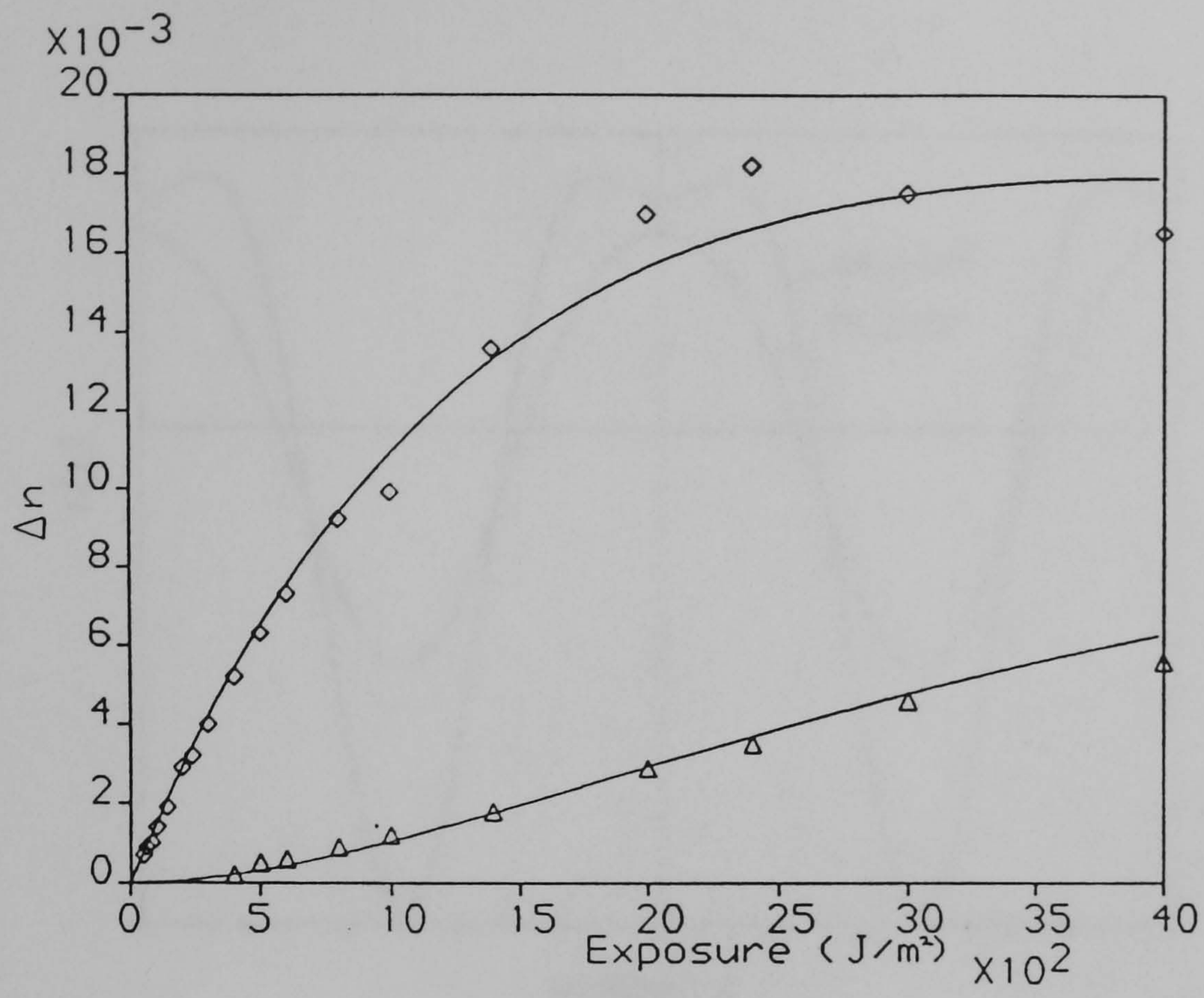

Figure 3.10: First and second harmonic grating amplitudes. Hologram 22073.

second harmonic out of phase with the first, agrees with the saturation model. The resulting grating profile for hologram 22073 is shown in figure 3.11 at two exposure levels of 1 and 4kJ/m^2. The lower exposure represents the peak diffraction efficiency, whereas the higher represents considerable overexposure. The unphysical appearance of the 4kJ/m^2 index profile is due to the neglect of the third harmonic, which, by the saturation equation, should have an amplitude of 0.0016.

A second set of efficiency results from a 649F plate (number 07011) recorded at 488nm are given in figure 3.12. Corresponding index modulations and a theoretical fit using $\beta = 6.5 \times 10^{-5}\mathrm{m}^2/\mathrm{J}$ and $\Delta n_m = 0.065$ are plotted in figure 3.13. Peak index modulation in these results occurs at the minimum in efficiency. β is significantly greater in these results by a factor of 4 due to greater sensitivity at 488nm. This is possibly due, in part, to the difference in absorption, which is a

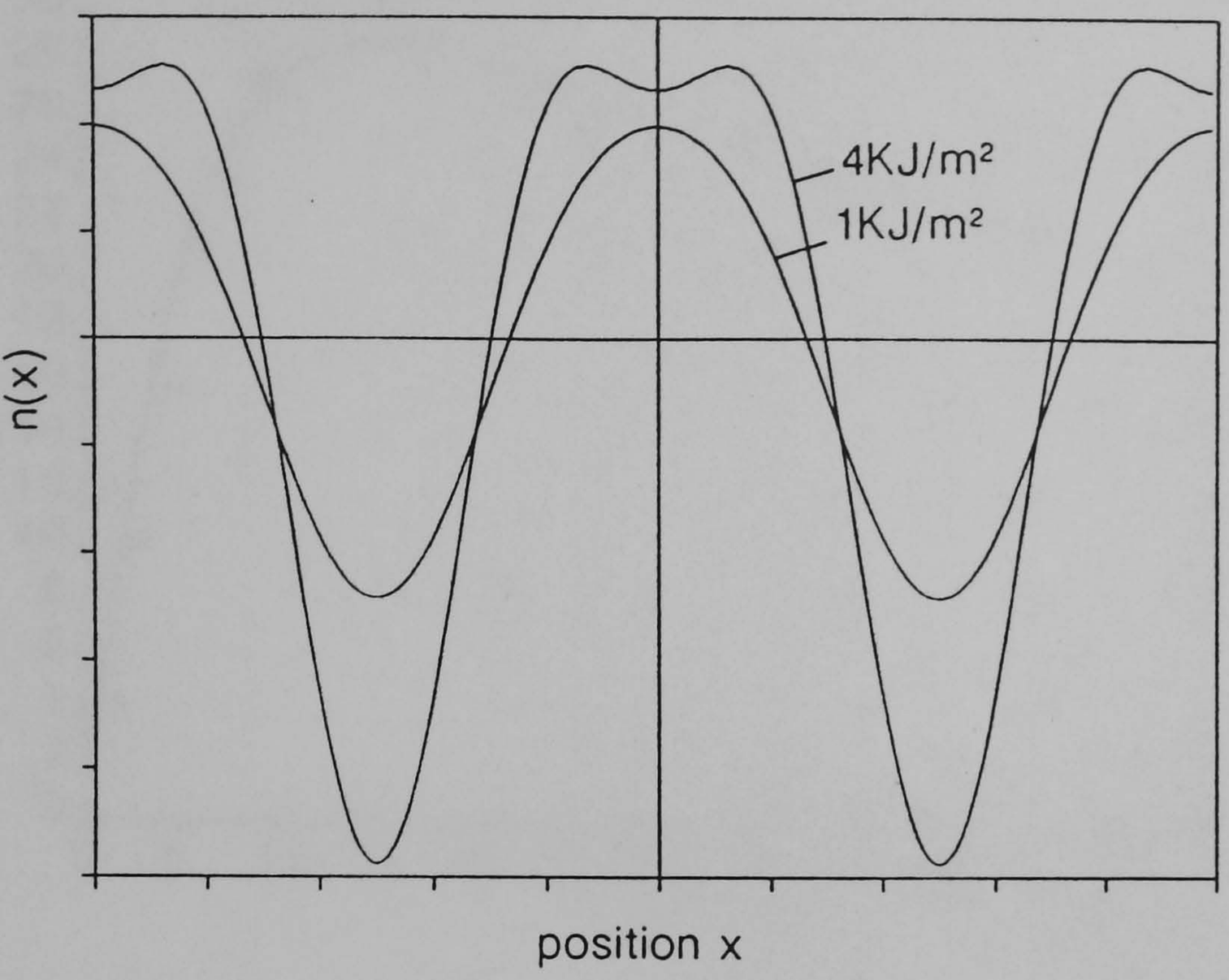

Figure 3.11: Calculated grating index profile. Hologram 22073.

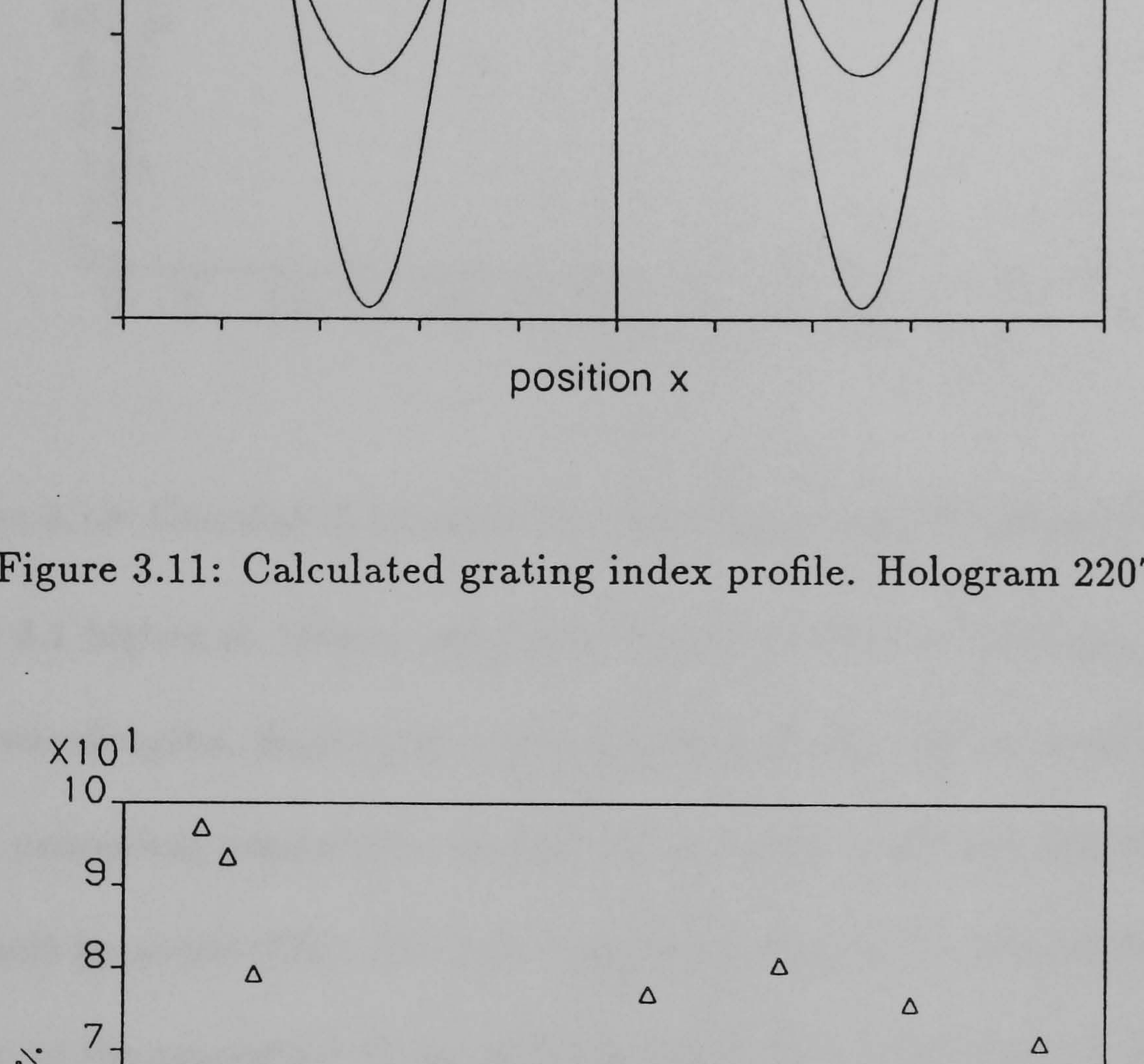

Figure 3.12: First order diffraction efficiencies. Hologram 07011.

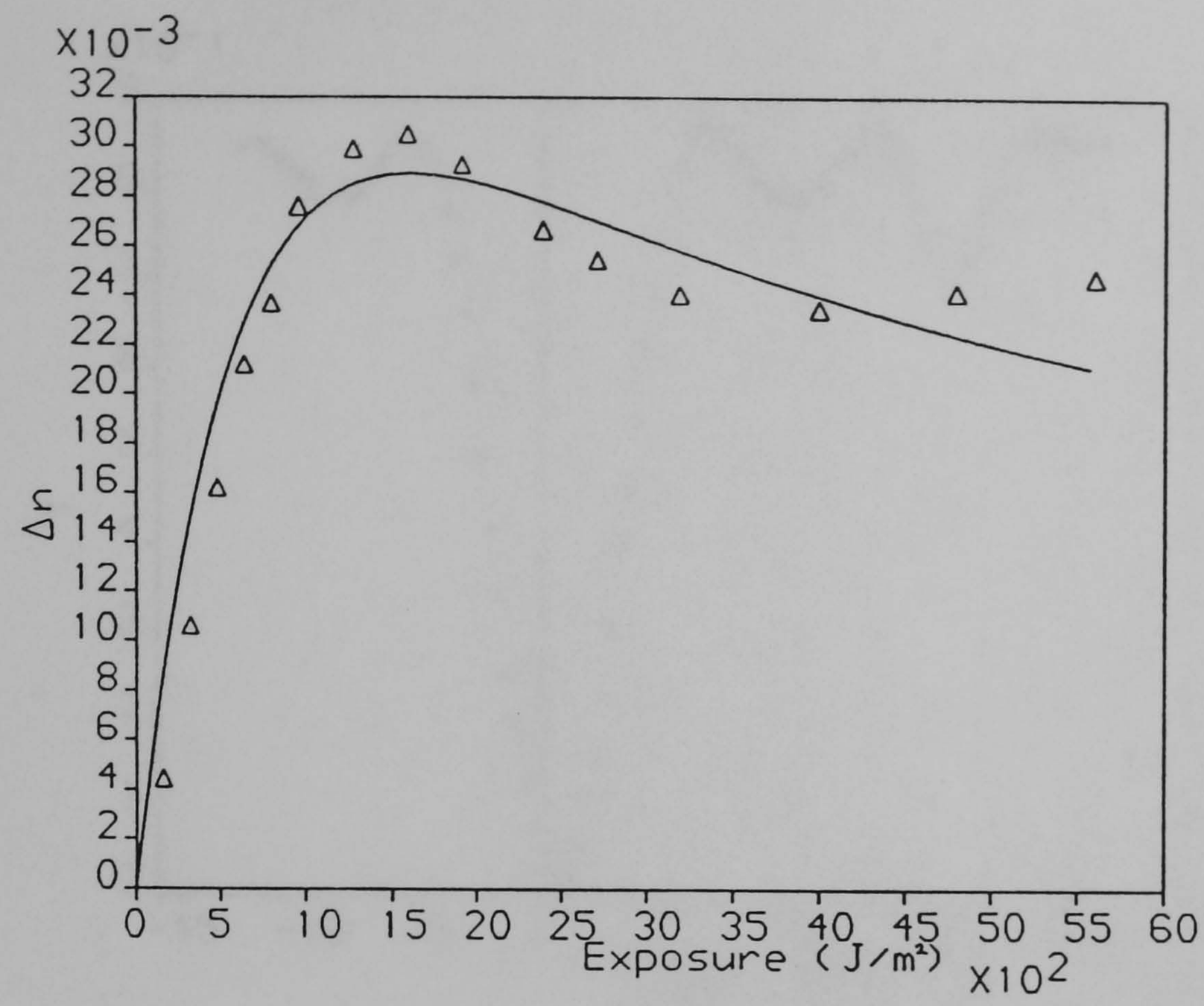

Figure 3.13: Calculated fundamental index modulations. Hologram 07011.

factor of 3.1 higher at 488nm and partly due to a different quantum efficiency at the two wavelengths. Sensitivity is also depends on the source of gelatin, and the different processing procedures, as does Δn_m, which is greater here than the previous result by about 60%. The two holograms were made from different batches of plates, so the properties of the gelatins would be expected to be different.

3.5 Angular response.

Results of an angular scan of a 649F hologram (30051) recorded and analysed at 514nm are given in figure 3.14. These results are presented as transmitted zero order powers because the transmitted zero order contains information on all diffraction directions, including those resulting from higher grating harmonics due

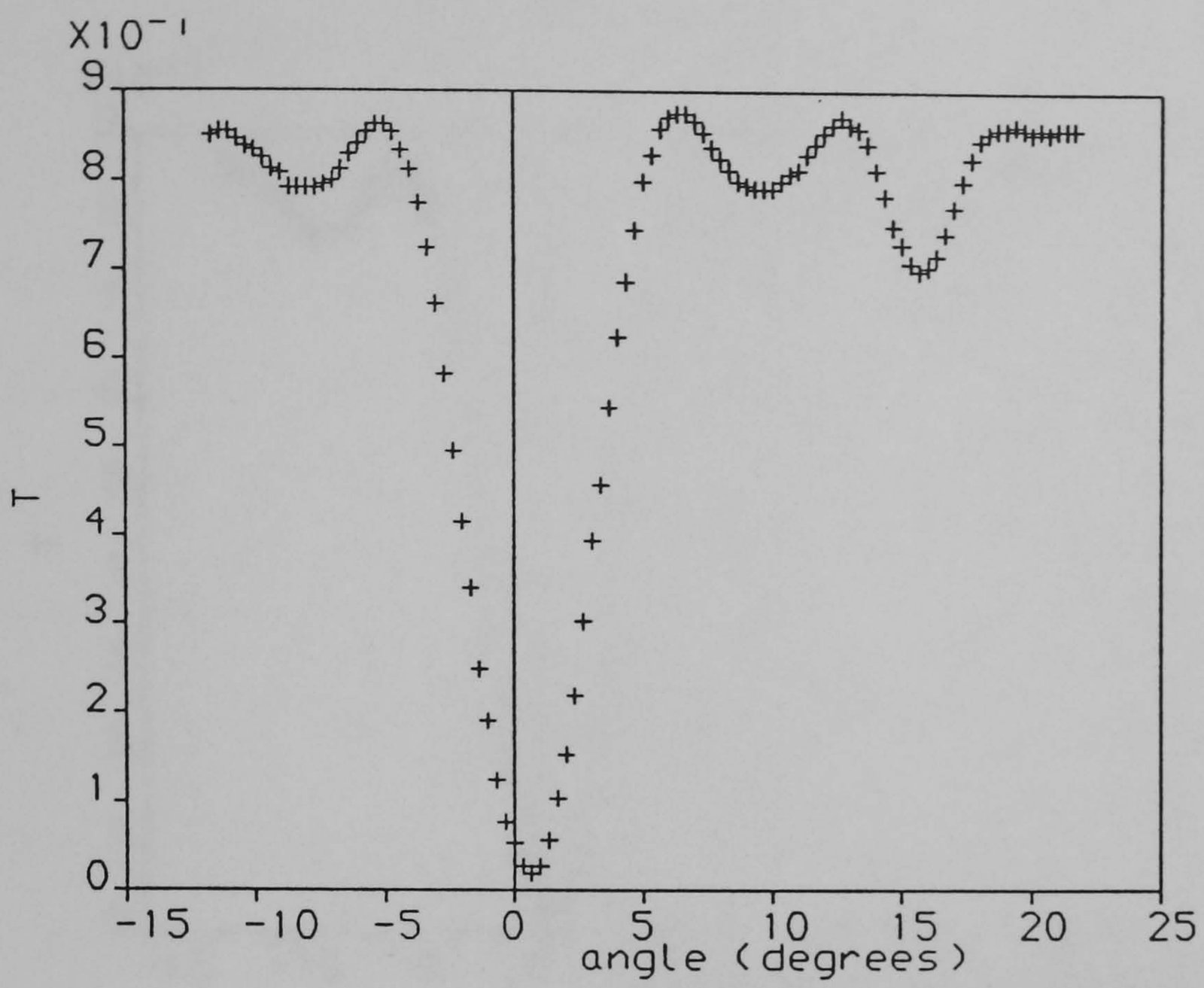

Figure 3.14: Transmitted power vs. angle. Hologram 30051.

to non-linearities. It will be seen in the analysis that this leads to a more complete picture of the fringe structure within the gelatin. This analysis technique is similar to that of Slinger et al [SLI85].

These results are exactly as measured, and have not been corrected for specular reflection or absorption losses. It can be seen that the maximum transmission value is 87%. This in fact is also the value of transmission of unexposed areas of the plate. This is less than the figure expected allowing for Fresnel reflection losses (91.5%), and indicates losses through absorption and/or scattering of 4.5%. Measurements show that in this case the loss is almost entirely due to absorption in the gelatin. (In a plate which is too soft, scattering may also appear in unexposed and lightly exposed regions, and may appear even in heavily exposed areas if the gelatin is very soft.)

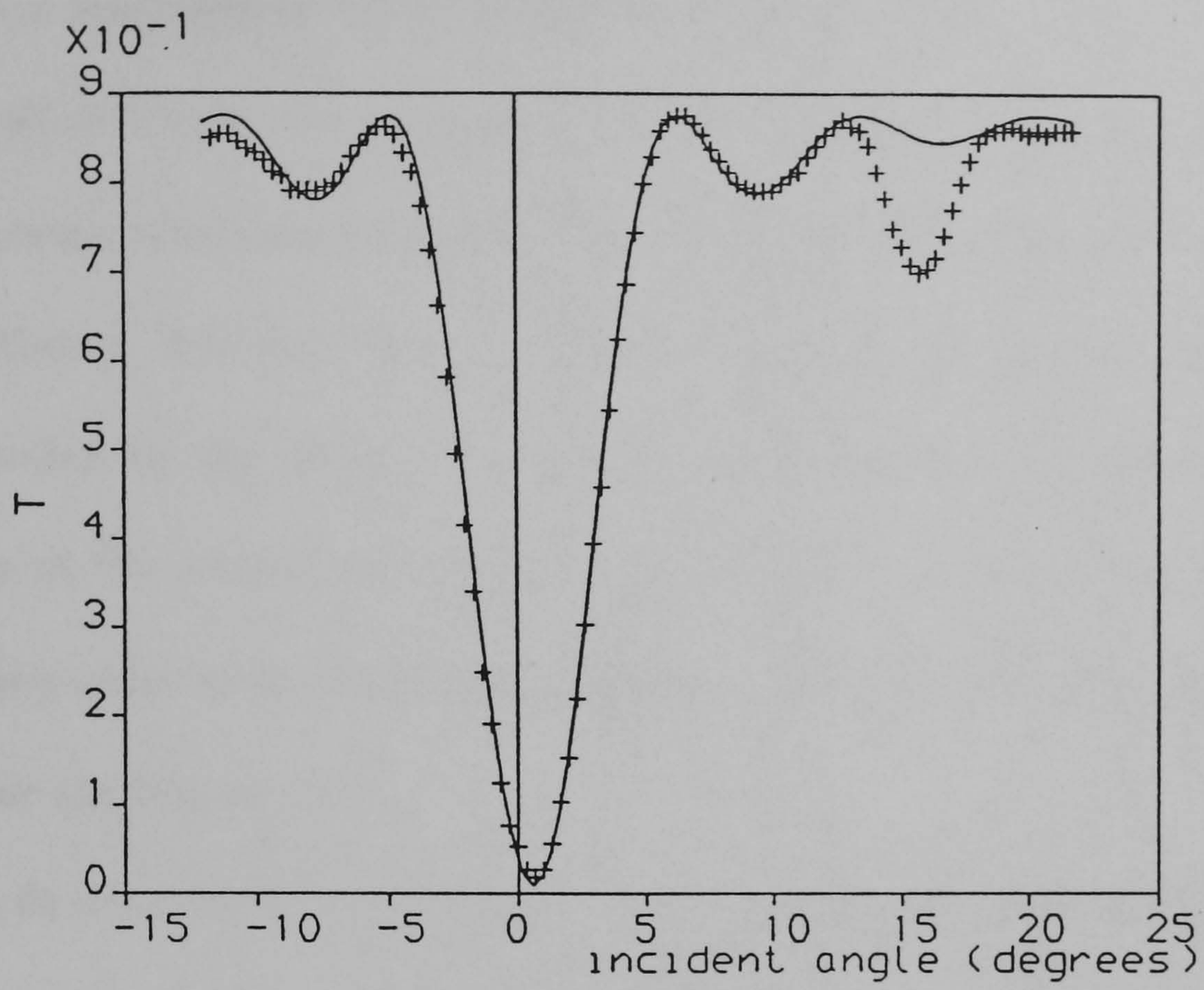

Figure 3.15: A simple coupled wave fit with experiment.

Shown in figure 3.15 is a theoretical fit using Kogelnik's two wave theory in a computer model. Losses have been taken into account. Note that the minimum falls at 0.7°, whereas the hologram was recorded with beams at 0° and 30°. We would therefore have expected the Bragg angle to be at 0° exactly. There are two parameters which may affect the position of the Bragg angle between recording and replay. These are a change in bulk refractive index, and a change in the thickness of the hologram. They are indistinguishable in their effect. However, in a separate experiment, thickness after sensitising was found to be 16.8μm and thickness after processing to be 13.0μm. Final refractive index was measured on an Abbe refractometer to be 1.493. The computer program was modified to include these changes, and, by trial and error, the refractive index during exposure was deduced to be 1.6$\pm$0.02. This is in good agreement with Newell's value [NEW87]

for gelatin sensitised at 5% concentration of around 1.59.

The fit of the theory is very good over the main dip, but not so good elsewhere. In particular, experimental results show a much stronger dip at 16° than predicted by the theory. But also, there is a slight asymmetry in the experimental results, not reflected by the theory, which is always symmetrical. Consideration of the position of the second strong dip suggests that it is due either to the second diffraction order of the fundamental grating, or to the first order from the second harmonic grating, or both.

The fit can now be improved by using the extended coupled wave model first to account for the secondary dip, and then to account for any non-uniformities which may be present.

By plotting only the diffraction efficiency of the negative second diffracted order, it was found that, in this case, the maximum efficiency is 1.9%. This is in the same position as the secondary dip, but is insufficient to account for its size. It is apparent that there is a component of the second harmonic present.

The strength of the harmonic grating was increased in the model until the secondary dip was accounted for. At such a relatively low efficiency, the effect of the harmonic does not extend far outside the immediate region of the dip, so the primary diffraction efficiency was unaffected. The amplitude of the harmonic was determined to be 0.0045, as compared to 0.018 for the fundamental. This agrees with the relative amplitudes calculated in figure 3.10.

Finally, the effect of the non-uniformity parameters were investigated in order further improve the fit with experiment. Figures 3.16 to 3.19 show the effects

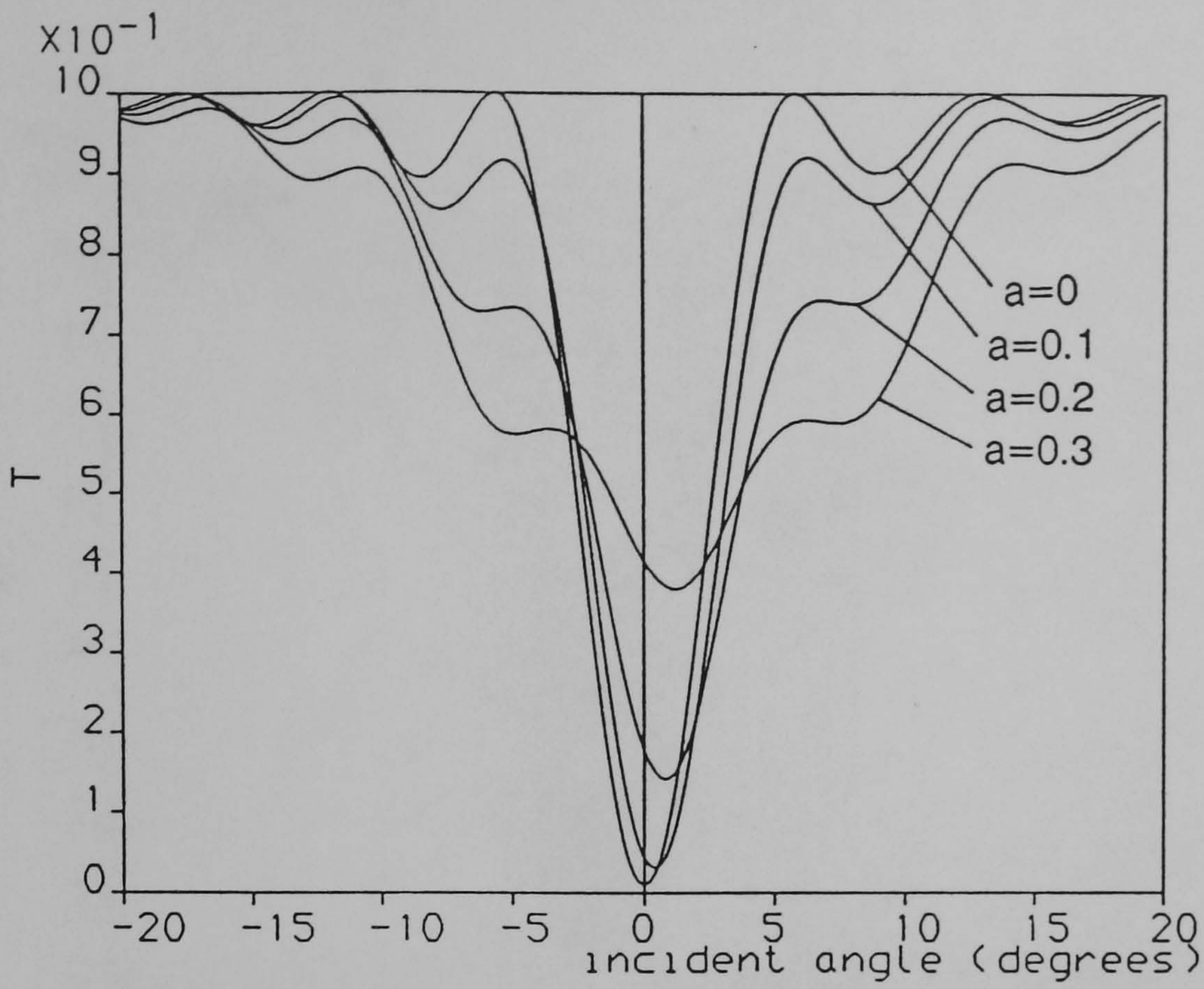

Figure 3.16: The effect of variation in a on angular response.

of varying the four non-uniformity parameters. Note that opposite signs of the linear factors a and c have identical effects. A negative quadratic variation in K exhibits reversed asymmetry, and in Δn depressed sidelobes. The parameters have distinctly different effects, although in practice it is found that they are not independent of each other, so that careful trial and error fits are necessary if large non-uniformities are to be accounted for.

The values found to match the experiment were $a = -0.005$, $b = 0.02$, $c = -0.7$, and $d = -0.6$, and the fit is shown in figure 3.20. Taken together, these values only have a small effect, and the percentage tolerances over which a good fit can be obtained are large. However, the low absolute values indicate that the non-uniformities in the hologram are minimal. The major effect on the angular results is therefore due to the presence of a harmonic grating resulting from saturation.

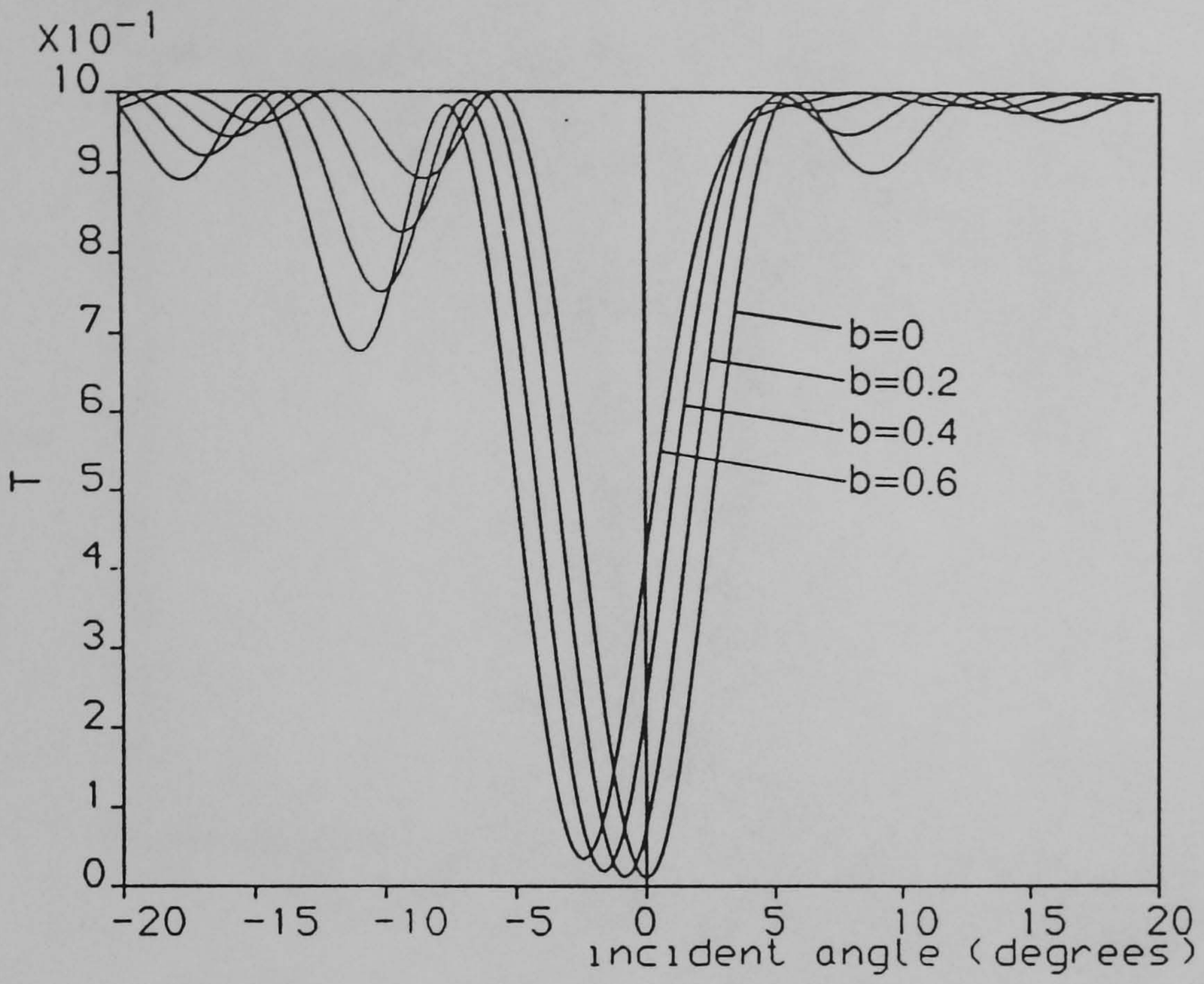

Figure 3.17: The effect of variation in b on angular response.

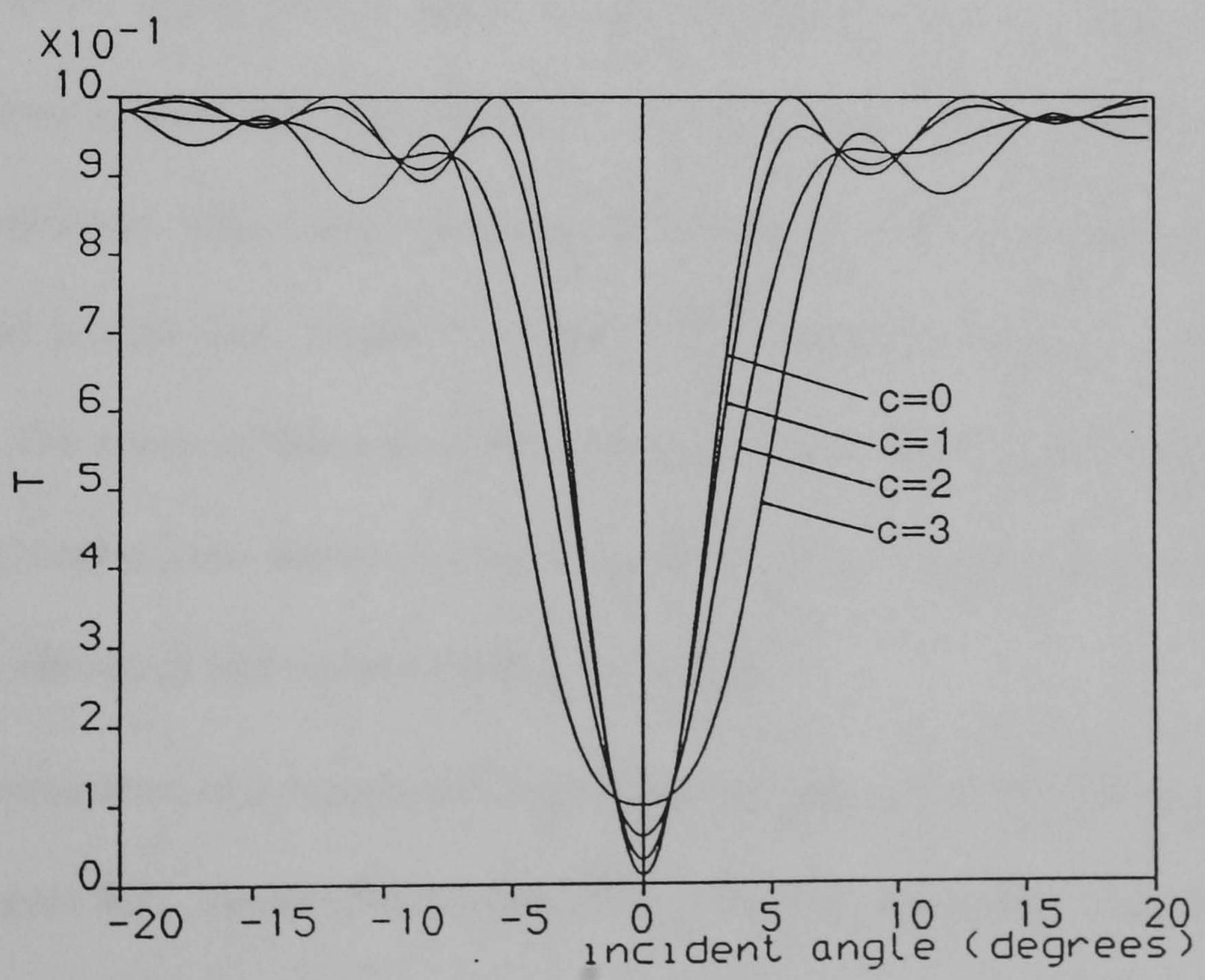

Figure 3.18: The effect of variation in c on angular response.

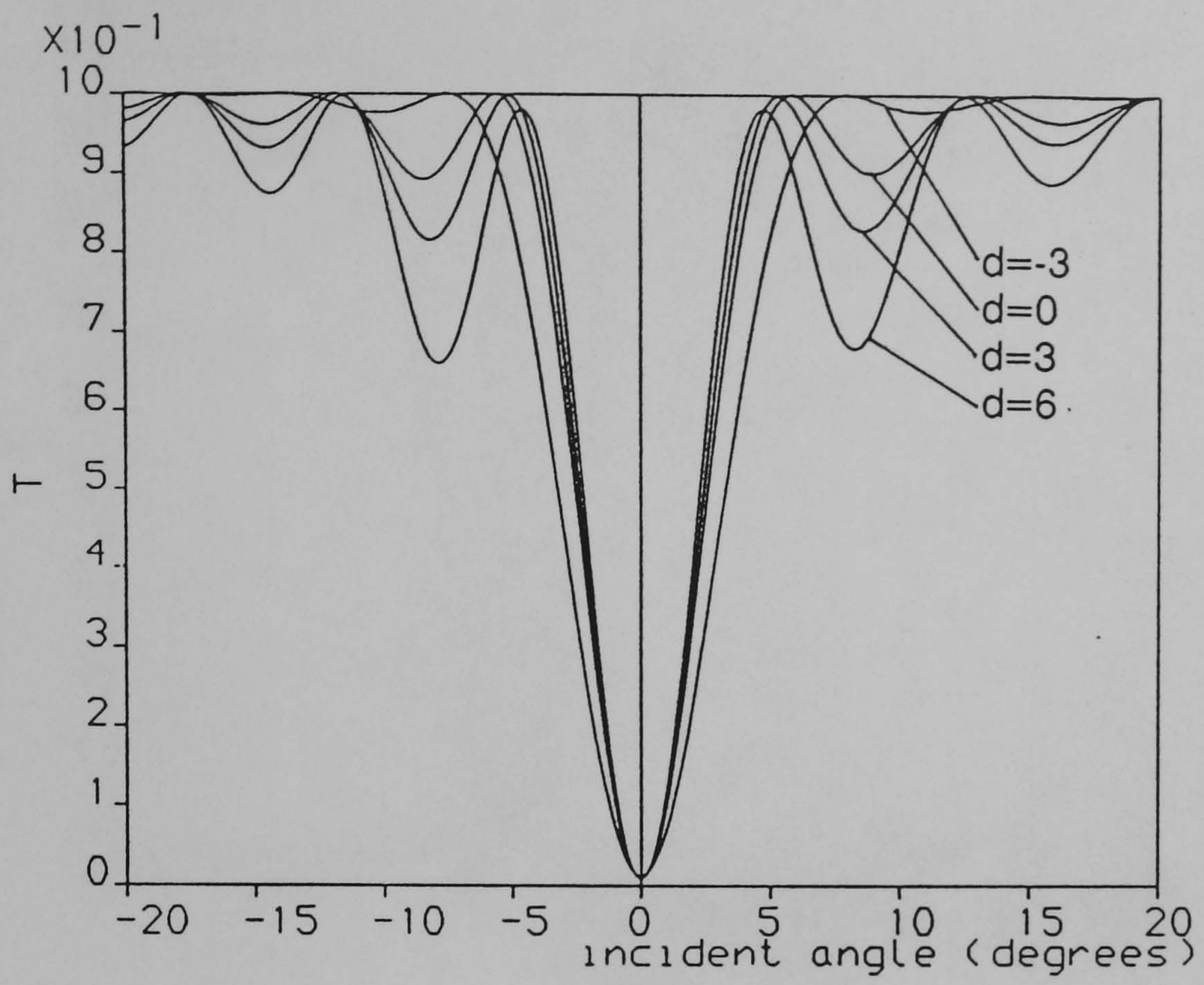

Figure 3.19: The effect of variation in d on angular response.

This is not always, the case, as shown by Au et al in much thicker (60μm) holograms in DCG. Their results show an obvious asymmetry and loss of sidelobes, implying strong quadratic variations in $K_x(x)$ and $n(x)$. Also, the non-uniformities are not consistent with simple absorption during recording, which would give an exponential modulation profile. In fact, Newell showed that in a re-processed hologram, the sense of the non-uniformities can be reversed. This indicates that processing mechanisms have a very strong effect, and may mask non-uniformities due to the effects of absorption during recording.

An angular scan of a transmission grating (hologram 22073) in 40μm gelatin is shown in figure 3.21, along with the best theoretical fit that could be obtained using the non-uniformity parameters already defined. The strong secondary peak at the second order Bragg angle is due to the combination of second order diffraction

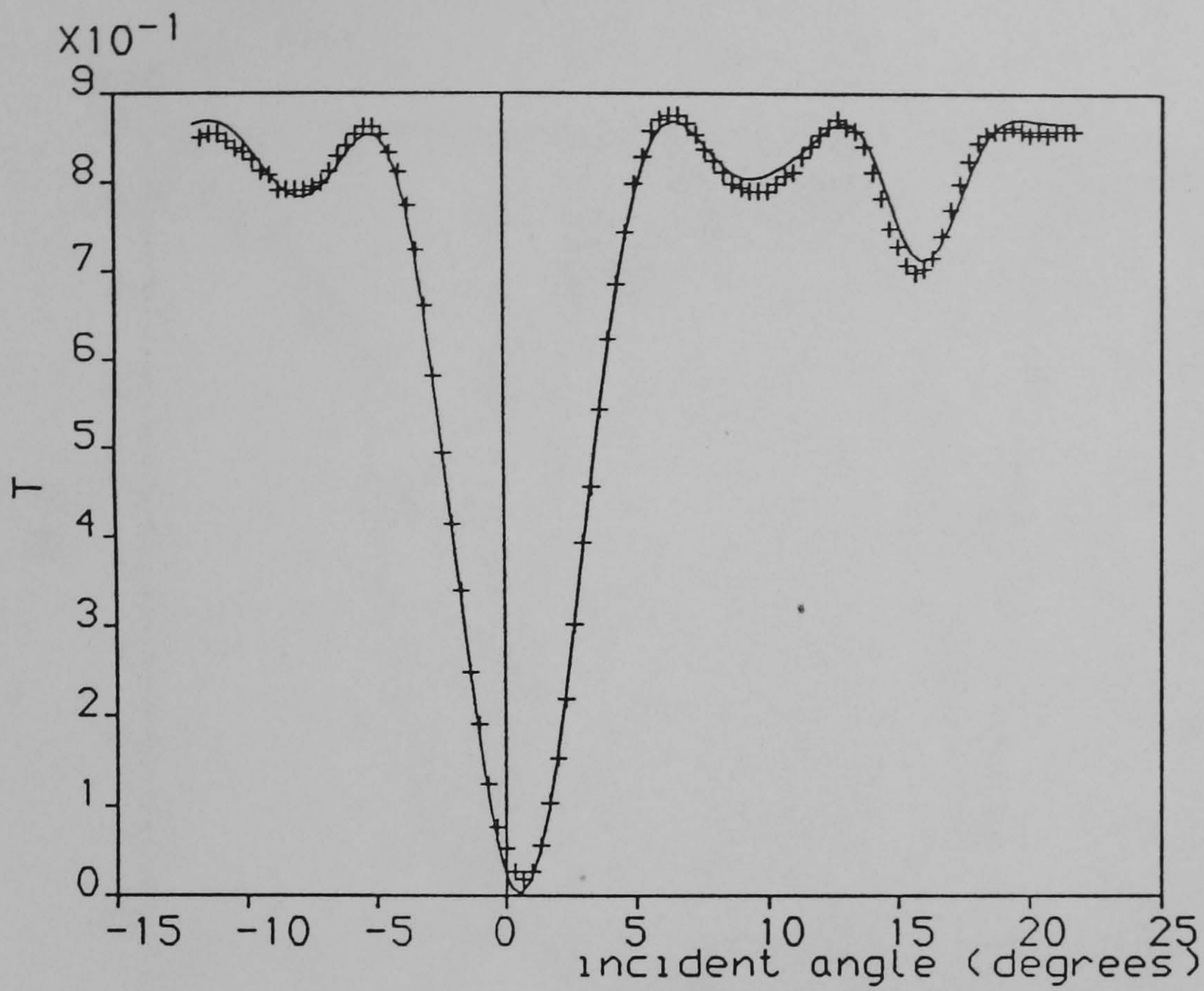

Figure 3.20: Best theoretical fit to hologram 30051, including second order diffraction, first harmonic grating and non-uniformities.

from the principle grating (amplitude 0.0055), and first order diffraction from the second harmonic grating (amplitude 0.0047). Such a strong second harmonic indicates that this hologram has been overexposed, and that the principle grating component has been considerably reduced due to severe saturation.

The non-uniformity parameters used here were $a = 0.015$, $b = 0$, $c = 4.4$ and $d = 10$. This corresponds to a small fractional variation in the grating vector, but a very large variation in index modulation. In fact, at $x' = 0.5$, modulation is about five times the average value. This confirms Newell's observations that nonuniformities are more significant in thicker gelatins. In addition, the inability to obtain a good fit indicates that a higher order polynomial is required to achieve a better fit. Such a polynomial is simple to include, but it is far from simple to

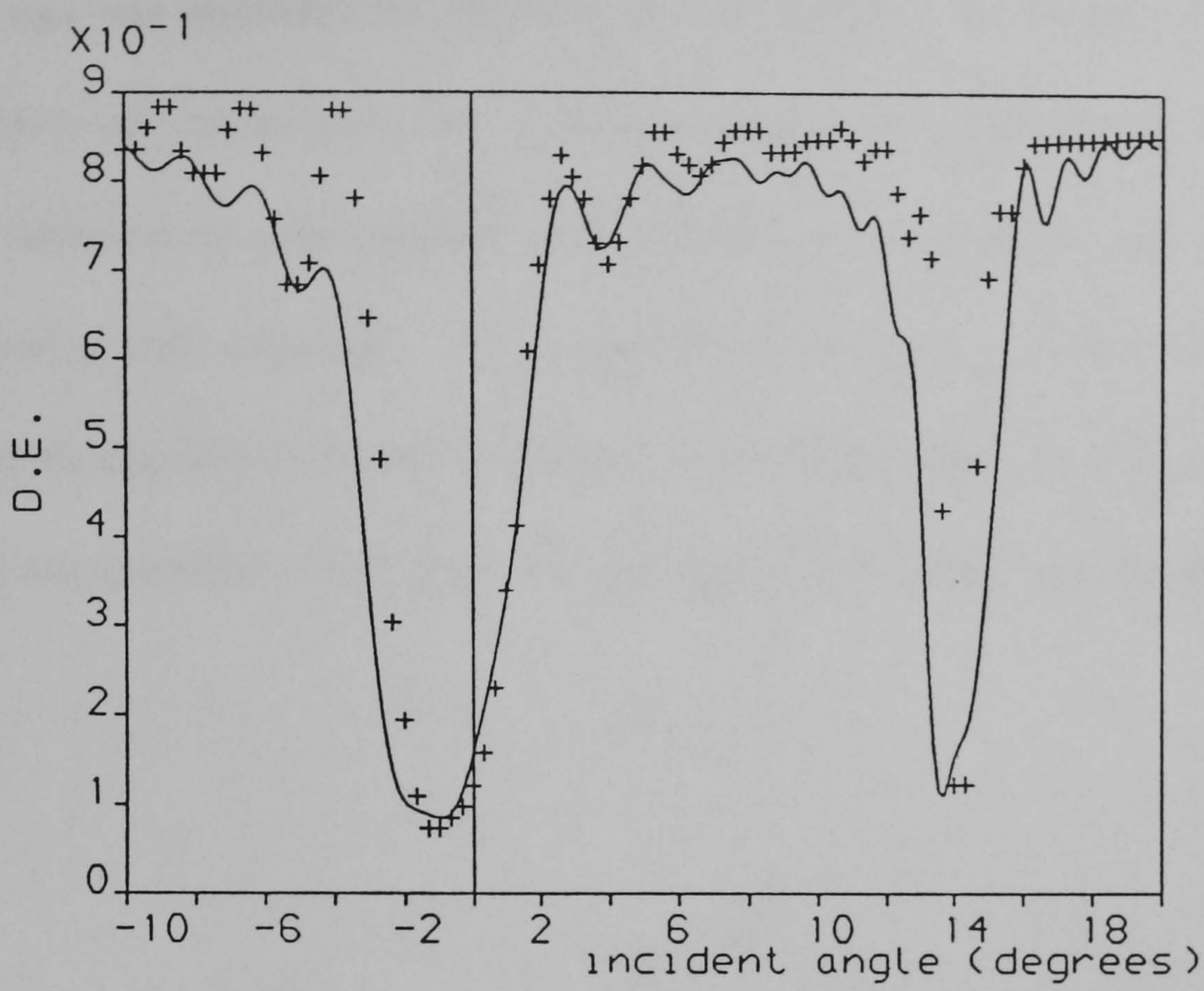

Figure 3.21: Experimental points and theoretical fit on a 40μm transmission grating.

obtain a good match with experiment when higher order terms are included. If the response of thick gelatins is to be accurately predicted in some application, it would be necessary to attempt a higher order fit. Ideally, the mechanisms behind the non-uniformities should be investigated.

3.6 Summary.

An extended coupled wave model has been developed for the computer solution of transmission holograms which includes the effects of higher diffraction orders and harmonic gratings. The effect of saturation of the index modulation was modelled with an exponential saturation description. This leads to a prediction of non-sinusoidal grating profiles containing harmonic gratings. The interaction between

these gratings was modelled successfully, supporting the saturation model.

The effects of non-uniformities in fringe spacing and refractive index modulation with depth were also included in the model, and empirical fits with experimental results were obtained. Non-uniformities in thick gelatins were found to be much more significant in thick gelatins. This is thought to be due to complex processing mechanisms which limit the transport of alcohol into the gelatin.

Chapter 4

Fan-out holograms.

Most HOE's are either simple plane gratings, such as beamsplitters and bandpass mirrors, or lenses, which have curved fringes. Both kinds of devices are usually alternatives to conventional non-diffractive optics, and they often have specific advantages, such as size, as in microlens arrays, or cost, as in head-up display mirrors, and weight. A type of HOE which is not easy to reproduce with conventional optics is one which splits a single input beam into many outputs - a fan-out device. Such devices are required for optical computing, as a method for generating large arrays of beams, and for interconnecting arrays of logic gates. It is very important that in elements of this type the overall efficiency is maximised in order to minimise the level of gain demanded from the logic devices, and that the power in each fanned-out beam is very similar, so that all logic elements respond in nearly identical fashion. Fan-out holograms may also be used in reverse, to fan-in, or combine a number of inputs into one. A typical application of this sort is to combine a number of phase-locked laser beams into one by including a

fan-in hologram as part of an external cavity arrangement.

In principle, a fan-out HOE can be produced simply by recording a hologram with the required input beam as the reference beam, and the required outputs as the composite object beam. In replay the hologram will certainly reconstruct the desired fan-out beams, but there usually are some problems. Fistly, unless the angle between the various fan-out beams is very large, it will be found that efficiency will be limited. Also, the relative weightings in the various beam powers will not generally be preserved. And finally, additional diffracted beams will be generated which may be unwanted, and constitute noise.

Before discussing possible sources of these problems, it should be noted that fan-out HOE's can be made in two ways. The first, in which all beams are present simultaneously during recording, is termed *coherent* recording because the object beams are free to coherently interfere with each other and generate extra gratings. The second, in which multiple exposures are made, each of which involves only the reference beam and one of the object beams, is termed , *incoherent* recording because there is no coherent relationship between the object beams used to create the hologram.

It may seem at first sight that the coherent method is bound to cause problems due to the unwanted additional gratings that are recorded, which must in turn produce unwanted diffracted beams. Also it would appear that incoherent recording should avoid these problems. However, in this study, many experiments in DCG using both methods and a variety of degrees of fan-out in different arrangements, and recorded in different thicknesses of gelatin, have been carried out,

and they show that the situation is not so simple. There is no clear division in results between the coherent and incoherent methods, and there is no simple way to achieve both high efficiency and faithful reproduction of beams even at low degrees of fan-out. It was therefore found to be necessary to return to the coupled-wave theory with the intention of extending it to model fan-out holograms.

4.1 The coupled wave model for fan-out holograms.

Su and Gaylord [SU75] and Case [CAS76] have investigated the special case of diffraction from gratings of arbitrary profile, which may be considered as a superposition of harmonic gratings. However, since we are not free to choose the directions of the individual beams in such a case, we will not consider this structure a fan-out hologram. Kowarschik [KOW78], Case [CAS75] and Solymar [SOL77] have considered the coupled wave theory for transmission holograms containing multiple arbitrary gratings with a common Bragg angle, with Solymar extending the theory to the 2-D, N-wave case. Alferness and Case studied the double exposure case using the grating decomposition approach [ALF75], and Kostuk [KOS86] and Kowarschik [KOW78] have investigated the multiple reflection grating case using coupled wave theory.

The coupled-wave computer model presented in chapter 3 was made as general as possible by the use of a coupling matrix. This can be entered manually by the operator, along with the desired recording waves, and the strengths of the gratings

formed, so that in principle the model is capable of analysing a multi-grating hologram, where the gratings are not necessarily harmonics. Slinger and Solymar have looked at the two-grating case specifically to investigate the spurious diffracted beams which emerge from such an arrangement [SLI86]. Here the technique is generalised by the inclusion of a coupling matrix and a method for deriving the diffracted beams.

To find a general method for defining allowed diffracted directions from a multiple-grating hologram, we begin with the simplest two-grating case. This implies that the gratings are recorded sequentially, and no grating is recorded between the object waves (i.e. this is the incoherent recording case). We will use the **K**-closure method to visualise the diffracted beams for its graphic simplicity, but within the computer, diffraction is modelled accurately by equation 3.19. The three principle waves involved are shown in figure 4.1 On replay, as Slinger and Solymar point out, the newly generated waves with wave vectors $\mathbf{k}_1$ and $\mathbf{k}_2$ may each interact with the grating corresponding to the other, if the Bragg responses of the two gratings overlap. This 'double diffraction' gives rise to two new waves, $\mathbf{k}_3$ and $\mathbf{k}_4$, not present at recording (figure 4.2). If we calculate the direction of $\mathbf{k}_3$, we get

$$\mathbf{k}_3 = \mathbf{k}_0 - \mathbf{K}_1 + \mathbf{K}_2 \tag{4.1}$$

If instead the hologram is recorded coherently, a third grating $\mathbf{K}_3$ will be generated between $\mathbf{k}_1$ and $\mathbf{k}_2$. A parallelogram may be formed between the ends of the wave vectors, showing that $\mathbf{k}_3$ is in the same direction as would be produced by a cross-grating between the object waves. Similarly, $\mathbf{k}_4$ would be produced directly by the

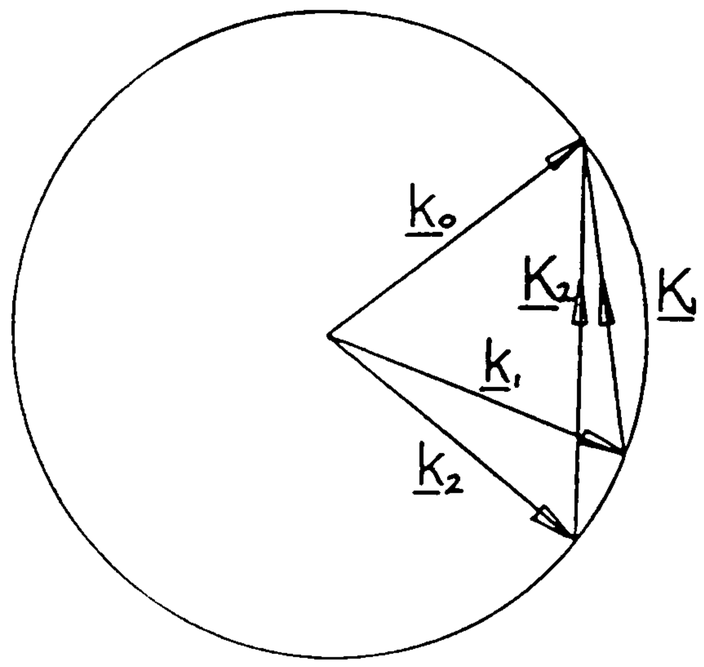

Figure 4.1: Principle wave directions in the 2 grating hologram.

cross-grating, but would be the opposite sign diffraction order to $\mathbf{k}_3$. Therefore, the *same* waves can be generated in both the incoherent and coherent cases. Even in this ideal linear holographic medium, unwanted waves will be generated due to the effects of off-Bragg diffraction. The following section discusses the importance of these waves and their dependence on experimental parameters.

4.2 Fan-out to two.

Fan-out to two holograms may be represented using the extended model by including the five wave directions, and calculating the appropriate coupling matrix. Since there are three gratings, the matrix subscripts must become arbitrary to some extent. We will use the subscripts chosen above to represent row and col-

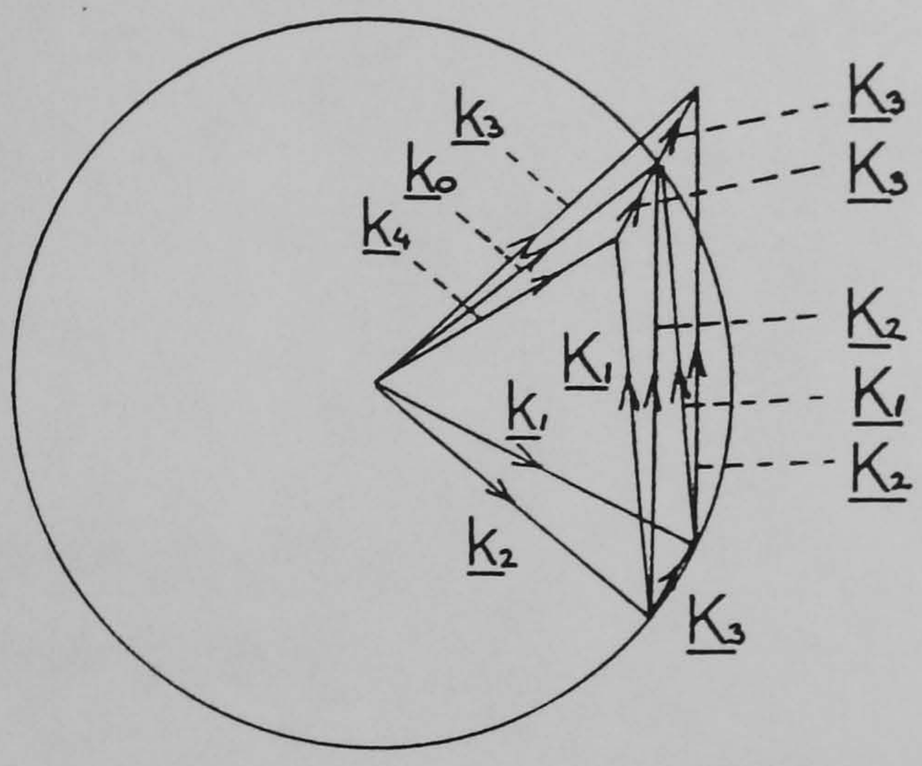

Figure 4.2: Principle and first pair of spurious waves in a fan-out to 2 hologram.

umn numbers, and, by looking at the diagram of all the waves (figure 4.2), and considering the coupling interactions, we get the coupling matrix

$$C = \begin{bmatrix} 0 & \kappa_1 & \kappa_2 & \kappa_3 & \kappa_3 \\ \kappa_1 & 0 & \kappa_3 & \kappa_2 & 0 \\ \kappa_2 & \kappa_3 & 0 & 0 & \kappa_1 \\ \kappa_3 & \kappa_2 & 0 & 0 & 0 \\ \kappa_3 & 0 & \kappa_1 & 0 & 0 \end{bmatrix}. \tag{4.2}$$

The variation of diffraction efficiencies of the four output waves can now be studied.

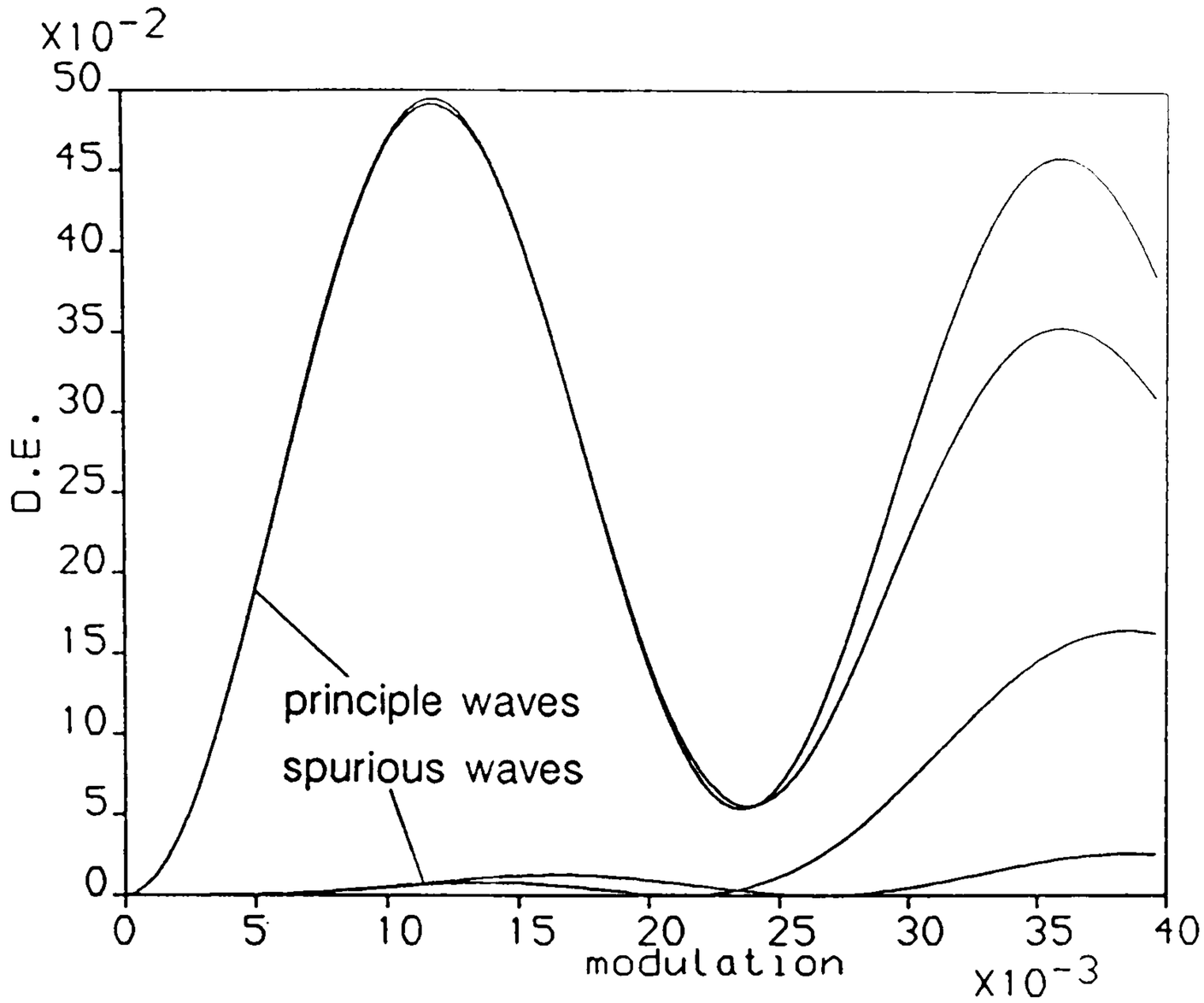

Figure 4.3: Diffraction efficiency vs. index modulation, Fan-out to 2, $\delta = 8°$.

4.2.1 Incoherent recording.

Fistly,we will look at the case where $\kappa_1 = \kappa_2$ and $\kappa_3 = 0$. This would correspond to a double exposure (incoherently recorded) hologram in a linear recording medium. The reference beam is held at 30° to the plate normal, and the average angle of the diffracted principle fan-out beams is kept at 0° in all cases. We allow the angle between adjacent fan-out beams, δ, to be adjusted to investigate its effect. The gelatin thickness is chosen to be 15μm and the wavelength is 514.5nm (typical experimental parameters). Diffraction efficiencies are plotted versus index modulation for three different values of δ, equal to 8°, 2° and 0.2°, in figures 4.3 to 4.5.

From these figures, it can be seen that the achievable sum diffraction efficiency of the principle output waves becomes limited when the angle between them drops

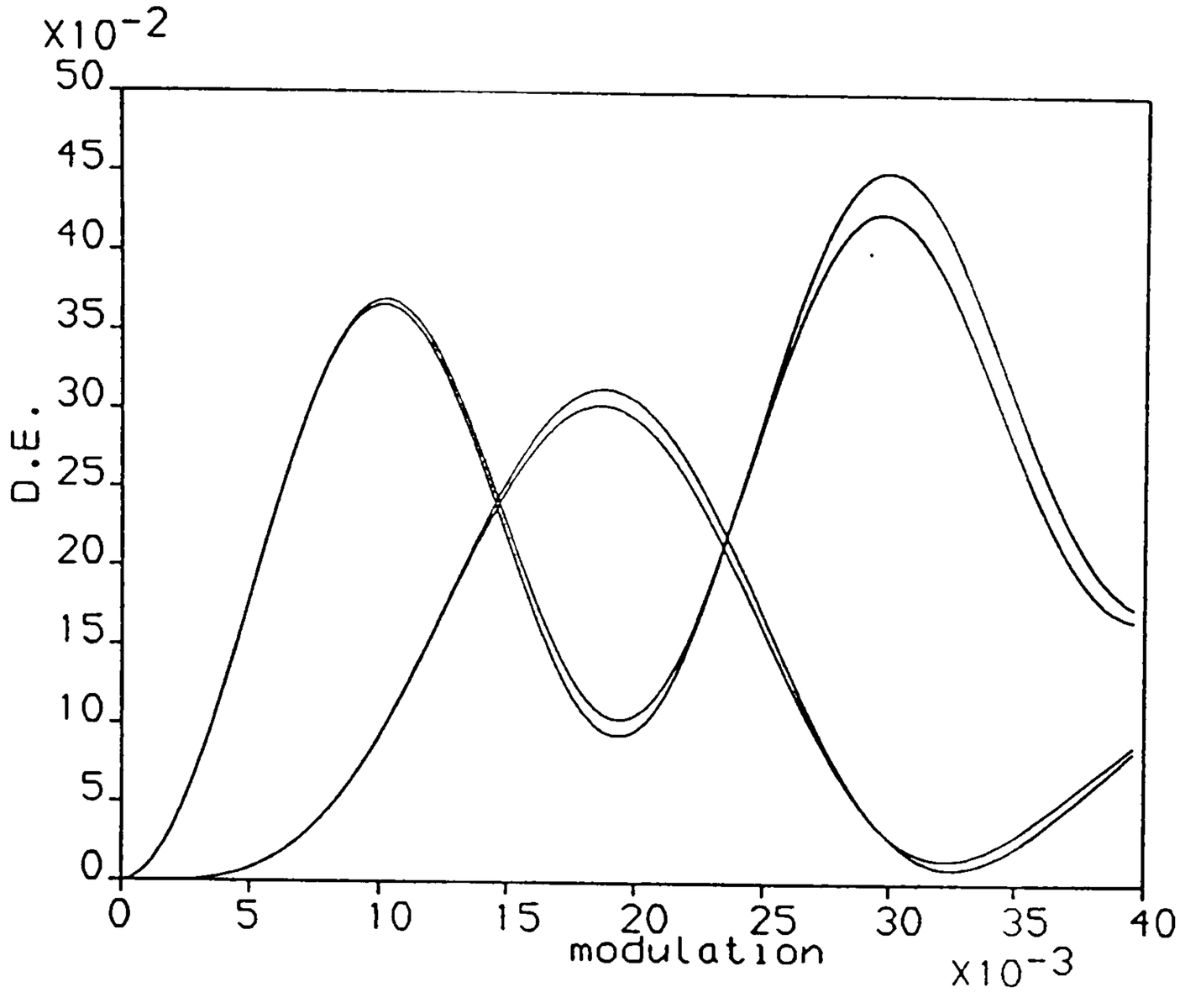

Figure 4.4: Diffraction efficiency vs. index modulation, $\delta = 2°$.

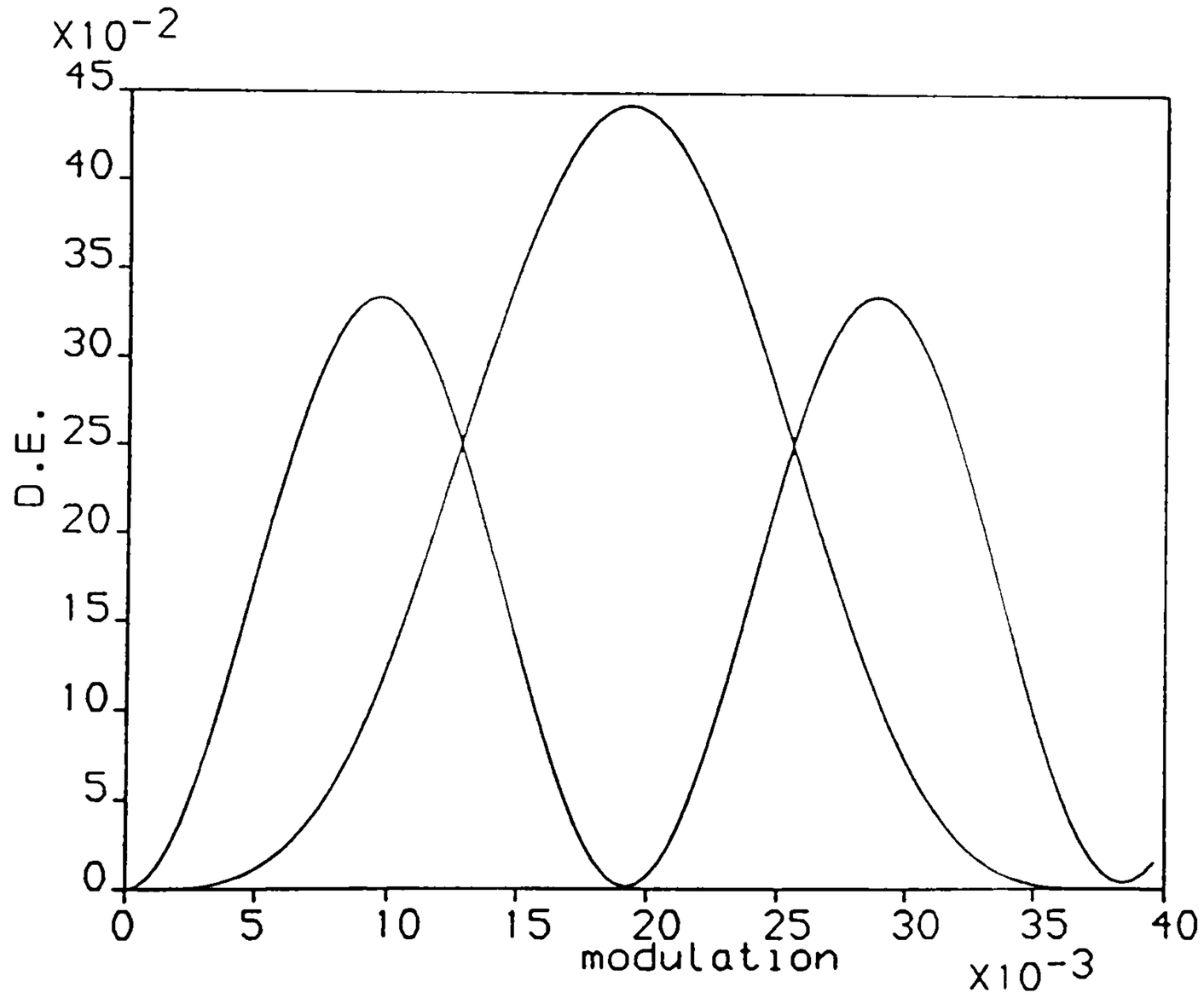

Figure 4.5: Diffraction efficiency vs. index modulation, $\delta = 0.2°$.

below a few degrees. It is also apparent that there is a slight imbalance in their powers which is at a maximum relative to total diffracted power in figure 4.4 where δ is an intermediate value. This intermediate value places a grating approximately on the maximum slope of the angular response curve of an adjacent grating. Therefore, it appears that fan-out effects are strongly dependent on the size of δ relative to the angular acceptance width, $\Delta\theta_B$, of a single grating. We can characterise the different regimes of δ in terms of the ratio $\delta/\Delta\theta_B$. The small δ regime corresponds to $\delta/\Delta\theta_B < 0.1$. In the large δ regime, that is, $\delta/\Delta\theta_B \geq 1$, effciency may approach 100%. For a 15μm thick hologram at 514nm, this means that δ must be greater than about 4.5°.

When δ is very small, it appears that almost 90% of the incident power can be coupled into $\boldsymbol{k}_3$ and $\boldsymbol{k}_4$. In fact, as shown below, if we include higher order multiple interactions (such as one involving $\boldsymbol{K}_1$, $\boldsymbol{K}_2$ and then $\boldsymbol{K}_1$ again) less power will be diverted into $\boldsymbol{k}_3$ and $\boldsymbol{k}_4$ and a significant amount will be diverted into the higher order interactions. However, power in the principle beams is not significantly affected by their inclusion until higher modulations than those needed for the first maximum are reached.

Inclusion of waves $\boldsymbol{k}_5$ and $\boldsymbol{k}_6$ as illustrated in figure 4.6 results in less than a 1% change in diffraction efficiency at the first peak for δ values under 0.5° or so, and negligible changes for larger δ. Inclusion of the next two waves derived in the same way has negligible effects even on δ values of 0.01°. Inclusion of more than the 5 waves $\mathbf{k_0}$ to $\mathbf{k_4}$ can be seen to have little effect on the results in the region up to the first efficiency peaks. This is likely to be the region in which we operate,

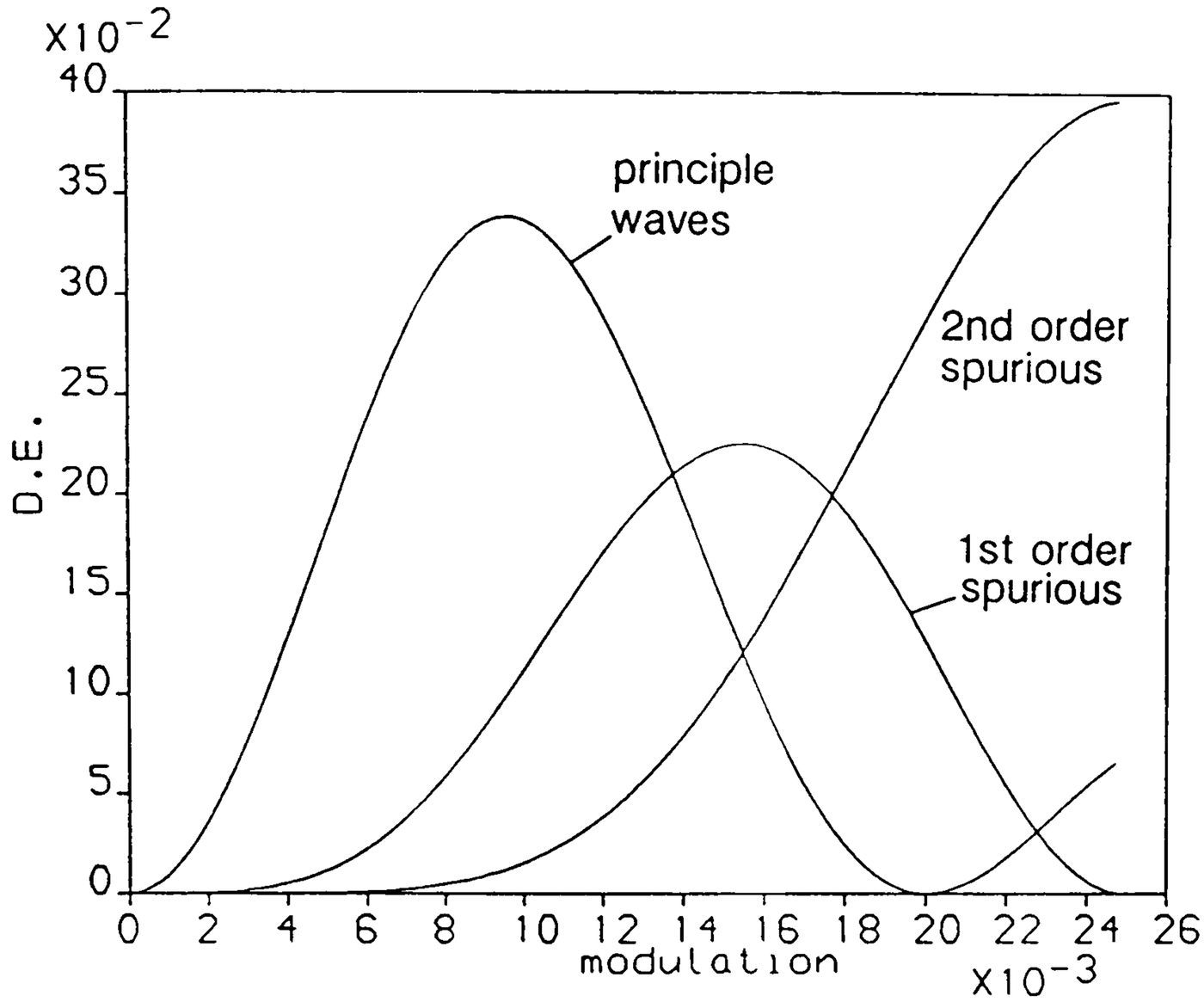

Figure 4.6: Inclusion of second order spurious waves k_5 and k_6.

since uniformity is best here, and we are generally limited in the modulation we can achieve by saturation. Total efficiency of the principle waves approaches 68% as δ decreases. This small δ region is of importance because the powers in the principle beams are very nearly equal.

An important feature which is illustrated by these graphs and graphs relating to higher levels of fan-out is the amount of index modulation required to reach maximum diffraction efficiency. It can be seen from the previous graphs that the modulation per grating that is needed is about 0.0012. The modulation required to reach the first maximum for the corresponding single grating is 0.017. It does not follow that only half the modulation is required per grating if there are two gratings present. In fact, as Case showed [CAS75], the *total* modulation required for N gratings is $\sqrt{N}$ times the single grating value. The extensions to the theory

that have been added here mean that this result is not exact, but it may be used as a guide to the modulation required.

4.2.2 Coherent recording.

Now we consider the effect of a non-zero κ_3. This occurs principally when the gratings are recorded in a single exposure with all recording beams present simultaneously (coherent recording). In a linear material, the grating modulation is proportional to $A_i A_j^*$, where A_i and A_j are the complex amplitudes of the recording waves. This dependence means that the amplitude of gratings recorded between two object waves may be controlled relative to gratings recorded between the reference and an object wave by varying the ratio of reference to average total object amplitude at the recording plane. If this ratio is made very large, the situation approaches that of the incoherent recording case. Unfortunately, an additional factor to be considered in a real experiment is that a high beam ratio leads, to some degree, to a build up of a DC refractive index due to the low modulation of fringes between a strong and a weak beam. Therefore, saturation of the refractive index is liable to occur before a sufficiently strong index profile is recorded. Saturation also causes additional problems which will be described in section 4.4.

Figures 4.7 and 4.8 show the dependence of diffraction efficiency on index modulation for a coherently recorded fan-out to two device as already discussed, with $\delta = 0.02°$ and $\delta = 0.2°$ respectively. The amplitude beam ratio is $\sqrt{2}$, corresponding to a total irradiance beam ratio of one. A total of 9 waves have been included to ensure good accuracy in situations when coupling to higher orders

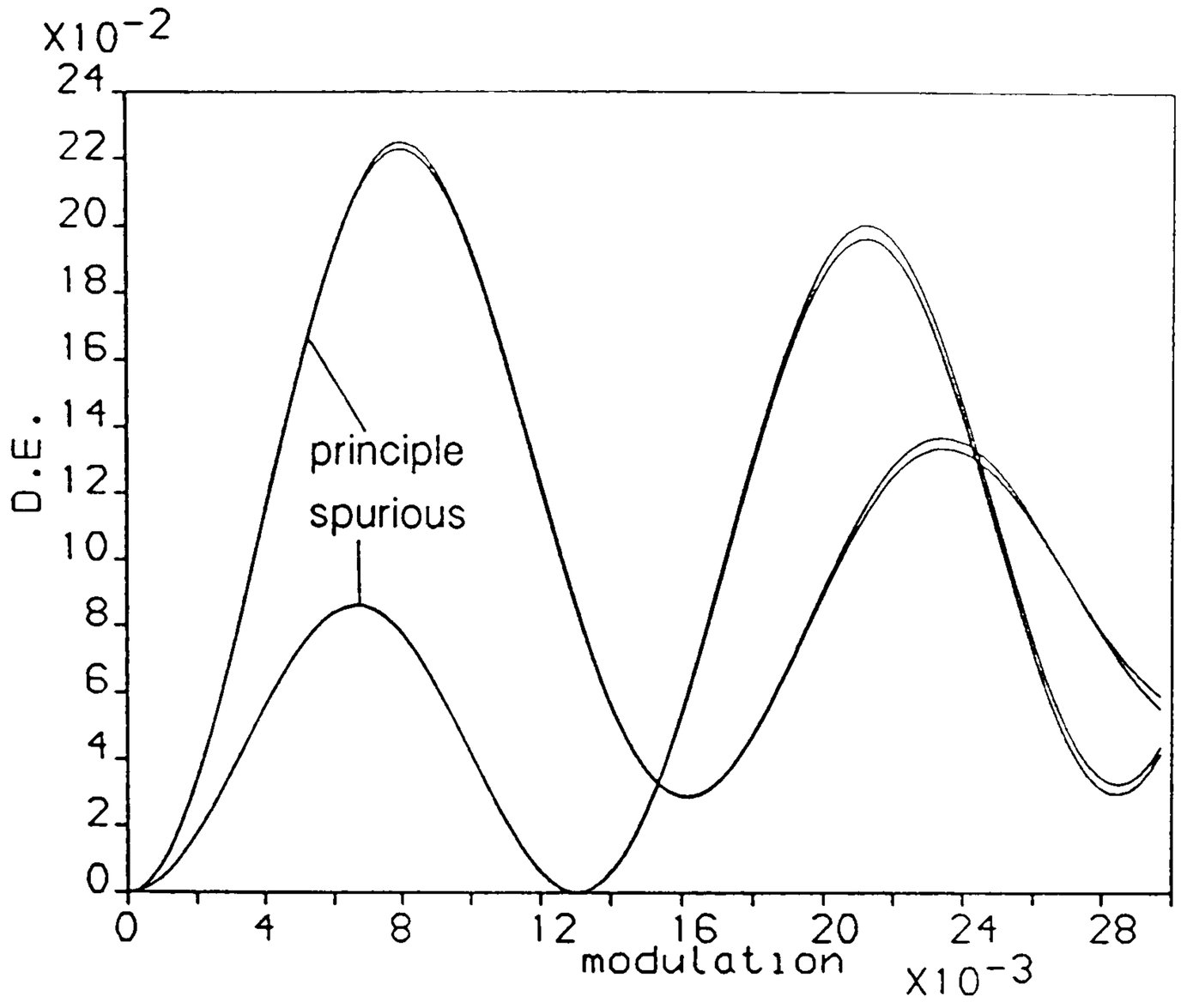

Figure 4.7: D.E. vs. Δn of a fan-out to 2 hologram. Beam ratio= 1, $\delta = 0.02°$.

is significant. It can be seen that the effect of the newly introduced cross-gratings is to reduce total efficiency to around 44%, and to unbalance the beam weightings. This imbalance is reduced by using smaller values of δ. Figures 4.9 and 4.10 show results for a higher irradiance beam ratio of 10. Efficiency has increased to 64% and uniformity of beam powers has improved. These results show that both overall efficiency and uniformity of diffracted powers in the small δ regime are best when coupling via the cross-gratings is a minimum.

4.3 Fan-out to higher numbers.

There is a great interest in the field of optical digital computing in methods of producing large arrays of focussing beams to act as a 'power supply' for 2-D

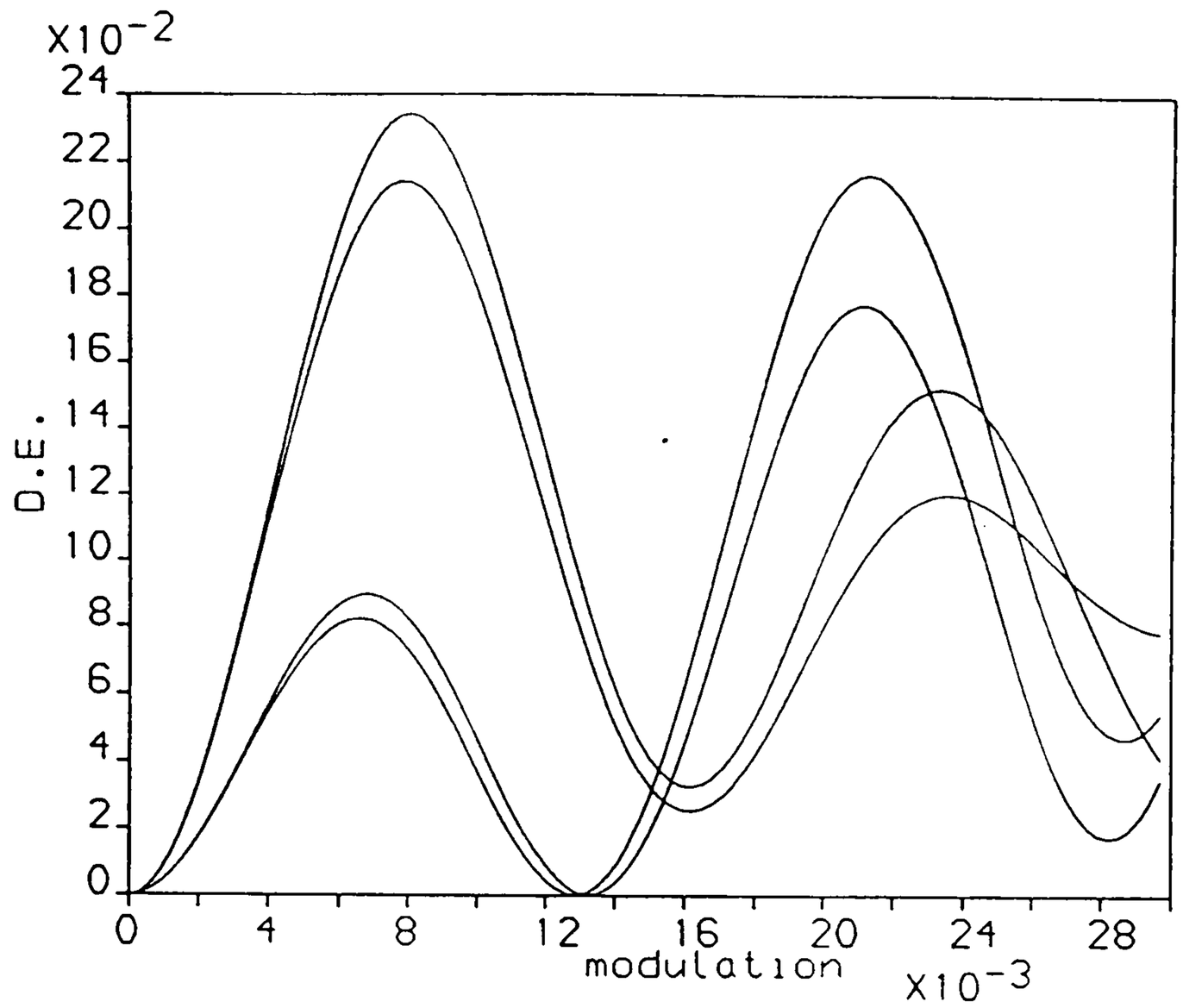

Figure 4.8: D.E. vs. Δn of a fan-out to 2 hologram. Beam ratio= 1, $\delta = 0.2°$.

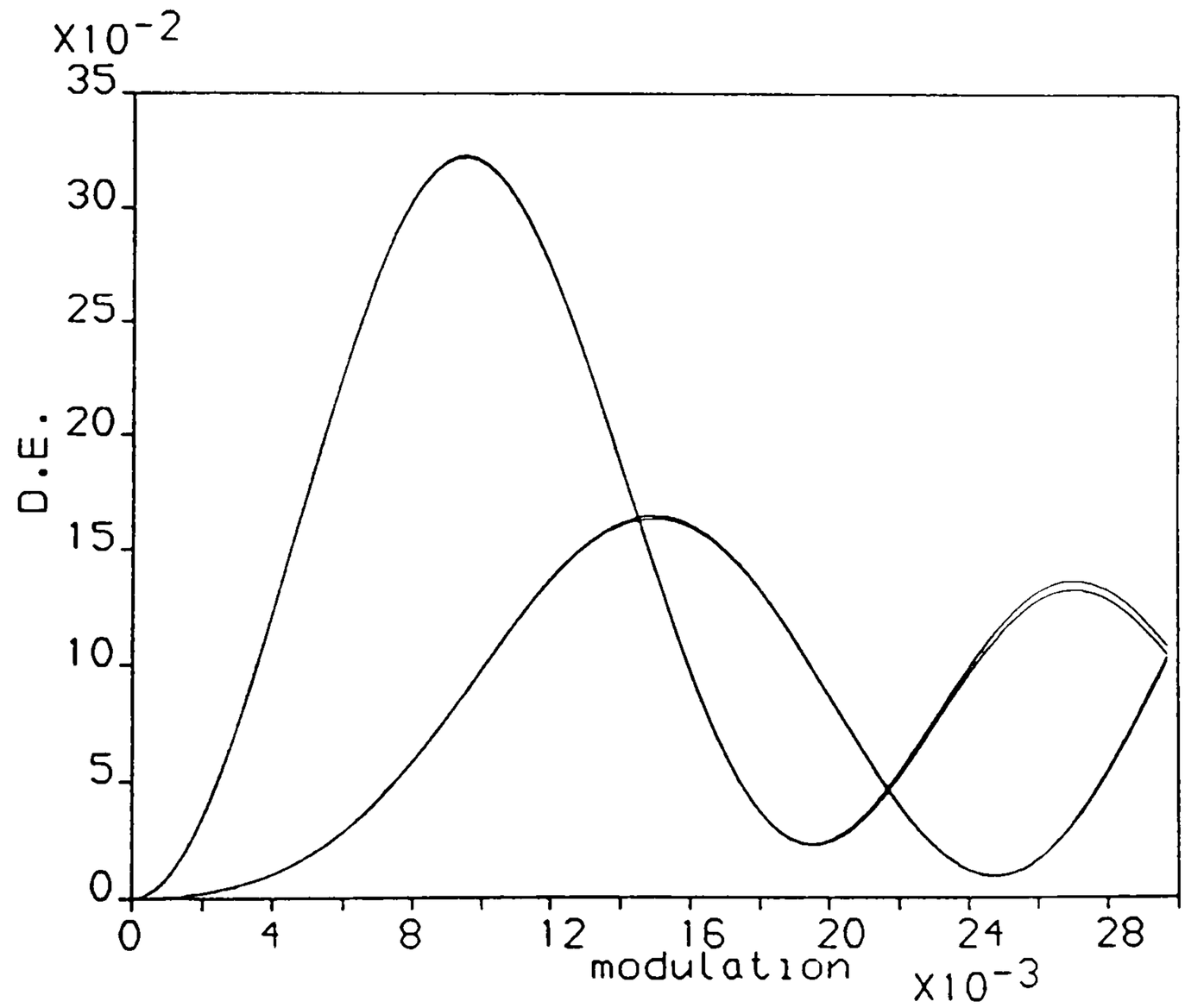

Figure 4.9: D.E. vs. Δn of a fan-out to 2 hologram. Beam ratio= 10, $\delta = 0.02°$.

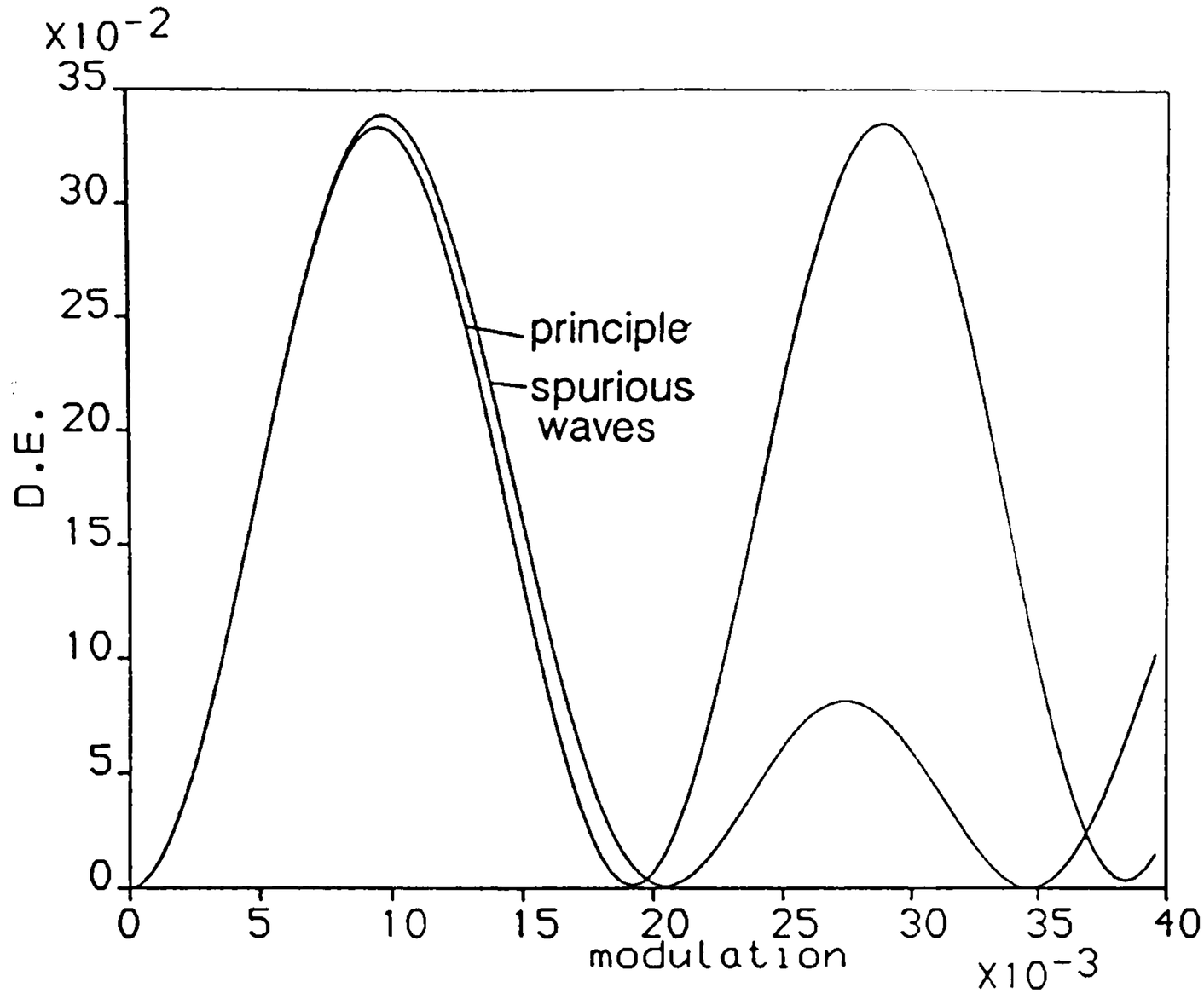

Figure 4.10: D.E. vs. Δn of a fan-out to 2 hologram. Beam ratio= 10, $\delta = 0.2°$.

arrays of logical devices. Such arrays of beams are not trivial to generate by conventional optics, whereas holographic devices in principle offer the possibility of array generation with relative ease and flexibility of fabrication. There are two principle holographic approaches to this problem. Firstly, arrays of individual lenslets can be recorded. This allows flexibility with high efficiency and good uniformity, and with an automated exposure system very large numbers of lenses may be included in an array. This technique will be discussed in chapter 6. The principle drawback with this method is that in order to obtain equal power in each focal spot, the array must be uniformly illuminated. This is not easy to do efficiently, since most laser beams do not have a uniform irradiance profile, and it is not a simple process to convert, say, a gaussian profile beam into a uniform, collimated beam.

The second holographic approach is to use a fan-out hologram which generates an array of collimated beams exiting at various angles from one collimated input beam, and use a single lens to convert these beams into an array of focussing beams. This avoids the need to supply a uniform illumination as an input. An unexpanded laser beam may be used as the input, producing an array of beams of the same profile. An interesting property of a device used in this way with a lens to produce tha focal spots, is that the focal spot diameter may be varied by varying the diameter of the input beam. This is because the diffraction-limited focal spot size is inversely proportional to the collimated beam diameter entering the lens.

The other potential application area in optical computing research for fan-out devices is that of array interconnects. A general array interconnect may be required to connect output signals form each pixel in one array to any number of pixels in the next logic array. Even digital image filtering using operations only on nearest neighbour pixels needs a minimum fan-out level of four. Therefore, in general, higher degrees of fan-out are of great interest in digital optical computing research.

4.3.1 Fan-out to three.

We begin by extending the investigation to a fan-out level of three. Theoretical results showing diffraction efficiency against δ are presented for four ratios of $\Delta n_p/\Delta n_c$ in figures 4.11 to 4.14, where Δn_p is the amplitude of the principle gratings, and Δn_c is the amplitude of the cross-gratings which directly connect

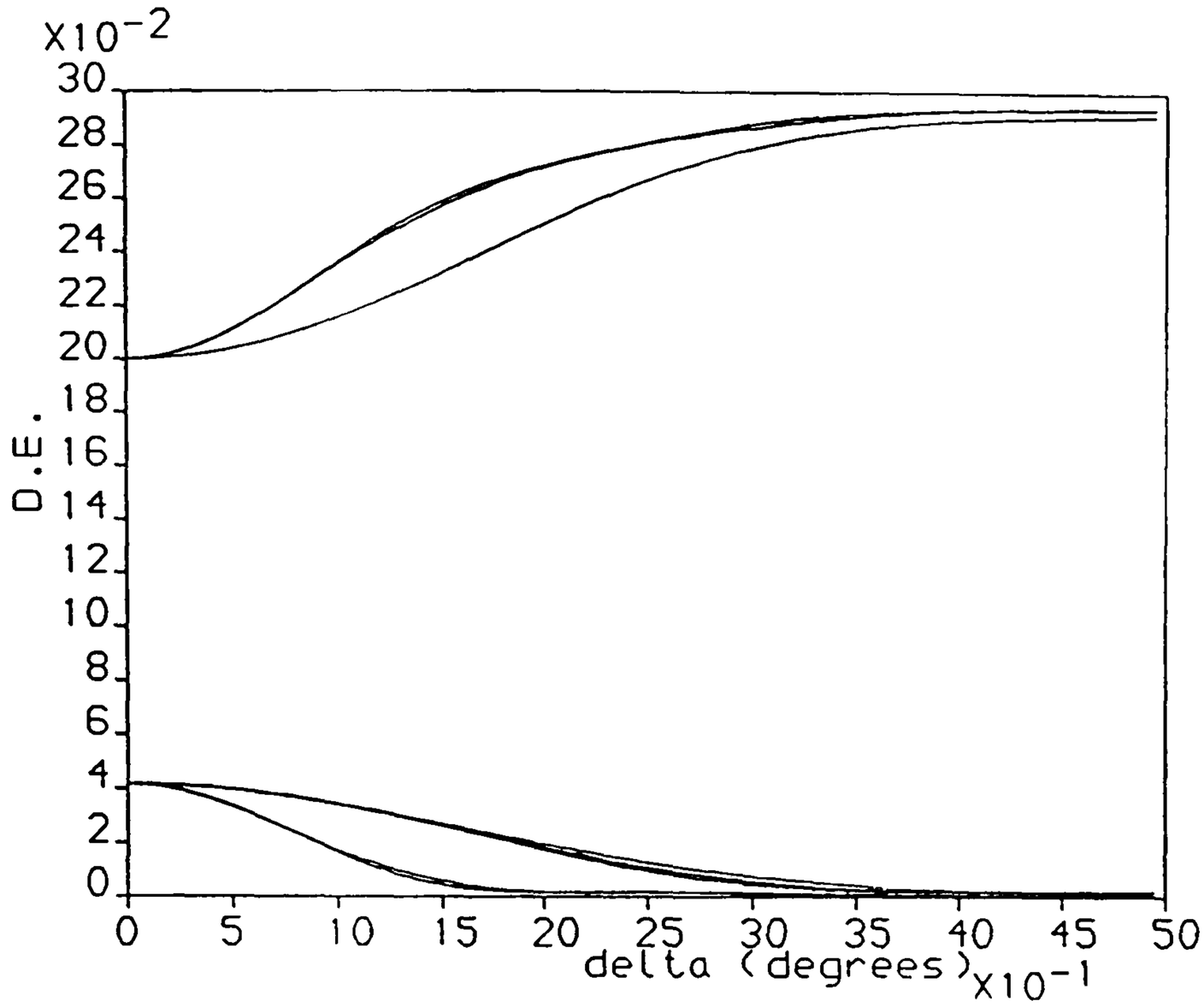

Figure 4.11: Fan-out to 3 D.E. versus δ. $\Delta n_p/\Delta n_c = \infty$.

each pair of principle diffracted waves. They include the case where $\Delta n_c = 0$, corresponding to the incoherent recording case. The parameters which are taken to be constant in these and following results are - thickness $d = 15\mu$m, wavelength $\lambda = 514.5$nm and reference beam angle $\theta_r = 50°$ to the plate normal. The average object beam angle is 0°. Δn_p is set at 0.0072 in the fan-out to three analysis because this is the value which gives the highest efficiency with $\delta \approx 0$. Generally efficiency can be close to 100% at large δ's and slightly greater Δn_p. The spurious orders are also given in these results, and are always the lower set of curves.

It can be seen that as in the fan-out to two case, highest efficiency is achieved at the highest δ values, and best uniformity occurs at δ close to zero when there are no cross-gratings. The presence of cross-gratings severely limits the region of good uniformity near $\delta = 0$. Total efficiency in fact reaches in excess of 99% at

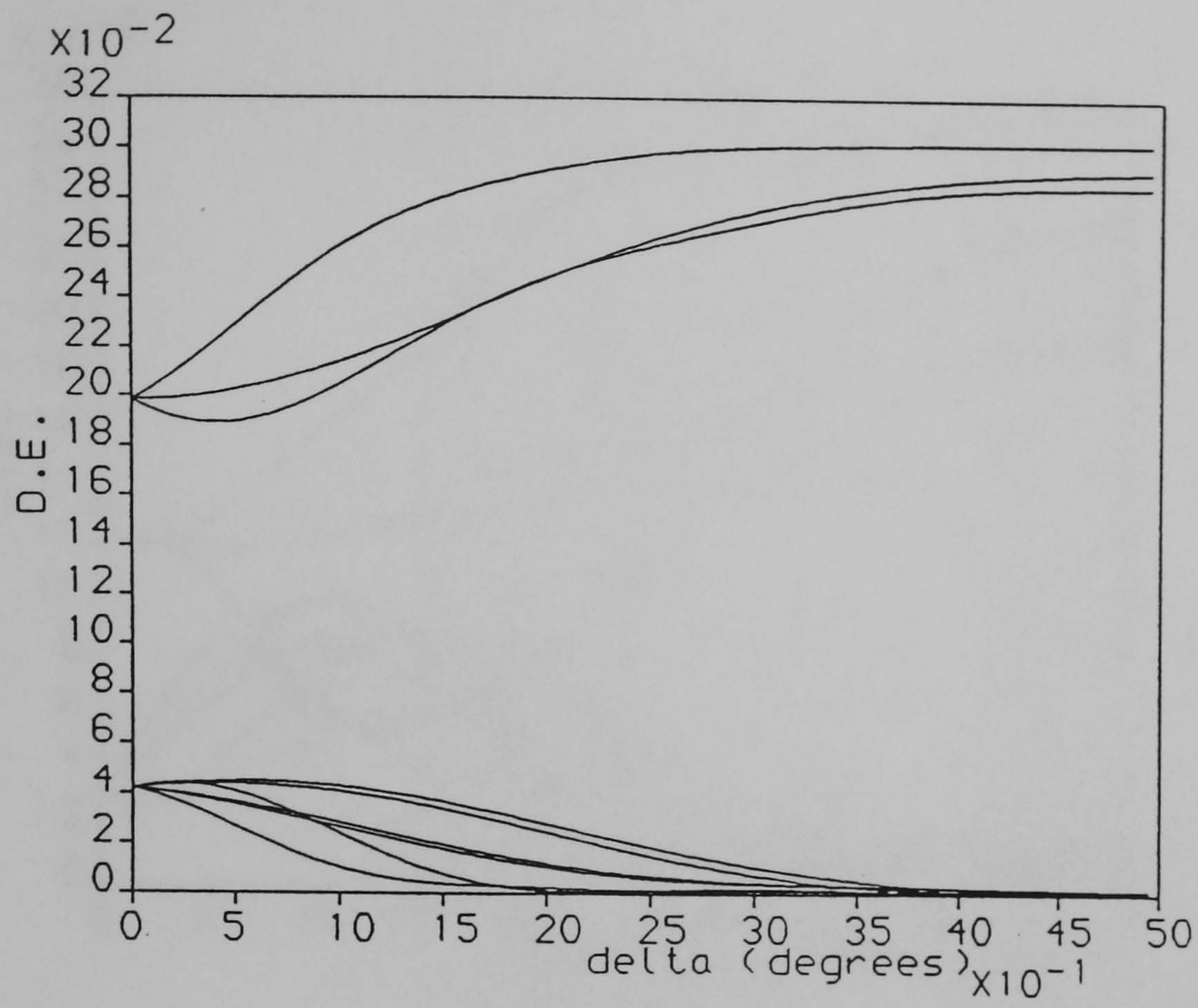

Figure 4.12: Fan-out to 3 D.E. versus δ. $\Delta n_p/\Delta n_c = 10$.

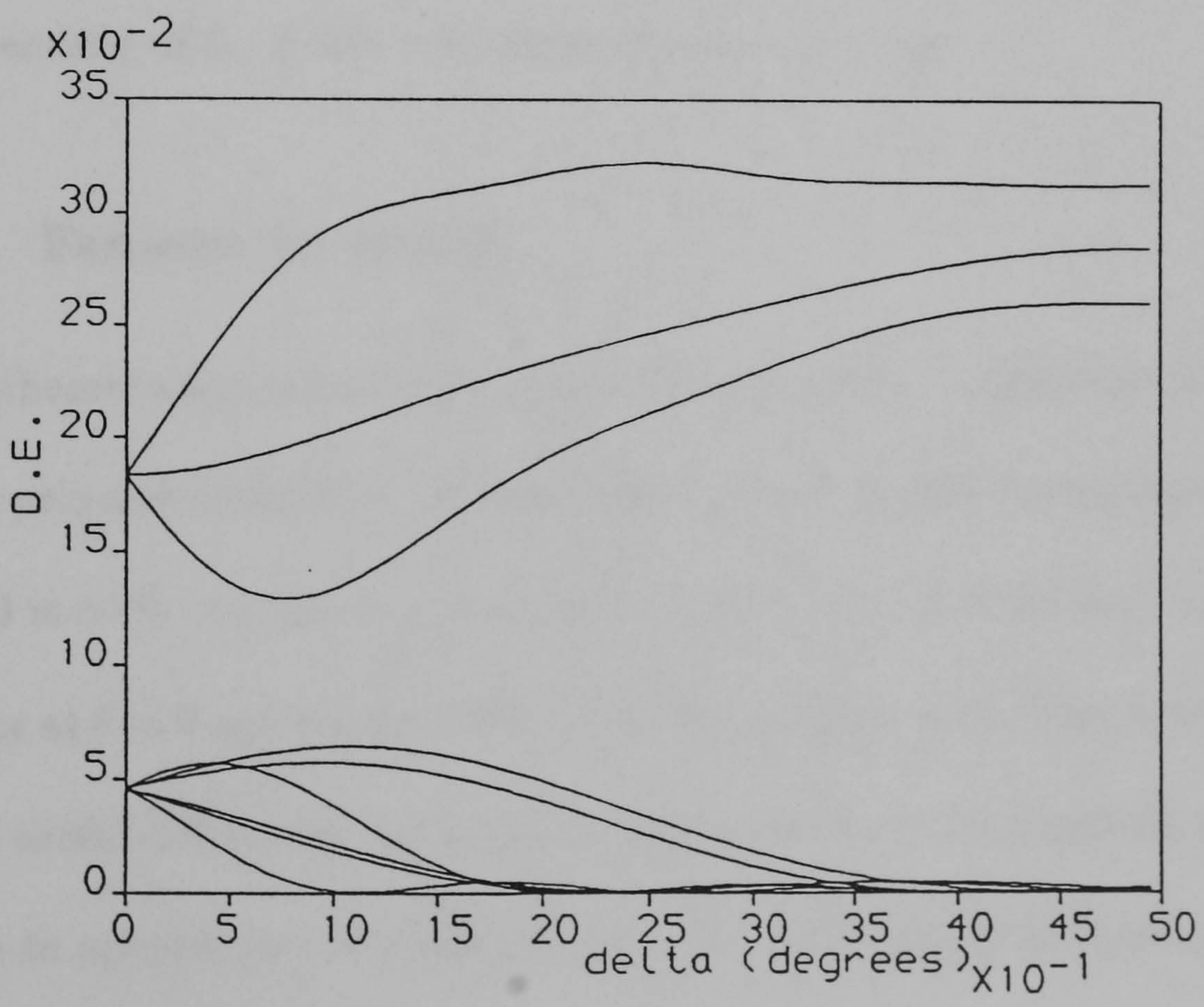

Figure 4.13: Fan-out to 3 D.E. versus δ. $\Delta n_p/\Delta n_c = 3$.

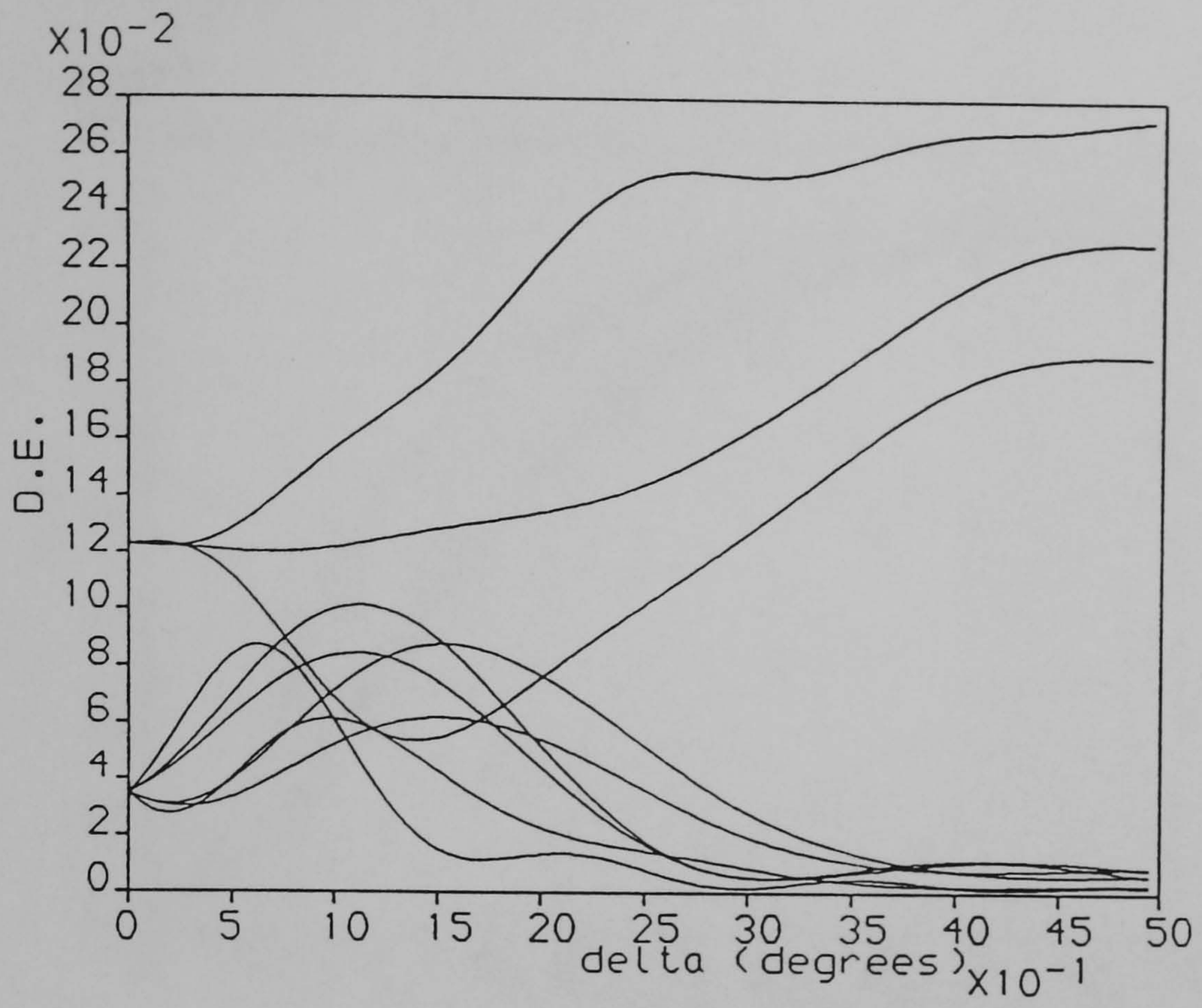

Figure 4.14: Fan-out to 3 D.E. versus δ. $\Delta n_p/\Delta n_c = 1$.

large δ for $\Delta n_c \approx 0$. Total efficiency at low δ is around 60% for weak Δn_c. This is independent of θ_r, d and λ for a great range of values.

4.3.2 Fan-out to many.

Similar theoretical results for fan-out to four are given in figures 4.15 to 4.18. Only the four principle diffracted waves are represented. In this case maximum efficiency at $\delta \approx 0$ is 56%. As the degree of fan-out increases, it was found that maximum efficiency at $\delta \approx 0$ approaches 50%, as shown in figure 4.19. This is places an upper limit on useful diffraction efficiency for high level fan-out holograms, assuming that we have to operate in the small δ regime to achieve good uniformity.

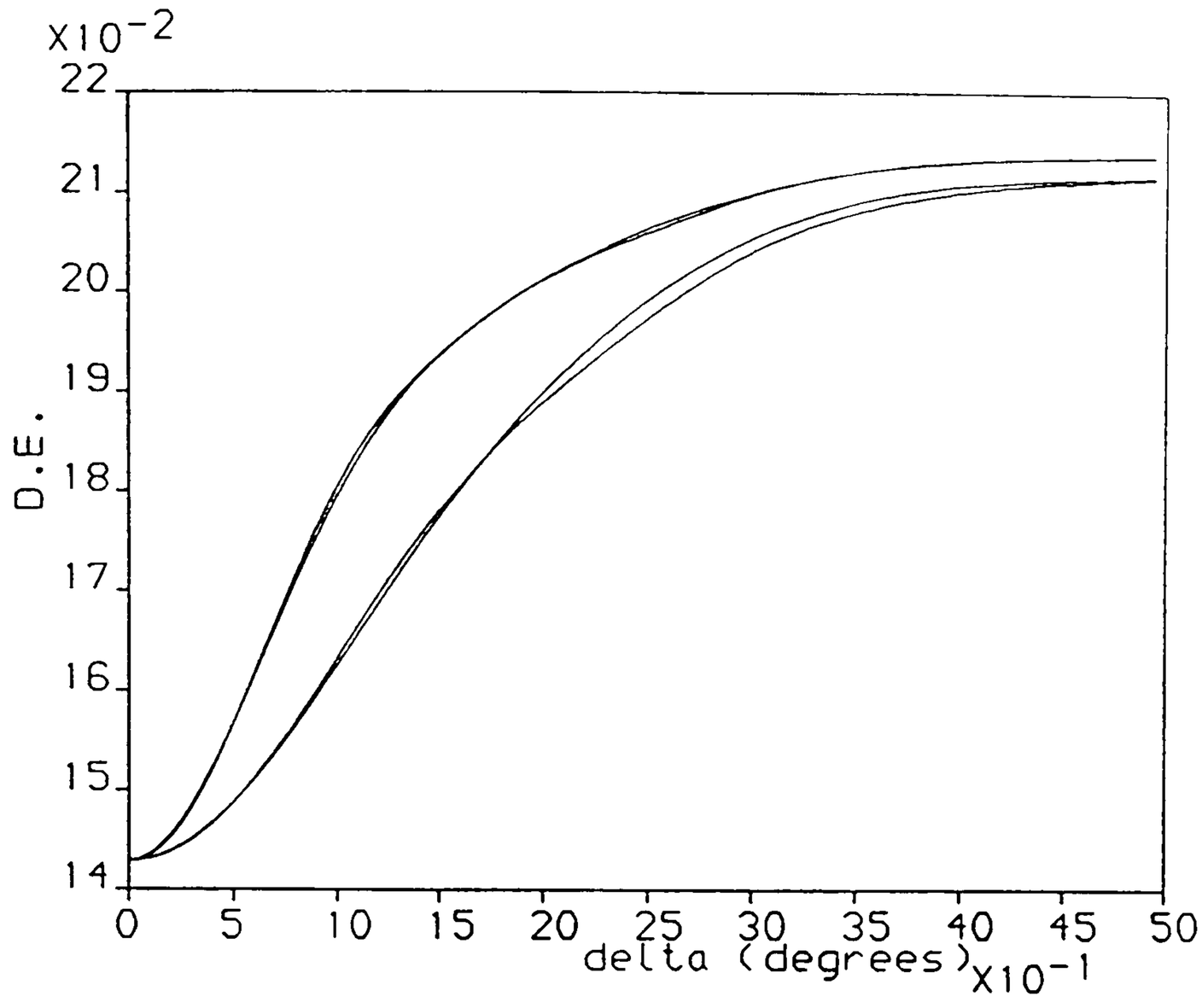

Figure 4.15: Fan-out to 4 D.E. versus δ. $\Delta n_p/\Delta n_c = \infty$.

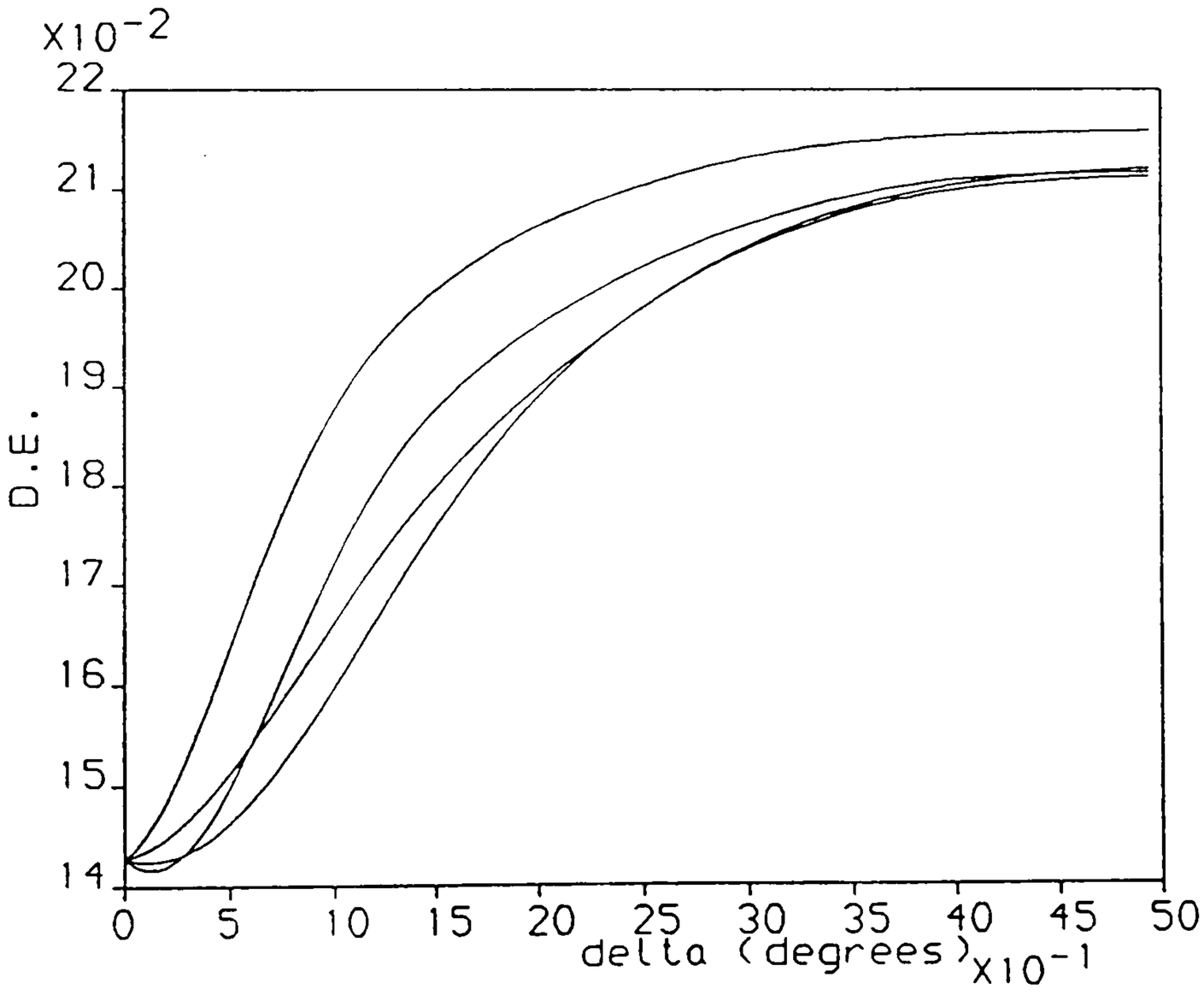

Figure 4.16: Fan-out to 4 D.E. versus δ. $\Delta n_p/\Delta n_c = 10$.

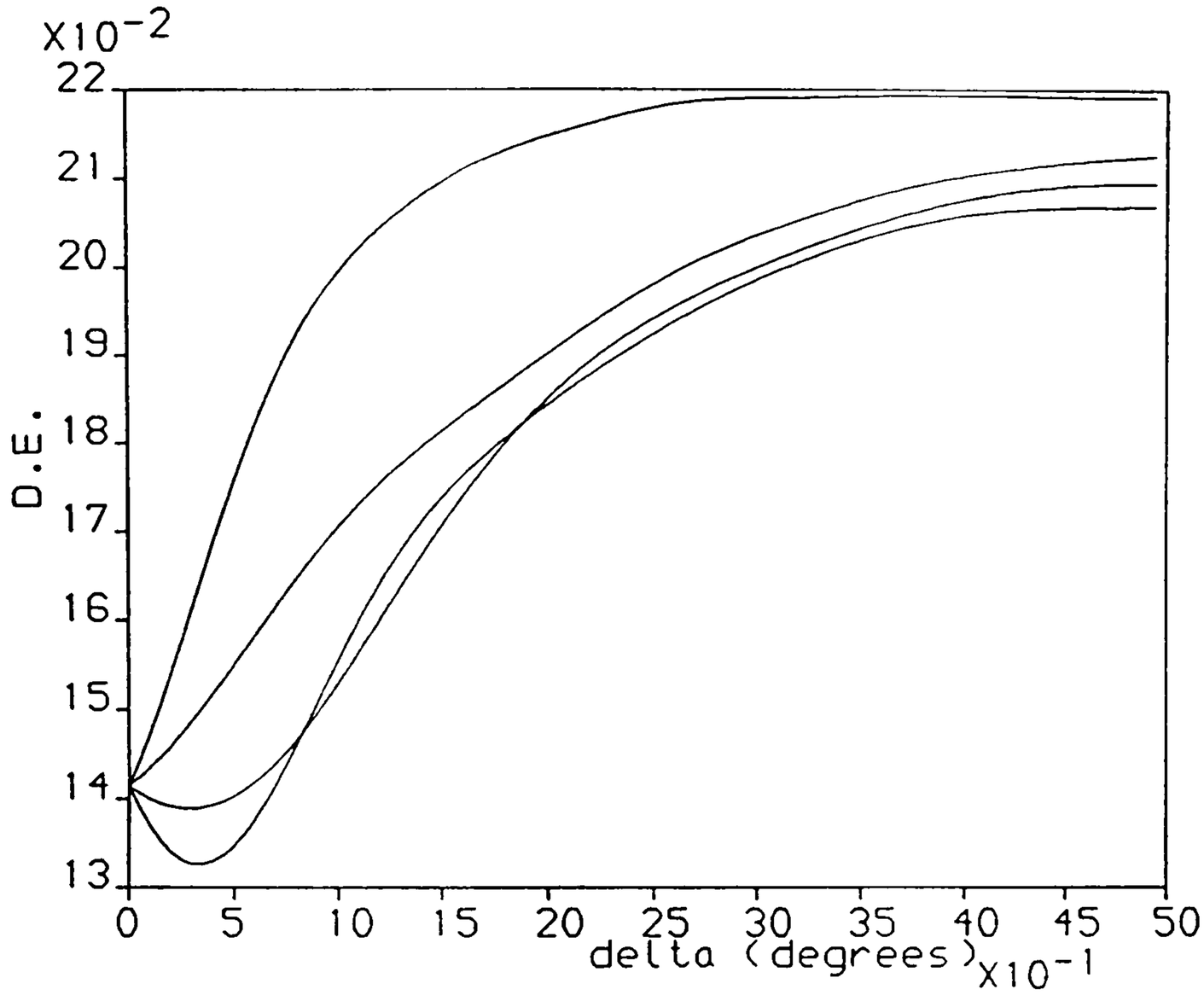

Figure 4.17: Fan-out to 4 D.E. versus δ. $\Delta n_p/\Delta n_c = 3$.

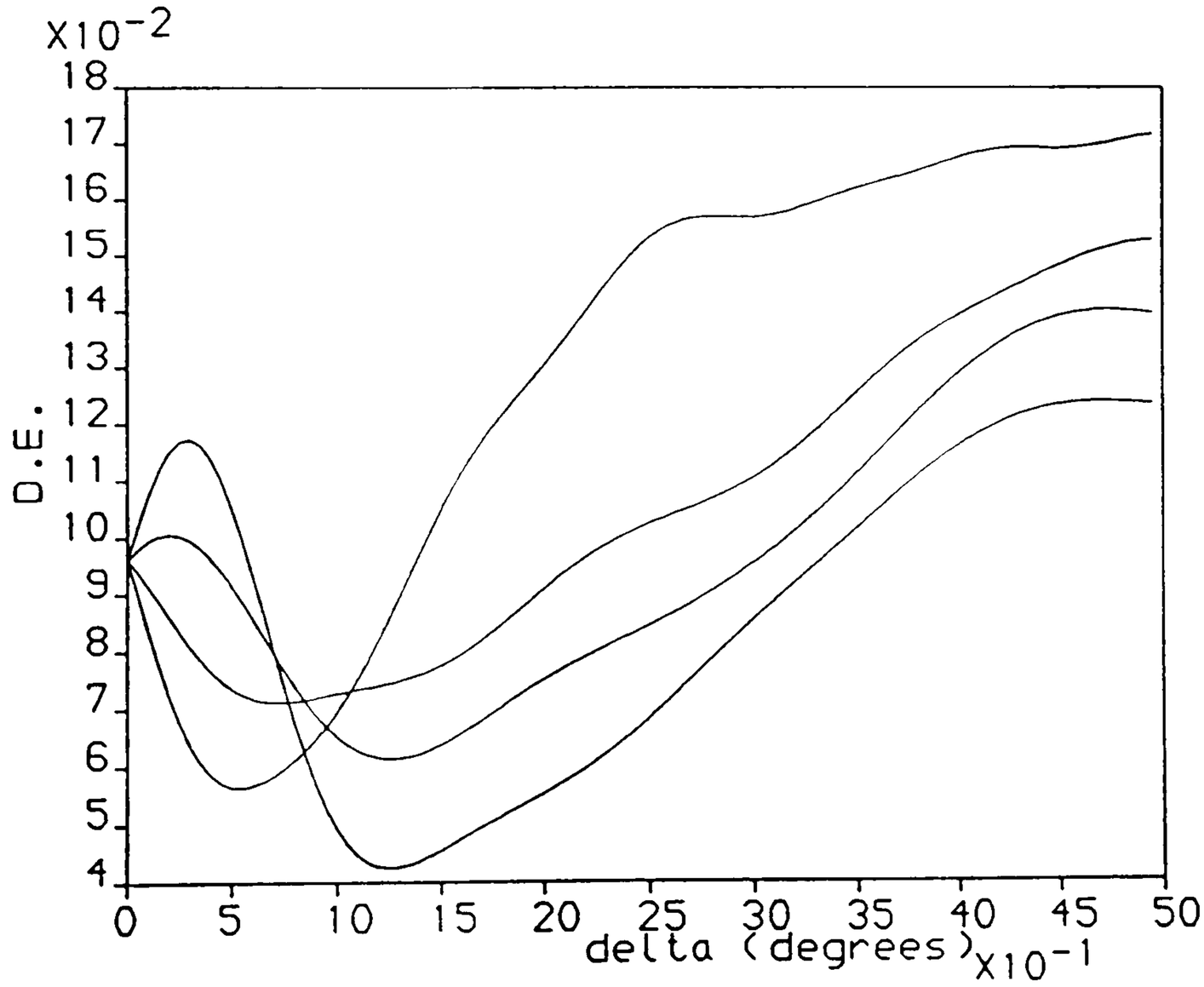

Figure 4.18: Fan-out to 4 D.E. versus δ. $\Delta n_p/\Delta n_c = 1$.

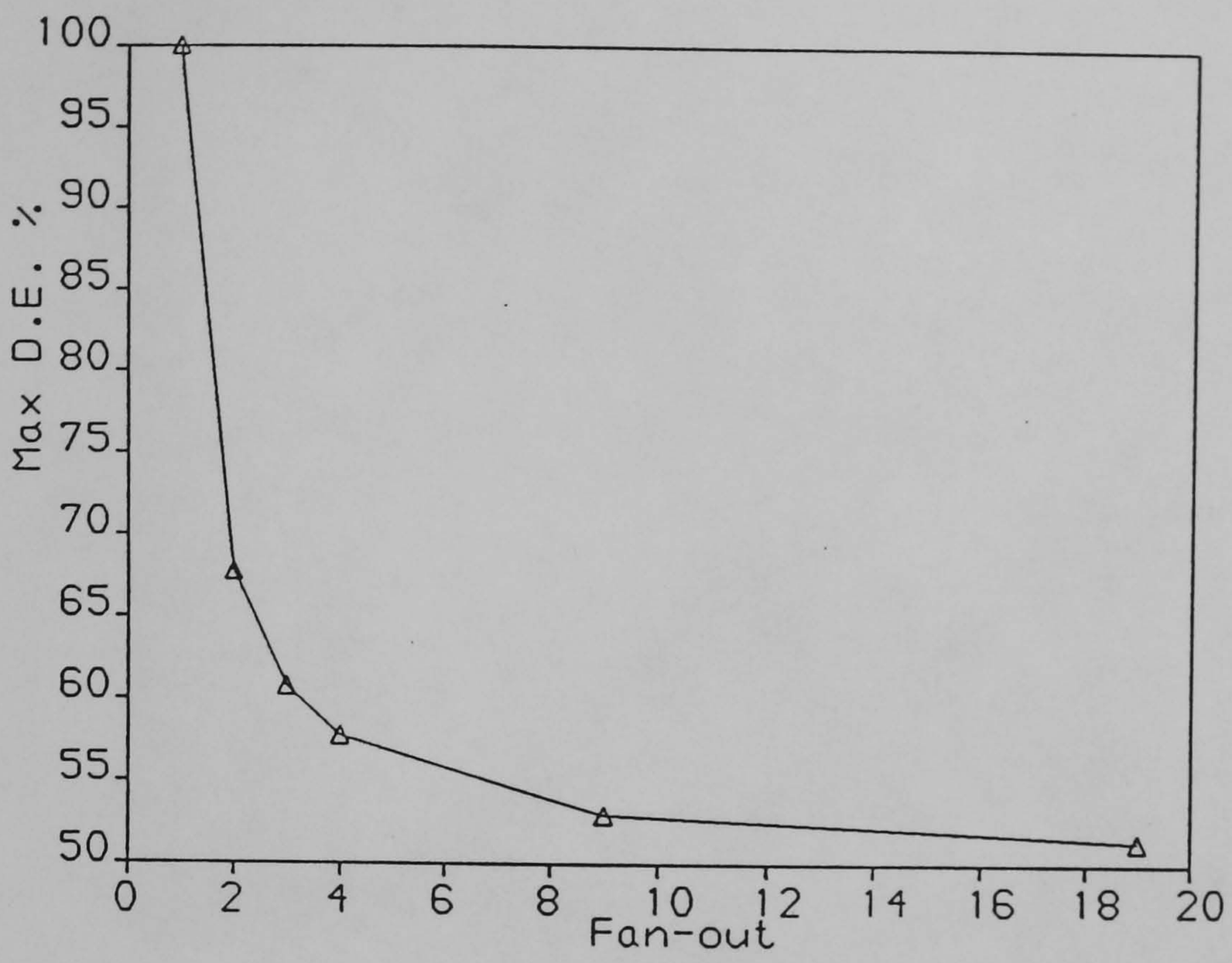

Figure 4.19: Maximum total diffraction efficiency versus degree of fan-out for $\delta \approx 0$.

4.3.3 Higher order spurious waves.

The previous analyses of higher level fan-out have assumed that only the first order spurious waves are present (those that result from first order diffraction from cross gratings, or double diffraction from only two of the principle gratings). Investigation of the importance of higher order spurious waves shows that they can contain appreciable amounts of power, especially at small δ. However, significant power is not coupled into these orders until the index modulation exceeds that needed to reach the first peak in the diffraction efficiency curve for the principle waves. This is illustrated in figure 4.20, which shows calculated results for a fan-out to three hologram with 16 waves in total included, $\delta = 0.3°$, and $\Delta n_p/\Delta n_c = 10$. The rise of the principle waves, then the first order spurious waves, and finally the

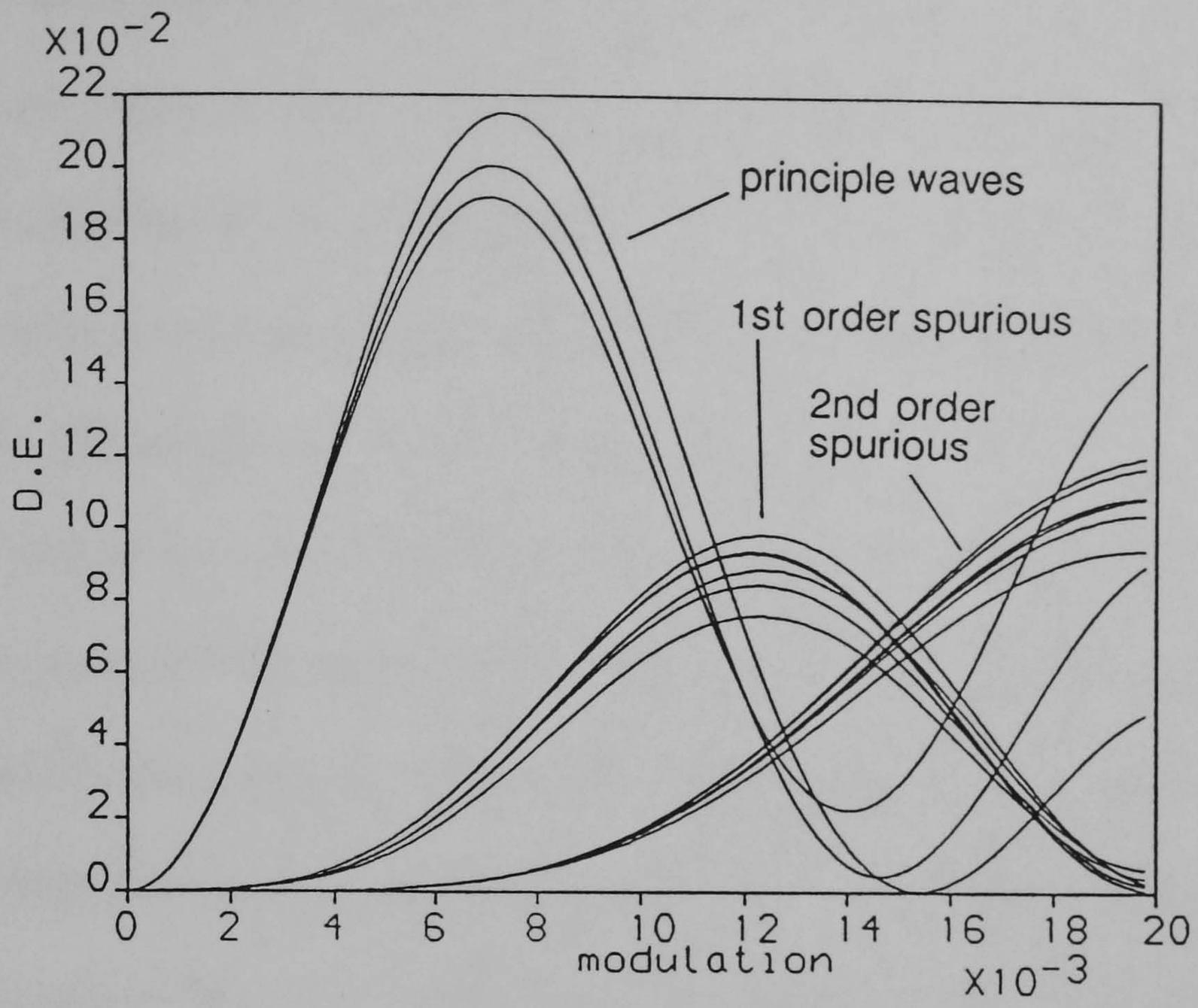

Figure 4.20: Inclusion of 11 spurious waves in a fan-out to 3 hologram. $\Delta n_p/\Delta n_c = 10$, $\delta = 0.3°$.

second order spurious waves can be seen as modulation increases.

4.4 Saturation in fan-out holograms.

As we know from chapter 3, saturation of refractive index modulation is very evident in DCG. Its effect on a single grating is to limit the amplitude of the grating, and to create a non-sinusoidal fringe profile which can be shown to consist only of harmonic grating components. When two or more gratings of different period and/or orientation are present in the same medium, saturation, in common with any non-linear effect, causes sum and difference frequencies to be generated in addition to harmonics of the individual gratings. Therefore, diffracted waves will be generated according to the grating equation. However, no *new* waves are

generated, since they all already exist through multiple grating diffraction. The powers in all these unwanted waves may be dramatically increased by the presence of the new gratings, which are Bragg-matched to these directions. Note that this is true for all δ, but as δ increases beyond the Bragg acceptance angle, the power in multiply-diffracted waves will become rapidly smaller.

In the case of a double grating fan-out hologram which has been sequentially recorded in a saturating medium, there will be a real third grating such as would be recorded by the interference of the two object beams. In addition, there will be a sum frequency grating, and higher harmonics of all these gratings.

The important feature of saturation in fan-out holograms is the generation of the difference gratings which, as already shown, lead to a loss of efficiency and a degradation of the uniformity of principle diffracted powers. Using the saturation model in chapter 3, we can estimate the effect in typical DCG holograms. Putting $\beta = 1.6 \times 10^{-5}$ and $\Delta n_m = 0.041$ (from hologram 22073 in chapter 3), and exposure energy $E = 500\text{J/m}^2$ per exposure into the saturation equation for a double exposure hologram, the resulting index profile was analysed into its principle grating components. This was done using a computer program which utilised a fast fourier transform algorithm to obtain a continuous spatial frequency spectrum. The resulting spectrum is shown in figure 4.21 for $\delta = 2°$, and a reference beam angle of 50°. The refractive index profile is shown in figure 4.22. Note that the resultant spectrum component *amplitudes* are dependent only on exposure and the saturation parameters, and do not depend on grating slants or periods. The graph shows the presence of the difference grating ($\mathbf{K}_3$ in our earlier double fan-out no-

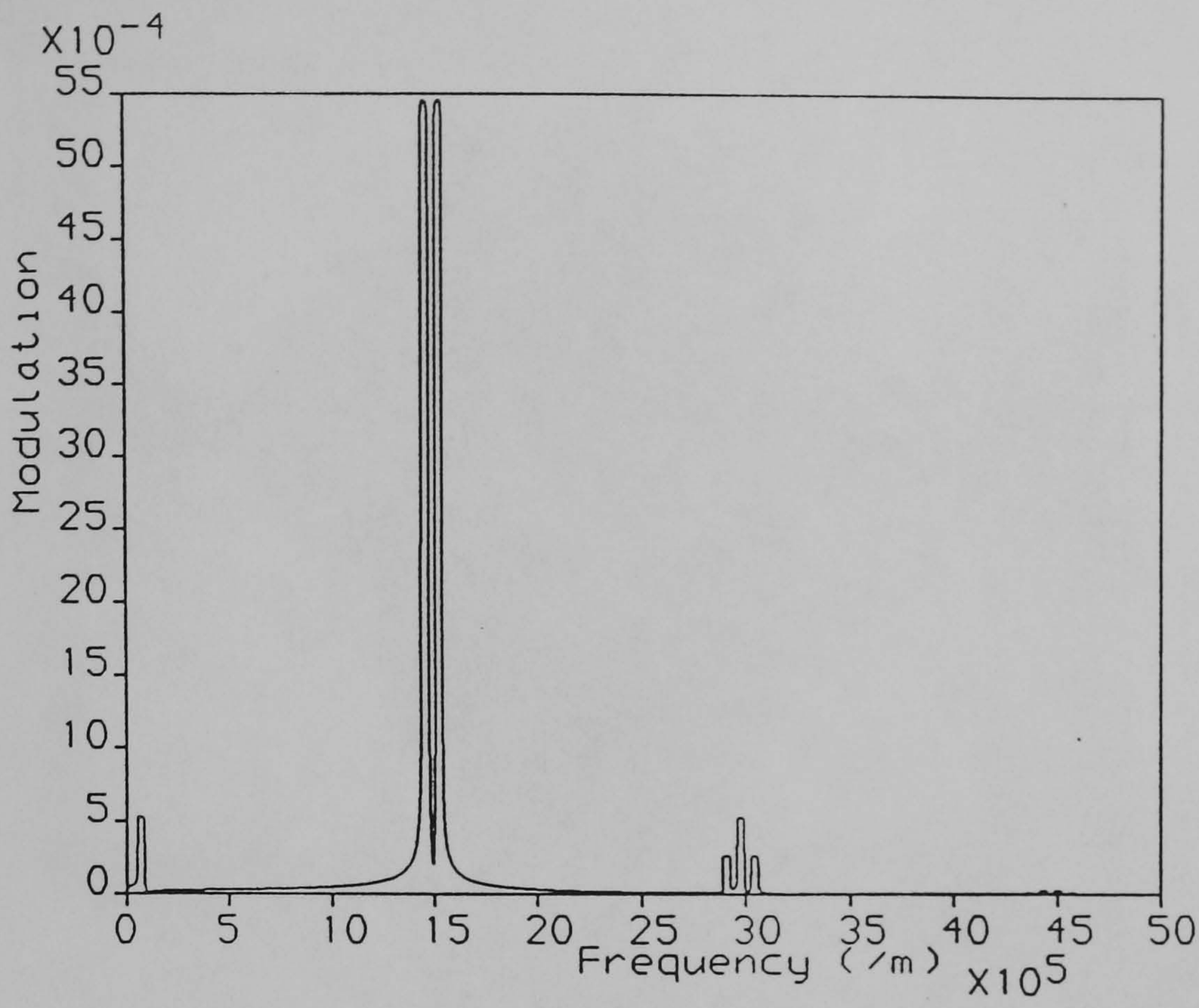

Figure 4.21: Spatial frequency components of the index profile in a saturated double exposure hologram.

tation) with a very low spatial fequency, the two principle gratings, $\mathbf{K}_1$ and $\mathbf{K}_2$, at around 15 $\times 10^5$ cycles/m, then a cluster of three gratings, representing the second harmonic of $\mathbf{K}_1$, the sum $\mathbf{K}_1 + \mathbf{K}_2$ and the second harmonic of $\mathbf{K}_2$ respectively, with increasing frequency. At higher exposure levels than this, higher harmonics and sums also begin to appear.

The grating amplitudes obtained by this method were then used in the extended coupled wave theory to determine the extent of the effect of saturation on efficiency and uniformity. Total exposure was taken to be the same as that which gave maximum efficiency in the single grating case. It was found that the two principle beams contained 23.8% and 22.2% of the incident power. Expressed as a fraction of the average diffracted power, this amounts to a $\pm 3.5\%$ uniformity. Setting the

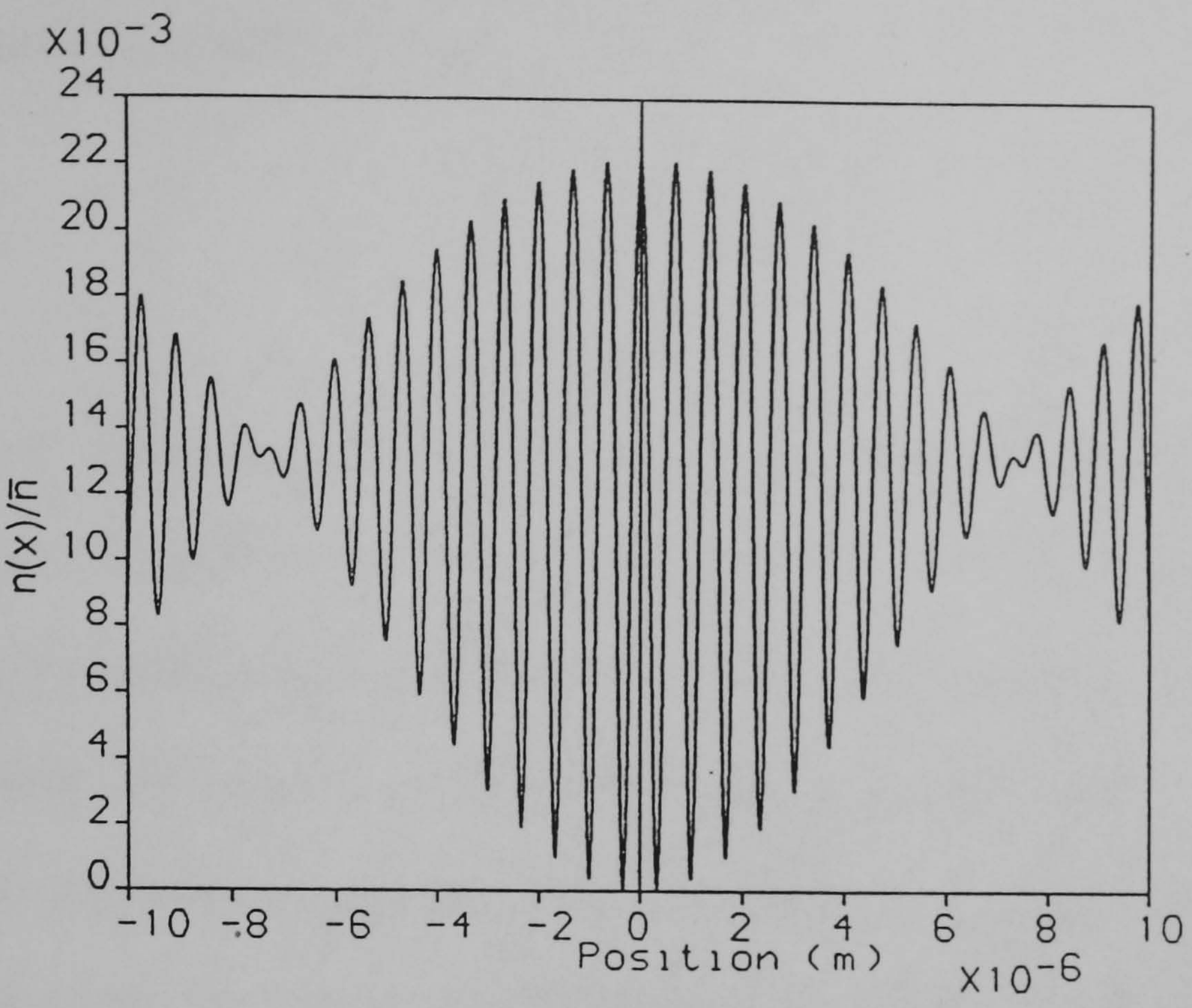

Figure 4.22: Refractive index profile of a saturated double exposure hologram.

amplitude of the difference grating, K_3 to zero in the same model (corresponding to the ideal linear recording medium), gives efficiencies of 23.00% and 23.07% - only an 0.3% uniformity.

A fan-out hologram recorded in a saturating medium by multiple, incoherent exposures can be equated to a single coherently recorded hologram in a linear recording material. They are not exactly the same, but may be considered so in the respect that the same principle and cross-gratings are present. In the saturated incoherent case, there will also be harmonics and sums of gratings present, but we ignore these on the grounds that they are far from Bragg incidence, and therefore have only a small effect. The ratio, R_g between the amplitudes of a principle grating, and a cross-grating is directly related to the irradiance beam ratio of a

coherently recorded hologram by

$$R_g = \sqrt{N R_b} \tag{4.3}$$

where N is the number of equal power object beams, and R_b is the irradiance beam ratio measured in the plane of the hologram. With the saturated hologram we have just investigated, R_g came out as approximately 10. Therefore this is equivalent to a coherent fan-out to two hologram with $R_b = 50$.

These results show that in typical holograms in DCG, multiple exposures do not give effectively decoupled principle gratings as a perfectly linear material would. Difference gratings of significant amplitude may be generated by the non-linear response of the recording medium. This effect is aggravated by the higher total exposure level that is required in fan-out holograms. This can only be avoided by using thicker gelatins for fan-out holograms.

A final effect of saturation in fan-out holograms is that when more than two principle gratings are present, saturation may alter the relative amplitudes of the gratings in the hologram. This is illustrated by the spatial frequency spectrum shown in figure 4.23. It can be seen that there is an imbalance in the amplitudes of the principle gratings of $\pm 1\%$ despite the fact that the exposure values are equal. The parameters taken here were - $\Delta n_m = 0.048$, $\beta = 1.3 \times 10^{-5}$, $\lambda = 514$nm, $d = 15\mu$m, exposure per grating $E = 1\text{kJ/m}^2$, $\theta_r = 40°$, object beam angles of -2°, 0°, 2°, 4°, grating phases all zero, and a sampling interval from x =-0.5mm to +0.5mm. The gratings oscillate primarily in the x-direction, and we assume the change in relative phases with depth due to tilted fringe planes to be negligible for

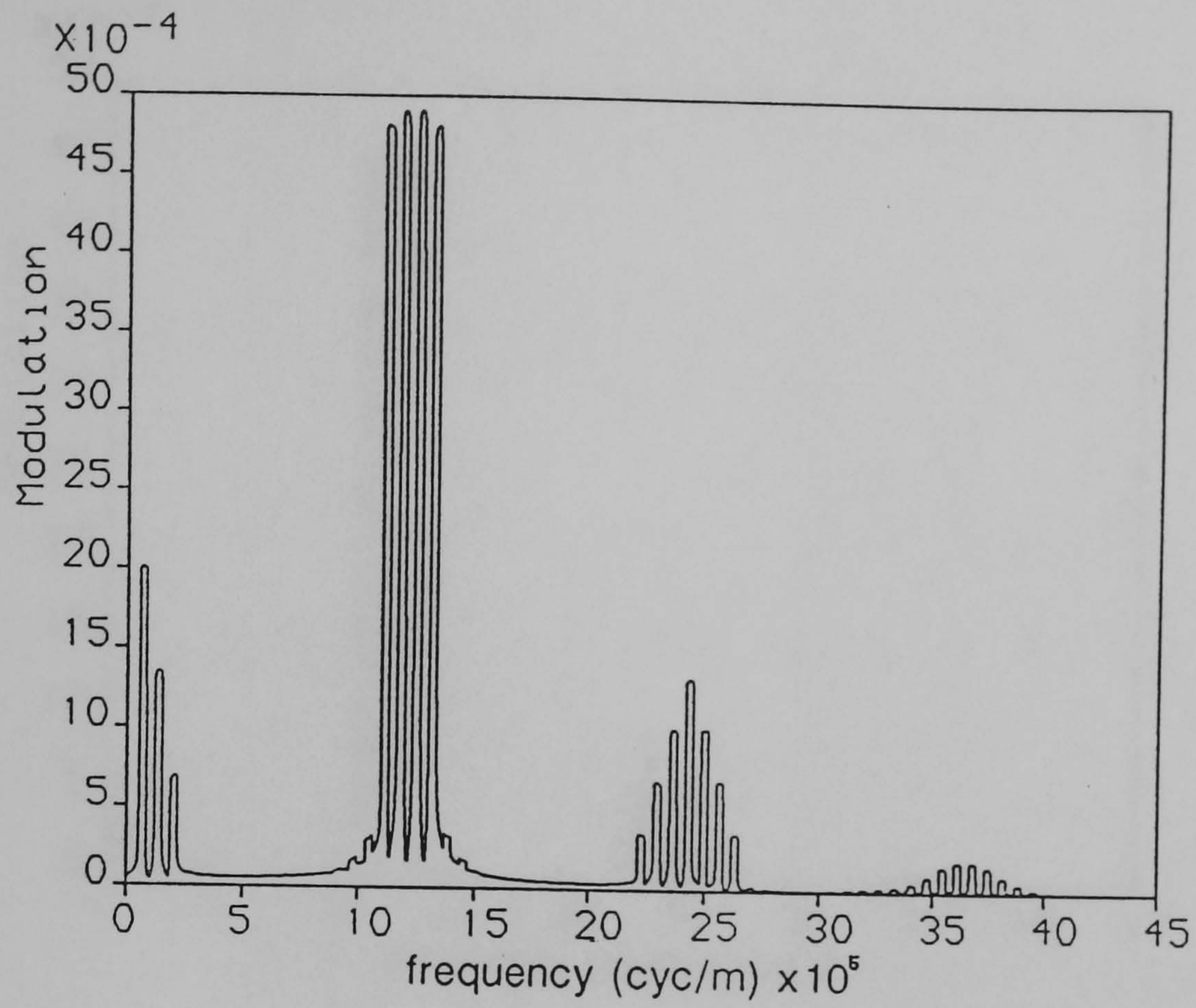

Figure 4.23: The effect of saturation on grating amplitudes in a fan-out to 4 hologram, $\phi_1 = \phi_2 = \phi_3 = \phi_4 = 0$.

the moment.

This effect depends on the relative phases of the gratings and the sampling region. This also greatly affects the amplitude and distribution of the difference and sum gratings, as shown in figure 4.24 where the phase of the highest frequency grating has been set to π.

4.5 Uniformity of modulation.

Real fan-out holograms recorded in DCG, both coherently and by multiple exposure with $\delta \leq 10°$, exhibited the trends in efficiency and uniformity predicted by the theory, but it was found that the magnitude of the total efficicency achievable differed from the expected. On inspection, double gratings show alternating

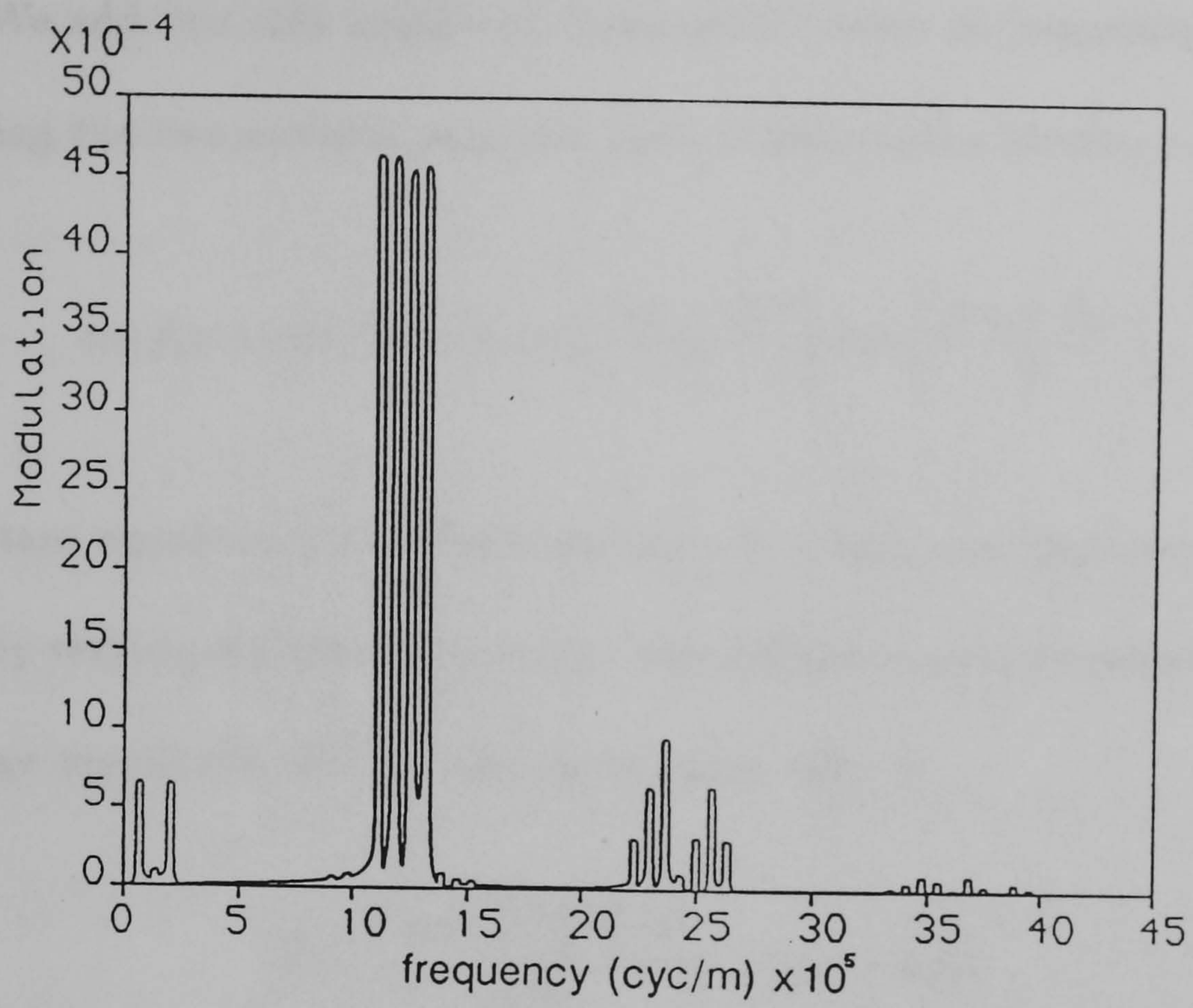

Figure 4.24: The effect of saturation on grating amplitudes in a fan-out to 4 hologram, $\phi_4 = \pi$.

stripes of high and low efficiency. The cause is simply the beating between the two grating frequencies. This is illustrated by adding two sinusoidal waves, as in figure 4.22. This results in a spatially varying modulation depth, and a varying efficiency.

If two gratings of slightly different frequencies are superimposed, there will be periodic regions where the modulations add to give twice the individual value, and areas where the amplitude of the modulation drops to zero. Holographically, these correspond to areas of high and low efficiency, so that the *average* efficiency will always be less than the local maximum efficiency. In a double grating case where the local maximum is 100%, the average will be of the order of 50%. In fact, the average modulation can be calculated as a fraction of the peak value simply as

follows. We add two unit amplitude cosinusoidal waves of frequencies f_1 and f_2, representing the two modulations, and use a trigonometric identity to obtain

$$\cos f_1 x + \cos f_2 x = 2\cos\left(\frac{f_1 x - f_2 x}{2}\right)\cos\left(\frac{f_1 x + f_2 x}{2}\right). \tag{4.4}$$

The resultant waveform is therefore equivalent to a high sum frequency modulated by a slowly varying difference frequency. The difference term therefore determines the average amplitude, and its average absolute value is

$$\overline{A} = \frac{\int \cos\left(\frac{f_1 x - f_2 x}{2}\right) \mathrm{d}x}{\int \mathrm{d}x} = 2/\pi = 0.64 \tag{4.5}$$

where the integral is over a half period of the difference frequency. Therefore, the average modulation of two superimposed gratings is 0.64 times the peak value. This does not then mean that average diffraction efficiency is 0.64 times the peak value. To calculate average efficiency, it is necessary to include the dependence of efficiency on modulation. For a first estimate, we can take Kogelnik's $\sin^2$ dependence, giving an expression for average efficiency

$$\overline{\eta} = \frac{\int \sin^2\left(\frac{\Delta n_p}{\Delta n_{opt}}\frac{\pi}{2}\sin x\right) \mathrm{d}x}{\int \mathrm{d}x} \tag{4.6}$$

where Δn_p is the peak index modulation, and Δn_{opt} is the modulation which would give maximum efficiency. If this integral is evaluated over one difference period, we get $\overline{\eta} = 0.652$.

This estimate of the average modulation and efficiency will in real holographic

media be modified by the effect of saturation, and this will tend to raise the average modulation and hence efficiency of a hologram.

It is interesting to note that Upatnieks and Leonard made a theoretical estimate of the maximum diffraction efficiency of a diffuse hologram which came out to be very close to this - 64% [UPA70]. This assumes a random linear superposition of gratings and considers the resulting statistically described modulation profile.

With only two gratings present, we can do nothing about the beating effect, but if more gratings are involved, we are free to vary their relative phases, and hence control the variation in depth of modulation. N gratings give rise to $N-2$ free parameters of phase. By carefully choosing the complete set of phases, the variation in total modulation depth can in principle be minimised over some limited region - the area of the hologram.

In general, the choice of phases is a non-trivial problem, even in one dimension (corresponding to the case where all beams are coplanar). Approximate solutions using only 0 and π phase values can be obtained by following Anderson's method [AND61], which was originally derived to solve similar communications problems. At present, no method is known for solving the 2-D case, where a hologram is required to produce a 2-D array of diffracted beams. A 'brute force' computer method may be feasible for low degrees of fan-out. This would typically work by minimising variations in modulation by making changes to one phase at a time (again limited to a few discrete values, such as 0, π), and only accepting the new value on an improvement. However, with N superimposed gratings, and P discrete phase values, a maximum of P^N combinations must be tried, each requiring a

number of sampled points to test the uniformity. This becomes a problem if we wish to generate a high level fan-out hologram, say 1 to 100. With two possible phase values for each grating, this means 2^{100} combinations must be tried. This would be impractical by the 'brute force' method.

Problems associated with attempts to record holograms with higher levels of fan-out without any phase control are more serious, because the gratings may combine in such a way as to give a 100% peak local diffraction efficiency, but a very low average efficiency - the modulation profile may be 'spiky'. Therefore, in order to achieve uniform modulation and to approach the best possible results given by the fan-out coupled wave model, it is necessary to first solve the phase choice problem, and then to devise an experimental method to observe and control the relative phases of sequential gratings. The experimental solution is possible to visualise - active phase control by feedback from a photodetector to a piezo-electric mirror is a well established technique [MAC77]. This must be extended so that the actual phase in the plane of the grating can be quantified and then set to the required value and locked there by feedback during each exposure.

4.5.1 Very large δ.

If the angle between two fan-out beams is sufficiently large, the angle between their corresponding gratings results in a significant change of phase between the gratings with depth. Therefore, there is now a three dimensional modulation profile to consider. This situation is illustrated in figure 4.25 in the symmetrical case where a normal incidence reference beam is diffracted into two object beams

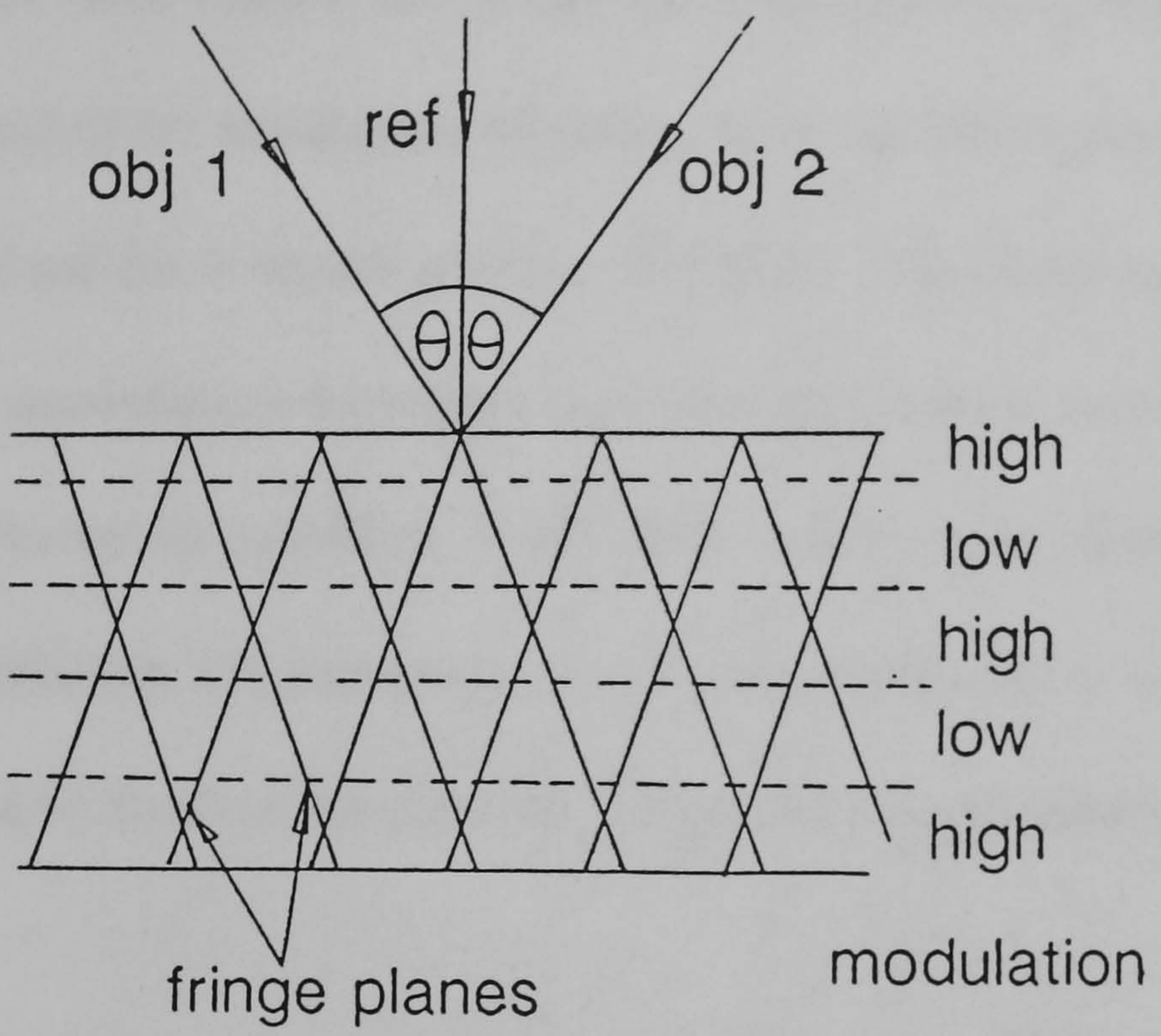

Figure 4.25: Index profile of a symmetric fan-out to 2 hologram with a large δ.

at $\pm\theta°$. In this case, the gratings actually have the same surface fringe period, so there is no 'beating' across the surface. Now, there are 'planes' of high and low efficiency which are parallel to the surface. We can see that the average modulation in the vertical direction (for a large number of periods) will be $2/\pi$ times the peak value. However, this differs from the small δ case since the incident beam no longer sees regions of varying modulation *across* the hologram, and the whole wavefront is diffracted with equal efficiency. The holograms's thickness has simply been effectively reduced, and this is not a barrier to efficiency. If enough modulation or thickness is available, 100% efficiency may be achieved.

This case was investigated experimentally by recording symmetrical holograms as shown in figure 4.25 with $\theta = 30°$. Such holograms could indeed achieve in excess of 90% diffraction efficiency with balanced powers. Also, such high efficiencies were

obtained with a total exposure energy about 2.5 times that for a single grating. This is in agreement with Case's investigation and this work, which states that the modulation required for maximum efficiency in a double exposure hologram is $\sqrt{2}$ times that required for a single grating [CAS75]. Case does not consider the spatial variation of modulation however, and this, as we have seen in section 4.5, leads to a further factor of $1/0.65 = 1.54$. The two factors together amount to an increase in modulation (or exposure, in a linear medium) of a factor of 2.18. Saturation will tend to further increase the exposure energy needed.

4.6 Holographic reciprocity law failure.

In photography, reciprocity refers to the linearity of recording with exposure. Therefore, if the aperture of a camera is doubled in area, the exposure time may be halved. This law fails at extremely long or extemely short exposure times, due to time-dependent effects in the latent image recording process in photographic materials.

In holography, 'reciprocity' has come to refer to the sequential exposure recording properties of a holographic material [JOH84,JOH85]. What is desirable is that each sequential exposure of equal energy results in a grating of equal amplitude. Johnson et al found that in photographic holograms there is a sequence-dependent effect, where later exposures must be extended in order to achieve the same grating strength. The effect is again connected with time-dependent processes in silver halide materials, where sensitivity depends on previous exposure history. This has serious consequences if a fan-out hologram is to be recorded with good beam

weighting uniformity, since each exposure time must then be varied to compensate.

Throughout the numerous experiments, involving both coherent and sequential exposures, and degrees of fan-out between two and one hundred, no evidence has been seen in DCG for such a reciprocity failure. This should be qualified, however, by stating that the non-uniformity in beam powers which results in fan-out holograms made to date has a masking effect which would make small effects indistinguishable from non-uniformity. In order to say whether there is or is not a reciprocity effect at all would require that the intrinsic non-uniformity problem be solved, or alternatively, that the phases of the various gratings be measured so that a model of the grating profile can be constructed, and efficiency and uniformity analysed.

4.7 Sensitivity to relative recorded exposures.

When recording real fan-out holograms, there will generally be some variation in power between the various object beams. For example, in a sequential exposure experiment, this may be due to fluctuations in the laser power between exposures. This will result in different amplitudes of gratings being recorded. This section briefly investigates the theoretical results of this effect on the replay of fan-out holograms.

Figure 4.26 shows theoretical plots of the diffraction efficiencies of the two principle beams in a fan-out to two hologram against the amplitude of one of the gratings, given by Δn_1. The other principle grating is held at an amplitude of 0.01, and the single cross-grating is held at 0.001. Curves for δ values of 0.1°, 1°

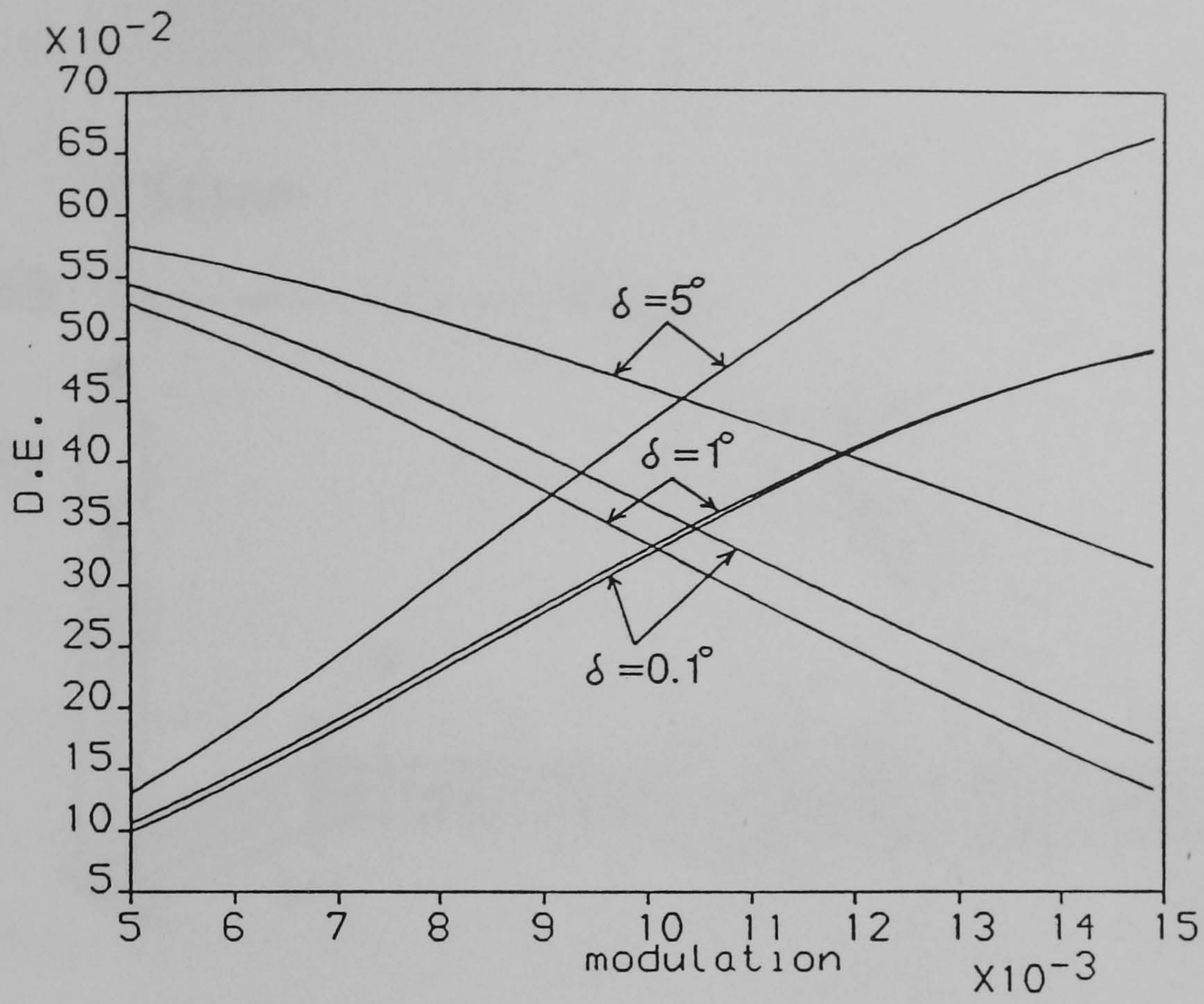

Figure 4.26: Diffracted power in a fan-out to 2 hologram vs. Δn_1. $\Delta n_2 = 0.01$.

and 5° are given, and in all cases it can be seen that a 10% increase in Δn_1 causes a greater than 10% increase in one beam power, and a greater than 10% decrease in the other. Therefore, non-uniformities in exposure levels cause a non-uniformity in output beam powers which is amplified by more than a factor of 2. A similar result applies in the perfectly incoherent recording case, where the cross-grating is set to zero, and in the fan-out to three case. These results indicate that the recording of fan-out holograms needs careful control of individual exposure values to attain uniformities approaching the theoretical optimum. This is in contrast to the single grating case, where the optimum exposure lies in a region of minimum sensitivity to exposure, on the top of a $\sin^2$ function.

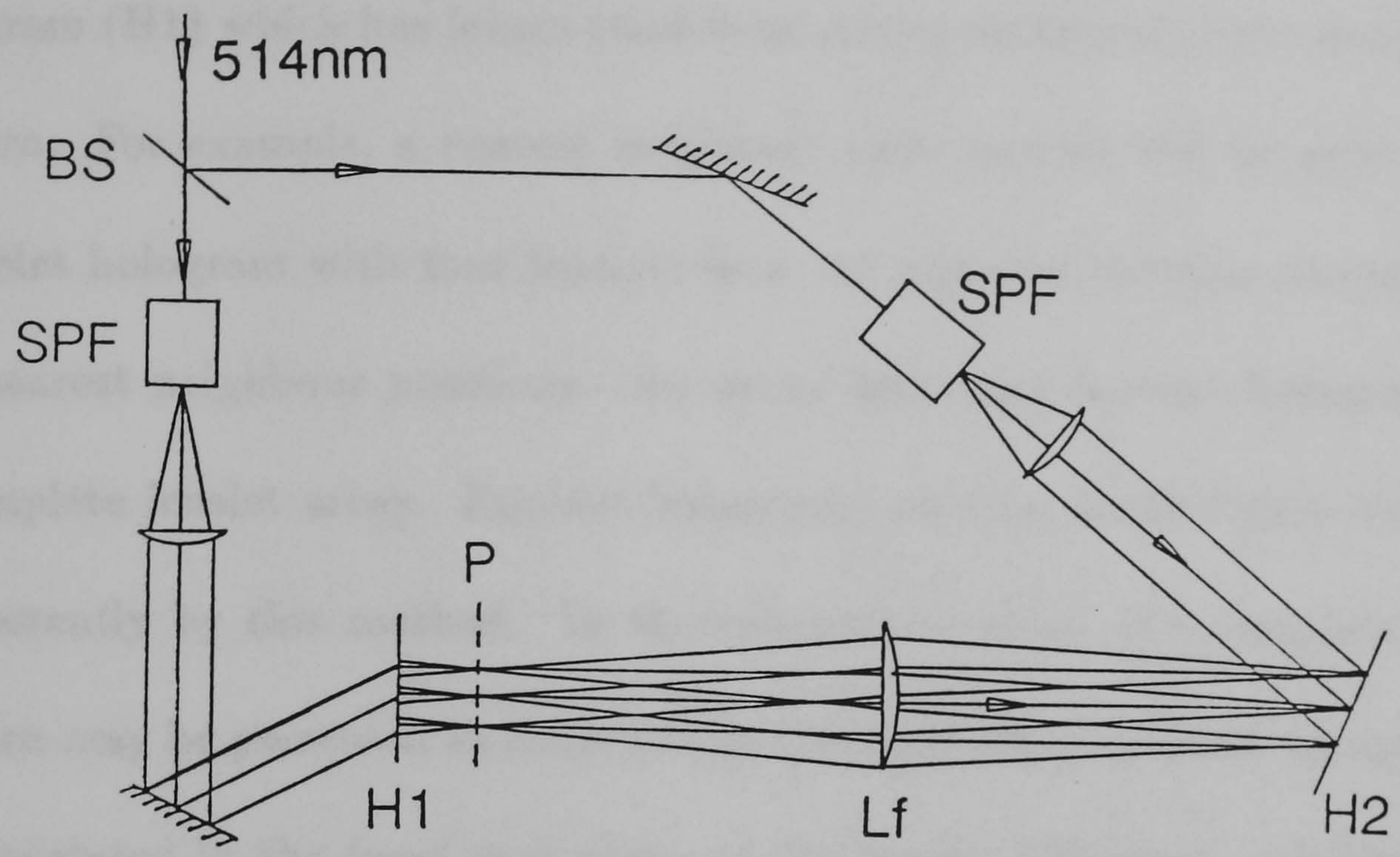

Figure 4.27: Recording geometry for a fan-out to 4 hologram.

4.8 Experimental.

4.8.1 Experimental arrangement.

Fan-out holograms were recorded using the arrangement shown in figure 4.27. To understand the arrangement, it should first be understood exactly what the hologram is required to do and how it does it. A fan-out hologram may be required either to generate a large array of focal spots from a collimated input, or to interconnect two arrays of optical logic devices. In the latter case, focal spots are required at both input and output planes.

In order to make either type of hologram, all that is required is to record the interference between a single collimated beam, and the Fourier transform of the desired output focal spot pattern (i.e. more collimated beams at the appropriate

angles). The spot pattern (at plane P in the figure) may be obtained from a lenslet hologram (H1) which has lenses (and focal spots) arranged in the desired fan-out pattern. For example, a nearest neighbour interconnect will be generated using a lenslet hologram with four lenslets in a '+' pattern, the tips corresponding to the nearest neighbour positions. An array generator fan-out hologram requires a complete lenslet array. Fan-out holograms may be made either coherently or incoherently by this method. In the coherent method, the complete focal spot pattern may be presented at once, and in the incoherent method, an aperture may be translated in the focal spot plane of the lenslet hologram, allowing only one beam at a time to be recorded.

The only difference between the array-generator type of hologram and the interconnect hologram is that the array generator needs only one transform lens on its output (assuming a collimated input), whereas the interconnect needs two lenses - one to transform the input and one to re-transform the output. A type of interconnect hologram will be discussed in more detail in chapter 6.

4.8.2 Alternative arrangements.

Any technique which can create the desired focal spot pattern as an input may be used in place of the lenslet array hologram. Possibly the only direct replacement for the holographic lenslet array is an array of refractive lenses, such as a fly's eye lens, or gradient index lenses. Generally, such methods are less flexible in this application. However, there are a number of methods for sequentially creating the pattern, one spot at a time.

An example of an alternative sequential method uses an optical fibre to create a point source. The fibre may be mounted on a translation stage or stepper motor and moved to the appropriate position corresponding to a desired output spot before each exposure. This is a more direct method, eliminating the intermediate lenslet hologram. A possible problem with the method is that it is likely to require phase stabilisation due to heating effects in fibres at the relatively high operating powers which are necessary to keep the total exposure time short. Also a single mode fibre is essential, and it is desirable that it is polarisation-preserving.

Another method which may be used is to generate the angled collimated beams directly by a tilting mirror. This may be removed from the hologram by a convenient distance by a 2 lens 4-f system. Such a system is shown in figure 4.28. This has the advantage that the plane of the mirror is imaged on to the hologram, so that if an aperture is imaged onto the mirror, it is then imaged on to the hologram, resulting in a hologram with a sharply defined area. In the lenslet intermediate hologram system the image at the hologram is the far-field diffraction pattern of an aperture, and a badly defined hologram area results.

4.8.3 Fan-out to two.

In order to avoid the problem of controlling phases in order to achieve spatially uniform modulation depth across a hologram, fan-out experiments must be limited to a fan-out level of two. Fan-out to three allows one free phase value which is experimentally random, and will affect the average and peak modulation amplitudes in the gelatin in a random way.

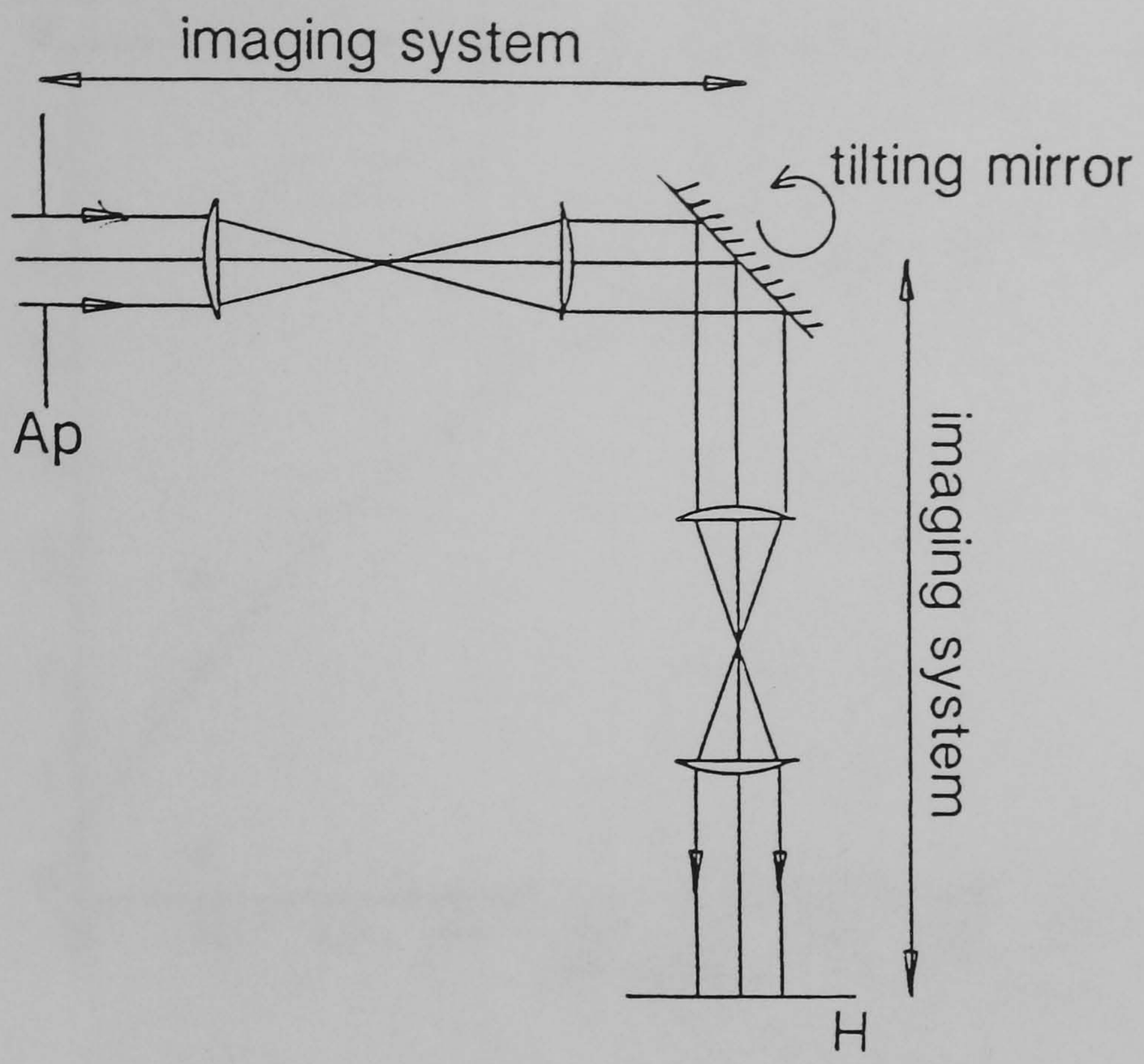

Figure 4.28: A tilting mirror system for recording fan-out holograms.

Uniformity in all experimental fan-out results is defined as

$$U = \pm \frac{p_{max} - p_{min}}{p_{max} + p_{min}} \times 100\% \tag{4.7}$$

where p_{max} and p_{min} are the highest and lowest powers in the diffracted beams of interest. Uniformity is equivalently defined as a percentage of the median beam power. It is the most appropriate measure of uniformity when overall system tolerances are to be considered, for example, in an optical logic circuit.

Figures 4.29 to 4.31 show experimental and theoretical diffraction efficiencies and uniformities for fan-out to 2 holograms which were incoherently recorded on approximately 14μm thick gelatin at 514nm. Triangles represent experimental points and crosses theoretical points. Upper points are efficiencies and lower uni-

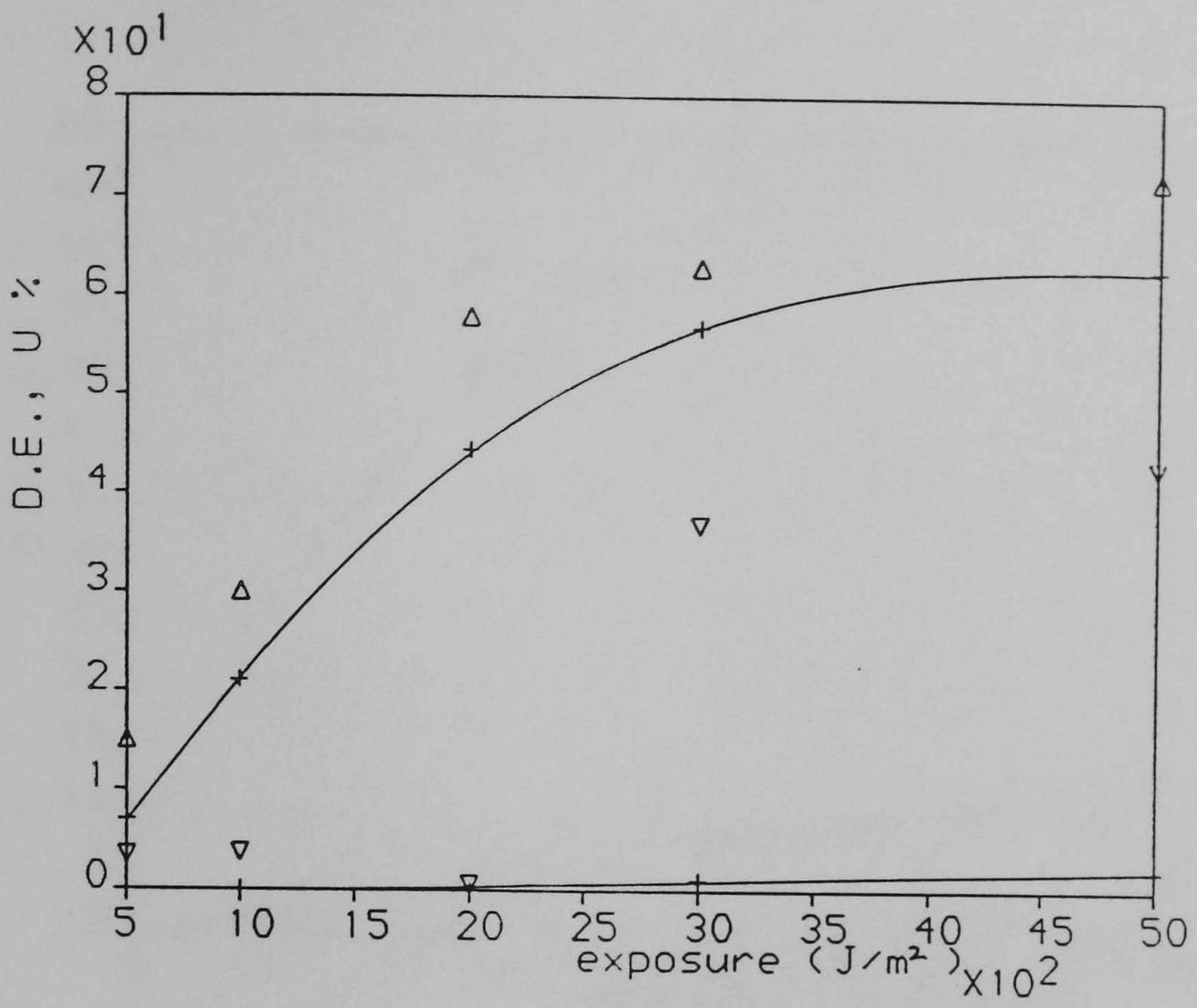

Figure 4.29: Fan-out to 2 experiment and theory. $\delta = 0.1°$.

formities. Fan-out beams are centred around normal incidence, and the reference beam is at 40° to the normal. Points are given for $\delta = 0.1°$, 1° and 3.8°, and for a range of exposures. The trends that can be seen in these graphs are firstly a limiting of efficiency (which is worse for small δ), and secondly a deteriorating uniformity with exposure. To compare these trends with those of the model, the gelatin's holographic response was first quantified from a series of single exposure gratings. The relevant parameters were found to be $\Delta n_m = 0.045$ and $\beta = 5 \times 10^{-6}$. This enables the index modulations of both the principle gratings, and the cross gratings in the double exposure holograms to be estimated by means of a Fourier analysis of the saturated doubly-exposed index profile. The effects that saturation has both in limiting grating amplitudes and in generating cross gratings must be considered in order to succesfully explain the form of experimental results.

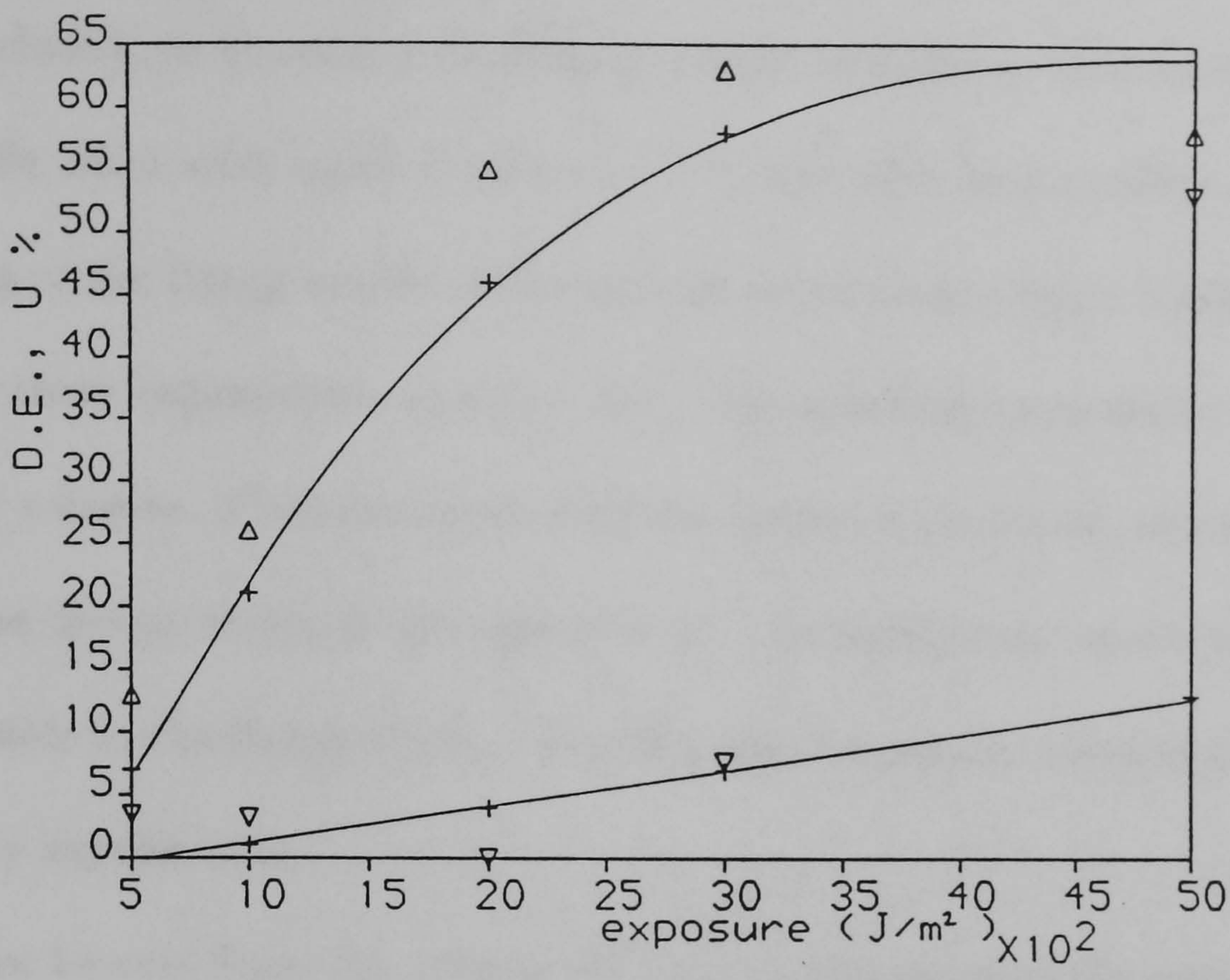

Figure 4.30: Fan-out to 2 experiment and theory. $\delta = 1°$.

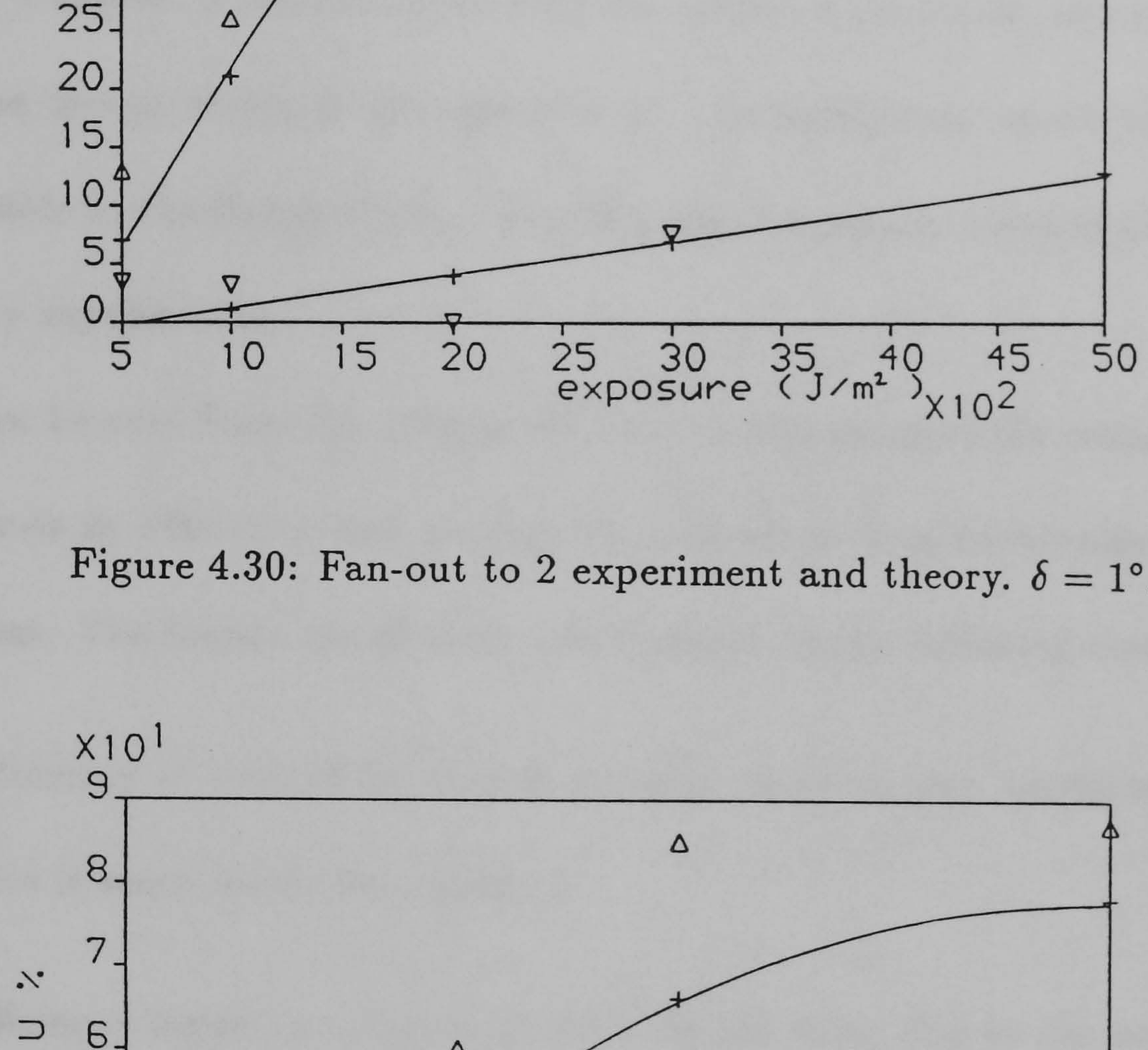

Figure 4.31: Fan-out to 2 experiment and theory. $\delta = 3.8°$.

In modelling the experiments, changes in bulk refractive index and thickness were included, as quantified in chapter 3. Such changes in fan-out holograms have negligible effect with small δ values ($< 1°$), but with larger values, the effect is a splitting of the Bragg angles of the various principle gratings. With the geometry used in these experiments and $\delta = 3.8°$, this splitting amounts to the order of a tenth of a degree. Therefore, even with the largest δ used here, this is unimportant since the Bragg width is the order of $5°$. In holograms where the splitting is comparable to the Bragg width, the effect may be major, and will limit the useful efficiency significantly.

It can be seen from the graphs that the model successfully estimates the correct trends in efficiency and uniformity, and there is a reasonable quantitative agreement. The trends are directly attributable to the following causes;

1. Efficiency is limited by double grating coupling into unwanted directions. This is more severe for smaller δ.

2. Efficiency tends to saturate at this limited value due to the combination of the higher modulation required for fan-out and saturation of modulation.

3. Saturation leads to the formation of the cross-grating which is responsible for increasing the degree of non-uniformity.

In addition, it was found that the energies in the first spurious orders agreed similarly with those predicted by the model, and the higher order spurious waves were insignificant in all cases, as predicted. Therefore, the total energy diffracted by the holograms was accounted for within experimental error.

Experimental uniformities are generally greater than those estimated by theory, and these may be at least partly accounted for by variations in exposure energy due to laser beam and power drift. This frequently amounts to as much as 5% over the course of an experiment. In addition, mode-hopping may dramatically reduce a grating's modulation if it occurs in mid-exposure. As noted earlier, variations in grating modulations due to exposure variations, movement or mode-hopping during recording are theoretically amplified by a fan-out hologram when it is replayed. Therefore, a hologram which ideally has perfect uniformity may easily develop 5% non-uniformity from a 2% power change between exposures. Because of the simple periodicity of the double-grating structure, it is likely that any uniformity discrepancies are attributable experimentally only to exposure variations.

The main discrepancy in the results lies in the absolute magnitude of the diffraction efficiencies. According to the earlier discussion of beating between gratings, the average efficiency would be expected to be $2/\pi$ times the local peak value (i.e. the value predicted by Fourier analysis of the index profile). Therefore, we should see efficiencies further limited to around 40% in the case of $\delta = 0.1°$ and $\delta = 1°$. In fact efficiencies are much higher than this, and are much closer to the values predicted by ignoring this effect. In the $\delta = 3.8°$ case, the gratings may change phase relative to each other by a significant amount in the depth of the hologram, so we would see higher achievable efficiency, but at a higher exposure. There is a clear increase in efficiency in the larger δ experiment, but again it appears to match the simpler theory better. This matter has still to be resolved.

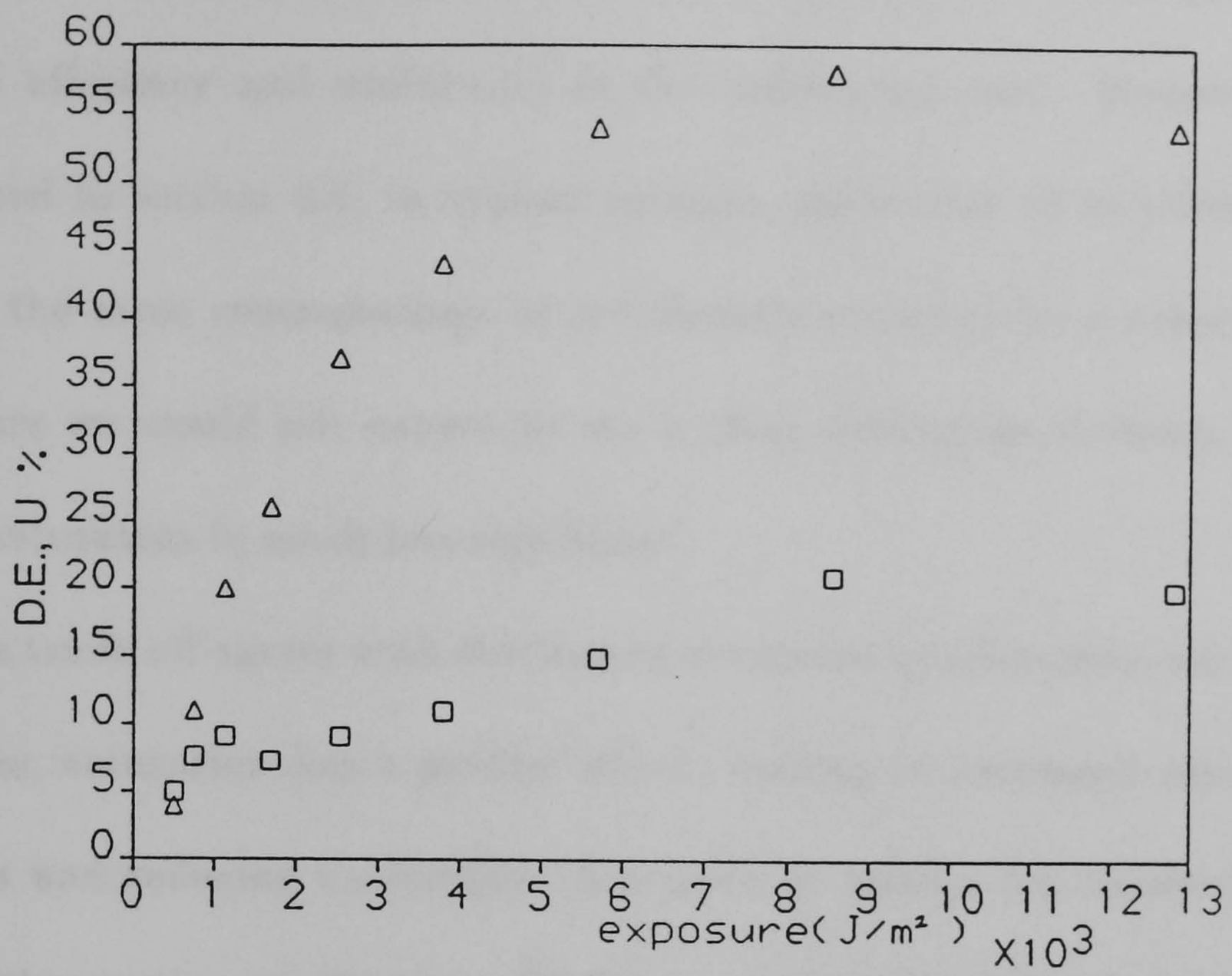

Figure 4.32: Diffraction efficiency and uniformity against exposure for a fan-out to 9 hologram.

4.8.4 Fan-out to more than two.

Shown in figure 4.32 are typical results of total diffraction efficiency and uniformity versus exposure for a real fan-out to 9 hologram. Diffraction efficiency (triangles) and uniformity (squares) are both given as percentages so they could be plotted on the same graph. The 9 output beams are arranged in a 3×3 square. This figure refers to a coherently recorded hologram with a beam ratio of 10, and $\delta = 0.38°$. The recording object beams had a uniformity of about 2%. The hologram was recorded in a 14μm 649F layer with a reference beam angle of 30°, and the object beams symmetrically arranged around 0°.

Here we can see the general trend observed in fan-out experiments - there is a trade-off between efficiency and uniformity. This effect occurs whether the

exposure method is coherent or incoherent, although there is a slight improvement in both efficiency and uniformity in the incoherent case. However, as already calculated in section 4.4, in typical gelatins, saturation in incoherent recordings creates the same cross-gratings as are directly recorded by a coherent recording. Therefore we would not expect to see a clear distinction between the two cases unless saturation is much less significant.

This trade-off agrees with the theory presented qualitatively, since as exposure increases, saturation has a greater effect, leading to increased coupling between gratings and reducing uniformity. As shown in section 4.4, saturation can affect the relative grating amplitudes, and this, in conjunction with the high sensitivity of fan-out holograms to grating amplitudes, leads to a further reduction in uniformity. In addition, fan-out holograms need greater index modulation (by a factor of $\sqrt{N}$) than single gratings to reach their maximum efficiency. Therefore, saturation affects results before the peak is reached. For example, a 3×3 hologram need 3 times as much index modulation as a single grating. This degree of modulation is greater than is usually available in a 14μm layer. In fact, what is required is that the product of $\Delta n \times d$ should be 3 times larger. Therefore, thicker layers are necessary to achieve a peak in efficiency.

Higher exposures than shown on the graph do not consistently increase the efficiency, but uniformity is always degraded, and the maximum efficiency that can be achieved varies from experiment to experiment. This is possibly due to variations in the parameters of the gelatin, and variations in the relative phases of the gratings.

The hologram shown reaches a maximum efficiency of 60% (when corrected for reflection and absorption losses. But, since the hologram is in a small δ regime, such a high efficiency indicates that saturation is actually raising the average modulation level well above the 'safe' level where the local peak corresponds to 100% efficiency. In an attempt to estimate the optimum exposure, we can take Upatnieks and Leonard's 64% maximum efficiency (derived purely on the basis of a statistical average modulation), and multiply it by our calculated maximum efficiency of 50% (resulting from coupling effects in the small δ regime in a high level fan-out hologram), to obtain an optimum theoretical efficiency of 32%. We may consider this to be the optimally modulated hologram. Looking at the experimental results, this efficiency corresponds to a uniformity of about 8%, which is 4 times greater than the recorded uniformity. Earlier theoretical investigations showed that non-uniformities in recording exposures cause efficiency non-uniformities of about twice the size. Therefore, the recording uniformity here of 2% would lead to a 4% uniformity in efficiency, leaving 4% unaccounted for. This may easily by taken up by the effects of saturation, resulting in real cross-gratings, and degraded uniformity. In fact, grating amplitudes of only a twentieth of the fundamental amplitudes leads to around 7% uniformity. Such grating strengths would be expected in real holograms in DCG.

4.9 Summary.

Experimental results showing non-uniformities in the output beam powers of fan-out holograms in DCG have led to a theoretical analysis using the extended coupled

wave theory developed in chapter 3. The analysis highlights the following points.

The relation between Bragg acceptance angle and object beam angular separation. The importance of multiple diffraction from more than one grating depends on the size of the angular separation, δ, of the diffracted beams relative to the Bragg acceptance angle, $\Delta\theta_B$ (defined as the deviation from the Bragg angle at which efficiency drops to zero for a single grating). Multiple diffraction reduces efficiency and lowers uniformity except in the region of small δ. Expressed as the ratio, $\delta/\Delta\theta_B$, the variation between output beam powers is reduced to about 3% when $\delta/\Delta\theta_B \approx 0.1$. This assumes the hologram consists only of the principle gratings. If good uniformity is required, this small δ region should be used, and thus an optically thin hologram is desirable, since its Bragg acceptance angle is large. Useful diffraction efficiency may approach 100% in the large δ regime, where $\delta/\Delta\theta_B > 1$. Again this assumes only the principle gratings are present, and both efficiency and uniformity degrade in the presence of cross-gratings.

Cross-gratings. The presence of 'cross-gratings' between object beams enhances the above effect, and reduces the acceptable size of δ in order to give good uniformity. These gratings may exist due to a coherent recording of all beams simultaneously, or due to saturation in a sequential recording.

Non-uniformity of modulation. Interference between gratings superimposed in the same volume leads to a spatially varying efficiency. This means that the average diffraction efficiency is in general lower than the local maximum. With more than two gratings present, the uniformity of modulation, and hence efficiency,

may be controlled in principle over some region by appropriate choice of the relative phases of the gratings. In order to achieve the best performance from fan-out holograms in DCG, the theoretical problem of choice of phases must be solved, and an experimental procedure must be devised to record holograms with this phase control.

Saturation. Exponential saturation in DCG as determined by experimental and theoretical analysis in chapter 3 is of a sufficient magnitude to cause significant cross-gratings (difference frequencies). Holographic materials with greater modulation range are therefore desirable. Saturation also can result in the destruction of the relative grating amplitudes that would be expected from a linear addition of exposures. This in turn further degrades the uniformity of diffracted powers.

Required index modulation. The product of total index modulation and hologram thickness which is required to reach maximum efficiency for a fixed wavelength and hologram geometry increases by a factor of $\sqrt{N}$ where N gratings are incoherently superimposed.

Experimental. Experimental results for the fan-out to two case show a good qualitative agreement with theory. Trends are correctly predicted and explained as the result of coupling effects and saturation. Quantitative agreement is good in terms of efficiency, uniformity, and spurious beam powers if the effects of beating between gratings are ignored. If this effect is included, then observed efficiencies are consistenly higher than those predicted by theory. This point remains unresolved. It is thought that a careful consideration of the propagation of diffracted

beams within this non-uniformly modulated medium may yield the answer without resorting to exact numerical theories.

Results for higher levels of fan-out show a trade-off between efficiency and uniformity which agrees qualitatively with theory. Results are not significantly better for incoherently recorded holograms because of the effects of saturation. Useful efficiency is typically limited to less than 20% for 5% uniformity in a fan-out to 9 hologram in the small δ regime, but this varies even between identically exposed holograms due to the uncontrolled relative phases of superimposed gratings.

It is felt that experimental problems may be alleviated somewhat with high level fan-out holograms if a random distribution of phases can be ensured. This case ensures a statistical distribution of grating phases, which will tend to make the resulting modulation depth more uniform. This approaches the diffuse hologram case that Upatnieks and Leonard showed could theoretically achieve 64% efficiency [UPA70]. Goodman and Knight [GOO68] also showed that in diffuse holograms good uniformity and low noise may be obtained by using high beam ratios. DCG is likely to be capable of superior results in this regime because of the greater thickness and index modulation available.

Chapter 5

Reflection Holograms.

Reflection holograms are formed by the interference of two wavefronts incident from opposite sides of the plane of the recording medium. Consequently, replay at the same wavelength yields a reflected reconstructed wave. Reflection holograms were first discussed and made by Denisyuk [DEN62]. Some years earlier, Gabriel Lippmann made a type of photograph with a photographic layer in optical contact with mercury which succeeded in replaying colour by interference [LIP94]. This is very similar in principle to Denisyuk's single beam reflection hologram, and Lippmann's name is still used to refer to reflection holograms.

The fringe planes of reflection holograms are substantially parallel to the surface, and so a reflection hologram exhibits the properties of a dielectric stack, such as an interference filter. The principle effect is that a reflection hologram exhibits a strong wavelength selectivity in reflection. In some applications, such as dichroic mirrors, holograms are alternatives to interference filters, and in others they they are unique, allowing lens properties and beamsplitting functions also to

be included.

Various authors have discussed the properties and applications of reflection holograms in DCG, notably McCauley et al [MCC73], Cullen [CUL82], Magarinos and Coleman [MAG85] and McGrew [MCG80]. Applications include aircraft head-up displays and laser protection eyewear, and interconnection devices for optical and electronic circuits [KOS85,FEL87]. Also reflection filters for demultiplexing wavelength encoded systems in telecommunications systems have been investigated [MCC85,DUN85]. These filters have a linearly varying fringe spacing, which means that the peak reflection wavelength varies with position across the filter.

5.1 Exposure geometry.

The simplest type of reflection hologram has fringe planes perfectly parallel to the surface of the recording medium, and is known as a 'conformal' hologram, or holographic mirror. It has the unique property that its surface fringe period is infinite, and therefore all higher diffraction orders collapse into the transmitted beam and first reflected order. It is a perfect reflector in the sense that only one reflected beam is present. This feature is important where a hologram is to be used as a mirror for human vision, such as in a head-up display, where the unwanted diffraction orders of any non-conformal reflection hologram may produce confusing extra images in the field of view. The exposure geometry for a conformal hologram may also be particularly simple, as shown in figure 5.1.

The single incoming beam passes through the plate and then the holographic layer before reflecting and emerging again through the layer. The incident and re-

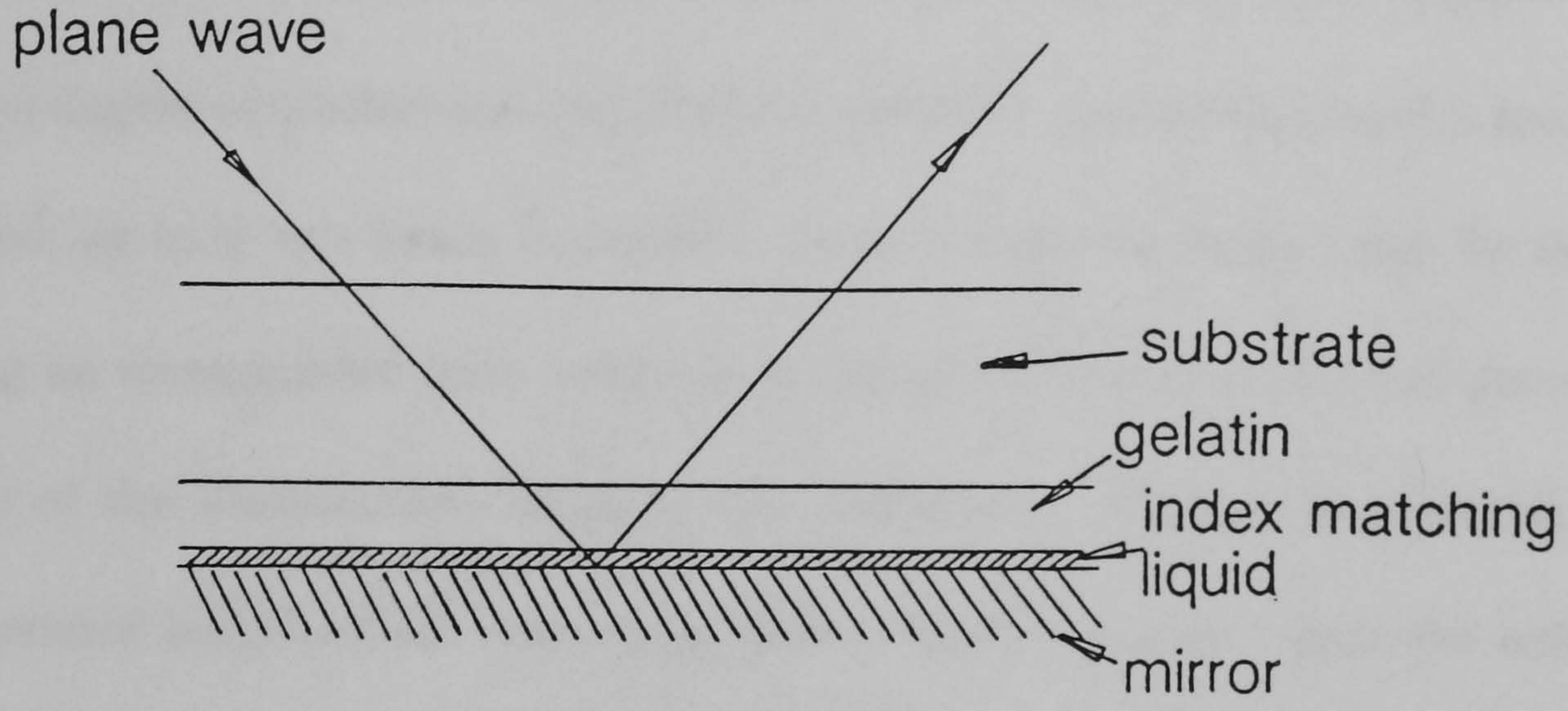

Figure 5.1: Exposure geometry for a conformal reflection hologram.

flected beams interfere to form a hologram which has interference fringes parallel to the mirror. If the mirror is in close contact with the gelatin, the fringes will be parallel to the surface of the gelatin. This may be achieved by index-matching the gelatin to a plane mirror. This also performs the important function of eliminating unwanted multiple reflections between the gelatin and mirror. A typical index matching liquid is xylene, which may be easily injected between plate and mirror, and simply evaporates after separation, but is highly toxic and a suspected carcinogen. Di-n-butly phthalate is more viscous, and does not evaporate, but is safe and may easily be removed by immersion of the plate in acetone or methanol immediately prior to processing.

As the plate and mirror will normally be held strongly by the index matching

fluid, this arrangement is mechanically very insensitive to vibration. This makes longer exposure times and hence larger holograms less of a problem. This is how large dichroic mirrors the order of 25cm square for head-up displays can be made easily, under conditions where a split beam technique would require a much improved degree of mechanical and thermal stability. In addition, optics are greatly simplified, as only one beam is needed. Such holograms in fact can be made by scanning an unexpanded laser beam in a raster pattern over the hologram, since stability of the illumination beam is not important. All that is required is that the coherence length of the recording illumination is greater than the total path length through the gelatin and index matching fluid and back.

Note that if the mirror is replaced by an object, a reflection hologram of the Denisyuk type will be formed, and if that object is another reflection hologram, a 'contact copy' of that hologram will be recorded. In the latter case, index matching fluid should again be used, and again the recording may be done with a scanning beam (this has been done successfully during this thesis using a simple beam scanner which uses two tilting mirrors for x and y scans), or a source of relatively limited coherence length, such as a spatially filtered low pressure sodium lamp.

The geometry shown suffers from the effects of unwanted internal reflections from the external surface of the plate, causing fringes to appear as a result of variations in the thickness of the glass substrate, and which modulate the efficiency of reflection across the hologram. A way to avoid these problems is to index match the reflected beam out of the plate and remove it by an absorbing neutral density filter, as shown in figure 5.2.

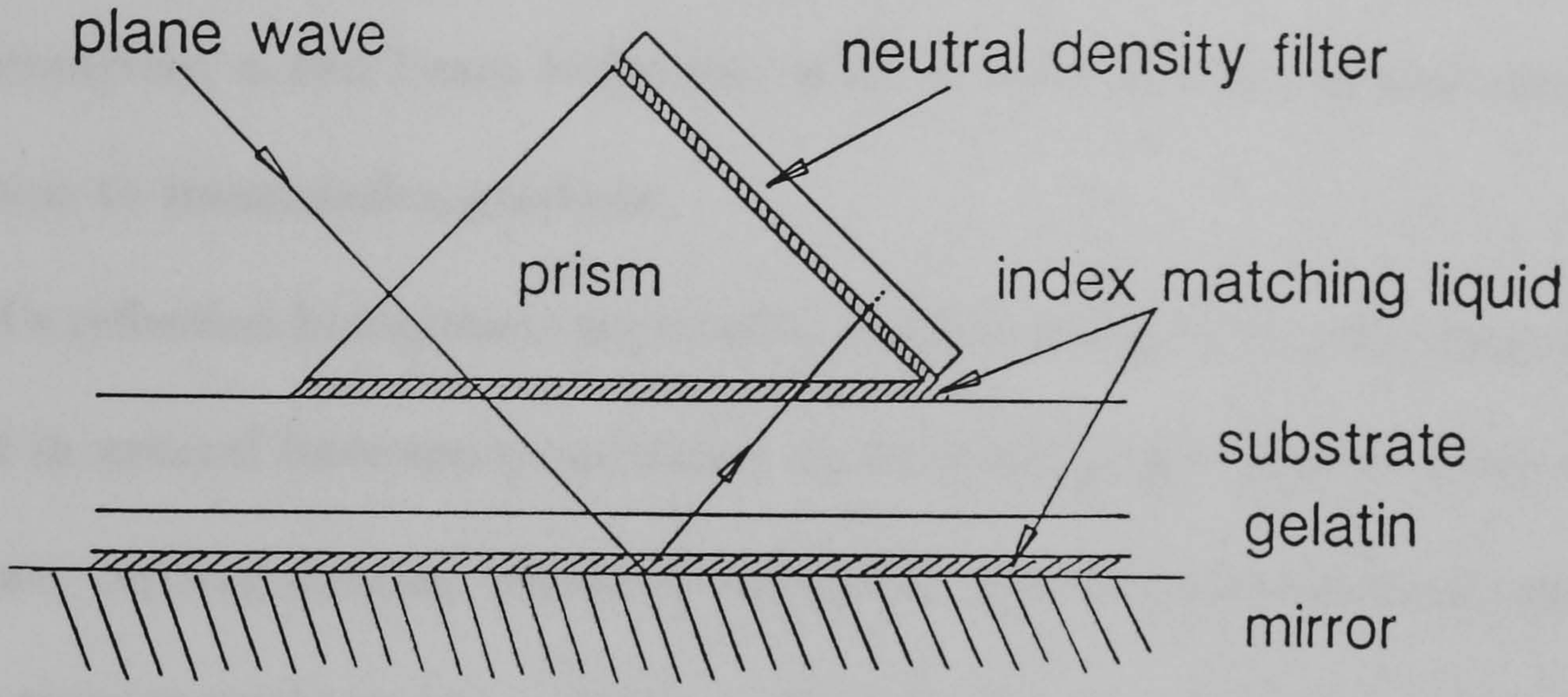

Figure 5.2: An improved geometry for recording conformal holograms.

The major restriction with the single beam method of recording reflection holograms is that only limited control of beam ratio is possible, and generally a beam ratio of unity is impossible to attain, since some light must be absorbed by the holographic layer on the first pass. Typical DCG transmission values are 25% at 488nm to 75% at 514nm in a 16μm layer, limiting minimum beam ratios (defined as I_{ref}/I_{obj}) to 16 to 1.8 at the external surface. Therefore, refractive index modulation would be expected to vary with depth, and the non-uniformity would be related to the transmission of the holographic medium. Calculations show that the index modulation should be a maximum at the mirror surface, with no DC bias, and a minimum at the external surface, with a maximum bias. However, it should be remembered that modulation formation and processing mechanisms

play a large part in affecting modulation profiles both transverse and in depth.

If a reflection hologram is required to have planar fringes which are not parallel to the surface, there must be an angle, and therefore a gap, between the holographic medium and the mirror. This may be filled by a prism or index-matching liquid. Alternatively, a two beam technique may be used, similar to that described in relation to transmission gratings.

If a reflection hologram is required to have focussing power, the fringe structure must in general have some curvature, and the hologram must be made either by contact copying another reflection hologram with an identical fringe pattern, or by a more general two beam method which has the focussing power in one or both arms.

5.2 Reflection hologram theory.

Kogelnik's approximate coupled wave theory gives simple expressions for the diffraction efficiency and near-Bragg response of thick reflection holograms, which may be amplitude, phase or mixed holograms [KOG69]. The efficiency of a pure phase grating at Bragg incidence is given by

$$\eta = \tanh^2\left(\frac{\pi n_1 d}{\lambda \cos\theta_0}\right) \tag{5.1}$$

where the symbols are as for the transmission grating equation 3.8. This represents the case of a conformal hologram with beams incident at θ_0 to the normal. The behaviour of the tanh function is asymptotic as the modulation, n_1, increases,

in contrast to the periodic nature of a transmission hologram. In addition, the angular acceptance of a reflection hologram is the order of twice as great as that of the corresponding transmission grating, and, as opposed to a transmission grating, as modulation increases, the bandwidth also increases.

More accurate theories for general reflection gratings only consist of the modal approach [CHU70], which results in an extremely difficult numerical problem for any reflection gratings, and improved coupled wave analyses. Moharam and Gaylord developed the exact coupled wave analysis for uniform gratings of either the transmission or reflection type [MOH81A], which may be slanted. They also discuss in more detail the case of the conformal reflection hologram [MOH81]. However, in [MOH82], Moharam and Gaylord point out that the coupled wave theory does not strictly apply in the case of a conformal hologram, since the grating is no longer truly periodic. This is due to the fact that in the conformal case, there is only a finite number of fringe periods, whereas whenever there is any slant of the fringes, the assumption that the hologram is infinite in its transverse extent means that there are an infinite number of fringe periods. Although this is also an approximation, for typical slant angles (say, 30°), the surface fringe period is around 1μm, and there are a thousand periods per millimetre. However, in the conformal case, a typical fringe period may be 150nm, and so a 5μm grating only contains 33 fringes. Obviously, the effect of the non-periodicity should be considered.

Moharam and Gaylord show that, as expected, the effect of non-periodicity becomes rapidly smaller with the thickness of the hologram, since the number of grating periods approaches infinity. When the error is significant, the actual

reflection value depends on the phase of the grating relative to the surfaces of the hologram. For all conformal gratings considered here, such effects are negligible. This can be proven by means of the modelling method which was chosen, which includes these effects. This model is similar to that of Moharam and Gaylord, and is based on the chain-matrix method commonly applied to single and multi-layer thin-film structures, such as interference filters. A similar approach was taken by Sharlandjiev and Todorov [SHA85], in which they simplified a periodic grating profile to a periodic two-layer system by equalising the Fourier harmonics of the two structures. This can make calculation faster especially for gratings with a large number of periods.

Sharlandjiev and Todorov also presented theoretical results for the spectral selectivity of conformal gratings recorded in an attenuating medium [SHA85A]. They calculate the fringe profile throughout the depth by assuming the incident waves are attenuated as they traverse the medium. The spectral response is then calculated based on this non-uniform profile. Their results are of limited use with respect to DCG because additional recording and processing mechanisms complicate the resultant profile. Therefore, it is not possible in general to predict response by such a simple method. Owen and Solymar [OWE80] looked at the diffraction efficiency of conformal gratings recorded in an absorbing medium by a unique coupled wave method which was later extended to a more general method with respect to nonuniformity profiles by Newell [NEW87]. The model developed here uses Newell's method of polynomial modulation profiles with a chain-matrix thin-film approach to calculating reflection values.

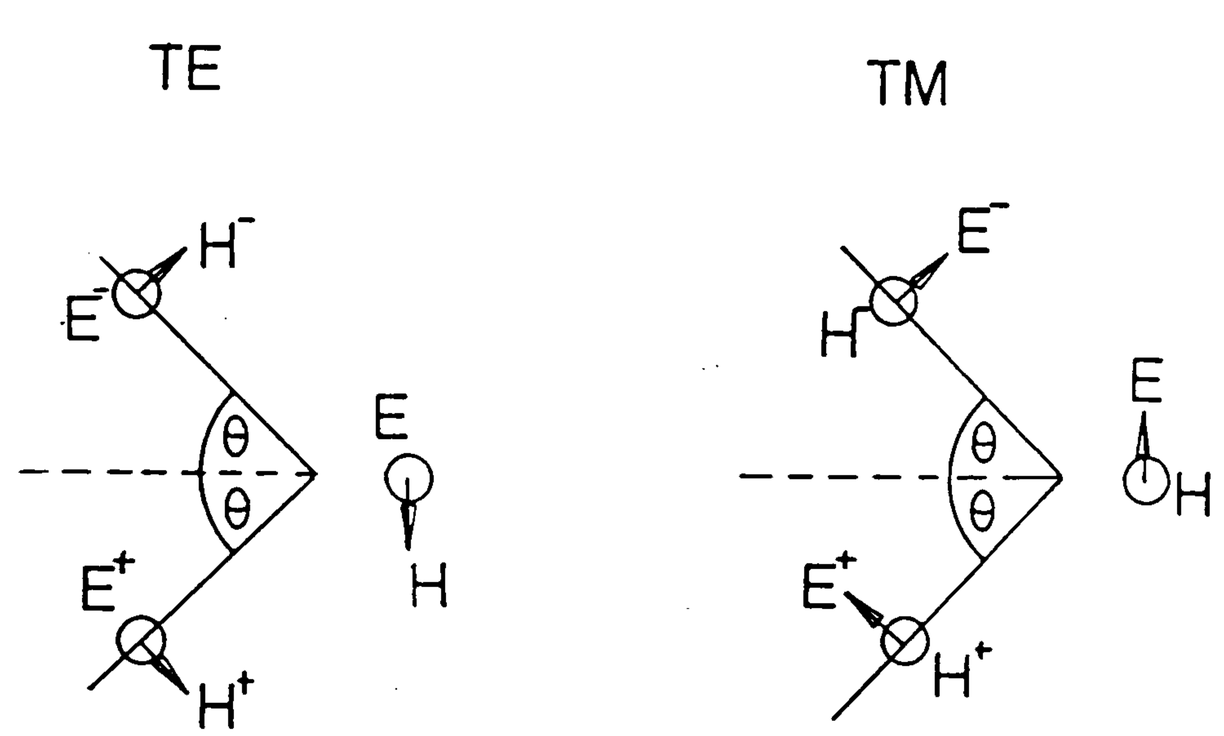

Figure 5.3: The variables used in matrix analysis of conformal holograms.

5.3 The conformal hologram model.

In this model, the grating structure is reduced to a stack of thin, plane, parallel slabs each of uniform refractive index. The reflection and transmission properties of such a stack can be analysed using the following matrix method.

If E and H denote electric and magnetic field amplitudes at a boundary and E^+ and E^- denote the travelling wave amplitudes moving to the left and right respectively, we can represent the relations between E, H, E^+ and E^- as shown in figure 5.3, for transverse electric (TE) mode,

$$E = E^+ + E^- \tag{5.2}$$

$$H = (H^+ - H^-)\cos\theta \tag{5.3}$$

$$= (E^+ - E^-)(\epsilon/\mu)^{1/2}\cos\theta. \tag{5.4}$$

Putting E and H into matrix form,

$$\begin{bmatrix} E \\ H \end{bmatrix} = \begin{bmatrix} 1 & 1 \\ g & -g \end{bmatrix} \begin{bmatrix} E^+ \\ E^- \end{bmatrix} \tag{5.5}$$

where $g = (\epsilon/\mu)^{1/2}\cos\theta$. Hence

$$\begin{bmatrix} E^+ \\ E^- \end{bmatrix} = \frac{1}{2} \begin{bmatrix} 1 & 1/g \\ 1 & -1/g \end{bmatrix} \begin{bmatrix} E \\ H \end{bmatrix}. \tag{5.6}$$

For transverse magnetic (TM) polarisation, the relevant eqations are

$$E = (E^+ + E^-)\cos\theta \tag{5.7}$$

$$H = H^+ - H^- \tag{5.8}$$

$$= (E^+ - E^-)(\epsilon/\mu)^{1/2}. \tag{5.9}$$

Putting E and H into matrix form,

$$\begin{bmatrix} E \\ H \end{bmatrix} = \cos\theta \begin{bmatrix} 1 & 1 \\ g & -g \end{bmatrix} \begin{bmatrix} E^+ \\ E^- \end{bmatrix} \tag{5.10}$$

where $g = (\epsilon/\mu)^{1/2}/\cos\theta$ (not the same as for TE). Hence

$$\begin{bmatrix} E^+ \\ E^- \end{bmatrix} = \frac{1}{2\cos\theta} \begin{bmatrix} 1 & 1/g \\ 1 & -1/g \end{bmatrix} \begin{bmatrix} E \\ H \end{bmatrix}. \tag{5.11}$$

In order to obtain a matrix for a thin film, the phase change, ϕ of a wave traversing a film with thickness δ and refractive index n is needed. This is given by

$$\phi = kn\delta\cos\theta \tag{5.12}$$

where k is the vacuum wave vector magnitude and θ is the angle of propagation in the film. The travelling wave amplitudes to the left (subscript l) and the right (subscript r) of the film are related by

$$E_l^+ = \mathrm{e}^{-i\phi}E_r^+ \tag{5.13}$$

$$E_l^- = \mathrm{e}^{i\phi}E_r^-. \tag{5.14}$$

The tangential field components on either side of a film, m, for both polarisations are then given by

$$\begin{bmatrix} E_m \\ H_m \end{bmatrix} = \frac{1}{2} \begin{bmatrix} 1 & 1 \\ g & -g \end{bmatrix} \begin{bmatrix} \mathrm{e}^{-i\phi} & 0 \\ 0 & \mathrm{e}^{i\phi} \end{bmatrix} \begin{bmatrix} 1 & 1/g \\ g & -1/g \end{bmatrix} \begin{bmatrix} E_{m+1} \\ H_{m+1} \end{bmatrix} \tag{5.15}$$

simplifying to

$$\begin{bmatrix} E_m \\ H_m \end{bmatrix} = \frac{1}{2} \begin{bmatrix} \cos\phi & -\frac{i}{g}\sin\phi \\ -ig\sin\phi & \cos\phi \end{bmatrix} \begin{bmatrix} E_{m+1} \\ H_{m+1} \end{bmatrix} \tag{5.16}$$

where g is appropriate to the polarisation being considered.

For a stack of films, the series of matrices are multiplied to relate the tangential field components on either side of the stack.

$$\begin{bmatrix} E_1 \\ H_1 \end{bmatrix} = M \begin{bmatrix} E_s \\ H_s \end{bmatrix} \tag{5.17}$$

where

$$M = \prod_{m=1}^{s-1} \begin{bmatrix} \cos\phi_m & -\frac{i}{g}\sin\phi_m \\ -ig\sin\phi_m & \cos\phi_m \end{bmatrix}. \tag{5.18}$$

s denotes the rightmost medium which is assumed to be infinite.

To obtain reflection coefficients, the incident and reflected electric fields, E_0^+ and E_0^-, are related to E_s^+ by

$$E_0^+ = \frac{1}{2} \begin{bmatrix} 1 & 1/g_0 \end{bmatrix} M \begin{bmatrix} 1 \\ g_s \end{bmatrix} E_s^+ \tag{5.19}$$

$$= \alpha E_s^+ \tag{5.20}$$

$$E_0^- = \frac{1}{2} \begin{bmatrix} 1 & -1/g_0 \end{bmatrix} M \begin{bmatrix} 1 \\ g_s \end{bmatrix} E_s^+ \tag{5.21}$$

$$= \beta E_s^+. \tag{5.22}$$

Then the amplitude reflection coefficient, r, is given by $r = \beta/\alpha$. Irradiance reflection magnitude, R, is then

$$R = \left|\frac{\beta}{\alpha}\right|^2 . \tag{5.23}$$

The phase of the reflected beam may also be obtained from the amplitude reflection phase, γ,

$$\gamma = \tan^{-1}\left(\frac{Im(\beta/\alpha)}{Re(\beta/\alpha)}\right) \tag{5.24}$$

where $Im(\beta/\alpha)$ and $Re(\beta/\alpha)$ represent the imaginary and real parts respectively of (β/α). To obtain the correct phase, the signs of the numerator and denominator in the $\tan^{-1}$ expression should be used to get the correct quadrant.

In the real modelling done here, the medium is taken to be non-magnetic ($\mu = \mu_0$) and non-absorbing (ϵ is purely real), although it is a simple matter to allow complex refractive indices by modifying the computer program. Refractive index, n, is related to the permittivity, ϵ, by $n^2 = \epsilon$. If absorption is zero, power is conserved and transmission can be obtained from $T = 1 - R$.

A computer program was written to calculate the matrices and perform the matrix multiplications to obtain reflectivity or transmission values.

5.4 Modifications to the model.

In addition to the method described above, some modifications were made to the computer model to allow a more complete description of holograms in dichromated gelatin. In similar fashion to the non-uniformity modelling done with transmission

holograms in chapter 3, we allow variation in reflection holograms of local average refractive index, n_0, and refractive index modulation, Δn, with depth, x. The variations are of the form

$$n_0(x) = n_0(1 + ax' + bx'^2 - b/12) \tag{5.25}$$

$$\Delta n(x) = \Delta n(1 + cx' + dx'^2 - d/12) \tag{5.26}$$

where n_0 and Δn are the overall average values, and x' is the normalised depth coordinate such that $-0.5 < x' < +0.5$. a, b, c and d are the free parameters we have to obtain a fit with experiment. The $b/12$ and $d/12$ terms ensure that the free parameters do not alter the overall average values.

The effect of the non-uniformity parameters were investigated by means of graphs of transmission versus wavelength. Wavelength was chosen as opposed to angle because reflection holograms are much more wavelength sensitive than angularly sensitive. It is therefore more appropriate to obtain wavelength scans in a spectrophotometer, whereas only limited information could be obtained from angular scans. With transmission holograms, the reverse is the case. Theoretical plots showing the effect of a, b, c and d respectively are shown in figures 5.4 to 5.7. The other parameters used in these graphs are thickness, $d = 15\mu$m, average refractive index (both inside and outside the hologram), $n = 1.52$, and wavelength, $\lambda = 514.5$nm. The recording beams are incident from both sides at

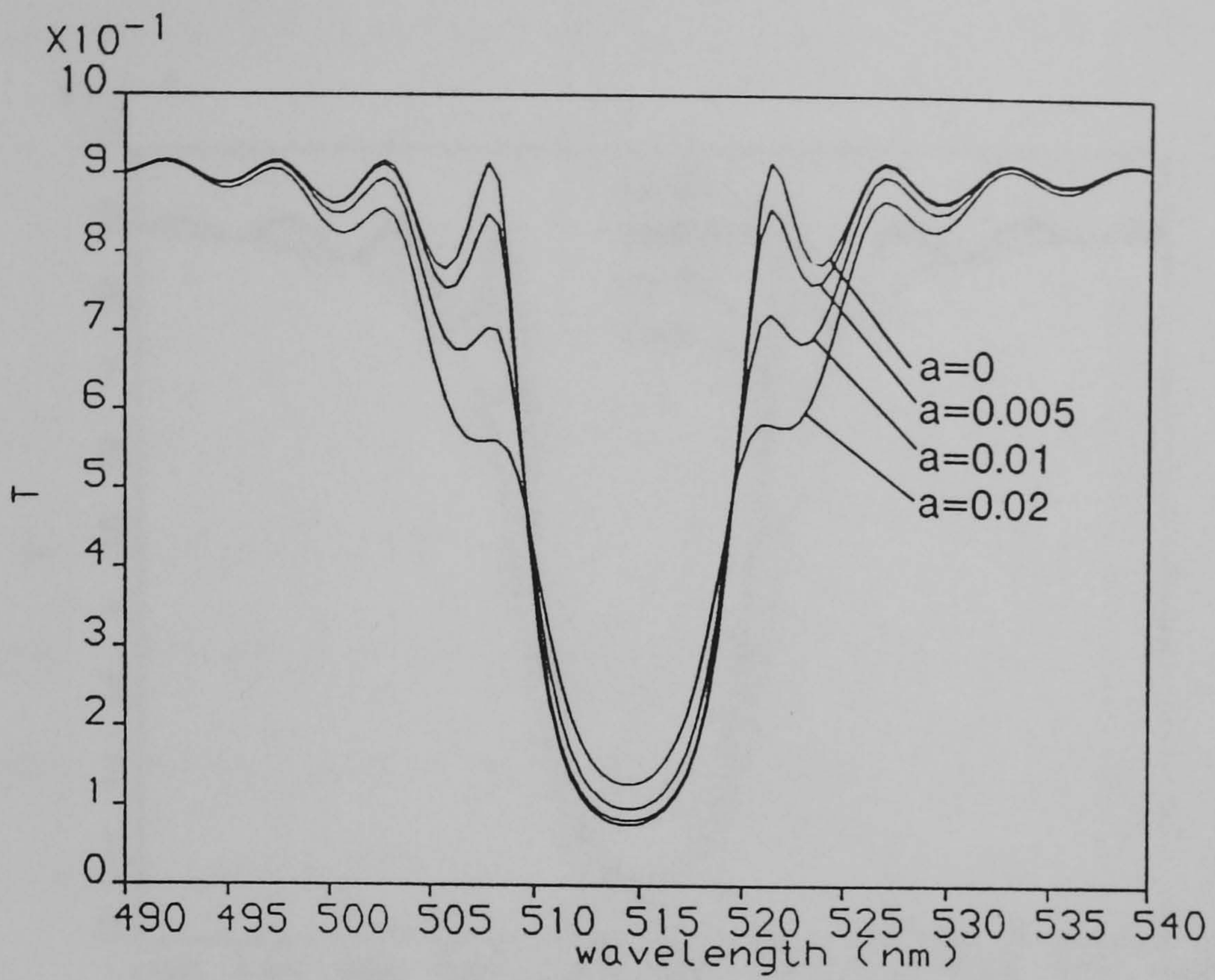

Figure 5.4: The effect of variation of a on transmission of a conformal reflection hologram.

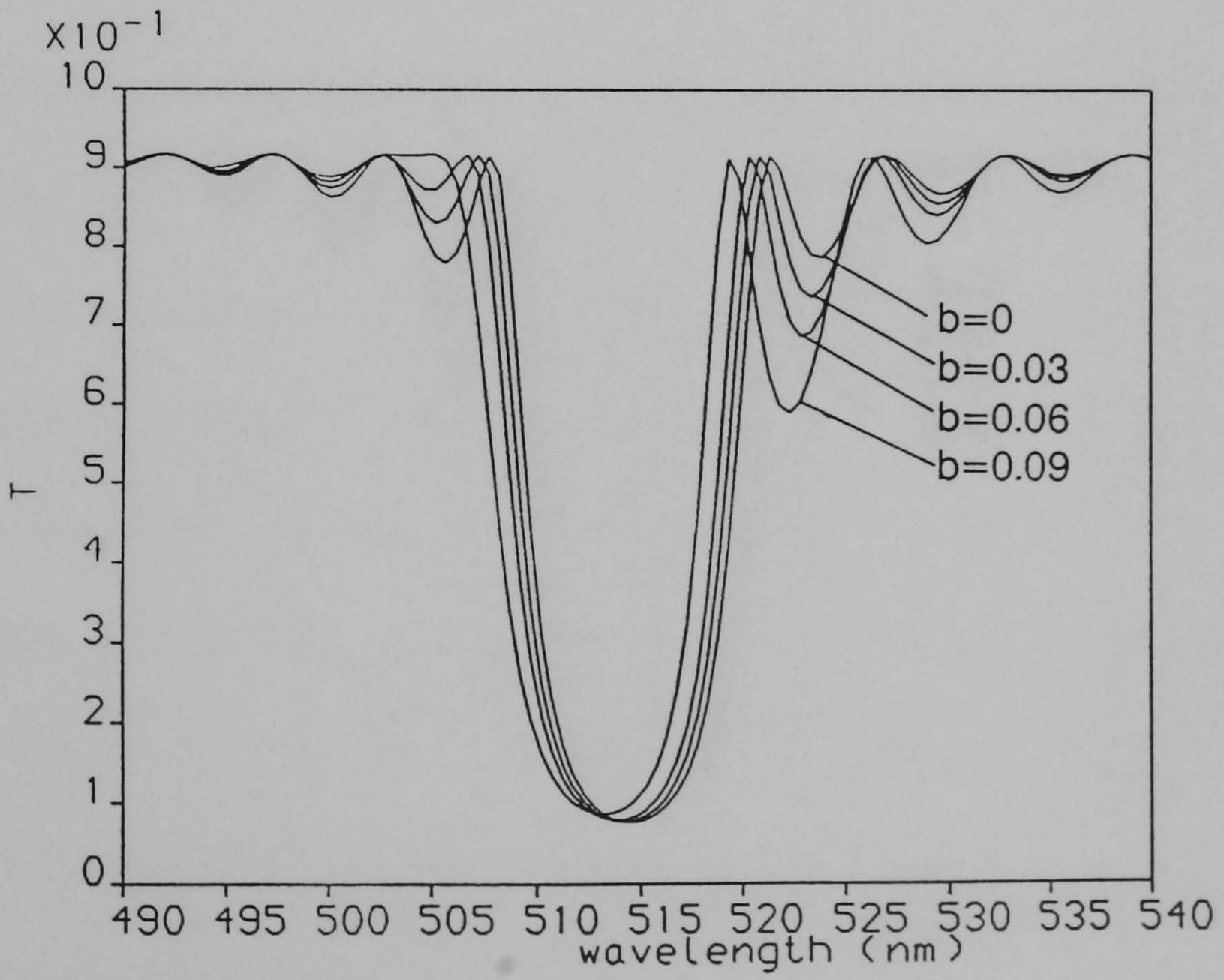

Figure 5.5: The effect of variation of b on transmission of a conformal reflection hologram.

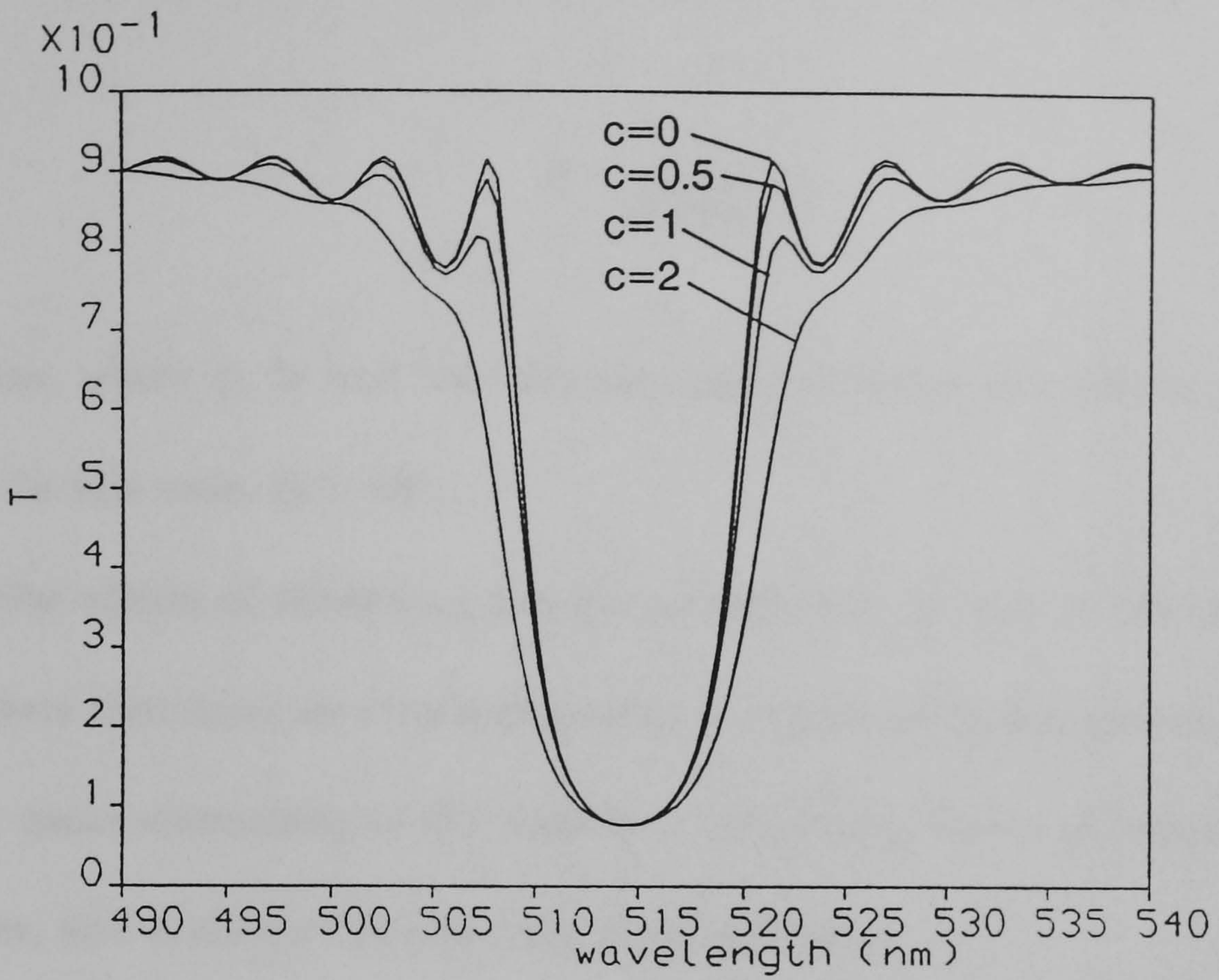

Figure 5.6: The effect of variation of c on transmission of a conformal reflection hologram.

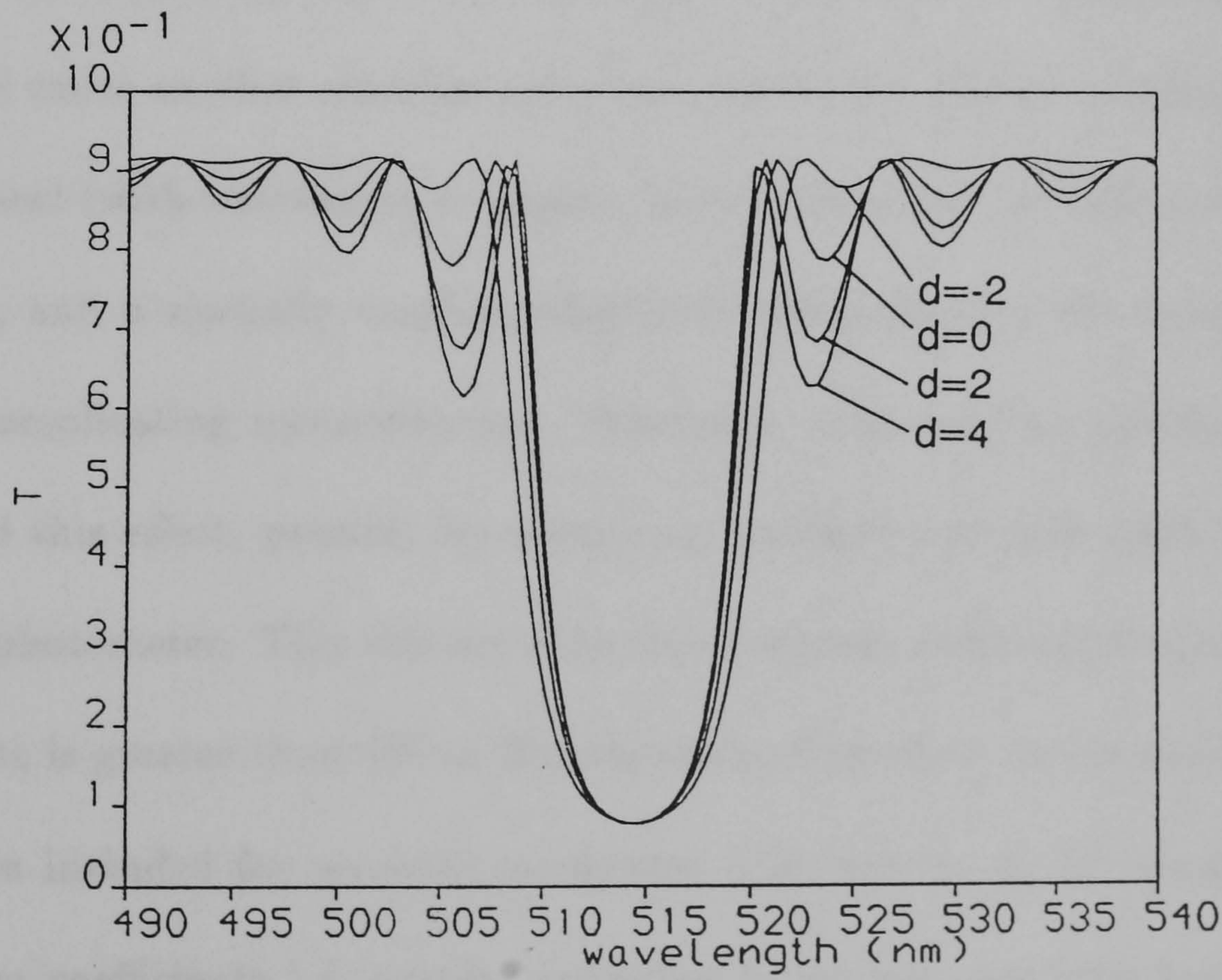

Figure 5.7: The effect of variation of d on transmission of a conformal reflection hologram.

normal incidence. This corresponds to a fringe period, Λ, given by

$$\Lambda = \frac{\lambda}{2n \sin \phi_i} \tag{5.27}$$

of 169nm, where ϕ_i is half the internal angle between the reference and object beams. In this case, $\phi_i = 90°$.

Similar effects of these four free parameters can be seen to the corresponding parameters that describe non-uniformities in transmission holograms in chapter 3. a and c cause smoothing of the sidelobes, whereas b causes an asymmetry in the sidelobes, and d affects the size only of the sidelobes.

In order to analyse a real conformal hologram, account must be taken of the reflections at the air interfaces. The model as given will take account of the first air/gelatin boundary, but if the substrate is included as another parallel slab, this will cause another coherent reflection, which will add an oscillating reflection component (with wavelength or angle). In fact, the substrate will never be parallel anyway, and a spatially varying reflectivity will exist over the hologram at any time, complicating measurements. Normally, measurement techniques will try to avoid this effect, possibly by using only partially coherent light, such as in a spectrophotometer. This will see only an incoherent reflection loss as long as the substrate is greater than 100 or 200μm thick. Therefore, in the model, provision has been included for separate incoherent reflection losses by using the Fresnel reflection coefficients. A simple correction factor has also been included for an absorption loss due to stain in the gelatin. If absorption had been significant in its magnitude, it would be necessary to include it as a complex refractive index in

each matrix of the stack calculation. This would be necessary to account for the partial absorption of the reflected light from each interface.

5.5 Experimental results.

A hologram was recorded using the arrangement of figure 5.2 and processed using the standard processing procedure of chapter 2. The hologram was recorded for a specific purpose (a miniature head-up display mirror for use inside a pilot's helmet), and was required to have a peak reflection of over 75% at 545nm at 45°, with a FWHM bandwidth of less than 20nm.

After drying, the hologram was analysed by placing it in a Shimadzu spectrophotometer which peformed transmission versus wavelength scans at various angles of incidence. Polarisers were placed in both the reference path and the sample path in the spectrophotometer in order to get calibrated transmission results with linear polarisation.

It was found that a good fit could be achieved at normal incidence, but the parameters used in this fit did not agree with results at larger angles. In fact, the form of the scans changed in a way that could not be accounted for by the model at all (sidelobes became blurred as the incident angle increased). Investigation of the spectrophotometer showed that it operates by imaging a slit onto the sample. Therefore, the probe beam cannot be perfectly collimated, and must consist of rays travelling in a range of angles. The range of angles was measured to be about ±1.5°. Trying a simple triangular weighting of the transmission values from the model gave a satisfactory match with the experiment.

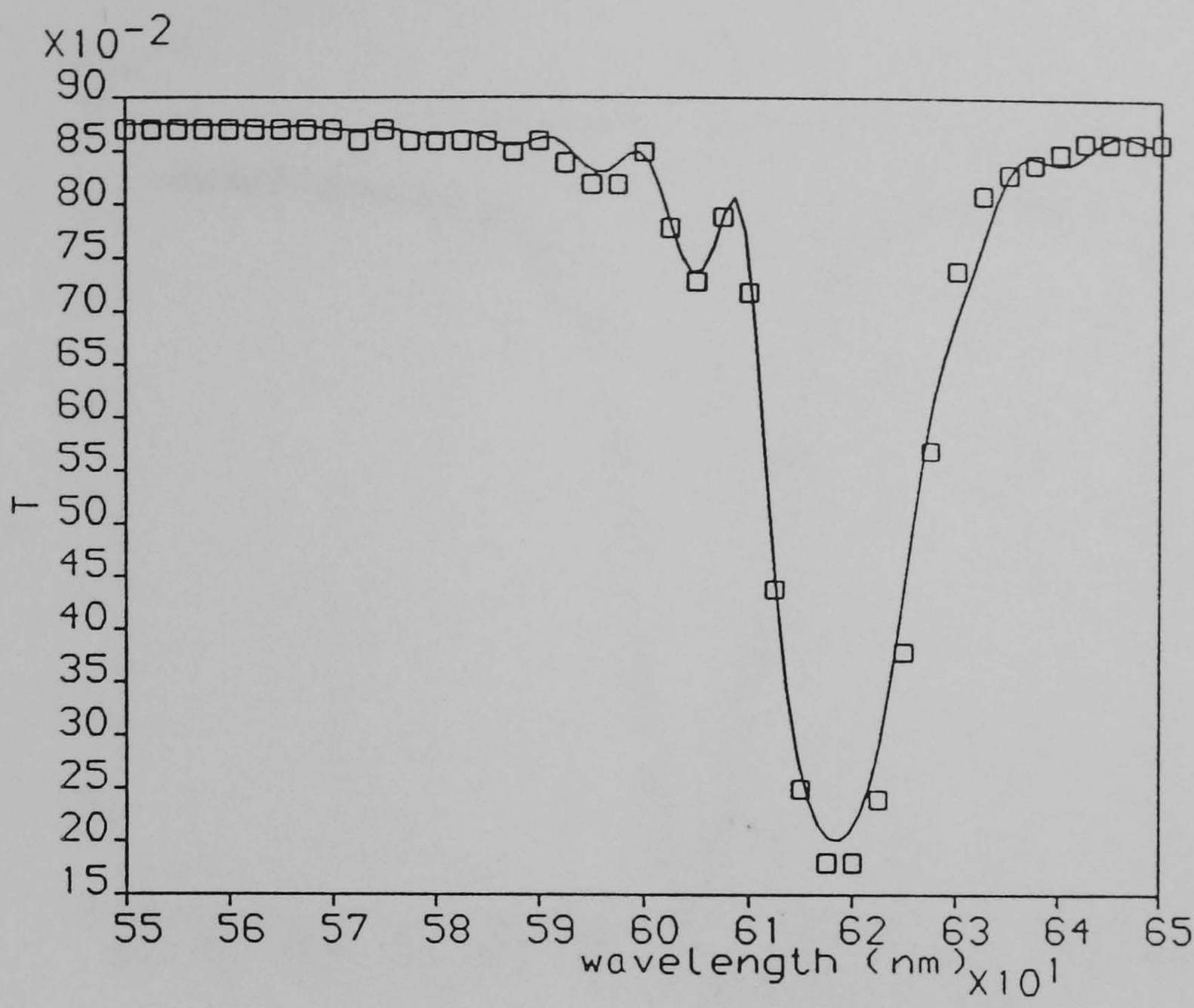

Figure 5.8: Theoretical fit (line) and experiment (squares) for a conformal hologram at 0°. $a = 0.015, b = -0.05, c = 1.7, d = 1.2$.

Graphs are given in figures 5.8 to 5.12 showing both experimental points and theoretical fits. The thickness of the processed hologram was measured as 14.0μm, its average refractive index was determined to be 1.495, and average index modulation, from the fit, is 0.020. The fringe period was calculated from the theoretical fit to be 206nm. Figure 5.11 shows experimental and theoretical response at 45° to TM polarisation (electric field in the plane of incidence), whereas the other graphs are for TE polarisation. In all graphs, the uniformity parameters are; $a = 0.015, b = -0.05, c = 1.7, d = 1.2$.

Figures 5.13 and 5.14 show the resultant bulk refractive index and modulation profiles within the gelatin. The bulk index shows a 2% variation, whereas the modulation shows a very large variation, from -65% to +100% of the average.

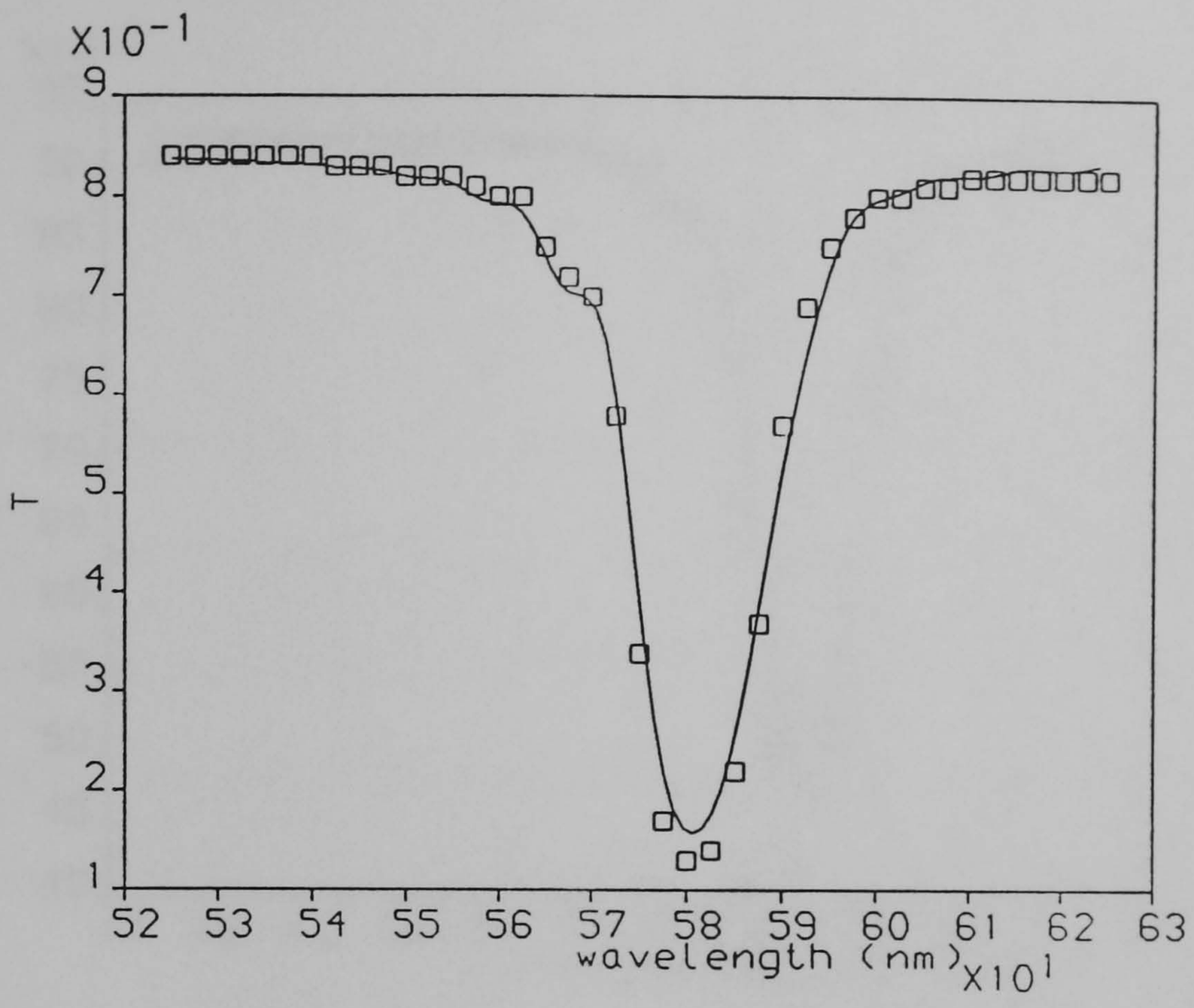

Figure 5.9: Theoretical fit (line) and experiment (squares) for a conformal hologram at 30°.

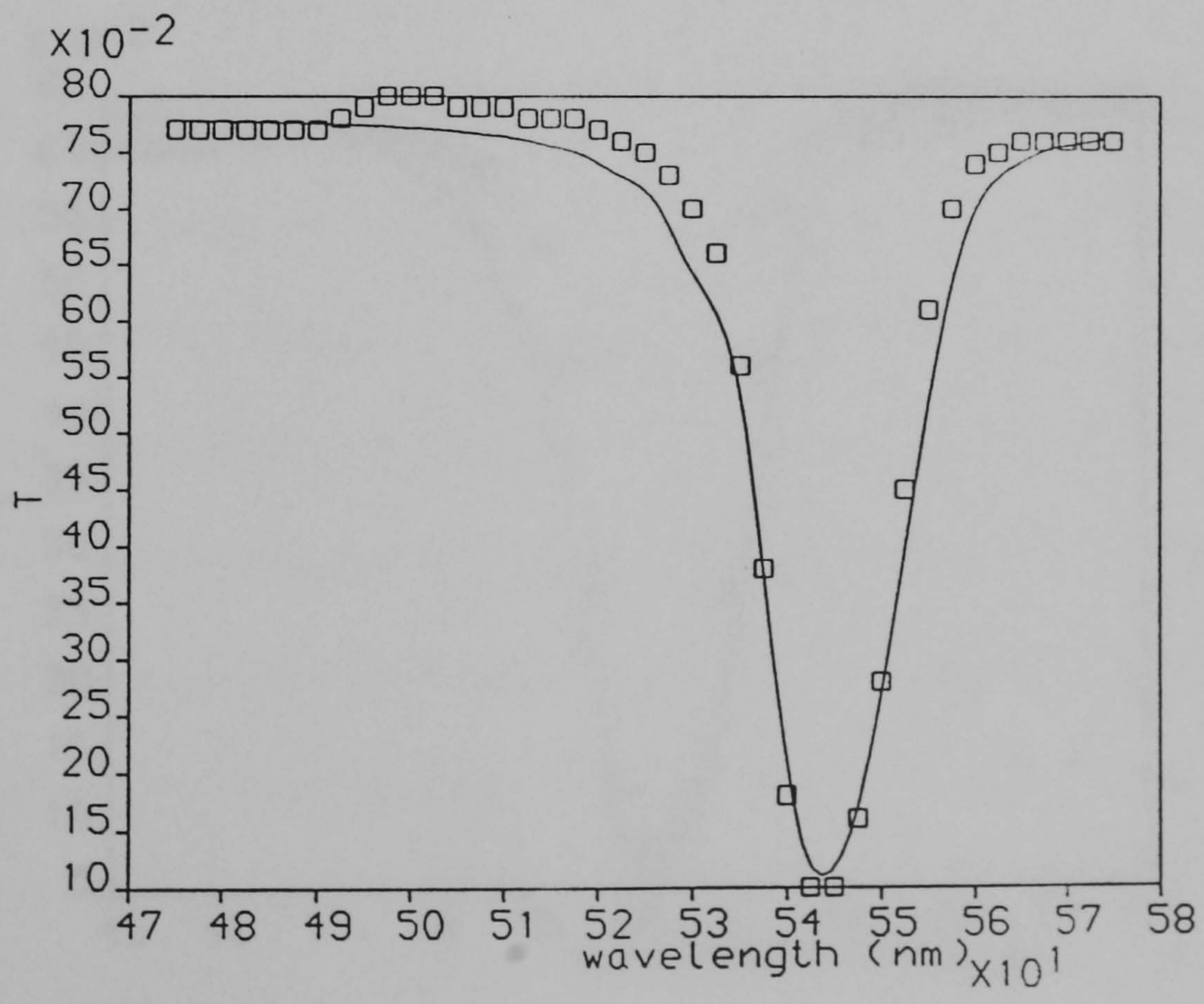

Figure 5.10: Theoretical fit (line) and experiment (squares) for a conformal hologram at 45°.

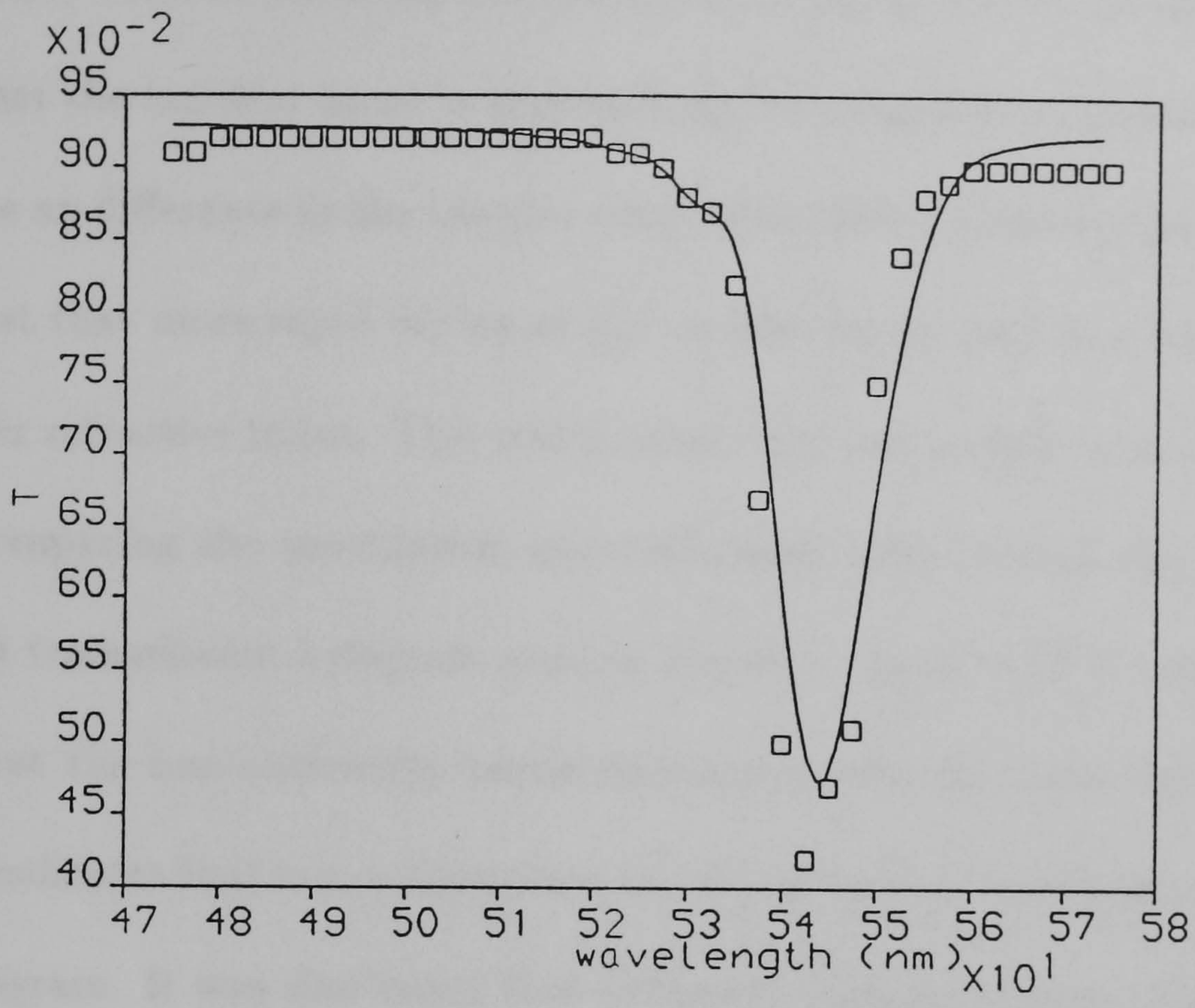

Figure 5.11: Theoretical fit (line) and experiment (squares) for a conformal hologram at 45°. TM polaristion.

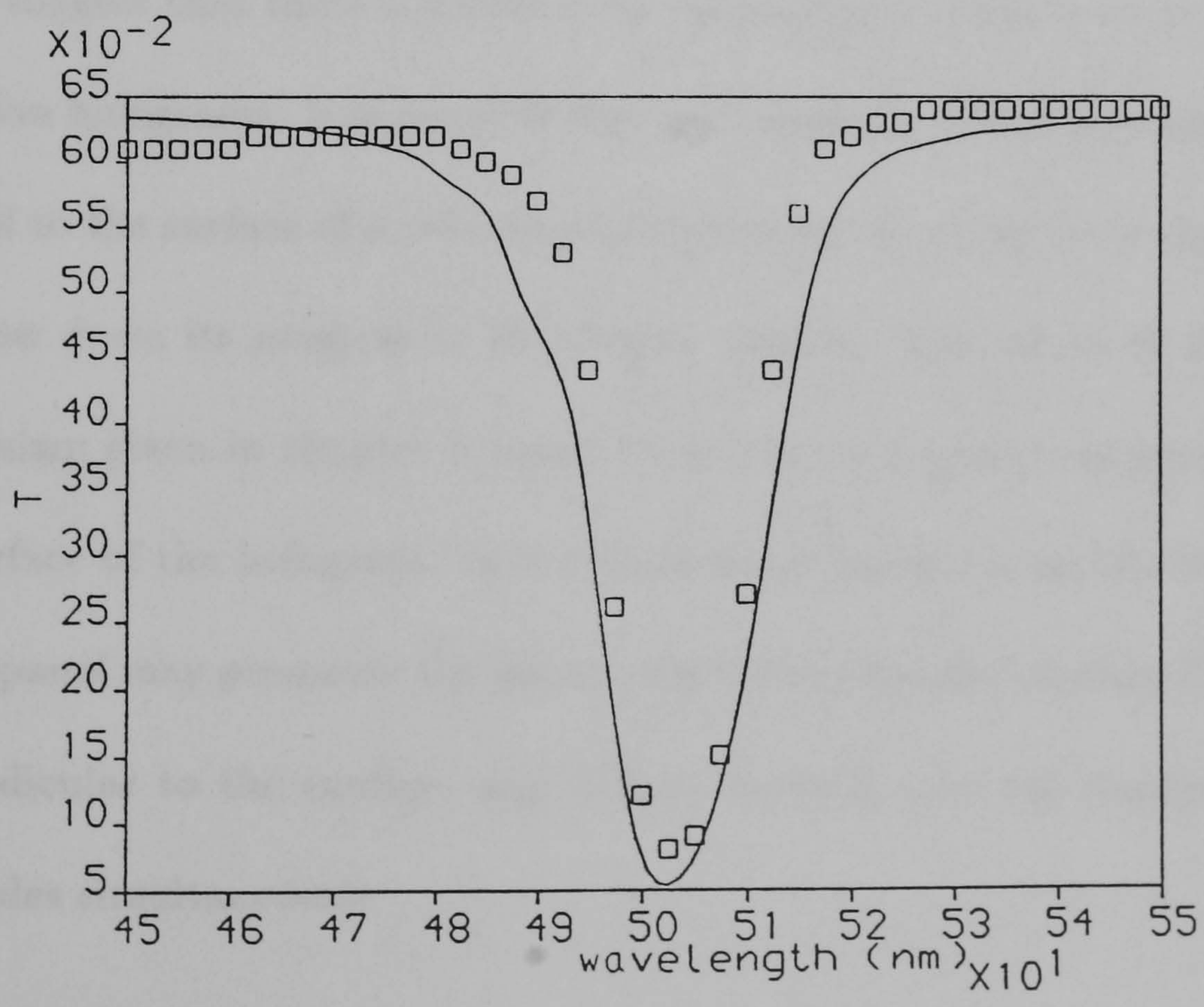

Figure 5.12: Theoretical fit (line) and experiment (squares) for a conformal hologram at 60°.

Note that without including absorption in the model it is not possible to determine whether the incident beam is approaching from negative or positive x' since there will be no difference to the angular scans. The model presented in chapter 3 would suggest that more rapid drying at the surface would lead to a lower density, and a lower refractive index. This would mean that the surface is at $x' = -0.5$.

Comparing the modulation non-uniformity with that of the identically processed transmission hologram grating shown in figure 3.20 in chapter 3, we can see that the non-uniformity parameters are greater by more than a factor of 2. This indicates that non-uniformities are dependent on the fringe structure within a hologram. It was also noted that reflection holograms take much longer to dry after processing, requiring a full 24 hours to stabilise as opposed to around one hour for transmission holograms in 14μm gelatin (at 40% RH, 20°C). These results would suggest that there is a differential drying rate which is more pronounced in reflection holograms. It is possible that the relatively rigid fringe planes which are parallel to the surface of a reflection hologram act as a barrier to the iso-propanol, and slow down its progress to the deeper regions. The model of the modulation mechanism given in chapter 2 would then lead to a greater index modulation at the surface of the hologram. In a transmission hologram on the other hand, the iso-propanol may permeate the gelatin via the unexposed 'channels' of soft gelatin perpendicular to the surface, and diffuse laterally into the harder regions from both sides simultaneously.

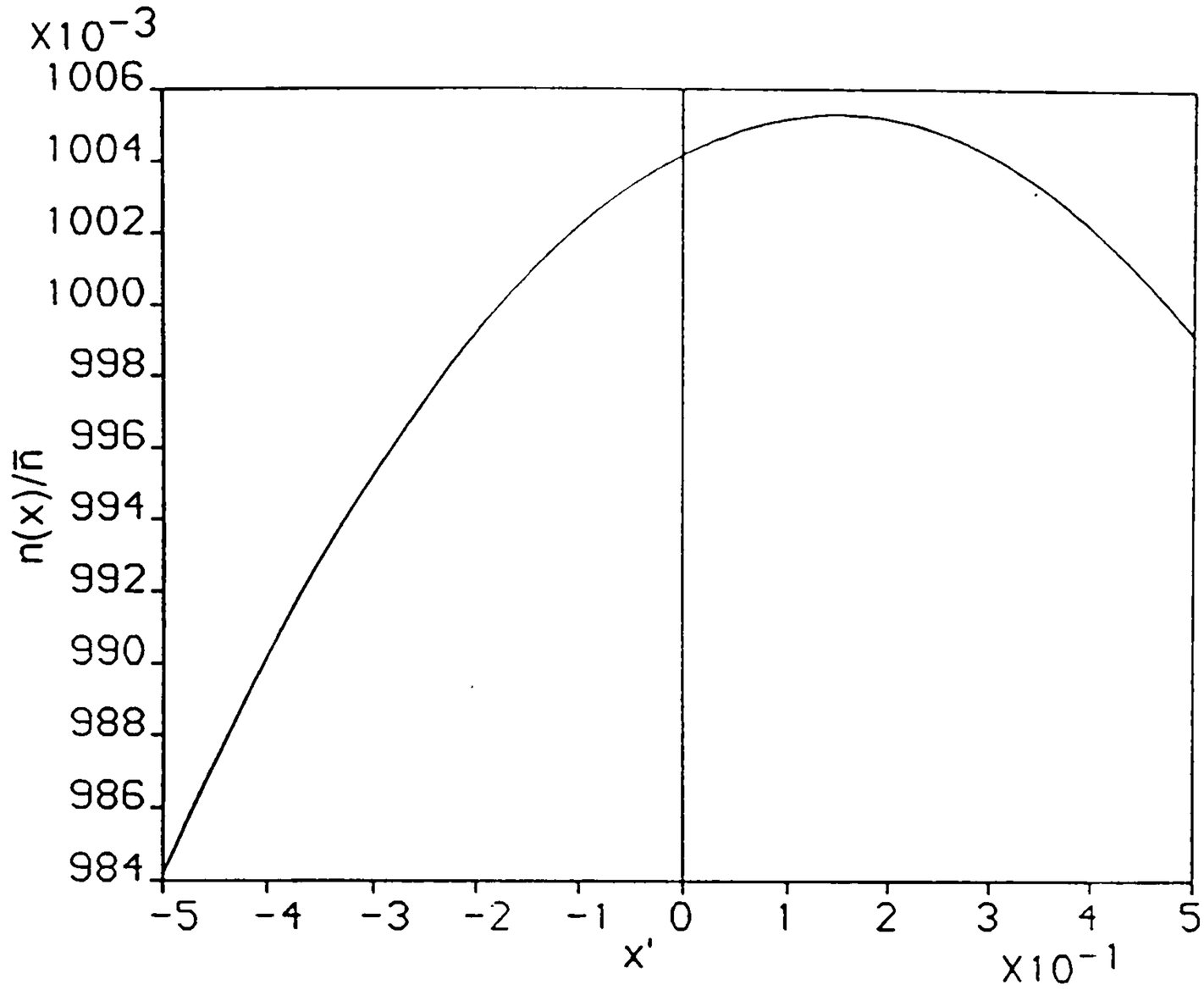

Figure 5.13: Bulk refractive index variation with x' in a conformal hologram.

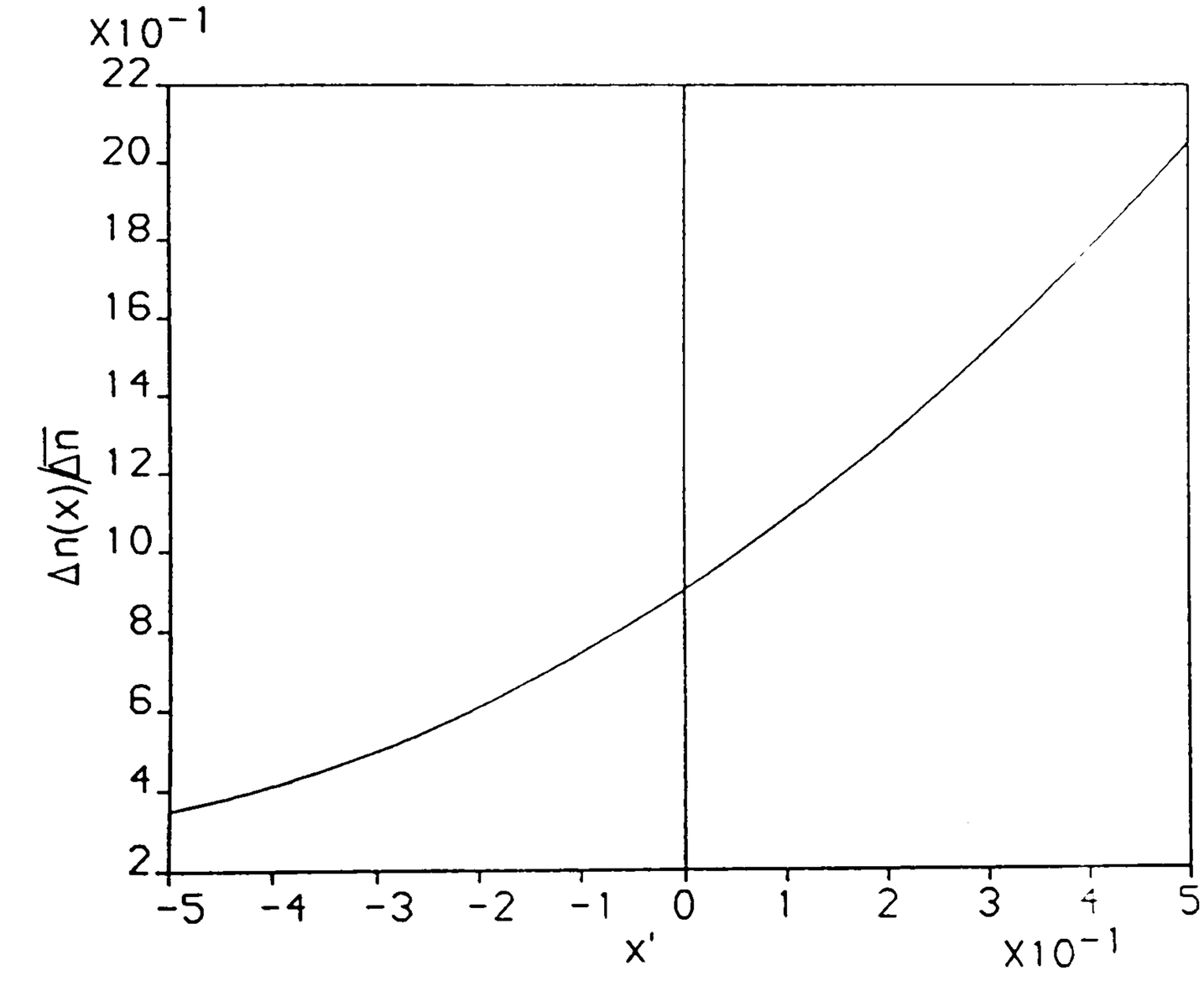

Figure 5.14: Refractive index modulation variation with x'.

5.6 Summary.

An experimental arrangement for recording conformal reflection holograms (holographic mirrors), has been described and used in practice to obtain holographic mirrors with specific properties. A theoretical model suitable for implementation on a computer has been given which models a conformal hologram as a stack of plane parallel slabs of uniform complex refractive index. Modifications to the model, including non-uniformities with depth in bulk refractive index and refractive index modulation, have been shown to be capable of satifactorily describing the structure of conformal holograms. The non-uniformities which match the theory with experiment are more than a factor of two greater than an identically processed transmission grating of the same thickness. This fact, in conjunction with the observation that reflection holograms take much longer to dry, indicates that drying rates and non-uniformities are dependent on the fringe structure within a hologram.

Chapter 6

Devices.

6.1 The Holographic Attenuator.

It is apparent from the angular scans of transmission gratings in DCG that a very high degree of attenuation of the incident beam is possible. This forms the basis of a very practical HOE for use with lasers - the variable laser beam attenuator [RED88].

The device is essentially a high efficiency transmission grating in DCG which has been optimised in its design and production to operate as a variable efficiency diffraction grating. The desirable properties of an attenuator are as follows.

1. Large dynamic range.

2. High power capability.

3. Low insertion loss.

4. Minimal beam deviation.

5. Minimal beam distortion.

6. Minimal spatial non-uniformites.

7. Insensitivity to polarisation.

8. Wavelength independence.

Of the above desired properties, it has been found that the holographic attenuator can equal or better the performance of a major commercial variable attenuator in all respects except wavelength independence and spatial non-uniformities at very high attenuation.

The device operates by rotating the holographic grating about a Bragg angle, thereby varying the amount of undiffracted light transmitted. The Bragg angle is chosen such that the centre of the required transmission range is achieved at normal incidence. (This minimises the beam translation that is introduced by the hologram and substrate at an angle to the beam.) For example, a 15μm gelatin hologram with Bragg angles at -2.5 and 30 degrees to the normal requires an angular range of about 5 degrees to cover the full range of attenuation, i.e. -2.5 to +2.5 degrees. With this type of hologram, transmission ratios of 100:1 may easily be achieved, with a maximum transmission of 90%. With anti-reflection coatings the maximum insertion loss can be reduced further.

For maximum transmission, the hologram should have minimum absorption. This can be achieved, as already mentioned, by omitting the pre-wash steps in the standard processing schedule. This trades off scatter against absorption, but in this application, low absorption is more desirable since typical absorption losses are

greater than scattering losses. More importantly, absorption causes a temperature increase in the gelatin which, if sufficient, may cause melting - hence limiting the maximum irradiance which the device can withstand before destruction. Power handling ability may be further increased by thorough drying, since the melting temperature of gelatin increases as its water content decreases. Drying can be done by careful baking (as described in chapter 2), vacuum drying or simply drying at STP in a zero-humidity atmosphere, such as in dry nitrogen gas.

Beam angular deviation is limited by the parallelism of the external surfaces of the substrate and cover glass used. Beam propagation quality is limited by the flatness of the surfaces. Thin microsheet glass (140μ and 200μ) was found to be insufficiently flat for use as cover glass, but 1mm glass slides cemented on to seal the HOE's were found to reliably maintain good beam quality, with a total beam deviation of less than 0.5 milliradians due to non-parallel faces. The optical cement used was Norland 61. This may not be the ideal cement, because its optical absorption was not measured, and absorption in the cement has the same affect as it has in the gelatin, i.e. it causes the gelatin to heat up under high illumination. Also the thermal conductivity of the cement should be considered as it effects the rate of removal of heat from the gelatin [TAG89].

The polarisation dependence of attenuators can be determined from coupled wave theory, which gives the coupling constant between beams as

$$\kappa = \frac{\pi n_1 \boldsymbol{s}_i . \boldsymbol{s}_j}{\lambda} \tag{6.1}$$

where $\boldsymbol{s}_i$ and $\boldsymbol{s}_j$ are the polarisation vectors of the i^{th} and j^{th} diffracted beams.

The efficiency, η, in turn depends on $\sin^2 \kappa$, and the transmission equals $1 - \eta$. Therefore, if a hologram has maximum efficiency for s polarisation, the efficiency for p polarisation will be lower, and transmission higher. In the standard attenuator format with beams at 0 and 30 degrees, this equates to a theoretical efficiency for p polarisation of 99.1% when that of s polarisation is 100%. However, by slightly over-exposing the hologram, the coupling for p-polarisation may be increased, raising its efficiency, while the s efficiency drops. The efficiencies for s and p polarisations may then be balanced and made equal to 99.8%, with intermediate polarisations having higher values, thus minimising polarisation dependence.

As the replay wavelength changes, the diffraction properties of a hologram change in a number of ways. Diffraction angles change, the Bragg angles move, and most importantly in this case, the required index modulation for maximum efficiency changes proportionately to the wavelength. Hence there is a decrease in efficiency to either side of the optimum wavelength, which limits the useful range of an attenuator. To maintain minimum transmission below 2% a full bandwidth of 20nm is typical.

Spatial non-uniformities have proved to be a problem with holographic attenuators. This appears to be mainly due to processing non-uniformities, and possibly thickness variations in the gelatin layer. The problem arises from the fact that a small change in efficiency when close to maximum attenuation will cause a much larger fractional change in transmission. We can analyse the approximate unifor-

mity required by considering Kogelnik's expression for efficiency,

$$\eta = \sin^2\left(\frac{\pi n_1 d}{\lambda \cos\theta_0}\right) \tag{6.2}$$

where the factors of interest here are the refractive index modulation, n_1, and the thickness of hologram, d. The transmission of the hologram will therefore be

$$T = 1 - \eta \tag{6.3}$$

$$= \cos^2\left(\frac{\pi n_1 d}{\lambda \cos\theta_0}\right). \tag{6.4}$$

When efficiency is very high, transmission is low, and a small change in efficiency will cause a larger fractional change in T. This fractional change increases as average efficiency increases. Any spatial non-uniformities in efficiency, such as may be caused by thickness variations of the gelatin, or non-uniform processing, will give rise to magnified non-uniformities in transmission. For example, if an attenuator has a transmission of 0.5%, then a 1% change in n_1 or d results in a 5% change in transmission. Alternatively, a 2% change in n_1 or d causes a 20% change in transmission. Therefore, to achieve simultaneously high attenuation range and good uniformity, the gelatin must be sufficiently flat optically, and care must be taken to ensure sufficiently uniform exposure and processing.

6.2 The holographic polarising beamsplitter.

Any grating may be considered to be a beamsplitter if more than one output beam is used. Volume gratings generally only produce a significant zero and single first order, and typically 95% of the incident power is split between these two beams. The relative power in the two beams may be chosen by setting the recording exposure energy. If the grating is a symmetric transmission grating, with its fringe planes perpendicular to the surface, then the beamsplitting ratio may be varied in use by slight rotation of the hologram while causing minimum deviation of the diffracted beam. This would correspond conveniently to, for example, a hologram placed at 45° to the incident beam which generates a split diffracted beam at 90° to the incident beam.

As described in section 6.1, volume gratings have polarisation-dependent properties which can be used to positive effect in a holographic polarising beamsplitter. From equation 6.1, it can be seen that if the angle between the polarisation vectors of the incident and diffracted waves is 90°, then the coupling parameter, κ, must drop to zero, giving zero diffraction efficiency, irrespective of the index modulation. This represents the case where the internal diffraction angle is 90°, and the polarisation vectors are in the plane of the beams (TM polarisation). If now TE polarisation is incident on the grating, the angle between the polarisation vectors is zero, and the coupling parameter is a maximum, defined by the exposure energy. This polarisation may therefore theoretically have 100% diffraction efficiency, while a TM polarisation beam is transmitted without diffraction. This device therfore operates as a holographic polarising beamsplitter (HPBS), which

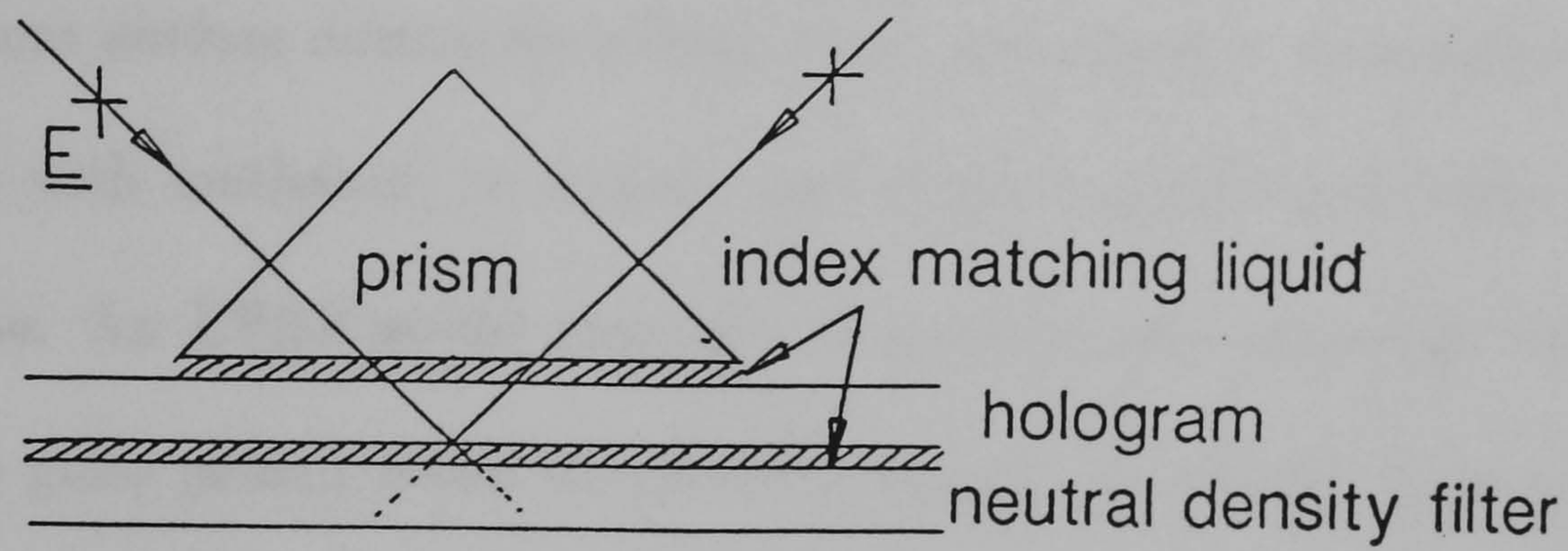

Figure 6.1: Recording arrangement for a transmission HPBS.

separates an incident wave into two orthogonal linear polarisations.

An HPBS may be made either as a transmission or a reflection hologram, the principle differences being in the angular and wavelength selectivities. A transmission HPBS will be more sensitive to angle than a reflection one, but less sensitive to wavelength. Which type is more appropriate will depend on its intended application. Experimentally, a reflection HPBS involves the simpler single beam holographic mirror type of arrangement, but it is generally necessary to 'tune' its thickness after processing, or experiment with the exposure geometry to obtain the correct final fringe spacing, even for final use at the original recording wavelength. Symmetrical transmission devices do not suffer from this at all, so experimental HPBS's were made by the split-beam transmission arrangement shown in figure 6.1.

Since an HPBS requires an *internal* diffraction angle of 90°, it is necessary to couple beams in and out by means of prisms, both at recording and replay. This is because it is impossible to achieve a 90° angle between the beams inside a hologram due to refraction at the surface. The prisms must be index-matched onto the front surface during recording, using, for example, di-n butyl phthalate (removable with methanol) or xylene, and index-matched onto both front and back for use. An HPBS would generally be permanently cemented between two right angle glass prisms when in use with an optical cement, such as Norland 61. The right angle surfaces of the prisms should be anti-reflection coated for the operation wavelength to minimise reflection losses and coherent 'fringing' due to multiple internal reflections.

An experimental HPBS made using the arrangement shown was measured to have a diffraction efficiency with TE polarisation of 91%, and a TM efficiency of 0.1% - a ratio of TE/TM of 910. Therefore the diffracted beam shows extremely good polarisation selectivity. However, equally important is the ratio of TM to TE power in the transmitted beam. This is not as good, showing approximately 97% of the TM light transmitted, but also 5.8% of TE transmitted - a ratio of 16.7. This is likely to be purely due to a non-optimal exposure during recording, since it is normally straightforward to reduce transmitted TE power to below 0.5% in the case of a holographic attenuator. In the experiment here, lack of time prevented further optimisation.

An important factor in obtaining a high performance HPBS is the control of the final bulk refractive index of the holographic layer. Processing alters its value,

and typically results in a final value of 1.490 to 1.495 [NEW87], which is generally lower than glass refractive indices (around 1.52 to 1.53). This will mean that the angle between the beams in the gelatin will not be exactly 90°, and therefore the hologram will have a non-zero efficiency for TM. In order to alleviate this problem, the prisms used in replay should ideally have the same refractive index as the gelatin layer.

6.3 A space-invariant interconnect hologram.

Fan-out holograms have been investigated for applications as interconnect devices between arrays of optical logic devices in optical computing research. In these experiments, fan-out devices may operate in either a space-variant or a space-invariant mode. The space-variant mode involves a separate interconnect hologram associated with each input pixel, and therefore the operation carried out on each pixel may be different. In the space-invariant mode an identical operation is performed on each input pixel. Here are presented details of such a space-invariant device which was used in a digital optical circuit to perform an edge-extraction operation on a binary input image.

To perform an edge-extraction operation, a hologram is required which 'fans-out' each input pixel to its corresponding four nearest neighbours in the output plane. Equivalently, this can be thought of as a fan-in to each output pixel from its nearest neighbours in the input plane. To realise this operation space-invariantly, a hologram may be used in the Fourier transform plane of a lens, as shown schematically in figure 6.2. This diagram shows the components in a straight line. In the

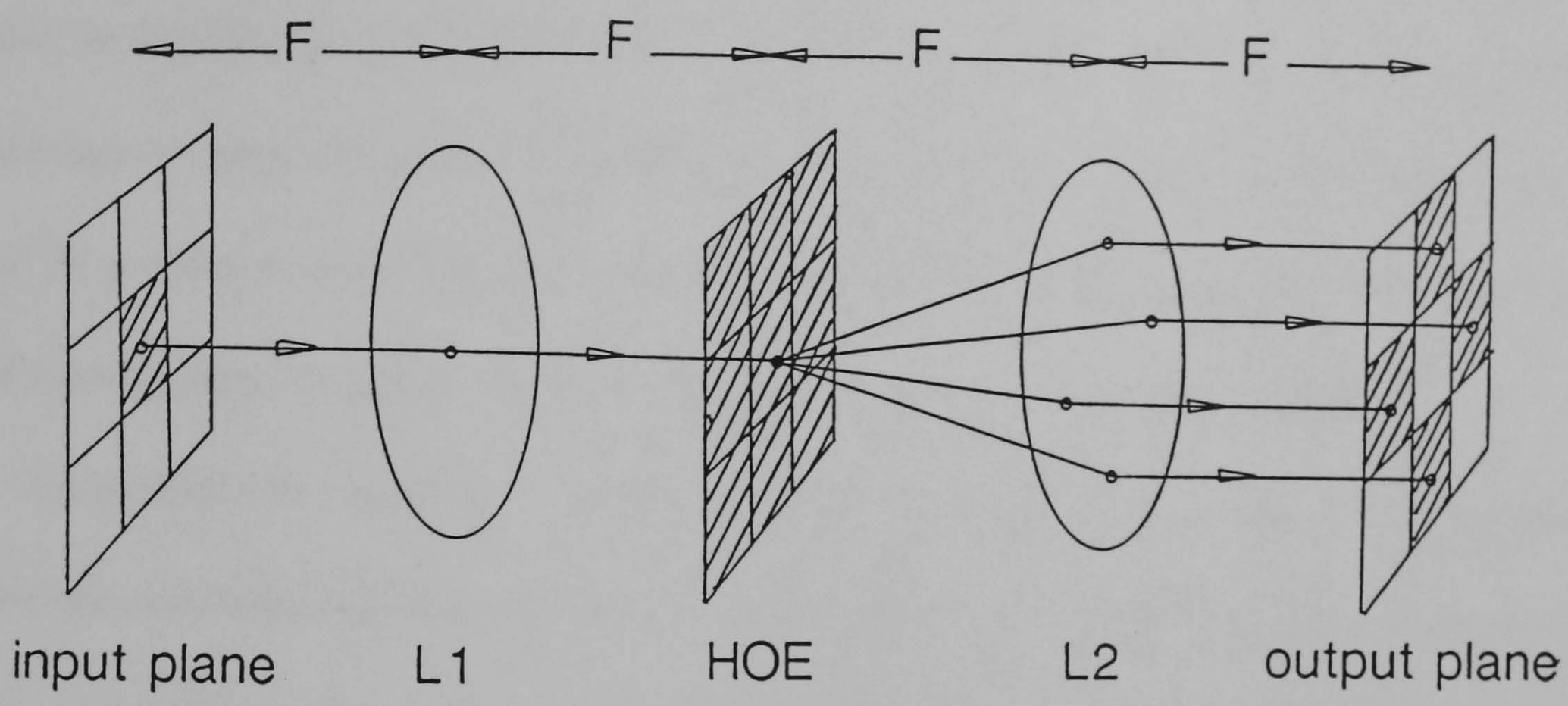

Figure 6.2: Schematic of the operation of a fan-out hologram for edge-extraction.

experiment, however, the hologram will impose an angle on the optical axis.

Each input pixel (which is a focal spot) is transformed into a collimated beam by the first lens L_1. This beam falls on the hologram and is angularly divided into four collimated beams, which are re-transformed by L_2 into focal spots at the nearest neighbour positions in the output plane.

Each input pixel is transformed into a beam at a different incident angle at the hologram, so it is necessary that the hologram has an angular acceptance (related to its Bragg response) which is larger than the range of incident angles. However, the hologram must have a certain holographic 'thickness' in order to achieve high diffraction efficiency. This means it must have a limited angular acceptance. In practice, the hologram should be made as 'thin' as possible (by reducing the angle between the reference and object beams), while still maintaining sufficient diffrac-

tion efficiency. In the real holograms used (14μm thick), the angular acceptance to the first zero in efficiency is about $\pm 4.5°$. Therefore the range of incident angles must be limited to well below this if a uniform response to all pixels is required. This can be done by using long focal length transform lenses. This in turn means that if a certain spot size is required, the lens and hologram aperture must be sufficiently large to allow a diffraction limited spot of this size or smaller.

An additional requirement of the design is that there is a linear relationship between the incident angle at the hologram and the diffracted angle. This is so that all beams in the output plane register accurately. In other words, we want to make sure that moving an input point by d moves its corresponding interconnect output by exactly d also. This does not follow in general if we consider the grating equation;

$$\sin\theta_0 - \sin\theta_1 = \lambda/d \tag{6.5}$$

where θ_0 here is given by geometric consideration of the function of the lens;

$$\theta_0 = \theta_B + \tan^{-1}(x_0/f). \tag{6.6}$$

θ_B is the Bragg angle of the hologram, x_0 is the position in the input plane relative to the axis of the lens, and f is the focal length of the lens. The resultant θ_1 from the grating equation leads to a focal spot position in the output plane given by

$$x_1 = f\tan(\theta_1 - \theta_B). \tag{6.7}$$

There is not a simple linear relationship in general between x_0 and x_1.

However, it is clear that what is required is that a change in θ_0 should cause an equal magnitude change in θ_1. Therefore, taking the derivative of the grating equation with respect to θ_0, we get

$$\frac{d\theta_1}{d\theta_0} = \frac{\cos\theta_0}{\cos\theta_1}. \tag{6.8}$$

Hence, $\frac{d\theta_1}{d\theta_0}$ can only be equal to 1 or -1 when $\theta_0 = \theta_1$ (no diffraction) or $\theta_0 = -\theta_1$. The latter corresponds to a symmetric hologram (where the fringe planes are perpendicular to the surface). There will also be a limited region in this case where $|x_1| \approx |x_0|$. The extent of the region can be calculated using the equations above, if the position tolerances, and hologram parameters are known.

Therefore, the hologram should be symmetric with the minimum values of θ_0 and θ_1 which give the required diffraction efficiency. This will ensure maximum uniformity of response in conjunction with optimum positioning accuracy.

The recording arrangement for the hologram is shown in figure 6.3. The fan-out hologram was recorded by exposing with the four object beams and the reference beam simultaneously. The object beams were derived from another hologram, which had four holographic lenses producing exactly the desired output spot pattern that the interconnect arrangement was to generate from a single input pixel. The focal spot plane was Fourier transformed onto the hologram using the same lens as used in the operation of the hologram, to ensure the accurate registration of the output focal spots on replay.

In this experiment, 300mm focal length lenses were used with a hologram of

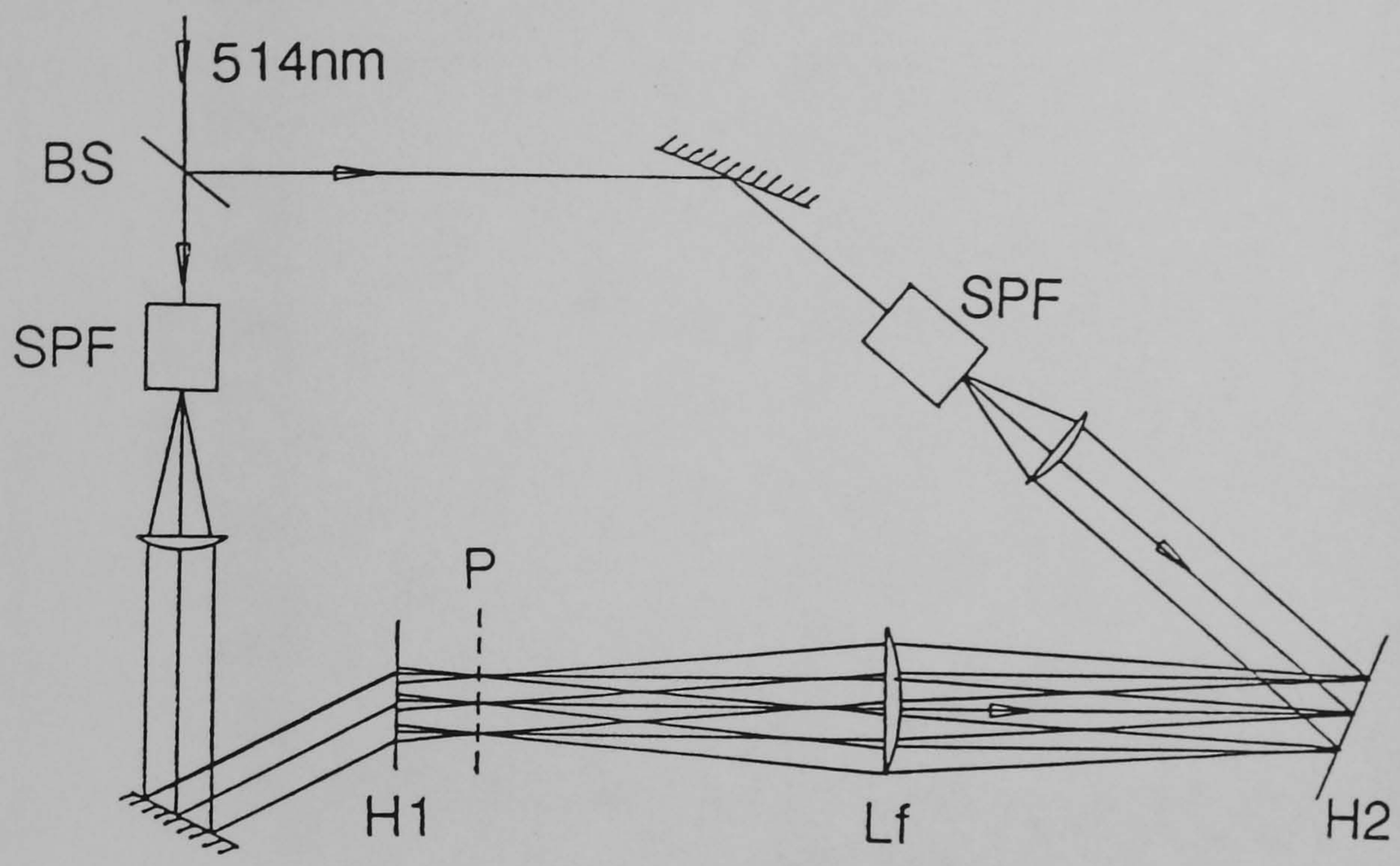

Figure 6.3: Recording arrangement for a fan-out hologram.

10mm square, and a fan-out angle of 0.38° in order to achieve the desired spot size of 30μm with a pixel separation of 2mm. As discussed in chapter 4, there is a trade-off between efficiency and uniformity of beam powers in fan-out holograms. Figure 6.4 shows this trade-off measured for a series of the holograms described here recorded with a range of exposures. The uniformity of the beams at recording was $\pm 1.7\%$, so it can be seen that good uniformity (2%) can be maintained up to about 40% efficiency.

6.4 Holographic lenses.

A holographic lens may be conveniently thought of as a holographic recording of a conventional lens. As such, when replayed with the identical reference beam as

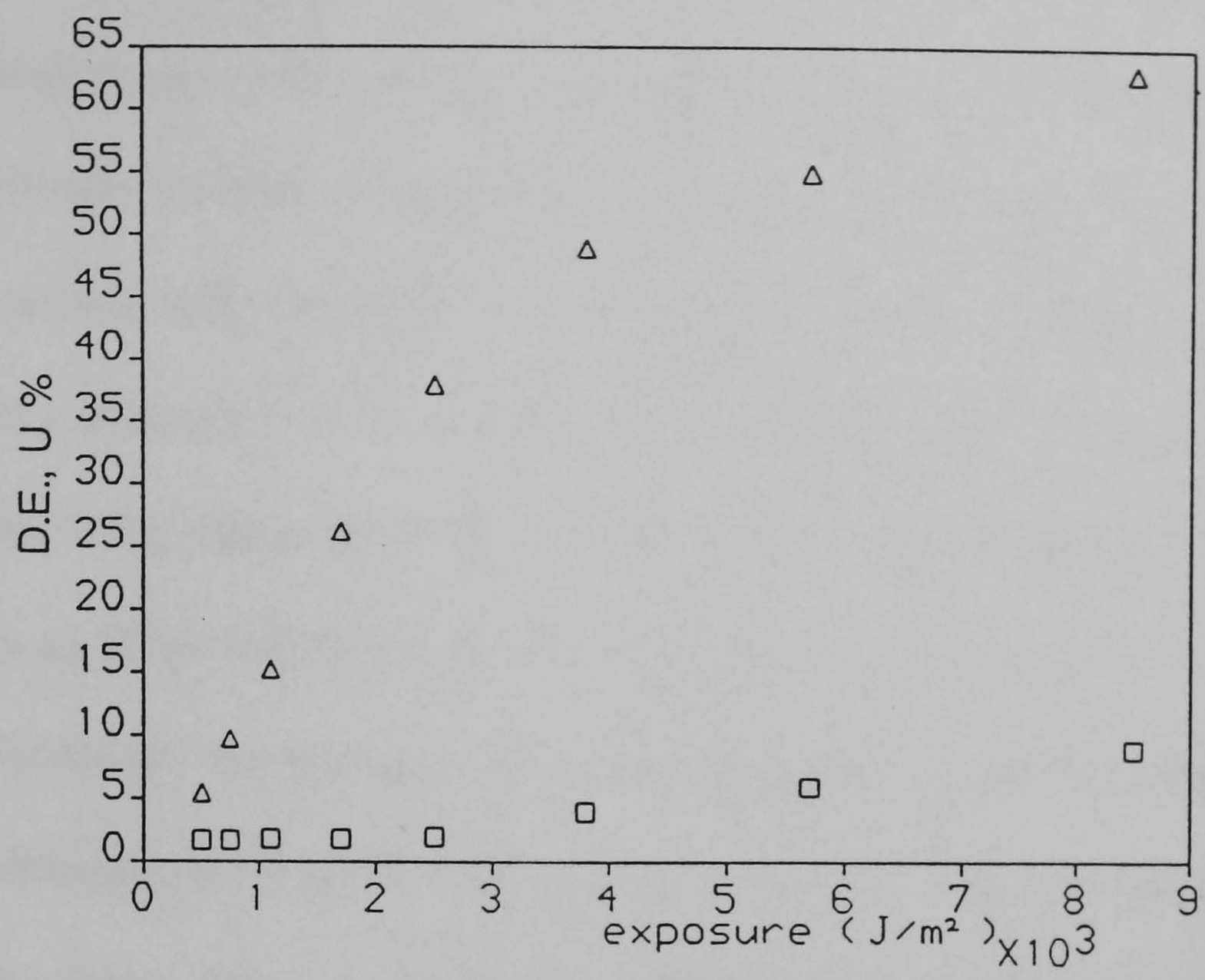

Figure 6.4: Efficiency (triangles) and uniformity (squares) versus exposure for the edge-extractor interconnect.

that used to record it, it will recreate the wavefront that the lens produced. The hologram therefore can replace the original lens, and will operate as a lens, to a limited extent. However, there are significant differences between holographic and conventional lenses which result from the fundamentally different physical processes involved. A conventional lens uses refraction of light at a dielectric boundary, and is governed by Snell's law of refraction. A holographic lens uses diffraction from a periodic structure, and is governed by the grating equation.

Whereas refraction is generally only slightly dispersive in visible optical materials, diffraction is by nature highly dispersive. This usually means that holographic optics will only operate successfully within a very limited range of wavelengths. Therefore, their use in monochromatic or laser-based systems is more common

since in such environments single wavelength holographic optics can perform as well as conventional optics. In fact, in such environments, holographic optics very often have other features which make them more desirable than conventional optics, such as size and flexibility. A holographic lens, for example, may easily be made with a dimension from $100\mu m$ up to 10×10cm and an f-number as small as 1 or less, with diffraction-limited performance, and an efficiency in excess of 95%. Such an HOE will typically be 15μm thick on a sheet of 1mm thick plane glass. In addition, the geometry and the conjugates of the lens may be chosen freely by changing the recording geometry, rather than by repolishing the optics. Holographic lenses may also be larger in aperture than the lenses used in their recording if required.

The diffractive nature of HOE's, however, means that all aberrations are zero only when the replay conditions are identical to the recording conditions, in terms of both geometry and wavelength. It is in general significantly more difficult to minimise holographic aberrations for non-ideal replay geometries than it is for conventional lenses, since holograms exhibit more severe aberrations in typical off-axis arrangements. Also, the Bragg properties of volume holograms mean that efficiency is also a consideration when replay conditions differ from those at recording. Neglecting changes in thickness and bulk refractive index, a hologram will have maximum diffraction efficiency only in the identical geometry, and any deviation from this in incident angle, incident beam curvature and incident beam wavelength will generally cause a degradation of efficiency.

It is possible to find a balance between both minimum aberrations and the

maximum efficiency across the hologram by means of aberration calculations or ray-tracing in conjunction with efficiency calculations to determine the optimum recording conditions. This will be discussed in detail in subsection 6.4.2.

The reason for investigating holographic lenses in this thesis was primarily as a method for generating large arrays of focussing beams to bias optically bistable threshold devices [SMI87,WAL88]. These devices are intended for optical digital computing applications in which the inherent parallelism of optical systems can be utilised to gain an advantage in processing power over electronic systems. Such systems must operate large numbers of channels in parallel. This may be achieved by defining 'pixel' arrays on optically bistable material, which are interconnected by free-space optical systems, such as conventional lenses and holographic interconnects. Each logic device requires power to be supplied to it, in this case to bias the gate into the correct operating region. This is where a method of efficiently generating a large number of equal-power beams is required. Despite its simplicity, the holographic lenslet array method has been very successful due to its ease and flexibility of fabrication, and its high efficiency and aberration peformance.

The use of holographic interconnects for electronic chip to chip interconnection has been investigated by Kostuk et al [KOS85], Feldman and Guest [FEL87] and Goodman et al [GOO84], and their use in optical computing by Jenkins et al [JEN84,JEN84A]. The optimisation of a holographic Fourier transform lens has been discussed using novel methods for generating aspheric wavefronts by Amitai and Friesem [AMI87,AMI88]. A holographic on-axis lens for position measurement has been investigated by Newell [NEW87], and holographic lenses in optical

component testing systems have been used for many years [CHE82].

Holographic aspheric lenses for the conversion of beam profiles have been designed in computer generated hologram (CGH) form by Han et al [HAN84] which may be copied into a phase volume medium such as DCG to get high efficiency. With advances in laser-diode based communication systems, holographic components for the infra-red are of interest, and one such device which combines lens and beamsplitting functions for a fibre communication link will be described in section 6.4.2.

6.4.1 Lenses for replay at the recording wavelength.

The principle of recording holographic lenses for replay at the same wavelength is similar to that for holographic gratings. Here we concentrate on transmission devices again for reasons of greater ease of use of transmission holograms in most applications. The arrangement used to record simple holographic lenses is shown in figure 6.5. It employs imaging systems in both arms in order that individual holograms are sharply defined, and therefore may be efficiently close-packed to form large arrays of lenses. The arrangement shown produces lenses which efficiently convert a collimated beam into a converging or diverging beam. If the processed hologram were placed in the arrangement shown and illuminated with the collimated beam only, a diverging beam would exit the hologram, whereas the same hologram rotated through 180° about an axis normal to the paper would produce a converging beam. The difference is simply that in the latter case, we are using the conjugate reference beam (i.e. reversed in its direction), causing the

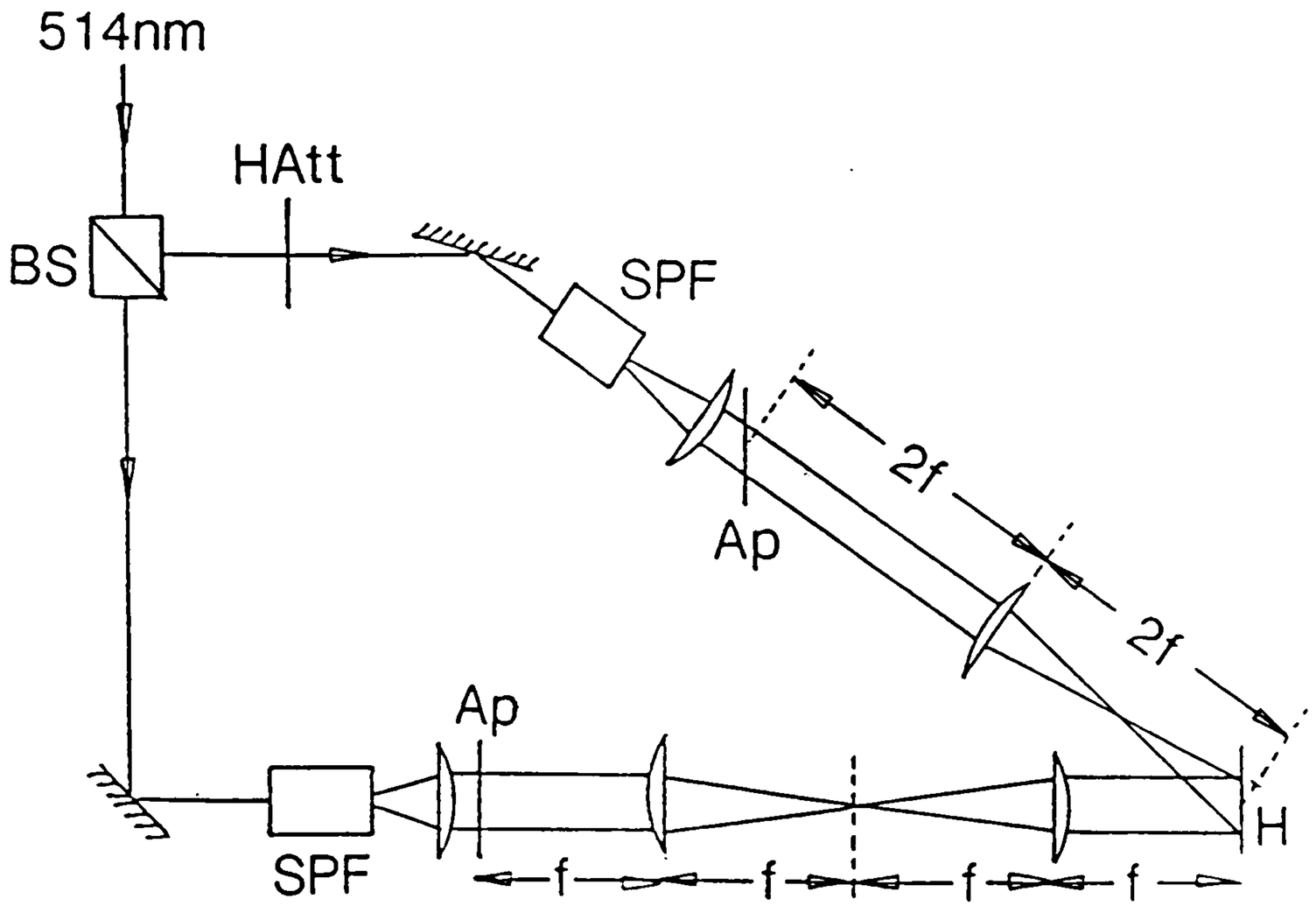

Figure 6.5: Arrangement for recording simple holographic lenses.

conjugate object beam to be diffracted by the hologram.

Using DCG as the holographic medium, lenses may be made with this arrangement with light of wavelengths shorter than about 530nm. During this work, DCG lens holograms were made using Argon ion laser wavelengths of 457, 476, 488 and 514nm. At all these wavelengths, in excess of 90% efficiency is easily achieved, along with diffraction limited focal spots (assuming the recorded spot is diffraction limited).

Lens arrays as large as 56×56 have been made by a simple automated step and repeat process with the hologram plate mounted on an x-y stepper motor stage controlled by computer. The dimension of each lenslet in the 56×56 hologram was 180μm square, with a focal length of 900μm, giving an f-number of 5. Focal spots again were diffraction limited at 5.5±0.5μm. The theoretical diffraction limit for

a lens of focal length f with a square aperture of side d_0 illuminated by a plane wave is given by

$$d = \frac{2\lambda f}{d_0} \tag{6.9}$$

where d is the miminum diameter of the focal spot measured to the first minima. At 514.5nm, this gives a theoretical spot size of 5.1μm which is within the observational error.

Typical variation in focal spot power in a lens array is better than $\pm 2\%$. This uniformity is defined by

$$U = \pm \frac{p_{max} - p_{min}}{p_{max} + p_{min}} \times 100\% \tag{6.10}$$

which is the same definition of uniformity as used when dealing with fan-out holograms in chapter 4. Uniformity is limited by variation in laser power between exposures, which normally can amount to a few percent, and on small diameter lens arrays by the positioning accuracy of the stepper motor, which in this set-up varied randomly by up to $\pm 20\mu$m. This causes overlap of, or gaps between, holograms. Overlaps greatly reduce the efficiency of the overlapped areas of both holograms involved, reducing the power in both the focal spots.

On arrays which cover large areas on a holographic plate (more than 20×20mm), there are often problems due to nonuniform processing and drying which causes slow changes of efficiency (and Bragg angle) across the plate. Ideally, a small central portion of a larger plate should be used if possible, and care must be taken to ensure consistent agitation during sensitising and processing. If possible, the

plate should be squeegeed immediately after removal from the isospropanol bath, but this usually causes scratches on the gelatin since the gelatin is actually dry and rigid by this stage, unlike photographic film, which is squeegeed wet. The hologram should be dried in a photographic drying cabinet with filtered air at room temperature to ensure a consistent drying rate which is not too rapid. Too rapid a drying rate increases non-uniformities and increases the risk of high scatter appearing as the gelatin 'cracks' under high stress.

The largest array area recorded was 32×32mm, consisting of a 32×32 array of 1mm holograms. The array came to within 5mm of the edge of the plate and showed considerable variation in the Bragg angle (about 3°) from the edge to within about 10mm from the edge. This is attributed to drying effects which proceed from the edge of the plate inwards, and more rapidly from the top of a vertically dried plate. Neglecting the holograms nearest the edge of the plate, overall efficiency was 92% with a uniformity of ±3% over the remaining 32×28 array. Losses in this case were primarily attributed to absorption within the gelatin.

There is usually a shift in the Bragg angle between recording and playback in holograms where the fringes are tilted (as opposed to perpendicular to the surface) due to changes in thickness and bulk refractive index. Therefore, the maximum efficiency angle of incidence does not correspond to the original reference beam direction. This causes aberrations to be induced in the focal spot. The magnitude of the aberrations depend on the f-number of the lens, and for typical lenses with f-numbers down to f/5 or so, the aberrations are negligible with an angular shift of typically 1 to 2°. If it is necessary to restore the optimum angle of incidence

to its original value, the plate may be baked gently, as described in chapter 2 or over-exposed initially and baked at higher temeperature to first restore the Bragg angle, and then to reduce index modulation until maximum efficiency is achieved. Alternatively, if freedom of choice allows, the hologram may be recorded with its fringe planes perpendicular to the surface, so that no shift in the Bragg angle occurs. To do this, the hologram must be symmetrical, i.e. the reference and object beams must be at equal and opposite angles to the normal. This leads to a focal spot plane with non-normally incident focussing beams, as shown in figure 6.6. In optical computing applications, this can be a useful arrangement, since some logical devices, such as non-linear interference filters are very sensitive to angle, and are difficult to fabricate with the correct parameters. Therefore, often a holding beam array is required which has individual beams incident non-normally. This would be difficult to achieve using conventional optics.

6.4.2 Lenses for replay at a different wavelength.

During the course of this work there has been an increasing demand for HOE's to operate in the near infra-red for use with laser diode-based systems (830 and 850nm) and Nd:YAG systems (1.06 and 1.3 μm). These HOE's are required primarily for optical computing research but also as elements of fibre-optic communication systems.

Due to the spectral sensitivity of DCG, it is not possible to directly record holograms at these wavelengths. Simple gratings, both transmission and reflection can easily be made at shorter wavelengths for operation in the red and infra-red,

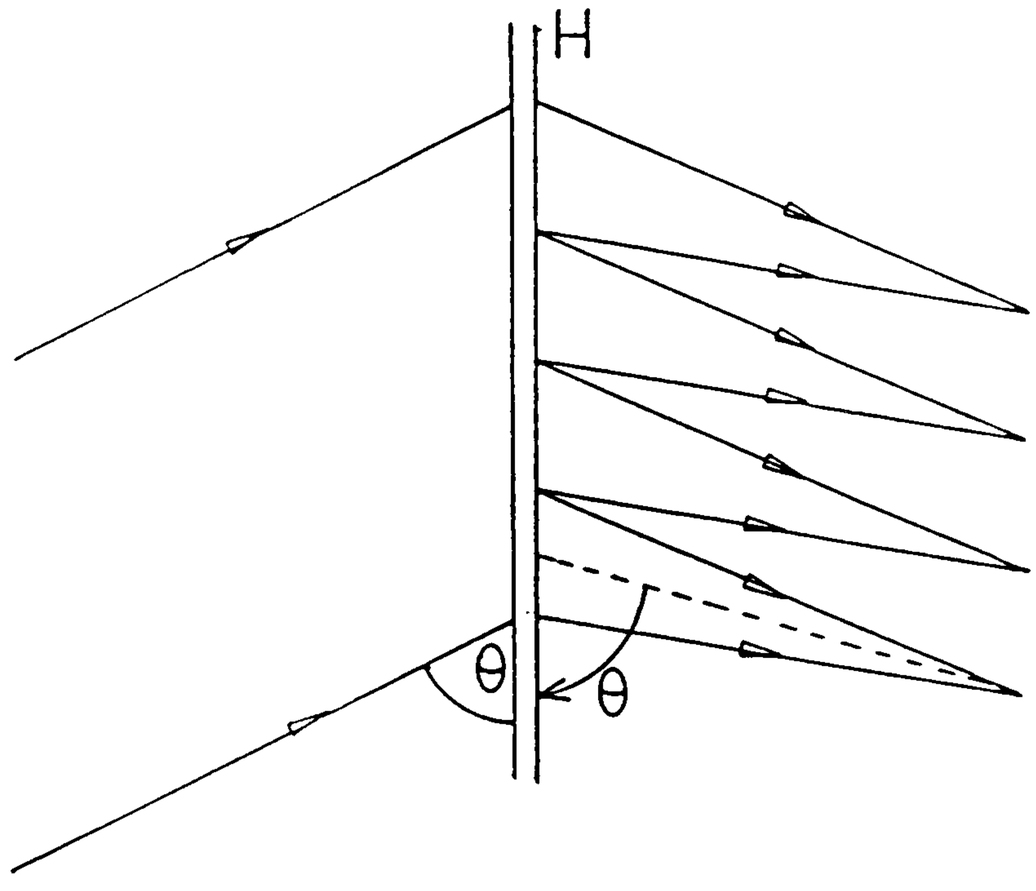

Figure 6.6: A symmetrical lens array hologram.

but if any focussing power is required, aberrations are induced by the wavelength shift, as a result of dispersion. The magnitude of the aberrations depends on the wavelength shift, the average diffraction angle, the numerical aperture of the HOE and the physical size of the HOE. This last feature is due to the fact that geometric aberrations scale in proportion to the size of the system. Therefore, a 100μm diameter hologram may show near diffraction limited performance, but at 10mm diameter the performance for the same numerical aperture may be far from diffraction limited, since the geometric spot will be 100 times larger although the diffraction limited spot size will remain the same. In an ideal non wavelength-shifted HOE, geometric aberrations are zero, so there is no problem in scaling up, but as soon as the replay conditions differ from the recording conditions, aberrations become a problem.

There is a second problem which appears when a hologram is replayed at a different wavelength. It is that the Bragg condition can no longer be satisfied at all points on the hologram at the same time. This comes about whenever the hologram has focussing power, and therefore its fringe period varies across its surface. Usually, there will be some incident angle (at the average Bragg angle) which gives a maximum efficiency overall, but the efficiency from point to point will vary, and the average will be lower than for a non-wavelength shifted lens. The degree of 'Bragg-matching' which can be achieved depends on the techniques used to design and record the HOE, and it is possible to either optimise wholly for optimum aberrations, and obtain poor Bragg matching, or vice versa.

Many papers have been published on the subject of aberrations in holographic lenses, following a variety of approaches. These are all generally applicable to quantifying aberrations, including those in wavelength-shifting problems, but not all give techniques for minimising the aberrations.

Leith et al [LEI65] and Meier [MEI65] classified the paraxial aberrations in a similar way to conventional lens aberrations, and considered the problems of magnification (Gabor's original motivations for using holography), as did Abramowitz [ABR69]. Champagne [CHA67] extended the paraxial treatment to non-paraxial properties, giving more accurate results. Offner [OFF66] used a ray-tracing analysis, with Ludwig [LUD73] generalising the method, whereas Miles [MIL73] used ray-tracing to evaluate the wavefront aberration as opposed to the geometric aberrations. Welford presented a simple vector ray-tracing formulation which does not explicitly involve the local fringe spacing of a hologram [WEL75]. Latta

presented detailed theoretical results of hologram aberrations with the aid of a computer-based paraxial analysis [LAT71A,LAT7BA] and also a ray-tracing analysis [LAT71C]. Prikryl studied image hologram aberrations by means of ray-tracing [PRI72].

A number of methods for minimising hologram aberrations on reconstruction with either a change in geometry or a wavelength shift, have been published. Many authors have based their techniques on the use of computer-generated holograms (see [LEE87] for a review of CGH techniques), such as Lee [LEE80] and Cederquist and Fienup [CED87]. Fairchild and Fienup [FAI82], Kedmi and Friesem [KED86,KED84] and Chen et al [CHE87] also importantly describe the use of a CGH in one arm of an optical recording arrangement, allowing high efficiency optimised elements to be recorded in volume phase materials such as silver halide or DCG. Chen et al also describe the use of an optically generated corrector plate made at a third, shortest, wavelength to reduce aberrations [CHE88].

A simple optical method which allows efficient wavelength shifting without any aberration balancing is given by Lin and Doherty [LIN71]. The method works by first recording directly the hologram that is required at the *replay* wavelength in some medium which is sensitive to that wavelength (such as dye-sensitised silver halide emulsions) and then copying into DCG in the blue or green. This ensures that the surface fringe period is faithfully copied, and therefore the diffraction properties at the replay wavelength are maintained after copying. The Bragg response must change, but this is more slowly varying, so it is possible by choice of DCG thickness and recording geometry to separately optimise the copy's effi-

ciency. This method gives aberration-free performance if the first hologram can be recorded. This limits its use to situations where suitable recording materials and lasers are available.

Bennett [BEN76] discussed minimising longtitudinal dispersion, such as for an eyepiece, by using two and three hologram cascades. This used paraxial theory based on Latta's work, and therefore is analytic and easy to apply, but limited to smaller aperture systems. Stone and George [STO85] used a similar but more accurate approach which included efficiency calculations to optimise angular and wavelength bandwidths of cascade systems.

Latta and Pole [LAT79] described a computer-based technique for wavelength-shifted lenses based on K-vector closure. This method breaks down the required HOE into small uniform volume gratings, and then calculates the rays corresponding to Bragg incidence at recording. The rays are traced to find the minimum blur circle point, corresponding to the best position for a recording point source. This method optimises efficiency primarily, and does not produce the best aberration performance.

Amitai and Friesem [AMI87,AMI88] described an analytic recursive technique for generating aspheric wavefronts from ancestor holograms recorded with spherical wavefronts. They applied the technique specifically to holographic Fourier Transform lenses in order to optimise their aberration performance over a range of incident angles (corresponding to a range of spatial frequencies). With Assenheimer [ASS88], they extend the principle specifically to wavelength-shifted lenses and achieve good results with an f/3 lens shifted from 514nm to 1064nm.

This is perhaps one of the most promising techniques for aberration balancing. Techniques such as this and the method presented below illustrate the relative simplicity of optimising HOE performance by optical means over a wide range of operating conditions.

The approach taken in this work is to optimise holographic recording using only spherical wavefronts. This is simpler than aspheric techniques, but for all the real applications dealt with in this work, results have been sufficient. The analysis technique is an exact ray-tracing one, yielding a geometric spot diagram and its position. The recording of the HOE has four free parameters, i.e. the 2-dimensional coordinates of the two recording point sources. The analysis assumes that the replay geometry and wavelength are fixed, and the positions of the two recording points are optimised with the aid of a merit function which includes the spot-size and the Bragg mismatch (and hence the overall efficiency), which may be chosen depending on the application.

Ray tracing.

The ray-tracing method presented here is based on Welford's method [WEL74], and includes Latta's modifications for holographic gratings [LAT71C]. Further modifications will be discussed in subsection 6.4.2. The model was implemented on a VAX 8700 computer in Fortran 77.

The relevant coordinate system and notations are illustrated in figure 6.7. Each ray has a known start point $P_{-1}(x_{-1}, y_{-1}, z_{-1})$ and initial direction given by its direction cosines (L, M, N). The problem is to calculate the point of incidence

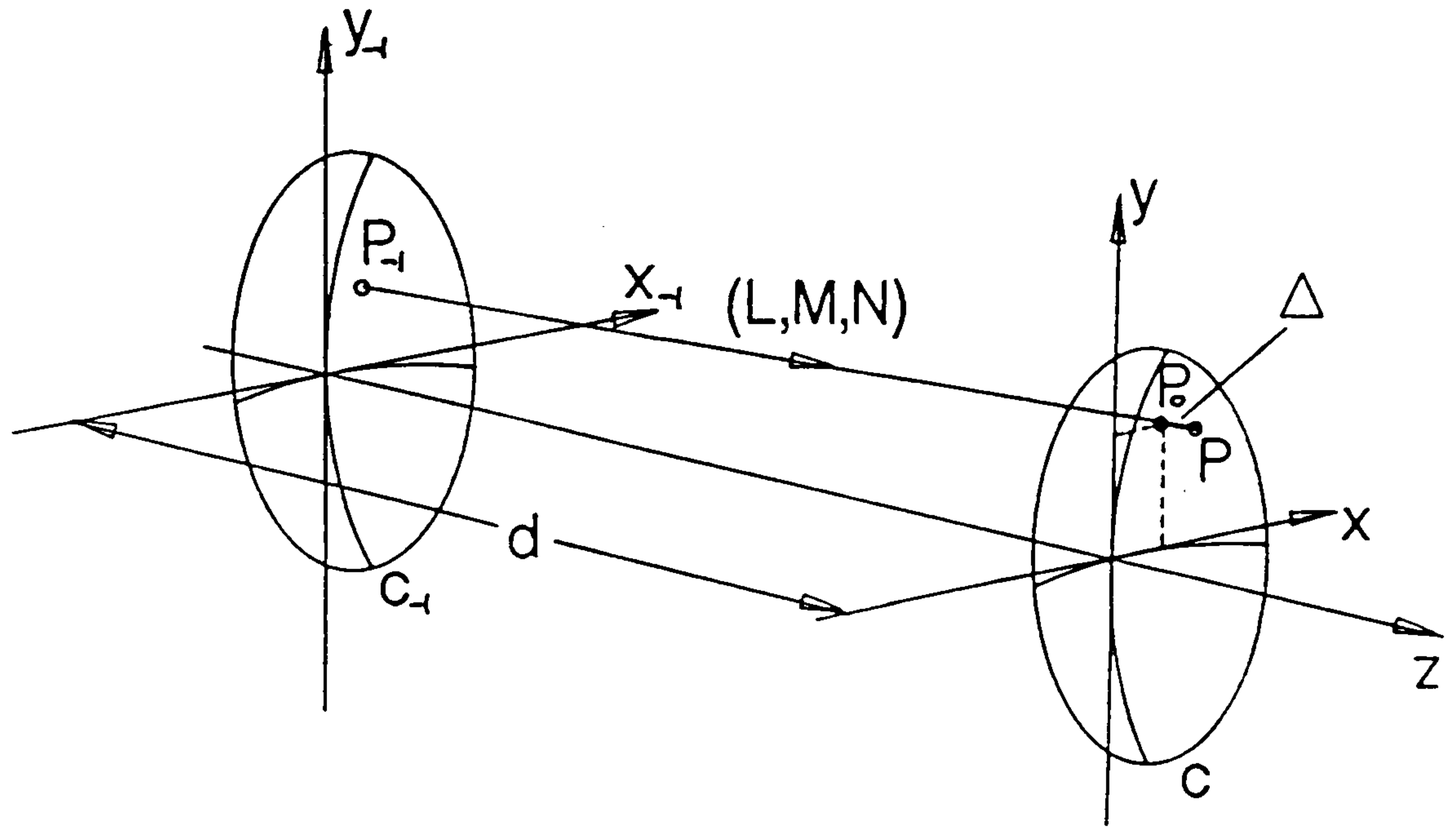

Figure 6.7: Coordinates and notation for ray-tracing.

of the ray on the next surface, P, and the new ray directions after refraction and/or diffraction after encountering that surface. We assume that all surfaces are spherical in this analysis with centres on the z axis. The surface is characterised by its curvature, $c = 1/r$, where r is the radius of the sphere. Planar surfaces have $c = 0$. To calculate a ray transfer to the next surface, we also need the distance to the next surface, given by the axial separation of the vertices of the two surfaces, d. We take the next vertex to be the new z origin. The point of intersection of a ray with the next surface in the new coordinates is then $P(x, y, z)$, given by

$$\begin{aligned} x &= x_0 + L\Delta \\ y &= y_0 + M\Delta \\ z &= N\Delta \end{aligned} \tag{6.11}$$

where x_0 and y_0 are the coordinates of P_0, the intersection with a plane surface instead of the general spherical surface, and Δ is the length of the segment from P_0 to P. x_0 and y_0 are given by

$$\begin{aligned} x_0 &= x_{-1} + \frac{L}{N}(d - z_{-1}) \\ y_0 &= y_{-1} + \frac{M}{N}(d - z_{-1}) \end{aligned} \tag{6.12}$$

and Δ by

$$\Delta = \frac{F}{G + \sqrt{G^2 - cF}} \tag{6.13}$$

where

$$F = c(x_0^2 + y_0^2) \tag{6.14}$$

and

$$G = N - c(Lx_0 + My_0). \tag{6.15}$$

The new direction cosines are dependent on whether the surface is refractive or diffractive. If it is refractive, the new direction cosines are given by

$$\begin{aligned} L' &= \frac{1}{n'}(nL - Kx) \\ M' &= \frac{1}{n'}(nM - Ky) \\ N' &= \frac{1}{n'}(nN - Kz + n'\cos I' - n\cos I) \end{aligned} \tag{6.16}$$

where

$$\cos I = \sqrt{G^2 - cF} \tag{6.17}$$

$$n' \cos I' = \sqrt{n'^2 - n^2(1 - \cos^2 I)} \tag{6.18}$$

$$K = c(n' \cos I' - n \cos I). \tag{6.19}$$

n and n' are the refractive indices of the incident and refracted media, and I and I' are the angles of incidence and refraction.

If the surface is diffractive, the relevant equations for the new direction cosines are

$$\begin{aligned} L' &= L + \frac{\lambda}{n' d_x} \\ M' &= M + \frac{\lambda}{n' d_y} \\ N' &= \sqrt{1 - L'^2 - M'^2} \end{aligned} \tag{6.20}$$

where d_x and d_y are the grating periods in the x and y directions. The grating periods can be obtained from the grating vector, $\mathbf{K}$, and are given by

$$d_x = L_k \Lambda \tag{6.21}$$

$$d_y = M_k \Lambda \tag{6.22}$$

where L_k and M_k are the direction cosines of $\mathbf{K}$, i.e. $K_x/|\mathbf{K}|$ and $K_y/|\mathbf{K}|$, and Λ

is the fringe spacing, defined by

$$\Lambda = \frac{2\pi}{|\mathbf{K}|}. \tag{6.23}$$

The grating vector $\mathbf{K}$ may be calculated from the recording arrangement if the refractive index and wavelength are known.

The way that specific diffraction gratings are included in the ray tracing is as follows. The hologram is sub-divided into a regular square or rectangular grid of sectors, as shown in figure 6.8 which are assumed to be uniform planar volume gratings. The recording geometry is used to trace rays into the holographic medium, which has a uniform bulk refractive index, where the grating vectors for each sector are calculated. The recording geometry cannot include any optics, and must consist only of a medium of uniform refractive index to the left of the hologram in which the recording spherical wavefronts propagate. The spherical wavefronts are specified by their focal points, and the recording rays are assumed to be travelling left to right as in figure 6.7. In order to analyse the hologram after the grating vectors have been calculated, ray directions are determined at the centre of each sector assuming the new replay point (real or virtual) in the medium to the left of the hologram. Tracing now proceeds by firstly a refraction at the HOE surface, then by diffraction from the grating, then propagation through the hologram bulk (which is assumed to be of constant refractive index), and finally through the substrate and remaining optical system, which may include further optics, including other HOE's, if desired.

The rays exiting the HOE are traced through a specified distance while the

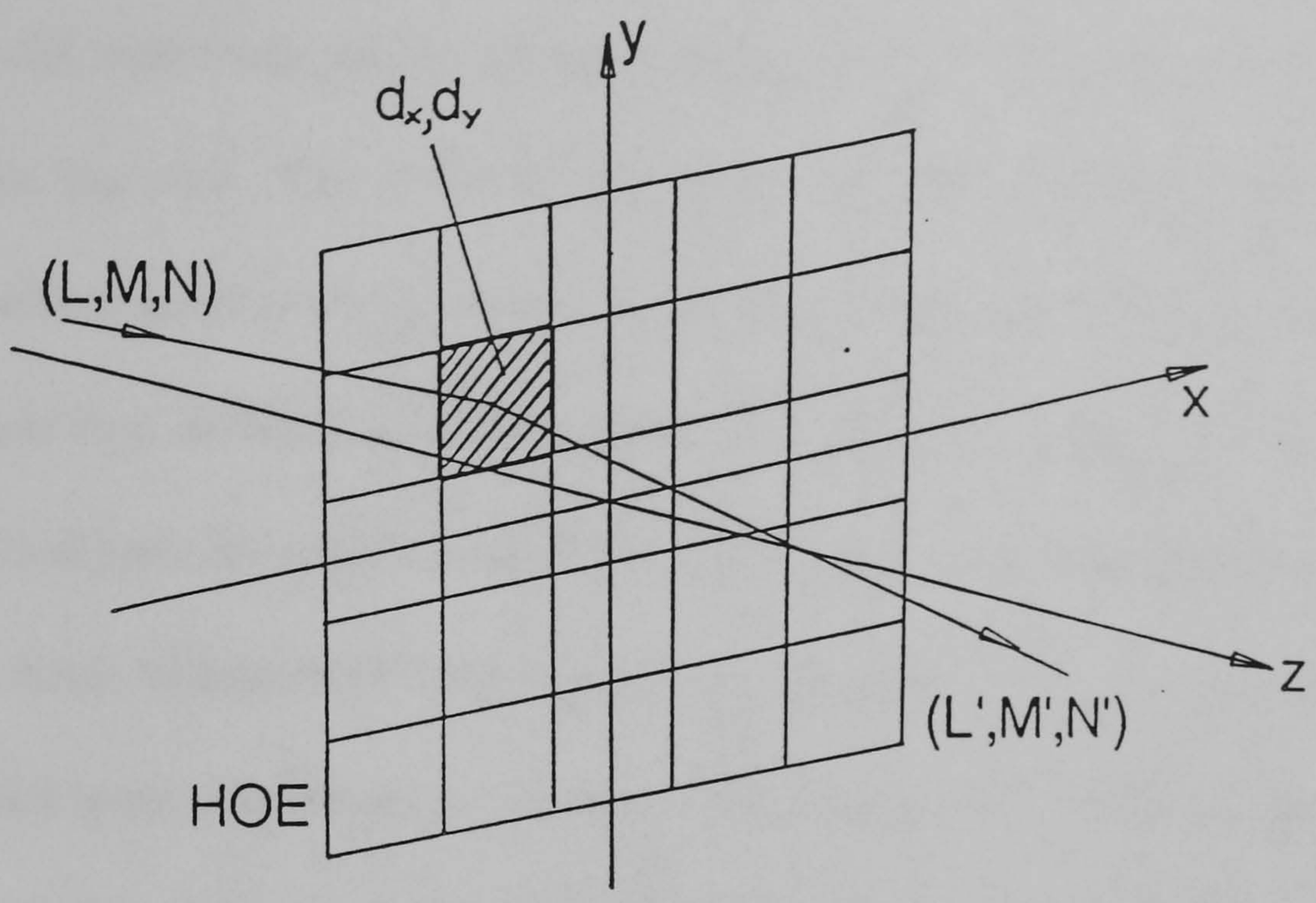

Figure 6.8: Ray tracing through an HOE.

spot dimension is regularly calculated. In this way, the best focal spot position is found.

The method by which the recording geometry is optimised is a simple nested search of possible recording point regions. These regions are defined in terms of (r, θ) coordinates rather than (y, z), since the average diffraction angle varies only slightly as the focal length of a wavelength-shifted lens is varied, and hence r and θ are relatively independent, allowing a coarser search. Once the best sub-region is identified, the search switches to that sub-region, which is then divided up again and searched, and so on. Such a nested 4-dimensional search takes some time, even on a mainframe computer, but is a one-run program, which may conveniently be run overnight.

Additional features.

The model described above assumes the grating is infinitely thin, which is obviously not the case. The finite thickness of real holograms in DCG leads to Bragg effects which modify the powers within the various diffracted orders. Specifically, the minus first order is generally strong, while other diffracted orders are negligible. This allows us to only trace the single order, as in the model, and ignore other orders. Also, although the zero order may be significant, its angular separation is large, and generally does not interfere with the main diffracted beam. A feature of major interest in holographic optics is the efficiency of the diffracted beam, and in the case of wavelength-shifted lenses, there will in general be local mismatch with the Bragg angle which varies across the hologram. This leads to a varying efficiency over the hologram which limits the maximum overall efficiency. In the ray-tracing program it is a simple matter to calculate the angular difference between the incident beam and the Bragg angle of each sector of the hologram. This must be minimised if efficiency is to be maximised. However, the optimum Bragg performance of an HOE does not in general correspond to the same recording conditions for minimum aberrations. This is easily seen from Latta and Pole [LAT79], where they assume the Bragg condition is met for each hologram sector after a wavelength change. This leads to rays which do not pass through a common focus. On the other hand, Lin and Doherty [LIN71] show how to ensure aberration-free performance with a hologram which may be very badly Bragg-matched.

This means that the recording geometry may be optimised for either aberrations, or Bragg mismatch, or both. Which is chosen depends on the application -

basically whether maximum power or maximum power density is required at the focal spot. Note that the power density will be ultimately limited by the diffraction limit of the lens. In other words, there is no point in making a great effort to reduce the geometric spot much below the diffraction limited size since its effect on spot size will be negligible. An estimate of the real spot diameter, d, to be expected is given in terms of the geometric and diffraction-limited spot diameters (d_g and d_d respectively) by

$$d = \sqrt{d_g^2 + d_d^2}. \tag{6.24}$$

If an accurate determination of the diffraction efficiency is needed, the details of each sector, and the incident beam can be fed into the coupled wave programs described in Chapter 3. The use of the ray-tracing and coupled wave programs allows accurate prediction of the aberration and efficiency performance at any replay geometry (involving point sources) and wavelength.

As discussed in chapter 3, in DCG there are changes in the thickness and bulk refractive index of the gelatin during processing which alter the Bragg angle and selectivity of a hologram. These features were included in the ray-tracing program since they directly affect both the Bragg mismatch and the spot dimensions if the holographic layer is taken to have finite thickness.

Results.

A typical example of the use of the ray-tracing program was in the design of a holographic lens array for 850nm. The array was required to have square elements of side 180μm and focal length 900μm. Replay was with a uniform collimated

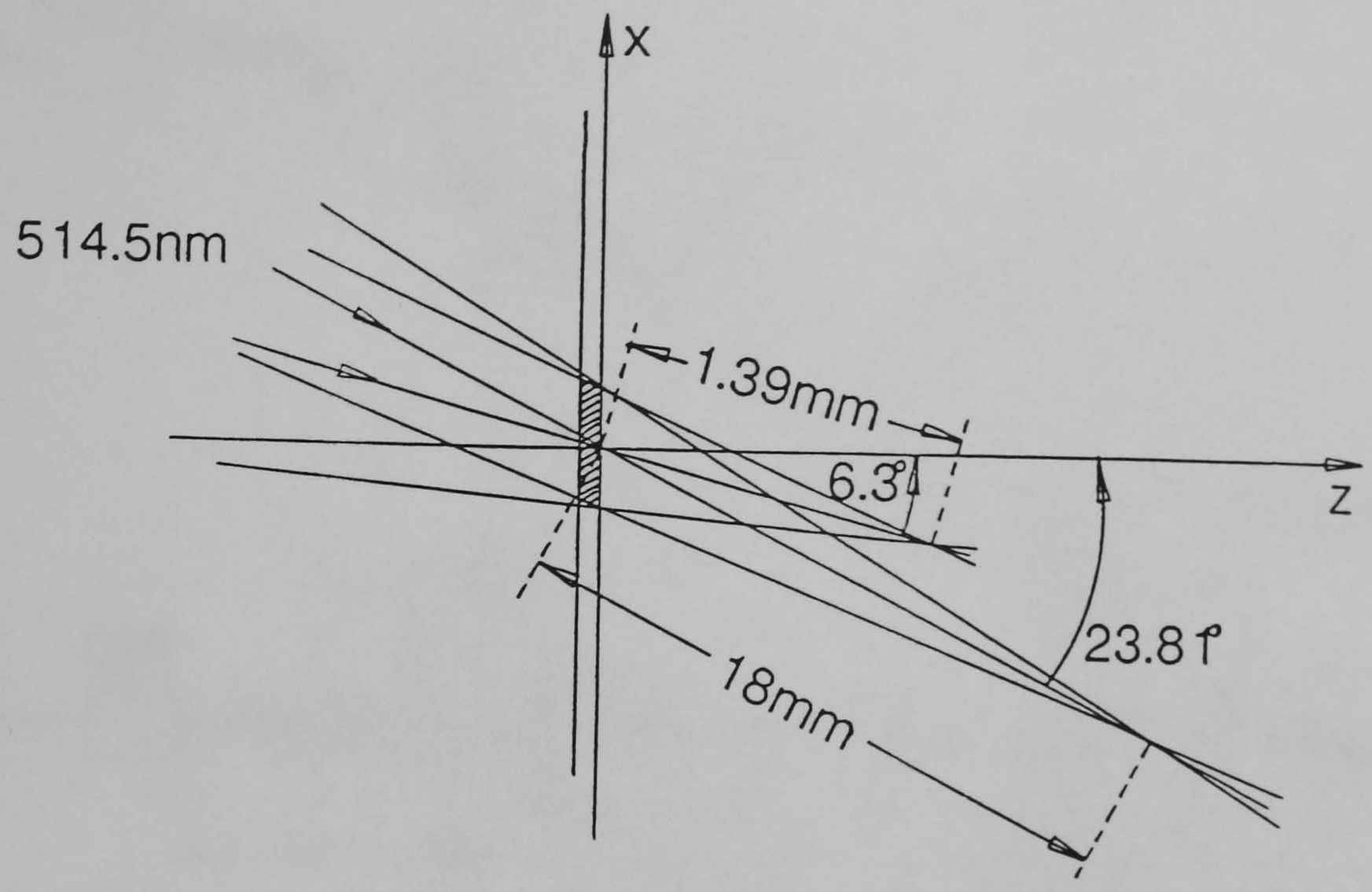

Figure 6.9: 514nm recording beams required for an HOE lens for 850nm.

beam at 30° to the normal, and the focal spots were on the normal from the centre of each lens.

The above parameters were entered into the tracing program in a search for minimum spot size. The recording wavelength was 514.5nm. The resulting best geometry is shown in figure 6.9, with the actual arrangement used to generate the required beams in figure 6.10, and the traced spot diagram in figure 6.12. In figure 6.10 it can be seen that there are more components than would be needed simply to generate the beams of figure 6.9. This is because in each arm we want to not only produce the desired recording beams, but also to image an aperture onto the plane of the hologram. This means that each hologram has a well defined area, and many holograms may be efficiently close-packed with minimum wastage and overlap.

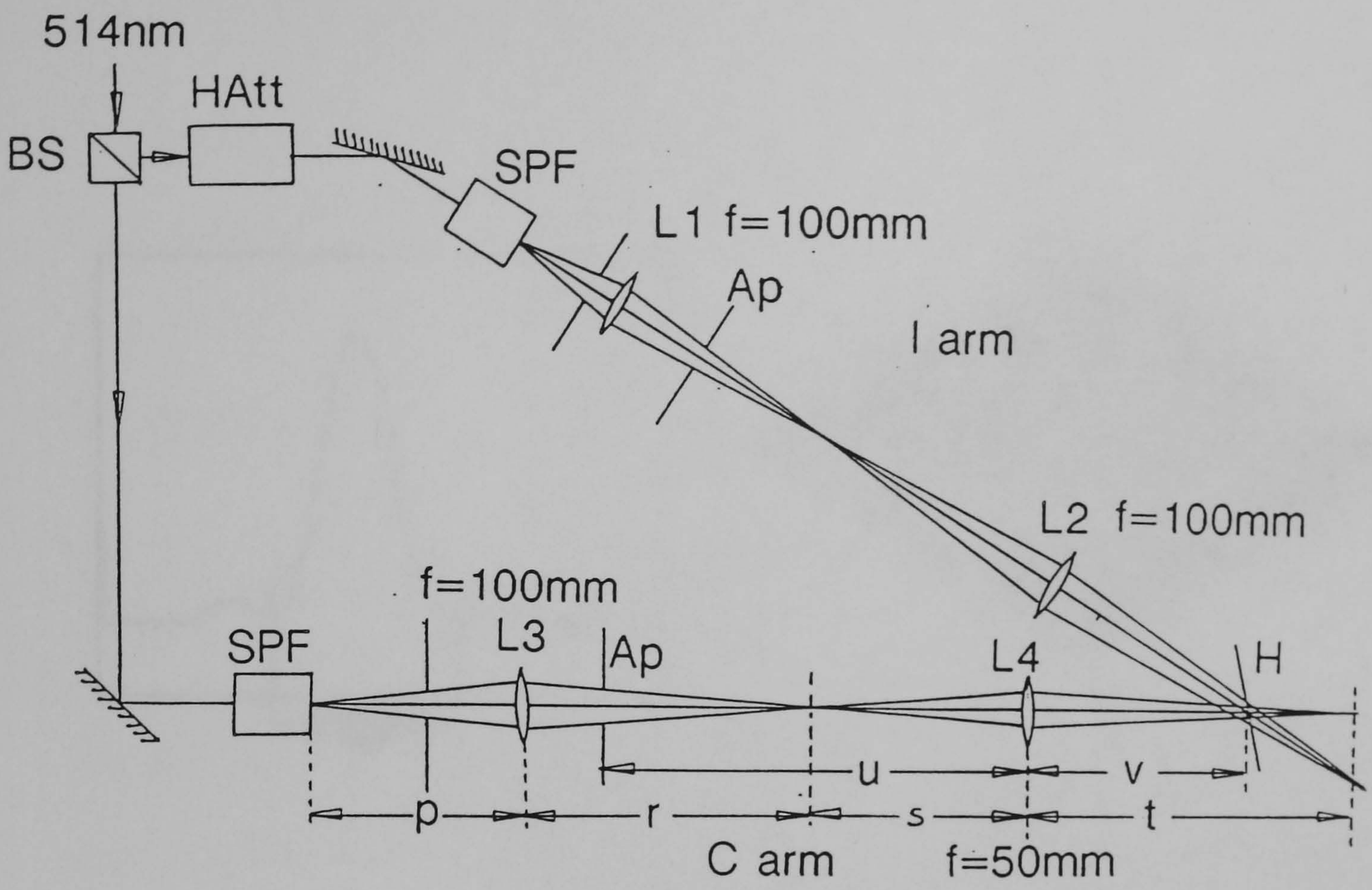

Figure 6.10: 514nm recording arrangement for an HOE lens for 850nm.

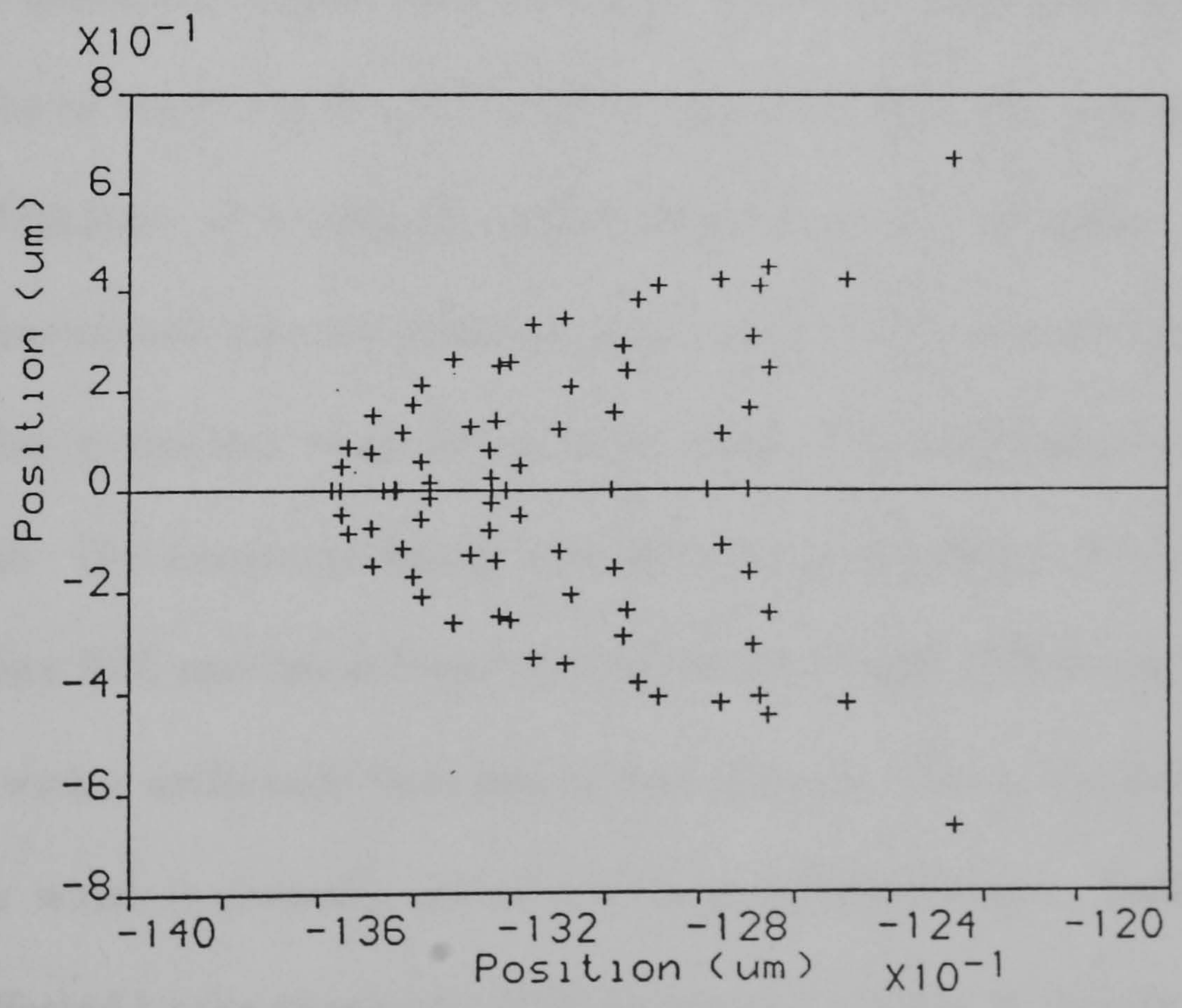

Figure 6.11: Ray-traced spot diagram at 850nm.

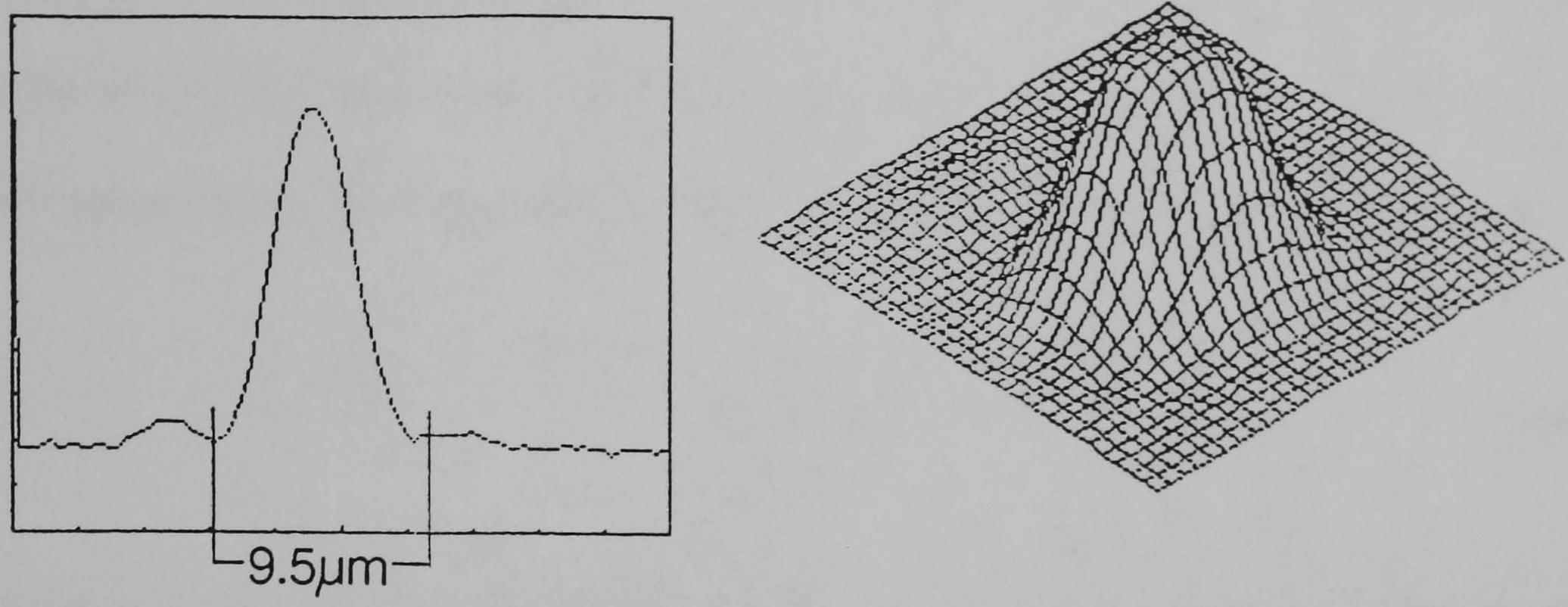

Figure 6.12: Spot scans at 830nm.

The traced focal spot is approximately 1μm in diameter, considerably smaller than the diffraction limited spot of 8.5μm. We would therefore expect the actual spot to be of the order of $\sqrt{8.5^2 + 1^2} = 8.6\mu$m. In fact, the measured focal spot was 10.0$\pm$0.6μm, at a distance of 940$\pm$20μm from the hologram. A linear and a two dimensional scan are shown in figure 6.12. These scans were performed at 830nm due to the lack of an 850nm laser diode, but the difference in spot size is negligible. The maximum Bragg mismatch was estimated to be 0.7°, leading to better than 99% maximum theoretical efficiency overall. Efficiency was measured as 92%, with a uniformity from lens to lens of $\pm$5%. This is typical of the level of efficiency which is normally achieved with non-shifted lenses. Uniformity should not be affected by the wavelength shifting process, and the value here is higher than normal, probably due to random errors in the motion of the stepper motor. The

error in the position of the focal spot is probably due to errors in the positioning of the recording optics. This is not a problem, since the measure of the depth of the focal spot, the Rayleigh range, has a value of about 70μm, indicating that a 40μm error is not too important. The Rayleigh range gives the distance over which a focussing Gaussian beam stays within $1/\sqrt{2}$ of its waist value, and is given by

$$z_r = \frac{\pi r_0^2}{\lambda} \tag{6.25}$$

where r_0 is the waist radius. Generally we are not dealing with Gaussian beam in lens arrays, but with 'top hat' beams, and so the Rayleigh range parameter is not exact, but it gives an idea of the depth of focus available.

A second application of wavelength-shifted lenses was for a bi-directional fibre-optic link at 850nm. This time the required hologram is as shown in figure 6.13. The HOE had to collect the light diverging from a laser diode or LED and focus it into an optical fibre. It also had simultaneously to collect light emitted from the fibre and direct it onto a photodetector. The numerical aperture of the HOE had to matche that of the fibre and the photodetector (0.2), and therefore fabrication of this HOE was more demanding than the previous f/5 (n.a.=0.1) lens array. The larger absolute dimension of this HOE (4.4mm) meant that aberrations would be worse.

This HOE also had to be a fan-out HOE, operating as a 50/50 beamsplitter for maximum efficiency. Therefore, the index modulation needed to achieve 100% efficiency was very high, since it needed to be a factor 850/514 higher than at 514nm, and a further factor of $\sqrt{2}$ higher for a double exposure to have maximum

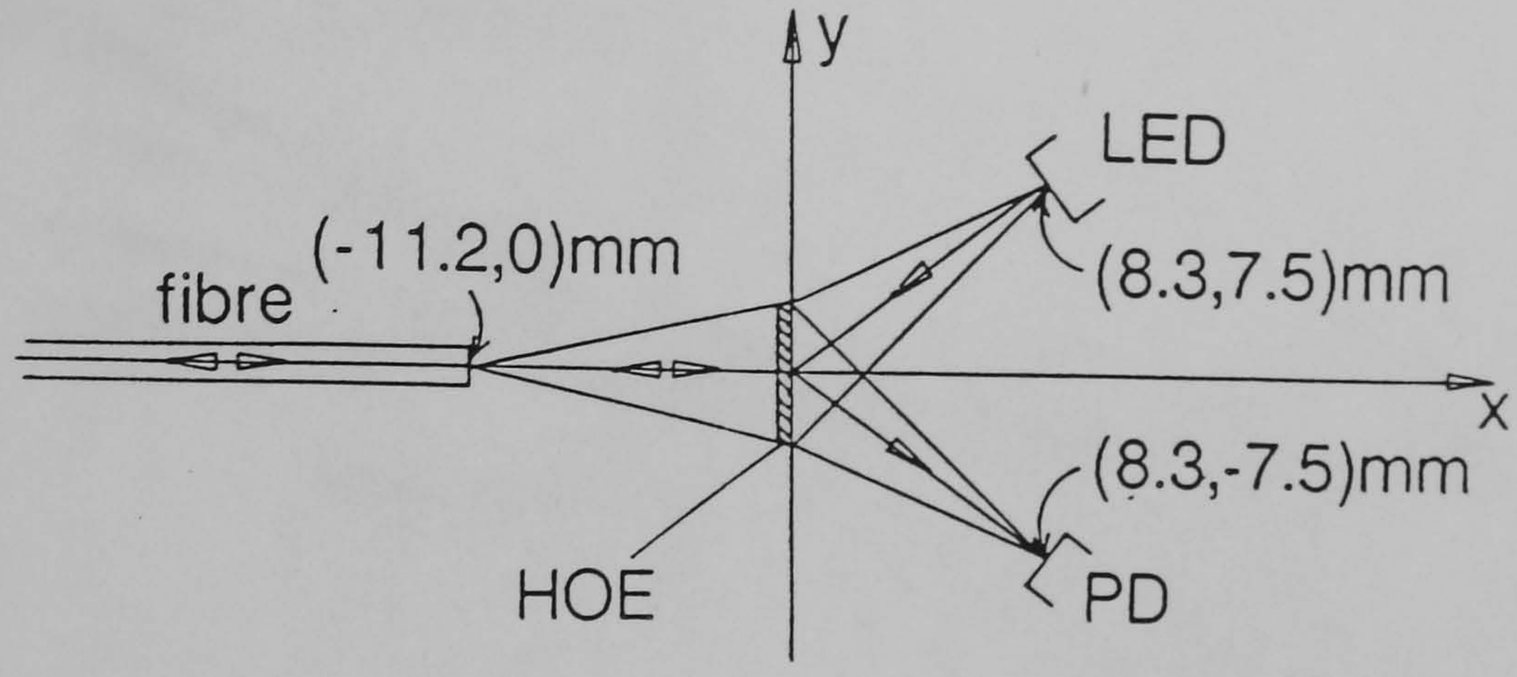

Figure 6.13: Schematic of an HOE for a bi-directional fibre link.

efficiency. This amounts to a factor of 2.3 more than that needed for a simple grating at 514nm. From the analysis in chapter 3 it is known that such an index modulation is not achievable in the standard 649F gelatin used in this work. In addition, there are effects due to beating of the gratings in the volume of the hologram which will further increase the modulation required. Therefore, the efficiency of the HOE was not expected to be high. However, for the particular application the other advantages of mechanical stability and ease of alignment were deemed to outweigh the efficiency limitation.

The ray-tracing program was run and yielded the geometry of figure 6.14. The actual arrangement that was used is shown in figure 6.15. The predicted focal 'spot' is shown at two positions in figure 6.16. Diagram (a) corresponds to the minimum spot size location (11.2mm, as required by the design), calculated by taking the

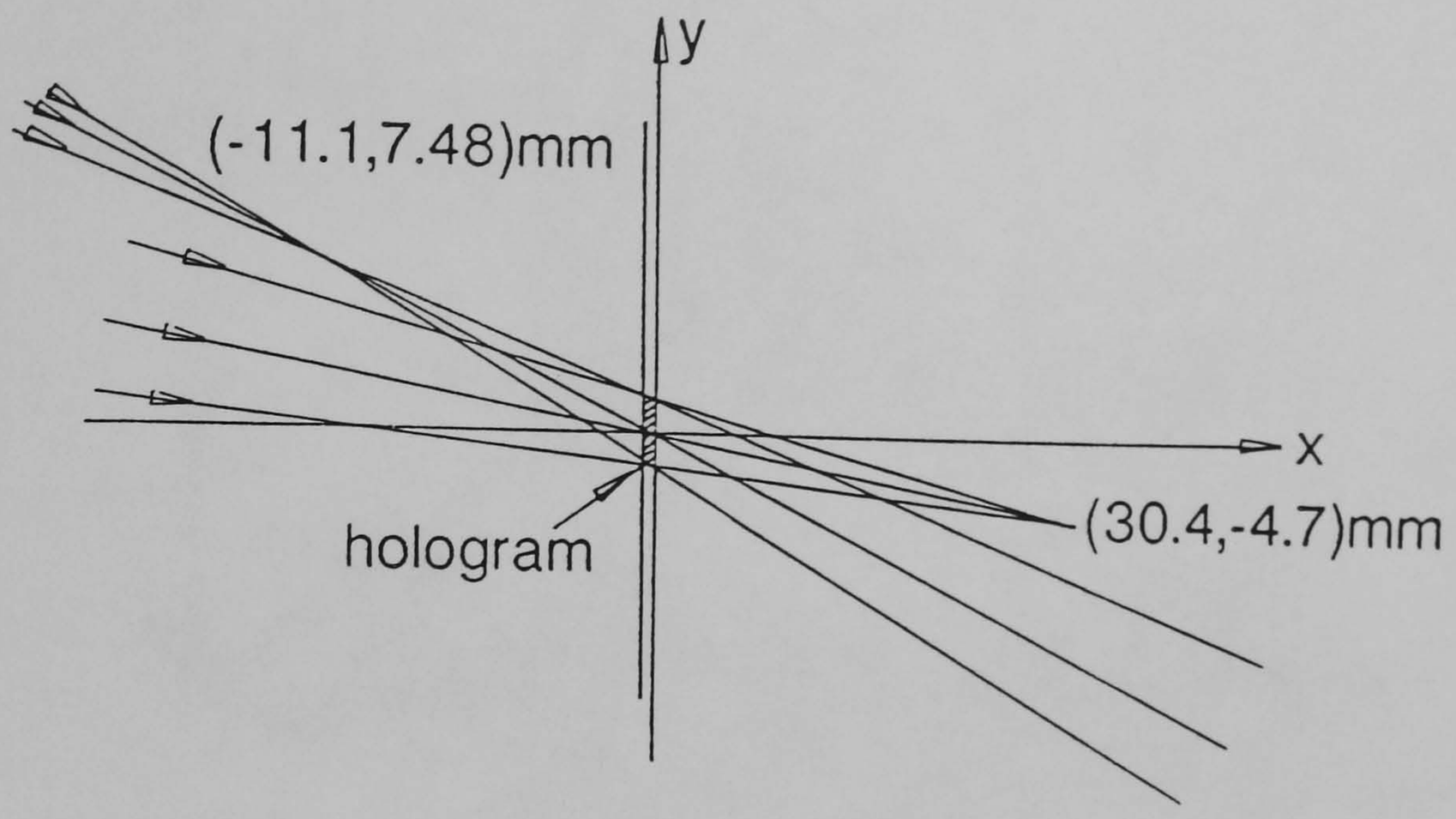

Figure 6.14: Fibre link HOE recording beams.

worst rays. (b) shows the spot at 11.3mm, which shows a greater concentration of rays, and therefore energy. The hologram was made by a double exposure, with the plate rotated by 180° between exposures. The exact registration of the plate in the two exposures is critical, or else the fibre-side beam, which should be common to both holograms, will not be in the correct position, and will result in increased aberrations in at least one of the three beams. Registration was achieved by marking the glass side of the holographic plate with a spot of ink, and illuminating the hologram from the gelatin side with a focussed spot from a helium-neon laser (to which DCG is insensitive). Before each exposure, the HeNe spot is aligned on the ink by translating the plate. In this way, registration accuracy of 10μm can be achieved.

The HOE was analysed with a laser diode operating at 830nm. This was dif-

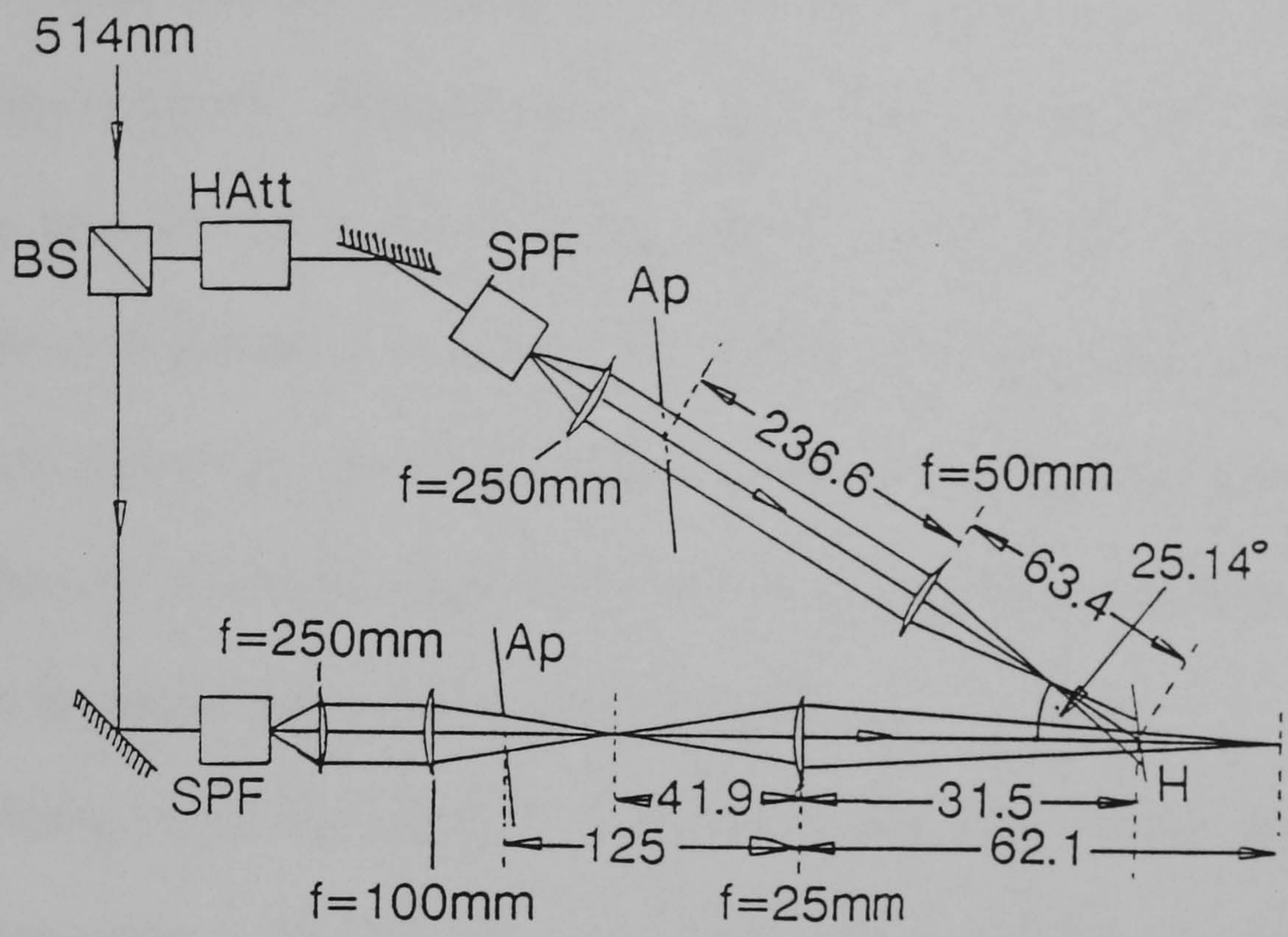

Figure 6.15: Fibre link HOE recording arrangement used.

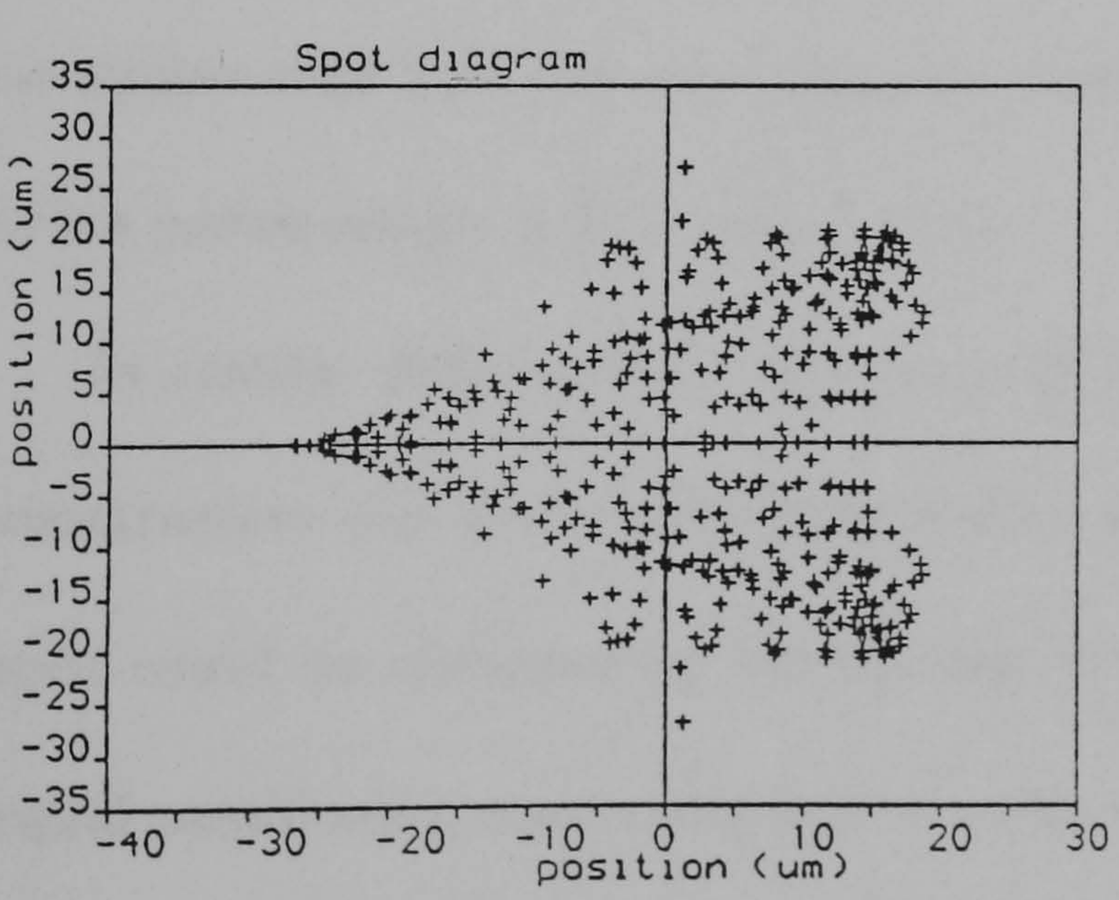

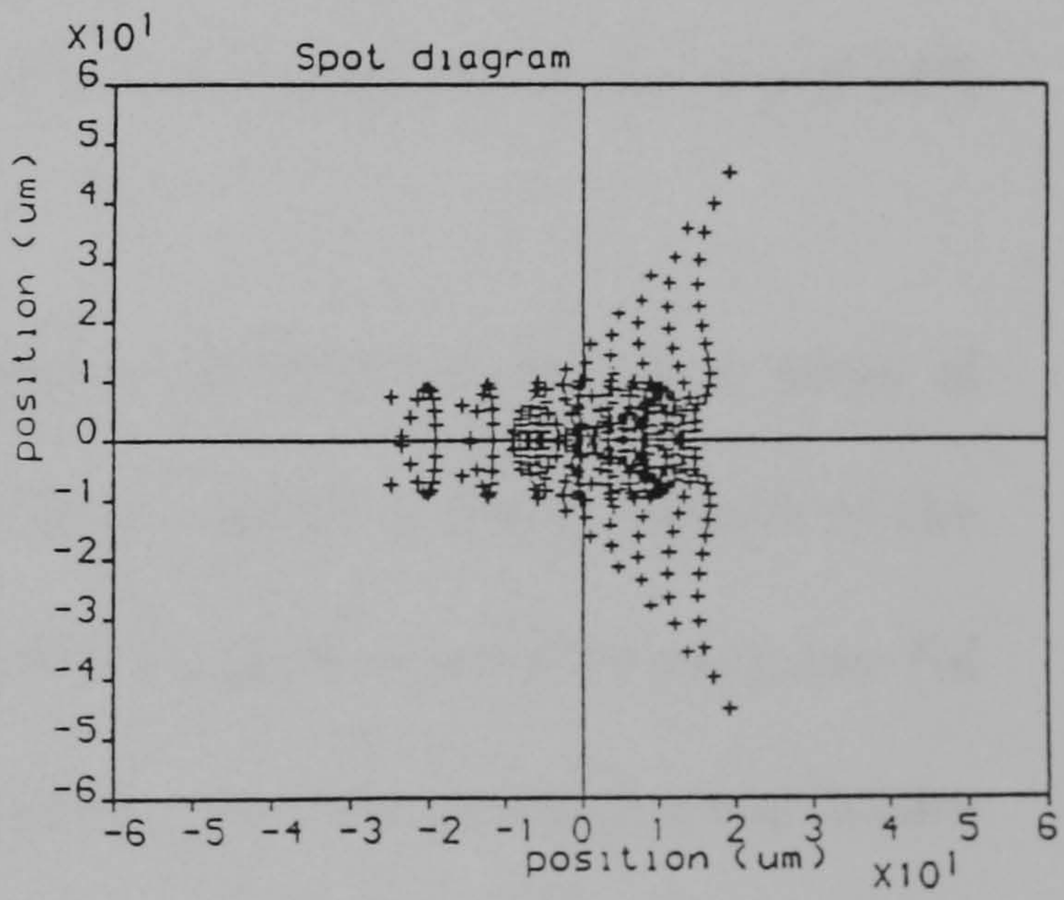

Figure 6.16: Fibre link HOE traced focal spot at (a) 11.2mm and (b) at 11.3mm.

ferent from the design wavelength (850nm) due to the lack of a suitable diode. However, tracing revealed a negligible difference in spot size, with only a slight change in spot position. When illuminated with a point source at (-8.32,7.49)mm, the output spot should be at (11.2,0) at 850nm, and (11.6,-0.2) at 830nm. At 830nm, this corresponds to a diffraction angle of 41.1°. The measured value corresponded to this within the experimental error of 1° of this, and the output lay within 200μm of the predicted spot position. This indicates that replay geometry should also be within these tolerances at 850nm.

The efficiency achieved was 38%, with equal power in each beam, and the spot size was measured at $33 \times 33 \pm 4\mu$m. In fact, this is significantly smaller than the estimated value of $47 \times 73\mu$m in figure 6.16(a). This is due to the fact that the model simply takes the worst case rays for its measure of diameter. A spot diagram at 11.3mm is shown in figure 6.16(b) which shows a much greater concentration of rays - about 75% of the rays are contained within a $25 \times 25\mu$m region. This compares well with the best experimentally measured spot, which contained 78% of its power within a $33 \times 33\mu$m spot.

In reality, differences in optical path lengths between rays result in areas of constructive and destructive interference across the spot. A better picture of the spot could be obtained by calculating the path length traversed by each ray (of equal amplitude), converting this to a phase value, and vector-summing amplitudes within small quantised regions to give local amplitude values. Irradiance values are then proportional to the square of the resultant amplitude. Further to this, the weights of individual rays may be calculated from the diffraction efficiency across

the hologram. The amplitude of each ray could be calculated using the coupled wave theory of chapter 3.

The 'quantisation' just mentioned is in fact a crude approximation to the effects of diffraction, which serve to limit the resolution of imaging of any system, such as an HOE. This causes a spreading of the light emanating from any point, such as on the hologram. Therefore, the field at any given point is a summation of the energy propagating, and diffracting, from all points on the hologram. The field is explicitly given by the Fresnel-Kirchoff equation. this is the most general way to calculate the field at any point in an optical system, and makes no assumption about the form of the optical system. The Fresnel-Kirchoff equation could, for example, in principle, be used to calculate exactly the field from a hologram illuminated under any conditions, without recourse to the grating equation or coupled wave theory. In practice, all but the simplest situations must be calculated by computer, and even so, many problems are impractical to solve.

6.5 Summary.

Some of the HOE's that have been fabricated during this work have been described in principle and practice. They range from simple gratings used as attenuators, to mirrors and beamsplitters, fan-out devices and to large lenslet arrays for use both in the visible and in the infra-red. A technique for optimising wavelength-shifted holographic lenses has been presented and shown to succesfully predict the performance of lenses in the near infra-red.

The flexibility and practicality of HOE's in DCG and their use in laser-based

systems has been clearly demonstrated, not only as replacements for conventional optics, but also as unique elements performing multiple functions in one device.

Chapter 7

Conclusions.

This thesis has attempted to demonstrate the practicality of dichromated gelatin as a medium for recording high performance HOE's. This has included aspects of the design, recording, processing and modelling of holograms in DCG.

All the known factors influencing the replay properties of DCG have been given with their effects, and a model of the modulation formation process in DCG has been given. The procedure of baking a processed hologram to tune its diffraction efficiency has been described, along with the use of thorough drying to increase its operating temperature and power handling capability.

Transmission and reflection holographic gratings have been studied using models which include the effects of changes in bulk refractive index and thickness during processing, as well as non-uniformities in both fringe spacing (or local average index) and index modulation with depth. In the case of transmission holograms, the coupled wave theory has been extended and generalised so that higher diffraction orders may be easily included, as well as harmonic gratings. These harmonic

gratings arise from the saturation of the index modulation. The saturation theory presented has been found to agree well with observed angular scans of gratings. Such scans also show clear evidence of severe non-uniformities in depth in thick transmission gratings (40μm), whereas in thinner 15μm gratings, significant non-uniformities are present only in reflection holograms. These non-uniformities have been attributed primarily to diffusion processing mechanisms, since their magnitude is too great to be caused by the more obvious cause of absorption of the recording beams. This model also agrees with the observed differences between transmission and reflection holograms.

The ease of recording fan-out holograms which generate many beams from one makes such holograms potentially very useful in many areas of optics. However, in practice, it is difficult to record fan-out holograms which are both efficient and which replay beam powers faithfully. The lack of knowledge of the causes of these problems motivated a detailed study of transmission fan-out holograms in DCG. Theoretically, the coupled wave model was further extended to account for the general case of multiply superimposed gratings of any orientation within the holographic medium. This model has shown how efficiency and uniformity of beam powers may be limited by multiple-grating interactions which generate unwanted diffracted beams. Problems are aggravated by the real presence of a cross-grating which directly links object beams. It has been shown that such a cross-grating may be generated even when the object beams are not allowed to interfere. In this case, saturation can generate a real 'difference' grating which is identical to the cross-grating. In DCG such difference gratings are significant at real exposure

levels, and become more prominent as the level of desired fan-out increases. The model has been matched qualitatively with fan-out experiments, and quantitative agreement may be obtained in the fan-out to two case. Quantitative agreement is more difficult to achieve in higher level fan-out experiments because the unknown relative phases of the gratings affect the results by altering the final modulation depth in the hologram. This effect is simply the result of beating between the gratings. The effect was also expected to reduce the average modulation of a double grating hologram, but experimental results show efficiencies as high as those predicted by ignoring this effect. It is believed that this is the most complete account to date of the factors influencing fan-out volume holograms.

A number of real holographic devices have been described both in their design considerations and in the practicalities of their production for specific applications. These have included holographic lenses recorded in the visible for use at infra-red wavelengths. This entailed the development of a ray-tracing computer program which models the recording of an HOE lens and its replay at a different wavelength. This was used to optimise the recording of the lens in the green using only spherical wavefronts. The performance of the real devices agreed well with that predicted by the ray-tracing program, achieving near diffraction-limited performance with 180μm f/5 lenses for 850nm, and approximately a 30μm diameter spot with a 4.4mm f/2.5 lens for 850nm. However, for more demanding applications, it is felt that aspheric recording wavefronts must be used in future. These may be obtained from ancestor holograms as described by other authors [ASS88], thereby keeping the recording a purely optical process.

Hopefully this work has shown that there is still great potential for optically recorded holograms in DCG, despite its reputation for being difficult to work with. This thesis has shown that, given the environmental control, reproducible high performance is easy to achieve with DCG. The performance of HOE's in DCG is still superior to any other optical material in most applications, and a number of real applications which demand high performance have been described to support this case. A measure of DCG's ability surely lies in the fact that in the department where this work was carried out, holographic gratings are routinely used as alternative variable attenuators, and holographic lenses are commonly used as direct replacements for conventional lenses because they may be smaller, lighter, or there just may not be a suitable conventional lens available. They can be fabricated to specification generally in days, and so can be of great use in general laser research in any application which can be fulfilled by a volume grating or lens. In one major area where there are limitations (in fan-out holograms), it is hoped that this work has added to the understanding of DCG, and more generally to volume holographic materials.

References

[ABR69] "Evaluation of hologram imaging by ray tracing." I. A. Abramowitz. Appl. Opt. 8 p403 (1969)

[ALF75] "Coupling in doubly exposed thick holographic gratings." R. Alferness, S. K. Case. J. Opt. Soc. amer. 65 p730 (1975)

[ALF75A] "Analysis of optical propagation in thick holographic gratings." R. Alferness. Appl. Phys. 7 p29 (1975)

[ALF76] "Analysis of propagation at the second order Bragg angle of a thick holographic grating." R. Alferness. J. Opt. Soc. Amer. 66 p353 (1976)

[AMI87] "Recursive design techniques for fourier transform holographic lenses." Y. Amitai, A. A. Friesem. Opt. Eng. 25 p1133 (1987)

[AMI88] "Design of holographic optical elements using recursive techniques." Y. Amitai, A. A. Friesem. J. Opt. Soc. Amer. 5 p702 (1988)

[AND61] "Minimization of the maximum amplitude in frequency multiplexing." D. R. Anderson. Proc I.R.E. p357 (1961)

[ASS88] "Recursive design for an efficient HOE with different recording and read-out wavelengths." M. Assenheimer, Y. Amitai, A. A. Friesem. Appl. Opt. 27 p4747 (1988)

[AU87] "Nonuniformities in thick dichromated gelatin transmission gratings." L. B. Au, J. C. W. Newell, L. Solymar. J. Modern Optics 34 p1211 (1987)

[BEN76] "Achromatic combinations of hologram optical elements." S. J. Bennett. Appl. Opt. 15 p542 (1976)

[BRA39] "A new type of X-ray microscope." W. L. Bragg. Nature 143 p678 (1939)

[BRA69] "Preparation of dichromated gelatin films for holography." R. G. Brandes, E. E. Francois, T. A. Shankoff. Appl. Opt. 8 p2364 (1969)

[BUR66] "Diffraction of a plane wave at a sinusoidally stratified dielectric grating." C. B. Burckhardt, J. Opt. Soc. Amer. 56 p1502 (1966)

[BUR67] "Efficiency of a Dielectric grating." C. B. Burckhardt, J. Opt. Soc. Amer. 57 p601 (1967)

[CAS75] "Coupled wave theory for multiply exposed thick holographic gratings." S. K. Case. J. Opt. Soc. Amer. 65 p724 (1975)

[CAS76] "Index modulation and spatial harmonic generation in DCG films." S. K. Case, R. Alferness. Appl. Phys. 10 p41 (1976)

[CAT65] "Three dimensional wavefront reconstruction using a phase hologram." W. T. Cathey. J. Opt. Soc. Amer. 55 p457 (1965)

[CED87] "Analytic design of optimum holographic optical elements." J. N. Cederquist, J. R. Fienup. J. Opt. Soc. Amer. A 4 p699 (1987)

[CHA67] "Non-paraxial imaging, magnification and aberration properties in holography." E. B. Champagne. J. Opt. Soc. Amer. 57 p51 (1965)

[CHA71] "Dichromated gelatin of improved optical quality." M. Chang. Appl. Opt. 10 p2550 (1971)

[CHA76] "Post processing of developed DCG holograms." B. J. Chang. Opt. Commun. 17 p270 (1976)

[CHA79] "Dichromated gelatin for the fabrication of holographic optical elements." B. J. Chang, C. D. Leonard. Appl. Opt. 18 p2407 (1979)

[CHA80] "DCG holograms and their applications." B. J. Chang. Optical Engineering 19 p642 (1980)

[CHE82] "Holographic Twyman-Green interferometer." C. W. Chen, J. B. Breckinridge. Appl. Opt. 21 p2563 (1982)

[CHE87] "Design of a holographic lens for the infra-red." H. Chen, R. R. Hershey, E. N. Leith. Appl. Opt. 26 p1983 (1987)

[CHE88] "Using holographically generated corrector plates to fabricate low f/no. HOE objectives and collimators." H. Chen, Q. Shan. Appl. Opt. 16 p3542 (1988)

[CHU70] R. S. Chu, T. Tamir, IEEE Trans. Microwave Theory Tech. MTT-18 p486 (1970)

[CUL82] "Some characteristics of, and measurements on DCG reflection holograms." R. A. Cullen. SPIE 369 p647 (1982)

[CUR70] "The mechanism of hologram formation in dichromated gelatin." R. K. Curran, T. A. Shankoff. Appl. Opt. 9 p1651 (1970)

[DAM71] "High efficiency in-line multiple imaging by means of multiple phase holograms." H. Dammann, K. Gortler. Opt. Commun. 3 p312 (1971)

[DEN62] "Photographic reconstruction of the optical properties of an object in its own scattered radiation field." Yu N. Denisyuk. Soviet Physics- Dolkady 7 p543 (1962)

[DUN85] "Tunable holographic filters in DCG operating in the near infra-red region." SPIE 523 (Applications of Holography) p196 (1985)

[FAI82] "Computer-originated aspheric holographic optical elements." R. C. Fairchild, J. R. Feinup. Opt. Eng. 21 p133 (1982)

[FAR87] "Comparison of binary encoding schemes for electron-beam fabrication of computer generated holograms." H. Farhoosh, M. R. Feldman, S. H. Lee, C. C. Guest, Y. Fainman, R. Eschbach. Appl. Opt. 26 p4361 (1987)

[FEL87] "Computer generated HOE's for optical interconnection of VLSI integrated circuits." M. R. Feldman, C. C. Guest. Appl. Opt 26 p3477 (1987)

[FIL71] "Sensitometric characteristics of hardened dichromated gelatin films." G. L. Filmore, R. F. Tynan. J. Opt. Soc. Amer. 61 p199 (1971)

[FUJ82] "Blazed gratings and fresnel lenses fabricated by electron beam lithography." T. Fujita, H. Nishihara, J. Koyama. Opt. Lett. 7 p578 (1982)

[GAB48] "A new microscope principle." D. Gabor. Nature 161 p777 (1984)

[GAY81] "Thin and thick gratings: terminology clarification." T. K. Gaylord, M. G. Moharam. Appl. Opt. 20 p3271 (1981)

[GOO68] "Effects of film nonlinearities on wavefront-reconstruction images of diffuse objects." J. W. Goodman, G. R. Knight. J. Opt. Soc. Amer. 58 p1276 (1968)

[GOO84] "Optical interconnection for VLSI systems." J. W. Goodman, F. I. Leonberger, S. Y. Kung, R. A. Athale. Proc IEEE 72 p850 (1984)

[HAN84] "Reshaping collimated lsaer beams with Gaussian profile to uniform profiles." C. Y. Han, Y. Ishii, K. Murata. Appl. Opt. 22 p3644 (1983)

[HAR84] "Optical holography." P. Hariharan. Cambridge University press (1984)

[JEN84] "Sequential optical logic implementation." B. K. Jenkins, A. A. Sawchuk, T. C. Strand, R. Forchheimer, B. H. Soffer. Appl. Opt. 23 p3455 (1984)

[JEN84A] "Architectural implications of a digital optical processor." B. K. Jenkins, P. Chavel, R. Forchheimer, A. A. Sawchuk, T. C. Strand, Appl. Opt. 23 p3465 (1984)

[JOH84] "Holographic reciprocity law failure." K. M. Johnson, L. Hesselink, J. W. Goodman. Appl. Opt. 23 p218 (1984)

[JOH85] "Multiple multiple exposure hologram." K. M. Johnson, M. Armstrong, L. Hesselnik, J. W. Goodman. Appl. Opt. 24 p4467 (1985)

[KAS73] "Diffraction by thick periodically stratified gratings with complex dielectric constant." F. G. Kaspar. J. Opt. Soc. Amer. 63 p37 (1973)

[KED86] "Optimised holographic optical elements." J. Kedmi, A. A. Friesem. J. Opt. Soc. Amer. A 3 p2011 (1986)

[KED84] "Optimal holographic fourier transform lens." J. Kedmi, A. A. Friesem. Appl. Opt. 23 p4015 (1984)

[KER66] "Nonuniform sinusoidally modulated dielectric gratings." J. Opt. Soc. Amer. 69 p1409 (1969)

[KIL77] "Coupled wave theory of hologram gratings with arbitrary attenuation." U. Killat. Opt. Commun. 21 p110 (1977)

[KOG67] "Bragg diffraction in hologram gratings with multiple internal reflections." H. Kogelnik. J. Opt. Soc. Amer. 57 p431 (1967)

[KOG69] "Coupled wave theory for thick hologram gratings." H. Kogelnik. Bell System Technical Journal 48 p2909 (1969)

[KOS85] "Optical imaging applied to microelectronic chip to chip interconnections." R. K. Kostuk, J. W. Goodman, L. Hesselink. Appl. Opt. 24 p2851 (1985)

[KOS86] "Volume reflection holograms with multiple gratings: an experimental

and theoretical evaluation." R. K. Kostuk, J. W. Goodman, L. Hesselink. Appl. Opt. 25 p4362 (1986)

[KOW78] "Diffraction efficiency of sequentially stored gratings in reflection volume holograms." R. Kowarschik. Opt. Quant. Elect. 10 p171 (1978)

[KUB76] "The diffraction efficiency of hologram gratings recorded in an absorptive medium." T. Kubota. Opt. Commun. 16 p347 (1976)

[KUB78] "Characteristics of thick hologram gratings recorded in an absorptive medium." T. Kubota. Optica Acta 25 p1035 (1978)

[KUB79] "The bending of interference fringes inside a hologram." T. Kubota. Optica Acta 26 p731 (1979)

[KOW78] "Diffraction efficiency of sequentially stored gratings in transmission volume holograms." R. Kowarschik. Optica Acta 25 p67 (1978)

[LAT71A] "Computer-based analysis of hologram imagery and aberrations. I. Hologram types and their non-chromatic aberrations." J. N. Latta. Appl. Opt. 10 p599 (1971)

[LAT7BA] "Computer-based analysis of hologram imagery and aberrations. I. Aberrations induced by a wavelength shift." J. N. Latta. Appl. Opt. 10 p609 (1971)

[LAT71C] "Computer-based analysis of holography using ray-tracing." J. N. Latta. Appl. Opt. 10 p2698 (1971)

[LAT79] "Design techniques for forming 488nm holographic lenses with reconstruction at 633nm." M. R. Latta, R. V. Pole. Appl. Opt. 18 p2418 (1979)

[LEE80] "Techniques for recording holographic lenses for infra-red wavelengths." W. H. Lee. Opt. Commun. 34 p29 (1980)

[LEE87] "Computer generated holography: an introduction." S. H. Lee. Appl.Opt. 26 p4350 (1987)

[LEI62] "Reconstructed wavefronts and communication theory." E. N. Leith, J. Upatnieks. J. Opt. Soc. Amer. 52 p1123 (1962)

[LEI65] "Microscopy by wavefront reconstruction." E. N. Leith, J. Upatnieks, K. A. Haines. J. Opt. Soc. Amer. 55 p981 (1965)

[LIN69] "Hologram formation in dichromated gelatin films." L. H. Lin. Appl. Opt. 8 p963 (1969)

[LIN71] "Efficient aberration-free wavefront reconstruction from holograms illuminated at wavelengths differing from the forming wavelength." L. H. Lin, E. T. Doherty. Appl. Opt. 10 p1314 (1971)

[LIP94] "Sur la theorie de la photographie des couleurs simples et composees par la method interferentielle." G. Lippmann. J. Physique. 3 p97 (1894)

[LUD73] "Generalised grating ray tracing equations." U. W. Ludwig. J. Opt. Soc. Amer. 63 p1105 (1973)

[MAC77] "Hologram fringe stabilization method." D. R. MacQuigg. Appl. Opt. 16 p291 (1977)

[MAG76] "Use of dynamic theory to describe experimental results from volume holography." R. Magnusson, T. K. Gaylord. J. Appl. Phys. 47 p190 (1976)

[MAG77] "Analysis of multiwave diffraction of thick holograms." R. Magnusson, T. K. Gaylord. J.opt. Soc. Amer. 67 p1165 (1977)

[MAG78B] "Equivalence of multiwave coupled wave theory and modal theory for periodic media diffraction." R. Magnusson, T. K. Gaylord. J. Opt. Soc. Amer. 68 p1777 (1978)

[MAG85] "Holographic mirrors." J. R. Magarinos, D. J. Coleman. Opt. Eng. 24 p769 (1985)

[MAZ82] "DCG for volume holographic recording with high sensitivity, Part II." M. Mazakova, M. Pancheva, P. Kandilarov, P. Sharlandjiev. Opt. Quant. Elect. 14 p317 (1982)

[MCC73] "Holographic optical element for visual display applications." D. G. McCauley, C. E. Simpson, W. J. Murbach. Appl. Opt. 12 p232 (1973)

[MCC85] "Position tunable holographic filters in DCG for use in single mode fiber demiultiplexers." D. J. McCartney, D. B. Payne, S. S. Duncan. Opt. Lett. 10 p303 (1985)

[MCG80] "Colour control in DCG reflection holograms." S. P. McGrew. SPIE 215 p24 (1980)

[MEE44] "The theory of the photographic process." C. E. Kenneth Mees. MacMillan Co. New York (1944)

[MEI65] "Magnification and third order aberrations in holography." R. W. Meier. J. Opt. Soc. Amer. 55 p987 (1965)

[MEY72] "Phase holograms in dichromated gelatin." D. Meyerhofer. RCA Review 33, p110 (1972)

[MEY77] "Dichromated Gelatin." D. Meyerhofer. Chapter 3 in "Topics in Applied Physics" vol. 20 (1977)

[MIL73] "Evaluation of the wavefront aberration in holography." J. F. Miles. Optica Acta 20 p19 (1973)

[MOH80] "Criteria for Bragg regime diffraction by phase gratings." M. G. Moharam, T. K. Gaylord, R. Magnusson. Opt. Commun. 32 p14 (1980)

[MOH80A] "Criteria for Raman Nath regime diffraction by phase gratings." M. G. Moharam, T. K. Gaylord, R. Magnusson. Opt. Commun. 32 p19 (1980)

[MOH81] "Coupled-wave analysis of reflection gratings." M. G. Moharam, T. K. Gaylord. Appl. Opt. 20 p240 (1981)

[MOH81A] "Rigorous coupled wave analysis of planar grating diffraction." M. G. Moharam, T. K. Gaylord, J. Opt. Soc. Amer. 71 p811 (1981)

[MOH82] "Chain-matrix analysis of arbitrary-thickness dielectric reflection gratings." M. G. Moharam, T. K. Gaylord. J. Opt. Soc. Amer. 72 p187 (1982)

[NEW85] "Holograms in dichromated gelatin- real time effects." J. C. Newell, L. Solymar, A. A. Ward. Appl. Opt. 24 p4460 (1985)

[NEW87] "Optical holography in dichromated gelatin." J. C. W. Newell. Ph.D. thesis, Oxford University (1987)

[NIN73] "Recording characteristics of volume holograms." Y. Ninomiya. J. Opt. Soc. Amer. 63 p1124 (1973)

[OFF66] "Ray tracing through a holographic system." J. Opt. Soc. Amer. 56 p1509 (1966)

[OLI84] "Dichromated gelatin holograms derived from Agfa 8E75HD plates." J. Oliva, P. G. Boj, M. Pardo. Appl. Opt. 23 p196 (1984)

[OWE80] "Efficiency of volume phase reflection holograms recorded in an attenuating medium." M. P. Owen, L. Solymar. Opt. Commun. 34 p321 (1980)

[OWE83] "Internal reflections in bleached reflection holograms." M. P. Owen, A. A. Ward, L. Solymar. Appl. Opt. 22 p159 (1983)

[PHA56] "On the diffraction of light by progressive supersonic waves." P. Phariseau. Proc. Ind. Acad. Sci. 44a p165 (1956)

[PRI72] "Studying hologram imagery by a ray-tracing method." I. Prikryl. Optica Acta 19 p623 (1972)

[RAM35] "The diffraction of light by high frequency sound waves." C. V. Raman, N. S. Nagendra Nath. Proc. Ind. Acad. Sci. parts I-V Vol. 2: p406, p413 (1935). Vol. 3: p75, p119, p459 (1936)

[RED88] "Continuously variable laser beam attenuator." Ian. R. Redmond, Mohammad R. Taghizadeh. European patent no. 88109667.1, U.S. patent no. 200 872, filed June (1988)

[ROB88] B. Robertson, measurements of thermal damage in DCG, Heriot-Watt University (1988). To be published.

[SAM80] "The mechanism of volume hologram formation in Dichromated Gelatin." D. M. Samoilovich, A. Zeichner, A. A. Freisem. Photographic Science and Engineering 24 p161 (1980)

[SHA68] "Phase holograms in dichromated gelatin." T. A. Shankoff. Appl. Opt. 7 p2101 (1968)

[SHA85] "Holographic mirrors- a thin-film optics approach." P. Sharlandjiev, T. Todorov. Opt. Quant. Elect. 17 p443 (1985)

[SHA85A] "Spectral selectivity of holographic mirrors recorded in an attenuating medium." P. Sharlandjiev, T. Todorov. Opt. Quant. Elect. 17 p277 (1985)

[SHI87] "Rectangular apertured micro-fresnel lens arrays fabricated by electron beam lithography." T. Shiono, K. Setsune, O. Yamakazi, K. Wasa. Appl. Opt. 26 p587 (1987)

[SLI85] "Nonlinear recording in silver halide planar volume holograms." C. W. Slinger, R. R. A. Syms, L. Solymar. Appl. Phys. B 36 p217 (1985)

[SLI86] "Grating interactions in holograms recorded with two object waves." C. W. Slinger, L. Solymar. Appl. Opt. 25 p3283 (1986)

[SMI87] "Restoring optical logic - demonstration of extensible all-optical digital syatems." S. D. Smith, A. C. Walker, B. S. Wherrett, F. A. P. Tooley, N. Craft, J. G. H. Mathew, M. R. Taghizadeh, I. Redmond, R. J. Campbell. Opt. Eng. 26 p45 (1987)

[SOL77] "Two dimensional N coupled wave theory for volume holograms." L. Solymar. Opt. Commun. 23 p199 (1977)

[SOL78] "A two-dimensional volume hologram theory including the effect of varying average dielectric constant." L. Solymar. Appl. Phys. Lett. 31 p820 (1978)

[STO85] "Wavelength performance of holographic optical elements." T. Stone, N. George. Appl. Opt. 24 p3797 (1985)

[SU75] "Calculation of arbitrary-order diffraction efficiencies of thick gratings of arbitrary grating shape." S. F. Su, T. K. Gaylord. J. Opt. Soc. Amer. 65 p59 (1975)

[SYM83] "Planar volume phase holograms formed in bleached photographic emulsions." R. R. A. Syms, L. Solymar. Appl. Opt. 22 p1479 (1983)

[TAG89] "High efficiency holographic optical elements for all-optical digital computing." M. R. Taghizadeh, I. R. Redmond, B. Robertson, A. C. Walker, S. D. Smith. Proc SPIE 1136 (1989)

[UCH73] "Calculation of the diffraction efficiency in hologram gratings attenuated along the direction perpendicular to the grating vector." N. Uchida. J.

Opt. Soc. Amer. 63 p280 (1973)

[UPA70] "Efficiency and image contrast of dielectric holograms." J. Upatnieks, C. Leonard. J. Opt. Soc. Amer. 60 p297 (1970)

[WAL88] "Optically bistable thin-film interference devices and holographic techniques for experiments in digital optics." A. C. Walker, M. R. Taghizadeh, J. G. H. Mathew, I. R. Redmond, R. J. Campbell, S. D. Smith, J. Dempsey, G. LeBreton. Opt. Eng. 27 p38 (1988)

[WAN88] "Interference filters as nonlinearision making elements for three spot pattern recognition and associative memories." L. Wang, V. Esch, R. Feinleib, L. Zhang, R. Jin, H. M. Chou, R. W. Sprague, H. A. McCleod, G. Khitrova, H. M. Gibbs, K. Wagner, D. Psaltis. Appl. Opt. 27 p1715 (1988)

[WEL74] "Aberrations of the symmetrical optical system." W. T. Welford. Academic Press, London (1974)

[WEL75] "A vector raytracing equation for hologram lenses of arbitrary shape." W. T. Welford. Opt. Commun. 14 p322 (1975)